Investigation of neuroanatomical subdivisions of the thalamic reticular nucleus upon brain states

PhD Thesis

Vladimir Visocky

Academic Supervisors:

I) Professor Judith Pratt

Dr. Shuzo Sakata

Professor Brian Morris

Industrial Supervisors:

Nick Brandon

John Dunlop

SIPBS

University of Strathclyde, Glasgow

September 1, 2018

This thesis is the result of the author's original research. It has been composed by the author and has not been previously submitted for examination which has led to the award of a degree.

The copyright of this thesis belongs to the author under the terms of the United Kingdom Copyright Acts as qualified by University of Strathclyde Regulation 3.50. Due acknowledgement must always be made of the use of any material contained in, or derived from, this thesis.

Abstract

The thalamic reticular nucleus (TRN), a part of the corticothalamic loop, plays a key role in selective attention and sleep spindle generation. Furthermore, sleep spindles are reduced in amplitude and duration in schizophrenia patients, implying clinical relevance of TRN functions. However, while the TRN is topographically organized, it remains unclear whether and how the TRN consists of functionally distinct sub-regions. Combining optogenetic and electrophysiological approaches in mice, we investigated changes in sleeping behavior and EEG oscillations caused by optogenetic stimulations in different parts of the TRN. Two inhibitory opsins Halorhodopsin (Halo) and Archaerhodopsin (Arch) were expressed specifically in either an anterior or posterior part of the TRN in parvalbumin (PV)-Cre mice using adeno-associated viral vectors. Effects of optical stimulation on cortical EEGs were assessed by delivering green light through chronically implanted optic fibers over 30 second periods in freely behaving animals. Tonic stimulations during awake states did not produce any significant change in EEG, whereas the stimulations during sleep significantly affected several frequency bands associated with TRN functions. The delta oscillation was decreased significantly during optogenetic inhibition in the rostral and caudal TRN. The sleep spindles, alpha waves, were significantly diminished only during the caudal TRN inhibition. The rostrally inhibited animals had a tendency for longer sleep and had a reduced proportion of the short sleep episodes relatively to the mice with caudally inhibited TRN. Lastly, we demonstrated that the caudal and rostral TRN are taking part in the brain state transition. The caudal part of the nucleus appears important for the wake – NREM sleep transition and the rostral TRN activation is associated with the sleep-wake transition. Although, it was a basic way to test the hypothesis, we concluded that rostral and caudal TRN consist of distinct subnetworks which have different activity levels during sleep. This is the first known description of TRN heterogeneity based on the location principles.

Contents

List of abbreviations

ACh - acetylcholine

AD – anterodorsal nucleus (n.)

AM – Anteromedial n.

ARAS - ascending reticular activation system

AV – anteroventral n.

BF – basal forebrain

CaBP – calbindin

CBP – calcium binding proteins

CCK – cholecystokinin

CL – central laminar n.

CM – central medial n.

CR – calretinin

CT – corticothalamic

GP – globus pallidus

HDB - horizontal diagonal band of Broca

IL – intralaminar n.

LC - locus coeruleus

LD – laterodorsal n.

LDT – laterodorsal tegmentum

LGN – lateral geniculate n.

LH – lateral hypothalamus

LP – lateral posterior n.

MCPO - magnocellular preoptic area

MD – mediodorsal n

MDc – central MD

MDl – lateral MD

MDm – medial MD

MGD – dorsal MGN

MGM – medial MGN

MGN – medial geniculate n.

MGV – medial MGN

MLT - melatonin

NA - noradrenaline

NBM - nucleus of basalis of Meyert

NPY - Neuropeptide Y

NREM – non-rapid eye movement sleep

NTS – nucleus tractus solitarius

PaV – paraventricular n.

PC – paracentral n.

PF – parafascicular n.

PO – posterior n.

Pom – posterior complex

PPT - pedunculopontine tegmentum

PrRP - Prolactin releasing peptide

PT – parataenial n.

PuL – pulvinar n.

PV – parvalbumin

RE – reunions n.

RH – rhomboid n.

PZ - parafacial zone

S-TRN – somatotopic part of the TRN

SI - substantia inominata

SN – substantia nigra

SOM - Somatostatin

TC – thalamocortical

TRH - Thyrotropin-releasing hormone

TRN – thalamic reticular n.

VA – ventral anterior n.

VB – ventrobasal complex

VIP - Vasoactive intestinal peptide

VL – ventrolateral n.

VLPO - ventrolateral preoptic n.

VM – ventral medial n.

VP – ventral posterior n.

VPL – Ventroposterolateral n.

VPM – ventral posteromedial n.

VTA – ventral tegmental area

ZI – zona incerta

5 – HT – serotonin

Acknowledgements

Yes, there were times, I'm sure you knew
When I bit off more than I could chew
But through it all, when there was doubt
I ate it up and spit it out
I faced it all and I stood tall
And did it my way

I would like to express my special appreciation and thanks to my supervisor Professor Judith Pratt. Professor Judith Pratt thank you for giving me the opportunity to be involved in this project. I appreciate your trust in me and the workflow freedom given to me. I greatly appreciate the support and patience of Dr. Shuzo Sakata, which weekly encouraged me during the whole project. Many thanks to Professor Brian Morris for his valuable input.

I am grateful for the fundings received towards my PhD from AstraZeneca. Thanks to Dr. John Dunlop and Dr. Nick Brandon for the support and timely feedbacks.

I also thank to my lab team, Dr. Josue Garcia Yague, Dr. Tomomi Tsunematsu, Dr. Daniel Lyngholm, Dr. David Mark Thompson and Miss Olga Lapies for their advice and jokes in the lab. Thanks so much for the support given to me by all BPU staff and members of SIPBS.

I would like to acknowledge my family and friends backing. Constant encouragement of my mum, father, aunt and grandparents made possible for me to finish this project. I am also indebted to my friend Roman Arhipenko, who insisted on finishing off this project during tough time

Chapter 1: Literature Review

1.1 Introduction

Neuroscience is slowly but consistently aiming to solve one of the biggest problems of civilization, brain diseases. Significant dysfunction in the brain leads to unbearable living quality and the path to the cure seems to be infinite. Although biomedical research techniques evolve at a high speed, the function of many brain areas is poorly understood. The thalamic reticular nucleus (TRN), an important part of the brain which seems to control other thalamic nuclei, is not an exception. Relatively minimal information about the TRN is available today; however, its importance for brain processes such as consciousness, sleep, memory, attention and sensory processing cannot be underestimated (Krol et al., 2018). My goal is to update the knowledge about this part of the brain using recently developed techniques.

The history of the thalamus began when Galen, one of most influential biomedical scientists of the Roman Empire, used the Greek word thalamos to name a specific area of the brain. Thalamos means an inner room or storeroom of a Greek or Roman house, a reservoir in the brain of vital spirit (Jones, 1985). The idea of the thalamus as the vital spirit storeroom was still extant even when Santorini described the geniculate bodies in 1725 and only lesion studies of early 19th century revealed its sensory role. Franz Nissl, one of the greatest neuropathologists of his day, described this region histologically, using his newly developed cell stain and named the thalamic nuclei in 1889 (Jones, 1985).

Ramon y Cajal (Garcia-Lopez et al., 2010) first proved, using a Golgi technique, that axons of the thalamic reticular nucleus (TRN) synapse in the dorsal thalamus. Later, Nissl (1913) demonstrated that telencephalon destruction led to cellular degeneration in the reticular nucleus, which emphasized the functional linkage between these two. The destruction of the cerebral cortex alone was sufficient to cause destruction of the TRN cells (Carman et al., 1964). Hence, it was believed that the reticular nucleus played the role of a final relay station for ascending sensory information. The introduction of autoradiographic and horseradish peroxidase histochemical techniques revealed that the TRN does not have direct afferent

connections with the cortex and that the cellular reaction was caused by close relationship with the dorsal thalamic nuclei and cortex (Jones, 1975).

These approaches together with physiological based approaches have enabled a detailed functional anatomy of the TRN and cortical regions to be described. The cerebral cortex and the thalamus are reciprocally interconnected by corticothalamic (CT) and thalamocortical (TC) axons, which send off collaterals to innervate the thalamic reticular nucleus (TRN). This GABAergic, shell-shaped nucleus covers the anterior, lateral and much of the ventral surfaces of the dorsal thalamus (Jones, 1975; Jones, 1985). The TRN receives excitatory synapses from CT and TC projections and sends inhibitory feedback to the nuclei of the dorsal thalamus. Inputs from the modality-related cortical regions and thalamic nuclei converge in the TRN, thus overlapping topographical maps representing sensory inputs are found in the nucleus. The TRN is in a strategic position between the cortex and the thalamus and the possession of the overlapping functionally distinct sectors contributed to Francis Crick's speculative hypothesis, the searchlight hypothesis. It stated that during selective attention, the TRN by intensifying corresponding TC circuits may act as the searchlight in the dusk. In other words, the TRN inhibitory projections "should be able to sample the activity in the cortex and/or the thalamus and decide where the action is" (Crick, 1984). Later, McAlonan et al. (2008) and Halassa et al. (2014) proved that modality associated attention is caused by the TRN inhibition of the lateral modalities neurons in the thalamus, which are not involved in the attention.

To understand better the mechanisms of proposed TRN functions, we will cover anatomy, morphology, neurochemistry and physiology of the TRN and its adjacent areas in the next sections.

1.2 Thalamus

The thalamus is not only a relay station for sensory information, but it also relays information from one cortical area to another (Sherman & Guillery, 2002). In addition, it significantly alters the nature of information propagated to the cortex (Rikhye et al., 2018). The thalamic relay is responsive to the brain states (arousal, wakefulness, sleep) and it modifies its cortical output according to the consciousness state. First order thalamic nuclei (lateral geniculate nucleus (LGN), ventrobasal complex (VB)) send the peripheral sensory information to the sensory cortices and receive modulatory corticothalamic afferents from pyramidal cells in cortical layer 6. Higher order nuclei (the mediodorsal (MD), the lateral posterior (LP)) receive very little or none of the sensory information from sensory organs. Instead they receive most of their afferents from pyramidal cells in cortical layer 5 and play a key role in the corticocortical or corticosubcortical communication. In addition, they receive modulatory afferents from cortex (layer 6) and subcortical modulatory inputs from the TRN and brainstem (Guillery, 1995; Sherman & Guillery, 2002a).

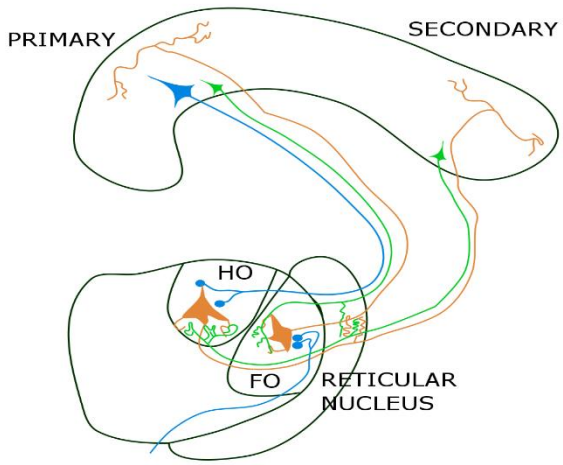

Figure 1.1 The difference is shown between first order (FO) and higher order (HO) nuclei in the thalamus. “Primary afferents” are in blue; the layer 6 corticothalamic fibers are in green and the thalamocortical fibers are in orange.

A small percentage of the afferent “drivers” transmit sensory information to the cortex. Other drivers are represented by the afferents from the inferior colliculus, the cerebellum and the mammillary bodies. All other inputs to thalamus can be regarded as “modulators”. They do not carry sensory message, but they can modulate the transferred message. A number of axons from the cortex and the TRN synapse to the thalamus as “modulators”. Drivers propagate the sensory information to the first order thalamic nuclei and do not innervate the TRN. Then, the first order relay thalamocortical axons propagate to their respective primary cortical areas, giving branches to the reticular nucleus on the way. Primary cortical areas send back two types of corticothalamic axons from layer 5 and 6. Layer 6 neurons send inputs to the relay thalamic nuclei and send off branches to the TRN (Figure 1.1). Silencing of these modulatory direct and indirect (feedback through the TRN) pathways produce minor changes in the receptive field. In contrast, the driver silencing would lead to a complete loss of the receptive field. Layer 5 neurons send driver like corticothalamic axons to the higher order thalamic nuclei. They share structural appearance and synaptic connectivity with ascending afferents to the first order relays and similar to them do not send any branches to the TRN (Guillery & Harting, 2003; Sherman & Guillery, 2002). Silencing of these CT pathways would lead to the loss of receptive field properties as well (Bender, 1983; Diamond et al., 1992). Layer 5 axons also branch to lower brain areas, brain stem or spinal motor centers. These axons represent the outputs that are going from cortex to lower centers and their thalamic branches serve to send copies of this output (corollary discharge) from one cortical area to another (Sherman & Guillery, 2002). Neurons from the higher order thalamic areas, similarly to first order, are reciprocally interconnected with the TRN. Therefore, the TRN not only modulates sensory information upcoming to cortex but also further facilitate the transfer of the corticocortical information.

In the early studies, the critical role of the thalamus for the sensory information transfer to the cortex was well recognized. Thus, attention was paid mostly to

thalamic relay areas, whereas 'non-relay' regions, also known as 'non-specific', despite relatively vast thalamic accommodation, were rarely mentioned. Higher order thalamic family are composed of anterior nucleus (anterodorsal (AD), anteroventral (AV) and anteromedial (AM)), mediodorsal nucleus (MD), intralaminar nuclei (central lateral (CL), paracentral (PC), central medial (CM) parafascicular (PF)), midline nuclei (parataenial (PT), paraventricular (PaV), rhomboid (RH) and reuniens (RE)), lateral nuclei (lateral dorsal and lateral posterior) and submedial nucleus (Vertes et al. 2016). The relay nuclei include posterior nucleus (PO), ventral lateral nucleus (VL), ventral anterior nucleus (VA), medial geniculate nucleus (MGN), ventral posteromedial (VPM) and posterolateral (VPL) nuclei, the lateral geniculate complex (LGN) and ventral medial nucleus (VM). Traditionally, thalamic nuclei were subdivided in three anatomical/functional groups: first order nuclei (also, principal or relay), the association nuclei (most of the higher order nuclei) and the midline and intralaminar nuclei (Witter & Groenewegen, 2004). The latter group is separated from other higher order nuclei, due to a distinct midline location, a prominent distribution pattern in both cortical and subcortical structures and due to their involvement in processes of arousal and attention (Witter & Groenewegen, 2004). Recently, an alternative classification was proposed and it similarly consists of 3 sets of thalamic nuclei: sensorimotor nuclei of thalamus, 'limbic' nuclei of thalamus and thalamic nuclei bridging these two domains (Vertes et al., 2016). Classifications variance is emphasized on Figure 1.2 below.

1.3 Topographical organization of the TRN

Although the receptive fields of reticular cells are larger than those of their thalamic or cortical counterparts (Yen & Conley, 1985), previous electrophysiological and staining studies indicated the non uniform nature of the TRN (Scheibel & Scheibel, 1972) and the existence of at least seven modality sectors 'slabs' in the TRN, five sensory (visual, auditory, gustatory, visceral and somatosensory), one limbic and one motor (Pinault, 2004a). Each sector found in the TRN sends projections to those

thalamic nuclei from which it receives projections (Jones, 1975). The first order connections (connections between first order thalamic nuclei and the TNR) are more clearly mapped in a topographic order than the higher order connections (Crabtree, 1992; Crabtree & Killackey, 1989). Thus, the modality specific projections to and from the sheet-like nucleus consist of structured components and can be mapped. However, we have to keep in mind that not all TRN modality areas have 'strict' topographical organization. Sensory and non-sensory sectors can have non- mapped projections or can send inputs to the thalamic nuclei with non-related modality. In the following sections, the thalamic nuclei physiological roles and interconnections with cortex and the TRN will be briefly characterized.

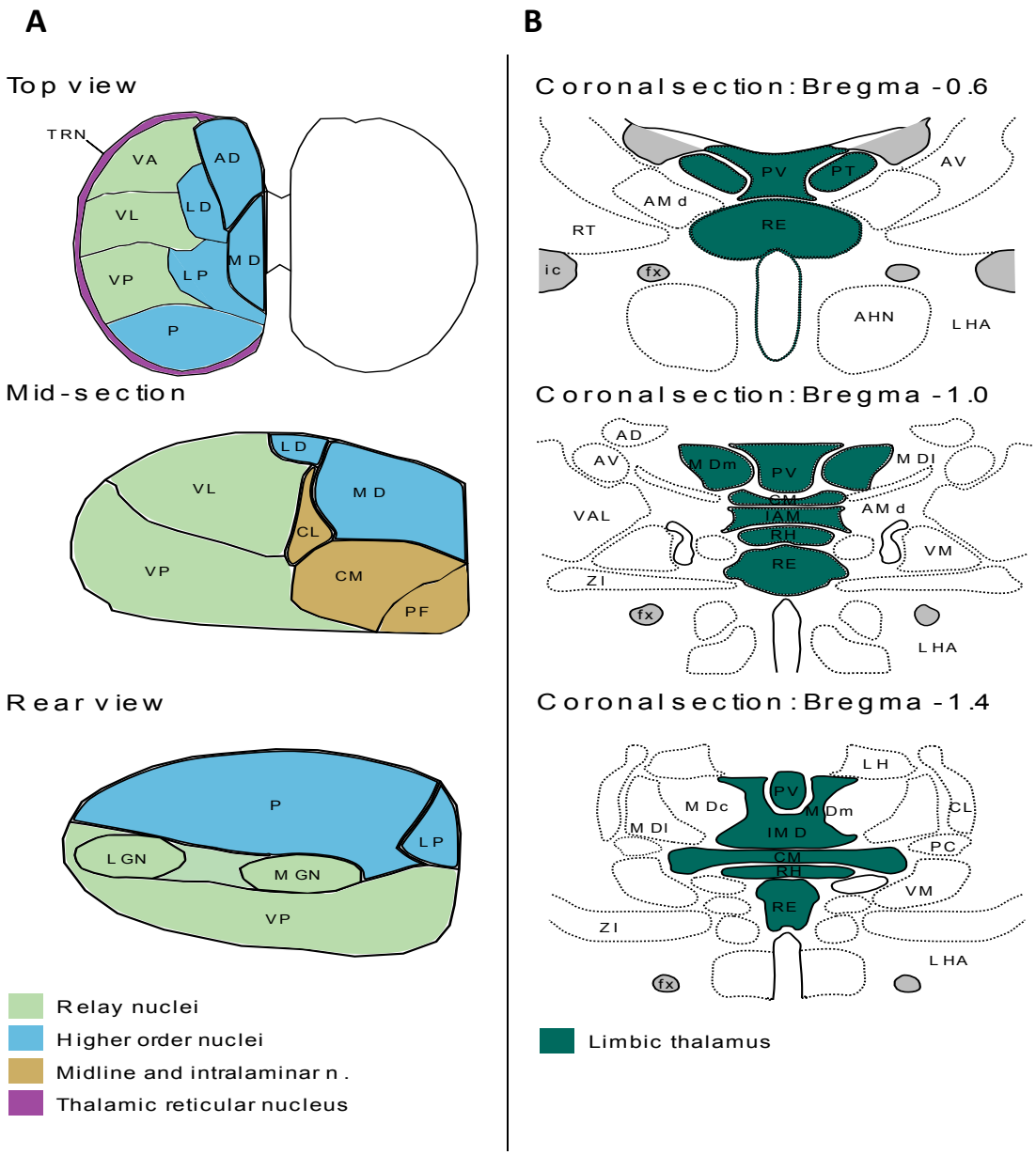

Figure 1.2 Two classifications of thalamic nuclei. **A** the traditional classification with three anatomical/functional groups: relay nuclei, the higher order nuclei, and the midline and intralaminar nuclei (Witter & Groenewegen 2004). **B** The alternative classification with three groups: the sensorimotor group (relay), the limbic group (MDm, midline and anterior nuclei), the limbic or 'bridging nuclei' group (lateral thalamus, intralaminar nuclei, submedial nucleus and MDc, MDi. VA – ventral anterior, VL – ventral lateral, VP – ventral posterior, P – pulvinar, LP – lateral posterior, LD – lateral dorsal, AD – anterodorsal, CL – central lateral, CM – central medial, PF – parafascicular, LGN – lateral geniculate nucleus, MGN – medial geniculate nucleus, PV – paraventricular, PT – parataenial, RE- reuniens, RH – rhomboid, MDm – medial mediodorsal, IAM – the interanteromedial nucleus, IMD - the intermediodorsal nucleus, ZI – zona incertia.

1.4 Higher order thalamic nuclei

1.4.1 Anterior Thalamus

The anterior thalamus (ATN), based on histological differences (Paxinos & Watson, 2007), can be subdivided into 3 subnuclei: anterodorsal (AD), anteroventral (AV) and anteromedial (AM). Mammillary nuclei, part of the limbic system, acts as the main subcortictical input to the anterior thalamus (Shibata, 1992). The thalamus is traditionally accepted as a relay nucleus, which propagates sensory and motor information in feed-forward manner to the wide areas of the neocortex. The 'limbic' areas of the thalamus, the anterior thalamic nucleus, in addition to the propagating functions appears to be important for cognitive functions (Wilton et al., 2001; Aggleton et al., 2010; Roth et al., 2016a). ATN is reciprocally interconnected with retrosplenial, subicular, cingulate, parahippocampal limbic, parietal and frontal association cortices (Paxinos & Watson, 2007; Van Groen & Wyss, 1995). Anatomical connections, lesion studies (Dalrymple-Alford et al., 2015) and the multiple cases of the diencephalic amnesia in subjects with thalamus trauma support the conclusion that the ATN is a part of the extended hippocampal-limbic processing network involved in learning and the retrieval of spatial and context-dependent information (Warburton et al., 2000).

There have been several studies probing the pathways between the TRN and the anterior thalamus. A series of experiments during which anterograde tracers were placed in the anterior part of the TRN in the Rhesus monkeys found projections to anterior thalamic nuclei group (AD, AV, AM), laterodorsal and mediodorsal nuclei. The TRN contacted the anterior thalamus using en passant axons, which allows it to create multiple synapses with local circuitry neurons in thalamus (Kultas-Ilinsky et al., 1995). Similarly, the rostral part of the TRN in rodents receives projections from the anterior thalamic nuclei; AV and AD connections are positioned dorsally and receive retrosplenial corticothalamic axons, whereas AM and mediodorsal nuclei project ventrally and cohabited with axonal branches from cingulate cortex. (Shibata, 1992; Lozsádi, 1994; Lozsádi, 1995; Gonzalo-Ruiz & Lieberman, 1995). Additionally, there

is clear evidence, that orbital and infralimbic cortexes project to the rostral TRN (Cornwall et al., 1990). Limbic cortex terminals, contrary to the sensory cortex axon bundles, do not cluster in slabs but occupy the entire thickness of the rostral TRN.

1.4.2 Lateral nuclei

Lateral nuclei (pulvinar) are also characterized as other higher order nuclei. In rodents and carnivores, the pulvinar nucleus is characterized as part of the lateral thalamic nucleus and in primates, it is recognized as an independent complex. Lateral nuclei consist of two nuclei: lateral dorsal (LD) and lateral posterior (LP). Both are anatomically and functionally related. LD and LP nuclei are found more on ventrolateral relatively to anterior ventral nucleus and are important for establishing and maintaining spatial orientation (Clark & Harvey, 2016). Previous lesion studies suggest, that the lateral thalamus does not take part in spatial learning and is vital during directing attention toward visual-spatial targets (Grieve et al., 2000). Lateral nuclei, like the anterior nuclei, project to the postsubiculum, retrosplenial and entorhinal cortex (Jankowski et al., 2013). The only distinction is that lateral nuclei do not propagate to PFC but have a strong reciprocal connection with dorsal striatum. Main inputs are incoming from tecta-pretectal pathways, superior colliculus and lateral geniculate inputs (Morin & Studholme, 2014). The lateroposterior thalamus, the rodent's pulvinar nucleus, has stronger reciprocal connections with primary and secondary visual cortical regions (Roth et al., 2016).

Retrograde tracer injection in the lateral dorsal nucleus of the rat labeled the dorsal part of the rostral pole of the TRN (Thompson & Robertson, 1987; Pinault & Deschênes, 1998). The projections from the lateral thalamus to the limbic cortical areas are organized in a loose topographical fashion (Thompson & Robertson, 1987). Interestingly, the lateral thalamus reciprocal connections with the TRN overlap with functionally related anatomically neighboring anterior thalamic nuclei. LD nucleus connection with the TRN overlaps with neighboring anterodorsal and anteroventral thalamic nuclei axons. The lateroposterior TRN connections are found caudally to the LD connections (Pinault & Deschênes, 1998).

1.4.3 Mediodorsal nucleus

The mediodorsal nucleus (MD) is a large non-homogenous structure, which contains medium-sized polygonal and fusiform cells. MD is overlapped by the midline and intralaminar thalamus. In early neuroscience years the prefrontal cortex was defined as the frontal lobe which receives projections from the mediodorsal thalamus (Rose & Woolsey, 1948). The danger is that the description of the MD inputs and the structure may vary among species. The human MD can be subdivided into seven sections (Dewulf et al., 1969). In primates, MD has three distinct subdivisions: the medial (magnocellular), the lateral (parvocellular) and extreme (paralamellar), and it is reciprocally interconnected with orbital and agranular cortexes and receives axons from piriform, cingulate, lateral and medial PFC (Ray & Price, 1993; Xiao et al., 2009). Paralemellar and magnocellular parts can be distinguished in carnivores. Rodents unlike primates or carnivores contain mostly magnocellular part and do not have connections with temporal and limbic cortical regions (Leonard, 1969). In rats the MD can be divided in three areas: medial (MDm), central (MDc) and lateral (MDl). The MDm receives axons from the basal forebrain, amygdala, hypothalamus, central gray, whereas the lateral MD receives projections from substantia nigra reticulata, superior colliculus, lateral habenula and paraventricular nucleus of the thalamus (Groenewegen, 1988; Erickson et al., 2004; Timbie & Barbas, 2015). Regarding the connectivity pattern, evidence from behavioral and electrophysiology studies suggests that the MD is important for cortical region communication during various cognitive functions, including memory processing, attention and cognitive flexibility (Lee et al., 2011; Parnaudeau et al., 2013; Browning et al., 2015).

Studies involving anterograde and retrograde tracers in primates, cats and rats revealed reciprocal connection between MD and TRN nuclei (Velayos et al., 1989; Tai et al., 1995; Gonzalo-Ruiz & Lieberman, 1995). MD projects to rostral part of the TRN, only MD inputs are located immediately ventral to the regions associated with anterior thalamic nuclei. Contrary to the limbic thalamic area, MD displays a high degree of topographical organization. Dorsolateral, intermediate and ventromedial parts of the MD associated TRN receive excitatory branches from discrete cortical

areas (cingulate, orbital and infralimbic cortexes) and have reciprocal connections with lateral, central and periventricular part of the MD, respectively (Gonzalo-Ruiz & Lieberman, 1995; Groenewegen, 1988; Cornwall et al., 1990b).

1.4.4 Midline nuclei

As mentioned previously, the midline nuclei consist of four nuclei with distinct functions: the nucleus reuniens (RE), the rhomboid nucleus (RH), the paraventricular nucleus (PaV),and the parataenial nucleus (PT). The dorsal midline nuclei (PaV, PT) are primarily involved in functions associated with emotions, when the ventral midline nuclei (RE, RH) is known for cognitive functions (Vertes et al., 2016).

The RE, the largest of the midline nuclei, is found in the anterior part of the thalamus. The nucleus is interconnected with the hippocampus (Ohtake & Yamada, 1989; Vertes et al., 2012; Varela et al., 2014). Mostly, all excitatory connections are received by the CA1 and subiculum of the hippocampus (Wouterlood et al., 1990). It is well known that the hippocampus profoundly targets the mPFC (Swanson, 1981; Hoover & Vertes, 2007) but there are no return projections from the mPFC to the hippocampus (Laroche et al., 2000). RE contains a relatively high percentage of cells with branching projections to the hippocampus and to the mPFC, therefore it might be important for memory consolidation and the synchronization of the theta rhythm during exploratory behaviors (Varela et al., 2014). RE, with a rather restricted output, receives a huge and varied array of afferents from the hippocampus, basal forebrain, hypothalamus, brainstem, cortex and amygdala (Herkenham, 1978; Sesack et al., 1989a; Risold et al., 1994; Vertes, 2002; Varela et al., 2014).

The rhomboid nucleus (RH) is a small, rhomboid shape nucleus found dorsally to nucleus reuniens. The rhomboid nucleus has very similar inputs and outputs to the RE, only the RH inputs are distributed to the wider cortex and subcortical areas, including somatosensory and temporal cortices, the nucleus accumbens, the basolateral nucleus and amygdala. (Berendse & Groenewegen, 1990; Van der Werf et al., 2002). Lesion/ inactivation studies were done usually on both nuclei due to their proximity and difficulty to separate them, and showed their critical involvement

in spatial working memory components associated with interaction of mPFC with the hippocampus (Hembrook et al., 2012; Prasad et al., 2013; Cholvin et al., 2013).

The paraventricular nucleus extends whole length of the thalamus below the third ventricle and mediodorsal nucleus. It sends axons to the wide range of the cortical and subcortical structures: mPFC, hippocampus, claustrum, lateral septum, amygdala and hypothalamus (Bubser & Deutch, 1998; Peng & Bentivoglio, 2004; Li & Kirouac, 2008; Vertes & Hoover, 2008). The major input source to PaV is from cortex and comes from mPFC and insular cortices, whereas the main subcortical afferent structures are the hypothalamus and brainstem (Krout et al., 2002; Kirouac et al., 2005; Vertes & Hoover, 2008). The parataenial nucleus (PT) is an elongated nucleus in the anterior thalamus, which borders with paraventricular nucleus. The PT is smaller than the paraventricular nucleus and propagates to similar locations. The main cortical targets are mPFC and hypothalamus, whereas major subcortical projections end up in claustrum, amygdala and nucleus accumbens (Vertes & Hoover, 2008). PT appears to receive similar inputs as the PaV (Vertes, 2004). PaV circuitry is directly involved in stress, anxiety, feeding behavior and drug seeking activities (Hsu et al., 2014). It is activated by wide range of stressors such as fear/anxiety, immobilization, and foot shock-induced stress (Bubser & Deutch, 1999) Posterior lesion of PaV blocks habituation to repeated restrain stress (Bhatnagar et al., 2002). Additionally, PaV cells are activated during reward stimuli and might act as part of appetitive functions (Bhatnagar et al., 2002). Lesion of PaV lead to suppression of drug seeking behavior (Marchant et al., 2010), and cocaine-seeking behavior strongly correlates with c-fos activation in PaV (James et al., 2011). PT functions are not well examined. TRN interconnections will be explained in the next section.

1.4.5 The intralaminar nuclei

The intralaminar nuclei are found laterally to the MD and are embedded in the internal medullary lamina. In rats, the rostral group of the intralaminar nuclei consist of central medial (CM), paracentral (PC) and central lateral (CL), whereas parafascicular (PF) and subparafascicular nuclei (SPF) are caudally located (Paxinos & Watson, 2007). Most of the intralaminar regions the target sensorimotor cortex and

the dorsal striatum, whereas CM propagates to the wider areas of the forebrain (Berendse & Groenewegen, 1991; Erro et al., 2002). The CM projections are comparable with medial and mediodorsal nuclei (Vertes et al., 2016) and a large number of afferents from the mPFC and brainstem are found in the CM nuclei (Sesack et al., 1989b; Bester et al., 1999). Although, anatomical projections of CM differ from the other intralaminar nuclei, they were never examined separately due to accessibility problems. Lesion or reversible inhibition of the rostral intralaminar group leads to a deficit in non-hippocampal-dependent working memory (Mair et al., 1998; Mair & Hembrook, 2008).

Similar, to the mediodorsal and anterior nuclei, the intralaminar and midline nuclei projections to the TRN are mostly restricted to the rostral pole (Cornwall et al., 1990c). Segregation is not complete, and axonal terminations overlap, but it is possible to conclude that the TRN projections to the intralaminar nucleus are found in the more ventrolateral part, whereas the projections to the midline nuclei are found on the dorsomedial side (Kolmac & Mitrofanis, 1997a). The reticular projections to 'non-specific' thalamic nuclei are far more diffuse than the reticular projections to the specific thalamic nuclei. The double-labelled studies show that reticular neurons in the rostral pole are able to contact more than one individual intralaminar nucleus, whereas in the caudal part of TRN this is rarely encountered. The mediodorsal and the intralaminar-midline sectors overlap (Kolmac & Mitrofanis, 1997a). According to Kolmac & Mitrofanis (1997) retrograde labeling study, an anatomical connection exists between rostral poles of ipsilateral and contralateral TRN.

As previously mentioned, midline nuclei are interconnected with hippocampus. Therefore, the rostral pole the TRN controls not only thalamic connections with cortex, but also connections with the hippocampal formation (Çavdar et al., 2008).

1.5 Sensorimotor thalamic nuclei

There is a misconception in the thalamic nuclei nomenclature, in that all thalamic nuclei do not act as purely a replay station. This concept is taken from the 19th century

telegraph relay station, which boosts signal strength that has been attenuated by the resistance of the wires. Action potentials do not attenuate with distance and the brain does not need for that 'relay nucleus' in that sense (Adrian, 1926). A more hypothetical concept of the relay was proposed in recent decades, where the signal can be switched off and on during different brain states (McCormick & Bal, 1997; Steriadeet al., 1993).

1.5.1 The ventrobasal complex

The ventrobasal complex (VB) consists of two nuclei: ventral posteromedial (VPM) and ventral posterolateral (VPL). Although, it is widely accepted as the main thalamic nociceptive nucleus, it's not the only one responsible for nociception in the thalamus (Yen & Lu, 2013). VB neurons can be dissociated onto nociceptive specific and wide dynamic range cells, propagating mostly tactile information (Yen & Lu, 2013). Both nuclei of VB complex are well known for the delivery of information encoding body position, touch, pain, temperature and itch. VPL receives sensory information from the body, whereas VPM receives information from the head and face, including taste (Lasiter, 1985). In rats and monkeys, VB receive projections from spinothalamic, corticothalamic tracts, dorsal column nuclei and medial lemniscus (Guilbaud, 1986; Li & Mizuno, 1997; Willis et al., 2001). The VB sends its afferents to somatosensory areas I, II and the caudate putamen (Herron, 1983; Erro et al., 2001). TRN interconnections will be covered in the next sections.

1.5.2 The posterior nucleus

The posterior nucleus (Po) is located caudally to the ventral posterior nucleus and rostromedially to the medial geniculate nucleus. It is a higher order nucleus, but it appears to be functionally related to the VB complex and involved in sensorimotor processing, including nociception (Park et al., 2017). The Po is an important part of sensory processing and might be linked with emotional aspects of somatosensation and Pavlovian fear conditioning (LeDoux et al., 1984; Motomura & Kosaka, 2011a). The Po is not a single structure and is subdivided at least in two parts based on distribution of afferents in cats and rodents (Heath & Jones, 1971). The medial division of the Po receives projections from the spinothalamic tract, while the lateral

division receives axons from inferior colliculus (Jones & Powell, 1971; Kudo & Niimi, 1980). In both rodents and cats, the Po sends afferents to the secondary somatosensory cortex, insular cortex, caudate putamen and amygdala (Ottersen & Ben-Ari, 1979; LeDoux et al., 1990; Motomura & Kosaka, 2011b).

Retrograde tracer injection in the VB complex and the medial division of the posterior complex of the thalamus resulted in the restricted labeling of the centroventral part of the TRN in rats, rabbits, cats and monkeys (Pollin & Rokyta, 1982; Yen & Conley, 1985; Shosaku, 1985; Harris, 1987; Crabtree, 1992; Crabtree, 1996). The medial part of the VB nuclei project to medial part (inner) TRN and vice versa, the lateral part (outer) part of the TRN projects to latter part of the VB. Although, the projections from Po and VB to the TRN overlap, Po projections lacks 'slab' like restricted topographical organization. Anterograde tracer injection in the primary sensory cortex labeled a similar area of the TRN (Crabtree, 1992; Crabtree, 1992). Face representing cells are found in the caudal parts of the somatotopic part of the TRN (S-TRN), whereas limbs representation is located on the rostral part of the TRN (Shosaku, 1985; Hoogland et al., 1987). Additionally, barrels columns representation can be found in the TRN with similar rod like shape orientation (Hoogland et al., 1987). Hartings et al. (2000) even claimed that the TRN contains neurons able to characterize whisker deflection, contradicting with the Shosaku (1985) study. The taste-related region is located in the ventromedial part of the sensory TRN (Hayama et al., 1994), whereas gustatory and visceral centers are found in the intermediate rostrocaudal levels of the TRN (Stehberg et al., 2001). The visceral TRN sector appears to overlap considerably with the gustatory TRN sector in the rostral sections of central TRN. Contrary to somatosensory TRN, the gustatory or the visceral sensory systems do not maintain a very strict topography.

1.5.3 The motor thalamus

The motor thalamus is well conserved across all vertebrates. In cats, there are four regions distinguished: ventral anterior (VA), posterior and anterior subdivisions of the ventral lateral region (VLa and VLp) and ventral medial (VM) region (Bosch-Bouju et al., 2013). In humans and other primates, the motor thalamus region is further

subdivided into numerous nuclei (Hirai & Jones, 1989). Rats are similar to cats having at least 3 nuclei, although the anatomical difference between VL and VA nuclei was discovered recently and is based on their afferents termination (Kuramoto et al., 2011). Nuclei responsible for the motor functions in the thalamus are interconnected with the cerebral cortex, deep cerebellar and basal ganglia nuclei. They also receive a substantial amount of axonal inputs from the spinal cord (Jones, 1985), superior colliculus (Bosch-Bouju et al., 2013) and pedunculopontine nucleus (Steriade et al., 1988). Previous lesion studies of the motor thalamus in mammals stress the importance of all motor thalamic nuclei in the maintenance of the posture, general movement and motor learning (Klockgether et al., 1986; Canavan et al., 1989). L, VM and VA nuclei are further special nuclei of the thalamus. There is a never-ending debate as to which thalamic family they belong; whether they are acting as a drivers or modulators. Possibly they are neither, and act as integrators of the motor information from different major motor centers of the brain (Bosch-Bouju et al., 2013).

TRN cells projecting to the ventral lateral nucleus (VL), or VM are found in the anterior, or anteroventral part of the central part of the TRN, respectively (Pinault & Deschênes, 1998). Although, in their previous work they did not manage to find connection between these group of nuclei and the TRN (Paré et al., 1987). Connection between VA and VL and the TRN was confirmed by anterograde and retrograde labeling study in the squirrel monkey (Hazrati & Parent, 1991a).

1.5.4 Medial geniculate nucleus

The medial geniculate nucleus (MGN) or the auditory thalamus propagates auditory information from inferior colliculus to the primary auditory cortex (Walker, 1937). MGN can be divided into three areas: ventral (MGV), dorsal (MGD) and medial (MGM) (Jordan, 1973). All three areas can be differentiated due to different cell types, efferent projections and functions. MGV is important for rapid transmission of auditory information, sharply tuned for frequency and projects to the primary auditory cortex (De La Mothe et al., 2006). MGD, similarly, project mainly to the primary auditory cortex, but unlike MGV, does not have tonotopic organization, can

be modulated by non-auditory stimuli and receives axons from lateral tegmentum (Bartlett, 2013). MGM is the most diverse nucleus of the MGN. It is tonotopically organized, but apart from the inferior colliculus, it receives afferent neuronal terminals from spinal cord (Ledoux et al., 1987), vestibular nucleus (Blum et al., 1979), hypothalamus (Papez, 1937; Turner et al., 1980) and superior colliculus (Henkel, 1983). In addition to that, MGM receives efferent axons from striatum (LeDoux et al., 1984). Both, MGM and MGD send inputs to amygdala (Turner et al., 1980). Additionally, to common connections such as cortex and inferior colliculus, MGN receives inputs from the cerebellum (Raffaele et al., 1969; Zimny et al., 1981) and globus pallidus (Moriizumi & Hattori, 1992; Shammah-Lagnado et al., 1996). It is important to mention that all auditory connections emphasized above are evolutionary conserved throughout the mammalian family tree (Keifer et al., 2015). Unilateral lesion of the MGN in humans abolish inputs to the ipsilateral auditory cortex (Fischer et al., 1995) , but affected patients are still able to detect sound with the contralateral ear. Bilateral lesion prevents nearly all auditory stimuli reaching auditory cortex and leads to deafness (Häusler & Levine, 2000). Although, lesion studies and early understanding perceived MGN as a simple relay nucleus, numerous studies demonstrated that the auditory thalamus manages to modify incoming inputs before relaying them to the cortex (Bartlett, 2013).

Injections of retrograde label in the MGN of the cat and rat resulted in labeled slab-like zones restricted a caudoventral sector of the TRN (Rouiller et al., 1985; Ohara & Lieberman, 1985a; Crabtree, 1998). Interestingly, inner and caudal cells of the TRN project to the pars ventral (MGV) and dorsal (MGD) nuclei, whereas outer and rostral cells mainly were interconnected to medial (MGM) nucleus. Cells projecting to different nuclei occupy overlapping territories. Furthermore, a substantial proportion of single cells in the TRN project to more than one nucleus of the MGN or even to somatosensory nuclei (Kimura et al., 2007).

1.5.5 Lateral geniculate nucleus

Lateral geniculate nucleus (LGN) or visual thalamus, is the most studied nucleus of the thalamus. It is a propagating station between retina and the visual cortex. In

monkeys, the LGN is divided in 6 layers: four dorsal parvocellular layers and two ventral magnocellular layers (Livingstone & Hubel, 1988). In addition, there are on-center and off-center neurons segregated in the laminar patterns (de Sousa et al., 2013). Each layer is monocularly driven from inputs of one hemiretina, either from the ipsilateral or contralateral eye (Ghodrati et al., 2017a). Laminar organization is poorly demarcated in small rodents (Reese, 1988), whereas it is quite distinct in monkeys and cats (Campbell, 1972). Monkeys and cat contain 3 major types of cells in the LGN: the magnocellular (M cells), the parvocellular (P cells) and the koniocellular (K cells) (So & Shapley, 1979; Casagrande, 1994). In short, the LGN has two spatiotemporal channels, the P cells are responsible for high spatial resolution and the M cells relay information with high temporal resolution. In addition, LGN got two color channels: red and green channels are conveyed by the P cells, whereas the blue and yellow are propagated by the K cells (Ghodrati et al., 2017). Interestingly, only a minority of axons in the LGN are incoming from retina (7%), the rest of inputs are incoming from different areas and act as modulators during different brain and behavioral states (Sherman, 2005).

The dorsocaudal part of the TRN projects to the lateral geniculate nucleus in rats, rabbits, cats and primates (Ohara & Lieberman, 1985a; Rodrigo-Angulo & Reinoso-Suárez, 1988; Crabtree & Killackey, 1989; Conley & Diamond, 1990). The same area of the TRN receives precise topographic projections from the primary visual cortex. The TRN visual sector is divided into non-overlapping subsectors representing distinct visual cortical and thalamic areas (Coleman & Mitrofanis, 1996) and it appears to contain an accurate retinotopic map (Montero et al., 1977). The pulvinar nucleus, a higher order visual thalamic nucleus, found in cats and monkeys, sends a small number of projections to the medial part of the caudal TRN (Rodrigo-Angulo & Reinoso-Suárez, 1988; Conley & Diamond, 1990).

1.6 Previous TRN studies

In the past, the works reviewing TRN inhibitory effects on dorsal thalamus stressed mostly two aspects: sensory and motor information propagation, without mentioning ‘cognitive’ modulatory effects of mediodorsal and anterior nuclei.

(Crabtree & Isaac, 2002). For example, Crabtree et al. (1998), explored first order and higher order nuclei relationships in the somatosensory TRN, the VB and the posterior complex (Pom). Later, Crabtree & Isaac (2002) expanded and included motor areas of the TRN and characterized relationships between the TRN cells associate with the VB complex, VL and caudal and rostral intralaminar thalamic nuclei. The TRN neurons linked with VB and Po interact with caudal intralaminar nuclei and both are engaged with sensory information propagations, whereas cells engaged in the motor information interact with motor thalamic nucleus (VL) and the rostral part of the intralaminar nuclei, a mixed-circuit sensory-related nuclear complex. A first attempt to compare 'cognitive' (limbic) and sensory TRN functions was accomplished by Halassa et al. (2014). His lab recorded from the TRN neurons associated with visual thalamus (LGN, sensory part of the thalamus) and the TRN neurons associated with anterior nucleus of the thalamus (ATN, limbic part of the thalamus) in freely moving mice during different states and found that both behave differently during wake and sleep. Although, Halassa is responsible for establishing the idea that TRN is non-homogenous structure and contains 'cognitive' (limbic) and sensory part, he never tried to locate and map these on the TRN. The map below is the first recorded attempt to draw the TRN interconnection with lower and higher order thalamic nuclei involved in the cognitive processes such as memory and learning (See figure 1.3).

It is important to note that the TRN is a 3D structure and a given map does not try to address the medial-lateral dimension. Crabtree (1999) in his review points out that the higher order thalamic nuclei linked with motor/sensory information propagation are located mostly medially in the thalamus, thus, they send their axons to the inner parts of the TRN. However, this is not the case with higher order thalamic nuclei propagating to the rostral pole of the TRN, as they sent their axons to both inner and outer parts of the rostral TRN (Gonzalo-Ruiz & Lieberman, 1995; Kolmac & Mitrofanis, 1997b; Pinault et al., 1997).

1.7 Pattern of the axonal connection to the thalamus

TRN topographical organization reflects the anatomy of the cortical and thalamic regions. Specific cortical or thalamic areas are represented in the adjacent TRN part,

'slabs', located perpendicularly to the thalamus (Crabtree, 1999; Pinault, 2004a). Though, this rule does not apply to all TRN neurons. Firstly, it is well recorded that these areas (slabs) do overlap and are mostly missing in the rostral TRN (Guillery et al., 1998; Pinault, 2003). Secondly, the functionally related cortical areas can send projections to the same TRN sector and a reticular sector can be linked with several functionally related dorsal thalamic nuclei (Pinault & Deschênes, 1998a). Due to these interconnection patterns of the TNR with thalamus, the thalamo-reticular projections form open loop and closed loop connections. Open loop connections, putatively, are important for lateral inhibition, required for modality specific attention/arousal (Pinault, 2004), where TRN plays a pivotal role (McAlonan, 2006; Halassa et al., 2014). Closed loop connections might act as a feedback loop, which could be involved in sleep spindles generation during non-rapid eye movement (NREM) sleep (Crabtree, 1999; Kim & Connors, 2012).

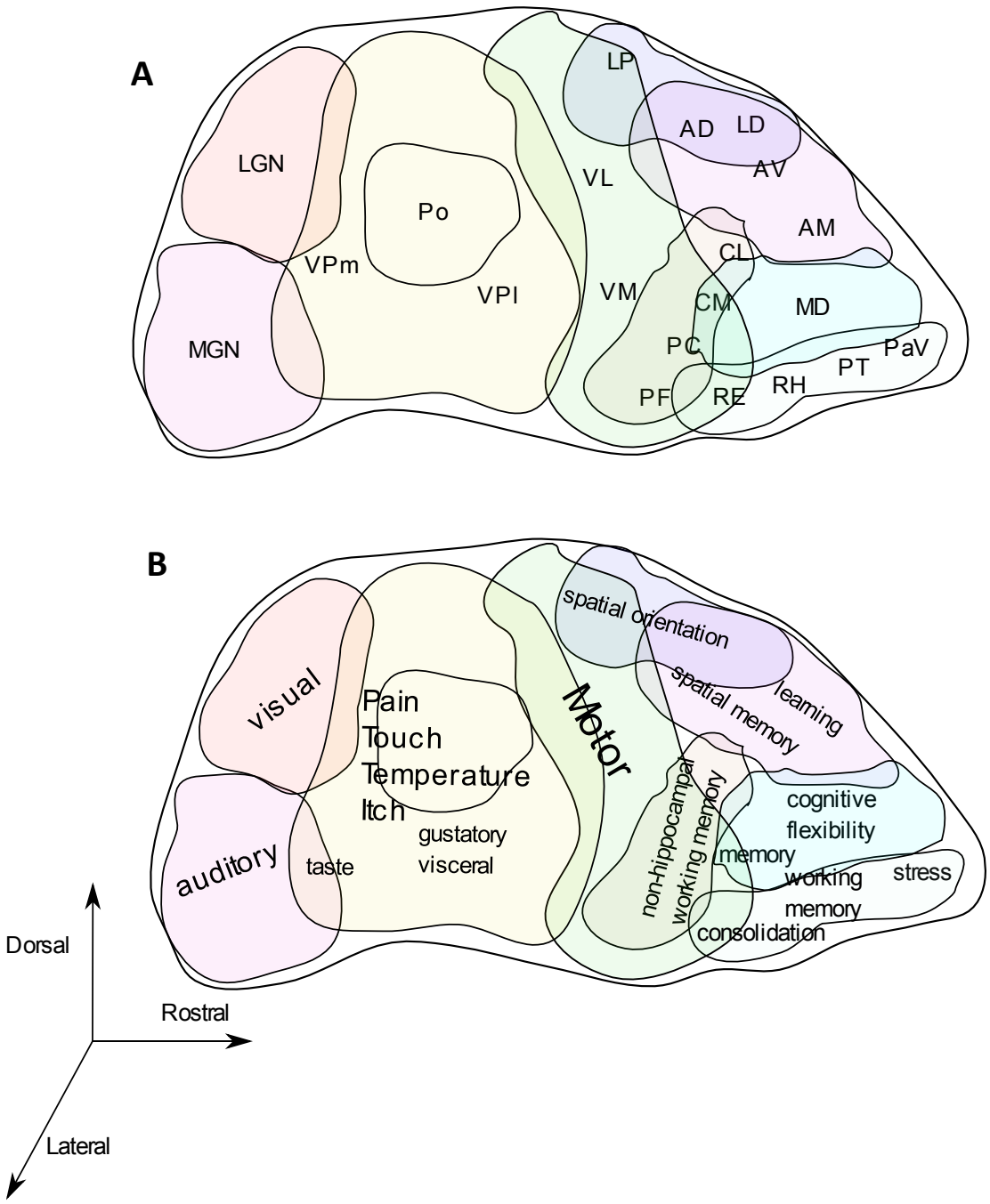

Figure 1.3 Schematic representation of the TRN (sagittal plane) interconnection with all thalamic nuclei. **A** The topographic map of the thalamic reticular connections with thalamic nuclei based on the previous anterograde/retrograde work mentioned above. Most of the higher order thalamic nuclei are interconnected with the rostral TRN, whereas all caudal TRN cells communicate typically with relay/first order thalamic nuclei. **B** The topographical map displays the functions of the thalamic nuclei connected to the specific areas of the TRN. Generally, 3 important functions of the higher brain are represented and spatially divided on the TRN: sensory, motor, cognitive. VA – ventral anterior, VL – ventral lateral, VP – ventral posterior, LP – lateral posterior, LD – lateral dorsal, AD – anterodorsal, CL – central lateral, CM – central medial, PF – parafascicular, LGN – lateral geniculate nucleus, MGN – medial geniculate nucleus, PV – paraventricular, PT – parataenial, RE- reuniens, RH – rhomboid, MD - medial mediodorsal.

1.8 Proposed evolution of the TRN

Consequently, all thalamic nuclei interconnections with the TRN associated with higher order functions such as memory, learning and executive functions, are localized in the rostral part of the TRN (See Figure 1.3). We can go bold and try to dissociate all brain functions into 4 segments, which can be mapped on the TRN in rostro-caudal manner (See Figure 1.4). Additionally, the TRN can be perceived as a small brain model with representation of all forebrain functions. That notion is not extra ordinary, if we keep in mind that, all three brain areas (the TRN, thalamus and cortex) are interconnected, topographically mapped and function as a finely orchestrated circuitry. Furthermore, the crude mapping of brain functions was done on the cortex plenty of times in the history of the neuroscience (Brodmann, 1909; Zilles & Amunts, 2010). Brodmann's approach of structural-functional relationship is quite helpful for better understanding of specific brain areas, even if it does not address a picture of the real neuronal network, which is composed of more heterogeneous structures.

The first segment of the TRN, located in the rostral part, contains neurons responsible for cognitive function modulation. The motor segment located adjacent to the cognitive part, deals with motor cortex associated information. Caudally located sensory parts of the TRN can be dissociated into another two parts. Rostrally located sensory TRN is responsible for propagation of pain, touch, temperature, itch and taste sensations, which had been developed during early brain evolution and did not evolve significantly after. Higher order sensation, visual and auditory, are found in the most caudal part of the TRN. All higher mammals contain abundant numbers of neurons in the caudal part of the cortex assisting demands of sophisticated vision and audition, therefore they require to have a larger thalamus and the TRN with extended caudal part. Although, this evolutional hypothesis of TRN is risky, there may be a rational basis, as the evolutional cortical growth is not possible without two cortical modulatory parts: thalamus and the TRN.

If we pay attention to studies of the established evolutionary scientist, Ann B. Butler, we will find a similar idea of TRN development enriched with facts from various

animal species (Butler, 2008a; Butler, 2008b). Butler terms the TRN as a crucial component of the thalamocortical circuitry/brain evolution.

The TRN appears to be a very old structure, which remained relatively unaltered during brain development. GABAergic neurons are found within the dorsal thalamic territory of lampreys (Butler, 2008b), zebra fish (Luo & Perkel, 1999) and amphibians (Hollis & Boyd, 2005) and might act as an early homolog of the mammalian thalamic reticular nucleus (Hollis & Boyd, 2005). In turtles, it is called the anterior entopeduncular nucleus and has circuitry similar to the mammalian TRN (Fowler et al., 1999; Kenigfest et al., 2005). A comparable GABAergic structure reciprocally interconnected with thalamus is found in crocodiles (Pritz, 1995) and birds (Pritz, 1995). Thereby, the variously composed TRN is found in sauropsids (birds and reptiles) and mammals. It is important to note, that evolutionary history of mammals is entirely separate from sauropsids and the mammalian line appeared 10 million years before the extinction of sauropsids. Therefore, Butler hypothesized that the TRN resembling structure was even found in in the earliest amniotes. In other words, the TRN, was developed in the brains of the common ancestors of mammals and birds at least 340 million year ago.

Additionally, Butler argues that the TRN is an important part of the brain responsible for higher order cognition and consciousness. According to Roth (2015), the number of cognitive functions found in birds and mammals, such as language perception (Fitch, 2011; Kaufman et al., 2013), working memory (Lee et al., 2015; Ditz & Nieder, 2016), and ability to rank something by making comparison (von Fersen et al., 1990; Wass et al., 2012) requires at least some level of consciousness. After evolutionary analysis of the birds and mammals' brain, Butler concluded that the neural substrate of higher-level cognition depends on a few brain anatomical features. Firstly, the brain-body ratio of both species is relatively high. Secondly, mammals and birds have an elaborated cortex, which contains large, glutamatergic neurons, extensive dendritic trees, extensive local and reciprocal interconnections, and GABAergic inputs from local interneurons.

And lastly, the cortex should receive sensory and other inputs from the dorsal thalamus, which should be regulated by the thalamic reticular nucleus.

We can conclude, that the TRN is an indispensable part of the brain's evolution and its functions were underestimated untill recently. The hypothesis of TRN functional segregation into four parts (cognitive, motor, lower sensory and higher sensory) over evolution requires more comprehensive analysis and studies.

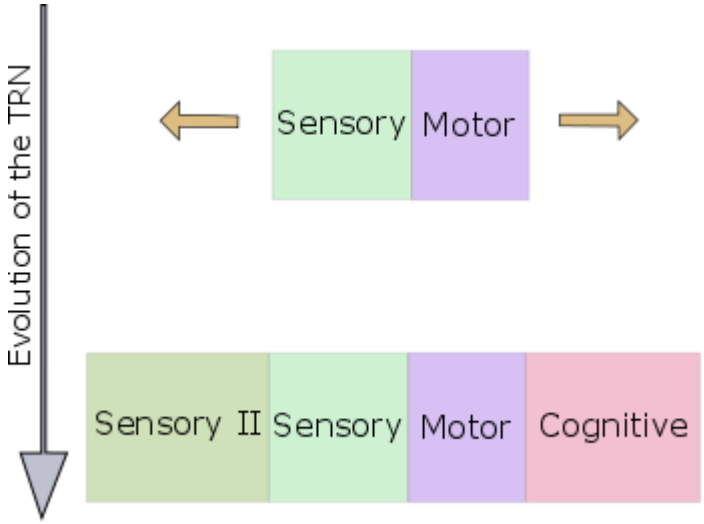

Figure 1.4 Schematic representation proposed evolution of the TRN over 300-million-years. As pallium (cortex), thalamus and sensory organs had advanced during evolution, they required to have a brain area responsible for the sensory information modulation. Probably, in the early years the TRN like structures were responsible for modulation of sensory and motor information only. As brain structure evolve, the sensory cortices grown to facilitate the consumption of the visual and auditory sensory information and the frontal cortex enlarged to facilitate more sophisticated behavior, required for survival. So, the TRN was following evolution of the cortex and thalamus, spread to rostral and caudal direction, in order to cope with demand of brain's increasing calculations.

1.9 The TRN connections with other subcortical areas

The TRN is an indispensable part of the corticothalamic loop and all major axonal projections to the TRN are incoming from the thalamus and cortex. These interconnections are known and well described. Connections of the TRN with other subcortical structures such as brainstem, basal forebrain and hypothalamus did not

get such good attention, but are vital in brain state modulations, especially, in the sleep/wake cycle.

1.9.1 Globus pallidus

The globus pallidus (GP) contains only GABAergic neurons (Jaeger & Kita, 2011), involved in the unconscious regulation of voluntary movements and their dysfunction causes movement disorders, such as in Parkinson's disease (Mallet et al., 2012). Interestingly, lesion of the GP leads to dramatic increase of wakefulness, probably through cortical disinhibition (Qiu et al., 2010)

The GP sends axons to the rostral/central part of the TRN in rodents (Asanuma & Porter, 1990; Cornwall et al., 1990d; Gandia et al., 1993), cats (Kayahara & Nakano, 1998) and primates (Hazrati & Parent, 1991b). The electrical or chemical activation of the GP cells decreases the mean firing rate in the TRN neurons (Pazo et al., 2013), whereas the inhibition of the GP neurons increases the firing rate in anesthetized rats. Both activation and inhibition of the GP does not modify the burst firing of the TRN neurons (Villalobos et al., 2016).

1.9.2 Brainstem

The brainstem is a posterior part of the brain, which contains multiple nuclei with various functions. Apart of motor and sensory roles, it is important for unconscious regulation of cardiac (Blevins & Baskin, 2009), respiratory (Smith et al., 2013), sleeping (Moruzzi & Magoun, 1949) and eating (Blevins & Baskin, 2009) behaviors. The TRN receives three times less projections from the brainstem than the thalamus (Paré et al., 1988) and these connections are derived mostly from the nuclei responsible for arousal: the noradrenergic locus coeruleus (LC) (Asanuma, 1992), the serotonergic (5-HT) raphe nuclei (Yoshida et al., 1984), dopaminergic ventral tegmental area (VTA) (Kolmac & Mitrofanis, 1998), GABAergic and the dopaminergic substantia nigra (SN) (Paré et al., 1990; Gandia et al., 1993; Kolmac & Mitrofanis, 1998; Anaya-Martinez et al., 2006), the cholinergic laterodorsal and pedunculopontine tegmentum (LDT/PPT) (Hallanger et al., 1987a; Cornwall et al., 1990a; Kolmac & Mitrofanis, 1998), the cholinergic parabrachial nucleus (Sofroniew

et al., 1985) and the periaqueductal gray matter (Rinvik & Wiberg, 1990; Kolmac & Mitrofanis, 1998; Mena-Segovia, 2016).

A nucleus of the brainstem with elevated activity during sleep, the nucleus tractus solitarius, also projects to the TRN, and during activation stimulates neuronal firing in the TRN (Nanobashvili et al., 2009). In contrast, stimulation of the brainstem nuclei associated with arousal, inhibits the activity of the TRN neurons. For example, brief rhythmic stimulation of the LC depresses the neuronal firing of the TRN (Nanobashvili & Narikashvili, 1985; Nanobashvili & Narikashvili, 1986). A similar diminishing effect on TRN activity is produced by stimulation of the dorsal raphe nucleus (Yoshida et al., 1984; Rodríguez et al., 2011) and the substantia nigra pars reticulata (Paré et al., 1990). Data dedicated to the cholinergic PPT and parabrachial nucleus stimulation effect on the TRN is missing, even so the application of acetylcholine to the TRN has a biphasic nature, due to the presence of nicotinic and muscarinic receptors (McCormick & Prince, 1986; Sun et al., 2013a). The hyperpolarisation caused by acetylcholine produces a firing pattern change in the TNR (Lee & McCormick, 1995), which does not lead to arousal. Ni et al. (2016) showed that selective stimulation of the cholinergic inputs activated GABAergic neurons by acting on nicotinic acetylcholine receptors, generated sleep spindles and promoted NREM sleep. However, Ni et al. explored non-physiological stimulation patterns and did not dissociate between basal forebrain and brainstem cholinergic inputs, therefore the cholinergic effect from the brainstem on the TRN is not clear yet.

Remarkably, the axonal terminals from the brainstem end up in distinct areas of the TRN. For example, the pedunculopontine nucleus (PPT) projects mainly to the ventral parts of the TRN, whereas the substantia nigra projects to the rostral and the rostrolateral pole of the TRN (Paré et al., 1990; Kolmac & Mitrofanis, 1998).

1.9.3 Basal forebrain

The basal forebrain (BF) is one of the cholinergic centres in the brain. The nuclei of the BF can be broadly divided into two major divisions: anterior and posterior. The anterior division of the BF projects to the hypothalamus and includes the substantia

inominata (SI), the horizontal diagonal band of Broca (HDB), the magnocellular preoptic area (MCPO) and the nucleus of basalis of Meyert (NBM) (Mesulam et al., 1983). The nucleus of the posterior BF, the ventral pallidum projects to the cortex (Zaborszky et al., 2015). Additionally, the BF contains non-cholinergic cells, GABAergic and glutamatergic neurons, which are involved in arousal and cortical activation (Zant et al., 2016). Activation of the GABAergic neurons of the BF sustains wakefulness and high-frequency rhythms, whereas chemogenetic inhibition increases sleep (Anaclet et al., 2015). The BF cholinergic neurons do not act as wake-promoting cells, but facilitate awake EEG by inhibiting slow oscillation (Anaclet et al., 2015). Cholinergic circuits of the BF contribute to sensory processing and experience-dependent cortical functioning, whereas loss of these neurons leads to cognitive decline, which is associated with Alzheimer disease (Shinotoh et al., 2000; Froemke et al., 2007; Pinto et al., 2013).

TRN neurons receive projections from the nucleus basalis of Meynert (Hallanger et al., 1987b; Asanuma, 1989; Spreafico et al., 1993), the vertical and horizontal limbs of the diagonal band, substantia innominata (Steriade et al., 1987; Parent et al., 1988; Cornwall et al., 1990c) and ventral pallidum (Parent et al., 1988; Cornwall et al., 1990c).

The basal forebrain synapses are found mainly in the rostral part of the TRN and in the thalamic nuclei associated with 'cognitive' TRN (Hallanger et al., 1987b; Cornwall et al., 1990c). Most of these neurons are GABAergic, parvalbumin containing neurons (50%) (Asanuma, 1989; Asanuma & Porter, 1990; Bickford et al., 1994) and only a minor part is cholinergic (20%) (Cornwall et al., 1990e; Jones, 1991). A significant portion (10-15%) of the neurons connecting the BF with the TRN is interconnected with cortex (Cornwall et al., 1990e).

To the best of my knowledge, there was no study investigating the effect of the BF on TRN neuronal firing. We can assume, that due to the GABAergic nature of the BF axons, their firing should lead to the inhibition of the neuronal firing of the TRN and consequently, promote the arousal and wakefulness.

1.9.4 Hypothalamus

The hypothalamus is a relatively small part of the brain responsible for whole-body homeostasis. The processes involved in energy regulation, such as sleep (Alam et al., 2014), feeding (Ikeda et al., 2015), drinking (Anacker et al., 2014) body temperature and activity (Anacker et al., 2014) are regulated by neuronal firing of the hypothalamus.

A bidirectional anatomical connection between the TRN and the hypothalamus implies that both areas can influence and regulate each other. Chemical or electrical stimulation of the TRN antagonizes the activity of the hypothalamic neurons (Barone et al., 1994). Electrically stimulated hypothalamic cells also have an effect on the TRN and induce: inhibition (66%), bidirectional response (6%) and excitation (7%) (Barone et al., 1994). For a long time it was accepted that only the TRN has direct projections to the hypothalamus, while the hypothalamus propagates to the TRN through the zona incerta (Barone et al., 1994). Later, Herrera et al. (2015), by exploiting various modern techniques in mice, proved that the TRN cells receive monosynaptic inputs from hypothalamic GABAergic cells, which are capable to induce negative current in the most cells (80%) of the TRN neurons.

Optogenetic activation of the GABAergic axons from the lateral hypothalamus (LH) in the TRN during NREM induced rapid awakening (several seconds) (Herrera et al., 2015a). Interestingly, the axonal stimulation in the rostral TRN introduced significantly faster brain state change, than in the caudal TRN stimulation. Herrera et al. (2015) assumed that this outcome was due to technical issue. Another possibility is that the heterogenous nature of the TRN was involved. According to provided tracing photos, the LH preferred to reach typically ventral and rostral parts of the TRN. Interestingly, bilateral optogenetic silencing of the LH-TRN pathways in the anterior part of the TRN significantly prolonged the duration of NREM episodes and induced the significant increase of delta oscillation, without sleep spindle effect. This raises the possibility that hypothalamus through acting on the anterior part of the TRN induce arousal.

1.9.5 Zona incerta

The Zona incerta was first described a century ago by Auguste Forel as a "region of which nothing certain can be said" (Mitrofanis, 2005). The ZI accommodates a small area, but at the same time forms the cytoarchitectonically and neurochemically most diverse neuronal nucleus in the thalamus (Kolmac & Mitrofanis, 1999), which propagates to almost every centre of the neuroaxis, from cerebral cortex to spinal cord (Romanowski et al., 1985; Power et al., 2001). These features allow the ZI to be involved in diverse functions: control of visceral activity (Tonelli & Chiaraviglio, 1993), arousal (Vidal et al., 2005; Power et al., 1999), sleep (Liu et al., 2017), attention shift (Shaw & Mitrofanis, 2002) and locomotion (Périer et al., 2002). Recently, Liu et al. (2017) identified a subpopulation of GABA neurons in the ventral zone incerta that promotes sleep. Interestingly, the ZI prefer to send their axons mostly to the non-sensory thalamic nuclei (Barthó et al., 2002).

The ZI propagates to the TRN in topographical manner and can be divided into four distinct sectors: rostral, dorsal, ventral and caudal (Cavdar et al., 2006). The rostral part of the TRN receives many axons from rostral and ventral sectors of the ZI. The intermediate part of the TRN receives inputs from dorsal and ventral segments of the ZI and the caudal part of the TRN receive slight number of the axons from the caudal ZI (Cavdar et al., 2006). The ZI-TRN interconnection led Cavdar et al. (2006) to propose that the ZI plays an important role in limbic and motor functions. Considering all extrathalamic-TRN interconnections and recently discovered functions of the ZI, we can also suggest that the ZI could be another brain state regulator of the TRN functions.

1.9.6 Summary of the afferent connections

Additionally, to the thalamic connections, extra-thalamic connections with the TRN highlight the heterogenous nature of the nucleus. There are afferent axons from various brain areas to the distinct parts of the TRN. For example, the afferents from the globus pallidus, substantia nigra, basal forebrain and zone incerta send axons mostly to the rostral part of the TRN.

1.10 Cellular Morphology

1.10.1 Neurons

The TRN neurons are found in sectors, which can be subdivided into three tiers (internal, intermediate, and external), with cell bodies lying parallel to the external medullary (Yen & Conley, 1985). The reticular tiers projecting to first-order nuclei display a well-defined topography, whereas those projecting to higher-order nuclei don't (Crabtree, 1996).

In the early studies, it was accepted that the neurons of the TRN resemble the brain stem reticular formation neurons in that they are multipolar, vary in size, shape (ellipsoidal, fusiform or triangular) and are wired by a complex matrix of presynaptic neuropil. The largest neurons, often 30 to 40 µm diameter, are found in the dorsal anterior section, and the smallest, about 20 to 25 µm diameter, lying along the lateral ventral sheets of the nucleus. (Scheibel & Scheibel, 1972). Spreafico et al., even identified three morphological types of the TRN cells in the adult rat found in different parts of the TRN (Spreafico et al., 1988; Spreafico et al., 1991). However, these investigations concluded that all cells in the TRN are similar in morphology and orientation, and Spreafico et al., results might be due to fact that neurons and the dendritic trees were viewed from the different angles (Lübke, 1993; Ohara & Havton, 1996).

1.10.2 Dendrites

Similarly to the cell bodies, the TRN dendrites resemble those of more caudal (brainstem) reticular areas (Scheibel & Scheibel, 1971). The neurons possess no more than four or five primary dendrites, which branch once or twice (Yen & Conley, 1985) and extend for relatively long distances, forming disc-shaped fields (Crabtree, 1999). They are perpendicularly oriented to thalamocortical, corticothalamic nuclei and characterized by unusually long filamentous spines, often 10 µm length, and with peculiar terminations, which resemble umbrellas or pom-poms (Lübke, 1993). Dendrites of the anterior dorsal sector of TRN leave the cell body at all angles and

show little or no dominant orientation of dendritic mass (Scheibel & Scheibel, 1965; Ohara & Lieberman, 1985b). Pinault (2004a) subcategorized the dendrites into three types in terms of their architecture: dendrites with dorsoventral ramification, dendrites with rostrocaudal ramification, and the dendritic ramification in all directions. The first two types of dendrites are observed in all regions of the TRN, whereas the third type is found only in the rostral and ventral parts of the TRN. The architectural types of the dendrites, apparently, are formed by the adaptation to the available space, which is largest in the rostral pole of the TRN (Pinault & Deschênes, 1998b).

1.10.3 Axons

The TRN axonal spreading inside the nucleus was a controversial topic for over few decades. Ahlsén & Lindström (1982) found an intrinsic chemical connection between the TRN neurons, which later was perceived as the facilitators for selective attention (Crick, 1984; Ahrens et al., 2015) and synchronous oscillations (Huguenard & McCormick, 2007). After, Cox et al. (1996) found up to 65% of the cells containing axons with intra-TRN collaterals. Pinault et al. (1997) in his early studies did not find any intra-TRN collaterals, although later he stated, that about 10% of all the TRN axons run exclusively in the TRN (Pinault, 2004). According to the latest study, which employed optogenetic and pharmacological approaches, the TRN of the mouse lacks intrinsic GABAergic connections, except during the first two weeks after birth (Hou et al., 2016). Alternatively, a few electron microscopy studies portrayed dendrites of the TRN neurons forming symmetrical synapses in rats and cats (Deschênes et al., 1985; Pinault et al., 1997; Csillik et al., 2005) and the function of these connections is mysterious.

Regarding thalamic connections, the axons of laterally lying TRN neurons tend to innervate more laterally located thalamic nuclei and vice versa (Pinault, 2004). Reticular axons show en passant feature and can innervate, perhaps, up to a thousand thalamic target neurons (Scheibel & Scheibel, 1965). Pinault and Deschenes (1998) specified that the single axonal arbor of the TRN neuron contains on average 4000 boutons, which tend to form grapelike clusters or strings and can contact at

least 630 thalamic neurons. The axons penetrate perpendicularly to the thalamus-TRN interface and their terminals are found onto perikaryon, main dendritic trunks and dendrites of medium and small size (Montero & Scott, 1981). Two types of the axonal projection exist: parallel towards a single thalamic nucleus and the divergent axonal projection connecting at least two separate nuclei (Pinault, 2004). Interestingly, the axonal arborization pattern of the TRN neurons can influence the level of the postsynaptic current (Cox, Huguenard & Prince, 1997). The existence of the contralateral projection from the TRN is still doubtful (Paré & Steriade, 1993; Hazrati et al., 1995; Pinault, 2004).

1.11 Neurochemical diversity

1.11.1 Calcium binding proteins

Over 250 varieties of the calcium binding proteins (CBP) have been described (Celio et al., 1996). These proteins, by binding to calcium, protect cells from excitotoxicity (Lukas & Jones, 1994) and modulate the dynamic cytosolic Ca^{2+} (Chard et al., 1993), which fluctuation is crucial for neurotransmission and intracellular operations (Katz & Miledi, 1969). A malfunctioning of the CBP influences neuronal excitability (Albéri et al., 2013), which consequently might lead to diseases like schizophrenia (Eyles et al., 2002; Steullet et al., 2017) and epilepsy (Köhr et al., 1991; Schwaller et al., 2004). Additionally, the binding proteins such as parvalbumin, calbindin and calretinin can act as an exceptional tool for differentiation between distinct chemoarchitectonic and functional domains within such a complex organization as the thalamus.

Parvalbumin (PV) is expressed in the majority of GABAergic cells in the cortex (Celio, 1986) and, along with contributions from glutamate receptor (Geiger et al., 1995) and potassium channel expression (Du et al., 1996), results in neurons with fast spiking rates (> 50 Hz) (Kawaguchi et al., 1987), which underlie the cortical gamma rhythm (Cardin et al., 2009). Parvalbumin is found throughout the TRN of reptiles (Pritz, 1995), rats (Celio, 1990; Arai et al., 1994), mice (Hou et al., 2016; Clemente-perez et al., 2017), monkey (FitzGibbon et al., 2000) and human (Steullet et al., 2017). There is discussion going on about the proportion of the PV expressing neurons in the TRN.

Even in recent studies, employing genetically modified animals and parvalbumin specific viruses, significantly different results were reported. Hou et al. (2016) claimed that the PV is expressed in almost all TRN cells (up to 98%), whereas in the study Clemente-Perez et al. (2017) the proportion of the PV neurons in the TRN of mouse was smaller than 80%. According to the majority of previous results in the various mammalian species, the parvalbumin is abundantly expressed, but not in all TRN neurons (Arai et al., 1994; FitzGibbon et al., 2000; Steullet et al., 2017). Even the TRN of reptiles has a number of neurons without parvalbumin expression (Pritz & Stritzel, 1993), therefore the putative discrepancies of the CBP expression between mammalian species are less likely to occur. Abundant parvalbumin expression in the TRN and no expression in other thalamic nuclei, makes the PV a great biomarker for the TRN function investigation (Arai et al., 1994).

Parvalbumin expression can be detected in the TRN at day P0 and it does not change at least till the day P90 in rats (Majak et al., 1998) and rabbits (Contreras-Rodríguez et al., 2002), therefore a decrease of the PV expression/expressing neurons is only associated with senescence (Schmalbach et al., 2015), disease (Steullet et al., 2017) or brain trauma (Schmalbach et al., 2015). However, the whole TRN is a vulnerable structure, and selective neuronal damage in the nucleus is common during cerebral ischemia (Ross & Graham, 1993; Kawai et al., 1995; Schwab et al., 1997). Neonatal stress also can interfere with TRN development and promote the reduction of cell bodies in pups (Salas et al., 1986).

The parvalbumin expressing neurons generate and modulate all the oscillations related to the TRN functions (slow and alpha oscillation) (Perez et al., 2017).

Calretinin and calbindin cells do not have such a rich distribution as parvalbumin neurons in the TRN. Calretinin is moderately expressed in the lateral and ventral part of the rostral TRN in rats, cats and humans (Arai et al., 1994; Fortin et al., 1996; Lizier et al., 1997; Fortin et al., 1998), although, the calretinin distribution in the TRN relatively to other brain areas is quite rich (Résibois & Rogers, 1992; Rogers & Resibois, 1992). A small number of cells expressing calbindin is located in the ventral

part of the middle and caudal parts of the TRN in rats and rabbits (Arai et al., 1994; Contreras-Rodríguez et al., 2003). Both CBP can be expressed individually or can be coexpressed with parvalbumin (Ulfig et al., 1998; Mitrofanis, 1992a). Usually, the neurons with calretinin and parvalbumin overlapping reside in the middle and caudal parts of the TRN. From an evolutionary point of view, calretinin and calbindin appeared in the TRN relatively late in evolution, as both CBP are not found in the nucleus of the reptiles (Pritz & Stritzel, 1991).

The functional roles of the neurons expressing these proteins were not investigated. Interestingly, the calretinin containing neurons found only in the rostral TRN are only interconnected with higher order thalamic nuclei like anterodorsal, midline, mediodorsal and intralaminar (Lizier et al., 1997).

1.11.2 GABA

The TRN contains two types of GABAergic receptors: the ligand-gated chloride channel, $GABA_A$, and the $GABA_B$ receptor, which affects calcium and potassium conductances through GTP binding proteins (Ambardekar et al., 1999). GABA receptor activation in the TRN has two basic responses: a fast increase in membrane Cl^- conductance mediated by $GABA_A$ receptors and a slow increase in K^+ conductance mediated by $GABA_B$ receptors (Crunelli et al., 1988). The malfunction of both receptors might lead to the 3-Hz spike wave discharge associated with absence epilepsy (Wan et al., 2003; Avoli, 2012; Zhou et al., 2015) and be one of the causes of schizophrenia (Ferrarelli & Tononi, 2011), whereas the normal Inhibitory postsynaptic potential of the TRN promotes powerful intranuclear inhibition and prevents epileptiform thalamocortical hypersynchrony (Huntsman et al., 1999; Huntsman & Huguenard, 2000).

There is numerous subunit isoform for the $GABA_A$ receptors, which determine the properties of the receptors. In human $GABA_A$ receptors might include 16 subunits (six α, three β, three γ, one π, one δ, one, one ε and one θ subunits) (Nutt, 2006). There are also 3 ρ subunits, which contribute to so called GABAC receptor (Barnard et al., 1998). $GABA_A$ receptor contains variation of five subunits and the minimal

requirement is the inclusion of both α and β subunits, which can combine with most other subunits. Important to mention that, γ subunits cannot be present with δ in the same receptors (Sieghart & Sperk, 2002). The most common type of $GABA_A$ in the brain involves a combination of two α , two β, and γ (α1β2γ2) (Connolly et al., 1996). Interestingly, that the individual subunits exhibit a distinct subcellular distribution. For instance, the most common combination (α1β2γ2) of subunits is concentrated in GABAergic synapses and in the extra synaptic membrane (Olsen & Sieghart, 2009a). In contrast, receptors containing variation of δ, α6 and β subunits are abundantly present in the extrasynaptic dendritic and somatic membranes (Nusser et al., 1998). Receptors containing these subunits (δ, α6 and β) exhibit relatively small channel conductance, a much longer open state time, and do not desensitize on the prolonged presence of GABA (Olsen & Sieghart, 2009). Tonic inhibition is three time larger than phasic inhibition and is mainly mediated by extrasynaptic receptors (α6β2/3, δ), whereas phasic inhibition is characteristic to the receptors found in synapse: (α1β2/3γ2), (α1β2/3γ2) and (α6β2/3γ2) (Nusser et al., 1998).

Inhibitory postsynaptic potentials of $GABA_A$ receptors in TRN neurons are more prolonged than in thalamocortical cells, due to expression of different subunits. The $GABA_A$ receptors of the TRN expresses α3/ β3 subunits, whereas the sensory relay nuclei have α1/β2 subunits (Fritschy & Mohler, 1995; Huntsman et al., 1996). The TRN is prominently stained for subunits α3, β3 and γ2, whereas thalamic nuclei are rich in α1, α4, β2 and, γ subunits (Sieghart & Sperk, 2002). $GABA_A$ receptors are antagonized by the convulsant bicuculline and modulated by benzodiazepines and barbiturates (Ulrich et al., 2007). Benzodiazepines increase inhibitory synaptic strength of the $GABA_A$ receptors in the TRN by binding to the α3/γ2 subunit junction (Christian & Huguenard, 2013). Interestingly, mice lacking α3 subunits had unaltered EEG during sleep and wake, but had significantly lower EEG power in 10-15 Hz frequency during transition from NREM to REM sleep and a slightly larger power in the 11-13-Hz band during transition from sleep to wake (Winsky-Sommerer et al., 2008).The $GABA_B$ receptor generates long lasting inhibitory postsynaptic potentials and has longer activation kinetics due to the different signaling pathways (Pinard et

al., 2010a). Activated $GABA_B$ receptors hyperpolarize neurons by decreasing Ca^{2+} and increasing K^+ membrane efflux, through direct coupling to GirRK channels (Fernández-Alacid et al., 2009). Two subunits of $GABA_B1\alpha$ and $GABA_B1\beta$ are expressed on the axons of the TRN neurons and efficiently inhibit the release of GABA to the thalamocortical cells (Ambardekar et al., 1999; Ulrich et al., 2007), as $GABA_B$ receptors are expressed on the presynaptic terminals and act as autoreceptors (Pinard et al., 2010). Postsynaptic $GABA_B$ receptors, mainly found on glutamate release sites are well known for the facilitation of the LTP in the different brain areas (Otmakhova & Lisman, 2004). Presynaptic $GABA_B$ receptors are located at a certain distance from release sites, extrasynaptic location, whereas postsynaptic $GABA_B$ receptors are present on dendritic shafts and on the extrasynaptic membrane of spines (Guetg et al., 2009). Activation of the $GABA_B$ receptors desynchronizes thalamocortical network (Cain et al., 2017), whereas their block promotes epileptogenesis (Sohal & Huguenard, 2003). The $GABA_B$ receptors are insensitive to bicuculline and are selectively activated by the agonist baclofen (Pinard et al., 2010).

The TRN receives GABAergic afferents from the basal forebrain (Asanuma, 1989; Asanuma & Porter, 1990; Bickford et al., 1994), globus pallidus (Asanuma & Porter, 1990; Cornwall et al., 1990d; Gandia et al., 1993), substantia nigra (Paré et al., 1990; Gandia et al., 1993; Kolmac & Mitrofanis, 1998), hypothalamus (Herrera et al., 2015a) and zona incerta (Cavdar et al., 2006).

1.11.3 Glutamate

Ionotropic glutamate receptors (AMPA, kainate, NMDA and δ receptors) share a similar architecture and composed of four large subunits that form a central ion channel pore. Glutamate receptors can be grouped into four distinct classes based on structural homology, AMPA receptors (GluA1-GluA4), the kainite receptors (GluK1-GluK5), the kainite receptors (GluK1-GluK5), the NMDA receptors (GluN1, GluN2A – GluN2D, Glu3A, and GluN3B), and the δ receptors (GluD1 and GluD2) (Traynelis et al., 2010). AMPA receptors by opening pass Na+ and sometimes Ca2+ pass through the channel into the cell, leading to an EPSP and NMDA stimulate the passage of the similar ions only during depolarized states (Sherman, 2014).

Metabotropic glutamate receptors (mGluR) consist of single polypeptide and evoke pre and postsynaptic effect through a cascade of biochemical reactions. Postsynaptic potentials (mGlu1 & mGlu5) produced in this way have a much longer time course than seen with ionotropic receptors, with a latency of 10 ms or more and duration of the hundred of milliseconds to several seconds or more (Govindaiah & Cox, 2004). There are eight different types of mGluRs in the brain. Activation of group I (types 1 and 5) act to prolong EPSPs, through closing of K+ channels; activation of group II (types 2 and 3) mGluRs leads to prolonged IPSP, mainly through opening of K^+ channels (Gu et al., 2012). Metabotropic glutamate receptors are found both presynaptically, on synaptic terminals, as well as postsynaptically, on dendrites (Sherman, 2014).

Glutamate is released by branches of thalamocortical and corticothalamic inputs, therefore glutamate receptors are abundantly expressed in the TRN. Glutamate receptors found in the TRN can be divided into metabotropic (mGluR1 and mGluR2) and ionotropic (AMPA and NMDA) receptors. Metabotropic receptors have prolonged effects and can cause depolarization (mGluR1) (Petralia et al., 1997) or hyperpolarization (mGluR2) (Cox & Sherman 1999) in the TRN cells. Recently, Copeland et al. (2017) showed that mGlu2 receptor activity reduces inhibitory transmission from the TRN to the thalamus with facilitation of nearby astrocytes. Additionally, the activation of the metabotropic receptors causes a long-term reduction of electrical current in the gap junction in the TRN cells (Landisman & Connors, 2005).

The AMPA receptor, a ligand gated channel composed of four subunits (GluA1-4), is mainly activated during thalamocortical activations (Henley & Wilkinson, 2013; Deleuze & Huguenard, 2016). However, AMPA receptors seems to be vital for TRN cortical activation. The TRN neurons express twice as much GluA2/3, and at least three times more GluA4 proteins than the thalamic relay nuclei (Lacey et al., 2012). Therefore, the TRN cells are more sensitive to corticothalamic excitation than the thalamus (Mineff & Weinberg, 2000) and epsp amplitude evoked by corticothalamic

fiber stimulation in the TRN is 2.5 times larger than in the relay neurons (Golshani et al., 2001). This current disproportion allows the TRN to inhibit the relay neurons after direct corticothalamic excitation (Paz et al., 2011). Interestingly, stargazer mice, a model of absence epilepsy, which shows corticothalamic imbalance due to dysfunctional trafficking of GluA4 protein, can be saved by deletion of AMPA receptors and replacement by NMDA receptors (Lacey et al., 2012).

Conversely, Deleuze & Huguenard (2016), stated that NMDA receptors in the TRN, composed of GluN2A, GluN2B and GluN2C subunits, are also largely involved in corticothalamic activations. Therefore, the thalamic input, employing AMPA receptors, in the TRN is larger and faster, while the cortical input is relatively smaller and slower in kinetics. The dynamic of the corticothalamic pathway activation is crucial: low frequency activity is suppressive for the thalamus, whereas high frequency activity is enhancing, due to plasticity introduced by the NMDA receptors (Crandall et al., 2015).

The GluN2C subunit found in the TRN is quite rare and is absent in pyramidal neurons of cortex and hippocampus (Karavanova et al., 2007). Interestingly, the blockage of the NMDA receptors *in vitro* hyperpolarizes the TRN neurons due to possession of the GluN2C subunit. Hyperpolarization resulting from NMDA blockade deinactivates T-type Ca channels and induces delta-frequency bursting, sensitive to D2 dopamine receptor antagonists (Zhang et al., 2009). It is important to note that enhanced delta oscillation is a common symptom of schizophrenia (Boutros et al., 2008).

1.11.4 Dopamine

Dopamine is one of the major modulators in the brain, and its malfunction is associated with various psychiatric disorders (McHugh & Buckley, 2015). The TRN expresses at least three subtypes of dopamine receptors: D1 (Huang et al., 1992), D2 (Khan et al., 1998; Zhang et al., 2009), D4 (Mrzljak et al., 1996; Govindaiah et al., 2010). Dopamine, by binding to the presynaptic D4 receptors located on the axons incoming from the globus pallidus, inhibits Ca^{2+} dependent GABA release (Florán et al., 2004; Gasca-Martinez et al., 2010). Stimulation of these D4 receptors on the

globus pallidus terminals lead to decreased locomotion, while the inhibition of the dopaminergic receptor disinhibits the TRN, promotes the traffic through the relay nuclei on the thalamus, and causes hyperactivity (Erlij et al., 2012). Interestingly, the altered signal propagation through thalamus (Rowe et al., 2005) and the malfunction of the D4 receptors(Li et al., 2006) are common features of the patients with attention-deficit hyperactivity disorder (ADHD). Therefore, ADHD is another disease associated with abnormal activity of the TRN (Wells et al., 2016).

The dopaminergic afferents are incoming to the TRN from the substantia nigra pars reticulata (Freeman et al., 2001; Anaya-Martinez et al., 2006; García-Cabezas et al., 2007) and, perhaps, from the ventral tegmental area (Kolmac & Mitrofanis, 1998).

1.11.5 Serotonin

Serotonin is one of the most important neurotransmitters related to the sleep/wake cycle modulation (Koella & Czicman, 1966). The TRN expresses two major postsynaptic serotonin receptors, 5-HT1A and 5-HT2A, located in the somata and dendrites (Rodríguez et al., 2011). The activation of 5-HT2 receptors deactivates a leaky K conductance (I_{KL}) and depolarizes neurons (McCormick & Pape, 1990). *In vitro*, the serotonin application inhibits burst firing and promotes the occurrence of single spike activity (McCormick & Wang, 1991), and *in vivo*, the excited TRN neurons by serotonin cause a long-lasting, very regular, high-frequency activity between about 35 and 120 Hz (Funke & Eysel, 1993). However, the latter seems to be caused by activation of the thalamic neurons.

The dorsal raphe nucleus is the main suppliers of serotonin in the TRN (Yoshida et al., 1984; Rodríguez et al., 2011).

1.11.6 Histamine

Histamine is involved in the control of arousal in the brain (Thakkar, 2011). Two receptors, H1 and H3 are expressed in the TRN (Manning et al., 1996; Jin et al., 2002). The histamine effect on the TRN neurons was not investigated yet.

The TRN receives histaminergic afferents exclusively from the hypothalamus (Manning et al., 1996).

1.11.7 Acetylcholine

Application of acetylcholine (ACh) to the TRN neurons results in rapid depolarization followed by a longer lasting hyperpolarization (Lee & McCormick, 1995). A rapid excitatory response is induced by nicotinic ACh receptors, followed by an inhibitory response, caused by activation of M2 muscarinic receptors (Sun et al., 2013b). Hyperpolarization, caused by increased membrane conductance to K^+, blocks tonic neuronal discharges and promotes the burst firing *in vitro* (McCormick & Prince, 1986) Microiontophoretically applied acetylcholine to the TRN *in vivo* inhibited tonic firing and often induced burst activity (Funke & Eysel, 1993). *In vitro*, brief optogenetic activation of cholinergic inputs from basal forebrain to the TRN synchronizes GABAergic cell firing (Pita-Almenar et al., 2014). *In vivo*, optogenetic stimulation of cholinergic axons in the TRN promoted NREM sleep and sleep spindle degeneration (Ni et al., 2016).

The cholinergic innervation of the TRN nucleus derives from brainstem: laterodorsal and pedunculopontine tegmentum (LDT/PPT) (Hallanger et al., 1987a; Cornwall et al., 1990a; Kolmac & Mitrofanis, 1998), parabrachial nucleus (Sofroniew et al., 1985) and from basal forebrain (Hallanger et al., 1987b; Asanuma, 1989; Spreafico et al., 1993).

1.11.8 Noradrenaline

Locus coeruleus (LC) is the main supplier of noradrenaline (NA) in the TRN (Morrison & Foote, 1986; Asanuma, 1992). *In vitro*, NA local application results in neuronal depolarization, mediated by activation of α_1 adrenoceptors, which deactivates a leaky K conductance (I_{KL}) (Pinault & Deschênes, 1992). NA application to the TRN *in vivo* elicited weak depressive action on the high frequency action, but during low oscillation prevented bursting firing and led to single spike firing (Funke & Eysel, 1993). Following bilateral lesion of the LC, TRN cells no longer displayed clock-like firing behavior. A few cells still discharged regularly for an hour, but after TRN cells were either silent or discharged in bursts (Pinault & Deschênes, 1992). Bizarrely, the noradrenergic effect on the TRN was not investigated appropriately so far.

1.11.9 Neuropeptides

Neuropeptides do not function as typical neurotransmitters, they are slower and act as fine tuners of neurotransmission (Baraban & Tallent, 2004). The TRN has a rich expression of the various neuropeptides receptors, including as: thyrotropin-releasing hormone, vasoactive intestinal peptide, cholecystokinin, neuropeptide Y, prolactin releasing peptide, somatostatin. The amount of neuropeptide expression in the nucleus prove that TRN is a finely tuned instrument for execution of imperative functions in the brain.

Thyrotropin-releasing hormone (TRH) is a 35-amino acid peptide secreted only by the hypothalamus. TRH receptors are strongly expressed in the TRN (Burgunder & Taylor, 1989; Mitrofanis, 1992b) and, like the parvalbumin expressing cells, are found throughout the TRN (Burgunder et al., 1999a). The TRH application to the TRN cells *in vitro* depolarised cells by blocking K^+ conductance and transiently changed neuronal firing pattern (Broberger & McCormick, 2005). According to previous clinical reports, TRH can affect sleep and epilepsy (Ujihara et al., 1991; Nishino et al., 1997).

Vasoactive intestinal peptide (VIP) is a 28-amino acid peptide, which is abundantly expressed in the various brain structures and can act as a modulator of the physiological functions (Magistretti, 1990) or as a neurotransmitter (Magistretti, 1986; Graber & Burgunder, 1996). VIP is found largely in the lateromedial part of the TRN (Burgunder et al., 1999), which is related to the motor function modulation. The neuromodulator seems to have a negligible physiological effect on the TRN in vitro, while it strongly depolarizes the thalamic relay neurons (Lee & Cox, 2003).

Cholecystokinin (CCK)-containing neurons and CCK binding sites are found in the TRN area. Application of CCK on the TRN neurons suppress a K^+ conductance in the dendrites (Sohal et al., 1998), which promotes in long lasting depolarization (Cox et al., 1995). CCK depolarized TRN neurons, changed their firing mode from phasic (burst) to tonic (single-spike) output (Cox, Huguenard & Prince, 1997), what leads to abolition of the spindle waves generated by thalamocortical neurons (Lee & McCormick, 1997). Interestingly, low concentrations of the CCK produce no effect on

the TRN neurons, like VIP application, although the probability of burst response was increased. Therefore, CCK can strongly modulate intrathalamic rhythms, depending on the CCK concentration and the resting state of neurons (Cox, Huguenard & Prince, 1997).

Neuropeptide Y (NPY) is expressed in most parts of the CNS (Allen et al., 1983) and is involved in numerous physiological and neuronal processes (Ekstrand et al., 2003; Hansel et al., 2001). The TRN predominantly expresses three subtypes of NPY receptors: Y1, Y2 and Y5 (Parker & Herzog, 1999; Wolak et al., 2003), which are located at the somata and dendrites (Molinari et al., 1987; Morris, 1989). Activation of the NPY1 receptors open GIRK channels, which facilitate K^+ conductance, whereas the activation of the NPY3 receptors leads to inhibition of high voltage activated Ca^{2+} channels (Sun et al., 2001). Therefore, activated NPY receptors produce an inhibitory effect, hyperpolarize neurons and deregulate GABA release (Sun et al., 2001). *In vitro*, NPY1 agonists suppressed oscillatory network responses in rat thalamus, and vice versa, an NPY1 antagonist augmented oscillatory network recorder in thalamus (Sun et al., 2003; Brill et al., 2007). So, NPY has a role of endogenous anticonvulsant, which inhibits the absence seizure (Stroud et al., 2005) and thalamic oscillations associated with sleep (Sun et al., 2003).

Prolactin releasing peptide (PrRP) is a 31-amino acid peptide responsible for a functional part of the hypothalamic-pituitary axis (Hinuma et al., 1998). Primarily, prolactin is known for the regulation of the physiological processes such as the development of the mammary glands and the promotion of milk synthesis (Powe et al., 2011) or body weight regulation (Gu et al., 2004). Additionally, PrRP can act as a neurotransmitter and the PrRP receptors (GPR10) are abundantly expressed in the reticular thalamic nucleus (Roland et al., 1999; Ibata et al., 2000). The PrRP by binding to the G-protein coupled receptor GPR10, enhances amplitude of the NMDA receptor-mediated excitatory postsynaptic current by 50-80%, and consequently, increases amplitude of $GABA_A$ receptor-mediated inhibitory postsynaptic current by 50-75% (Xia & Arai, 2011). Deleuze & Huguenard (2016) stressed that NMDA

receptors in the TRN are primarily used by the corticothalamic pathways, therefore PrRP by acting on GPR10 receptors might prioritize top – down processing. *In vitro*, PrRP application to the thalamic slices suppresses artificially evoked oscillatory burst activity, while *in vivo*, intracerebroventricular injection of a small concentration of PrRP in sleeping animals significantly suppresses sleep oscillations and promotes arousal, but large concentrations of PrRP suppress absence epilepsy (Lin et al., 2002).

Somatostatin (SOM) is a well-known peptide present in GABAergic cells of the TRN of various species (Bendotti et al., 1990; Burgunder & Young, 1992). Up to 20% of cells in the TRN coexpressed SOM and PV, whereas up to 30 % of neurons in the TRN express only SOM without PV (Clemente-Perez et al., 2017). SOM, by activating SST5 receptors, can suppress the TRN GABAergic cells via presynaptic inhibition of glutamate release and postsynaptic activation of GIRK channels (Sun et al., 2002). Application of SOM *in vitro* leads to the dampening of both spindle-like and epileptiform thalamic network oscillations, whereas stimulation of the SOM containing cells *in vivo* does not have any effect on oscillation (Sun et al., 2002; Clemente-Perez et al., 2017). Additionally, Clemente-Perez et al. (2017) showed that the PV neurons send axons to the sensory thalamus, while the SOM cells project to limbic parts of the thalamus. However, it might be an overestimation reflecting viral expression, as they used the data from two nuclei only (VMP and ATN), as proof.

So, the neuropeptides, by modulating the neuronal membrane potential of the TRN neurons, can change the firing pattern accordingly to the current brain state. Apparently, most of the neuropeptides reaching the TRN are released from the areas responsible for arousal, such as brainstem and hypothalamus (Lechner et al., 1993).

1.11.10 Melatonin

Melatonin (MLT) is synthesized in the pineal gland and it has a hypnotic effect (Brzezinski et al., 2005). The physiological actions of MLT in brain are mediated by two high-affinity G-protein-coupled receptors, MT1 and MT2. MT2 receptors are abundantly expressed in soma and dendrites of the TRN neurons (Lacoste et al., 2015). Microinfusion of a partial agonist of MT2 receptors in the TRN promotes

NREMS, by enhancing the bursting firing in the TRN (Ochoa-Sanchez et al., 2011). Interestingly, MT2 knockout mice display decreased time of NREM sleep with diminished delta oscillation (Comai et al., 2013).

1.11.11 Endocannabinoids

Endocannabinoid's receptors (CB1R) are present in the TRN and can enhance the physiological levels of thalamic synchrony (Sun et al., 2011).

1.11.12 Summary of the TRN neurochemical diversity

The TRN importance in various physiological processes is emphasized by the diverse neurochemical expression shown above. The TRN is a state dependent generator/modulator of the cortico-thalamo-cortical pathway oscillation, due to to the rich number of the sleep/wake modulating receptors expressed in the TRN. The heterogenous pattern of the expressed receptors in the TRN was not surprising, due to outline of the afferents from the thalamus and other subcortical structures. For example, SOM containing neurons, putatively, propagate to the higher order thalamic neurons and VIP receptors are found only in the rostral part of the TRN.

1.12 Electrophysiological properties of the TRN

1.12.1 Intrinsic circuitry characterization

TRN cells communicate between each other through dendrodendritic and at least 2 weeks after birth through axodendritic (axonal collaterals) synapses (Pinault et al., 1997; Hou et al., 2016) .

Before Hou et al., (2016) work, it was generally accepted that mutual inhibition of the neighboring neurons is a quite common way of interaction in the TRN (Ahlsén & Lindström, 1982). Dendrodendritic and axodendritic junctions, apparently, are useful in the lateral inhibition during modality specific attention. The axodendritic synapses existence is still questionable, and apparently, some intrinsic axon collaterals have the ability to disappear during brain maturation (Cox et al., 1996; Pinault et al., 1997; Hou et al., 2016).

Landisman et al. (2002), using paired cell recordings, discovered the presence of functional electrical cellular couplings in the TRN neurons of young rats and mice. Connexin-36 plays an important role in the cellular synchronization especially of low-frequency events such as low-threshold Ca^{2+} spikes. Long et al. (2004) suggested that 'electrically coupled small neuronal clusters may be a major determinant of the spatial and temporal activity patterns of TRN'. Gap junctions in the TRN might be involved in the Ca^{2+} related oscillation or they might be controlling dendritic Ca^{2+} currents.

1.12.2 Electrophysiological properties

The extracellular recording from the TRN *in vitro* revealed that neurons either fire in burst firing or discharge in a tonic, single spike pattern. (Bal & McCormick, 1993). Intracellular injection of hyperpolarizing current into TRN neurons produces rhythmic burst firing, whereas intracellular injection of depolarizing current generates tonic, single spike activity. Hyperpolarization de-inactivates low threshold T-type calcium channels and induces rhythmic burst firing. The transition between two firing states can occur within a change of a few millivolts of membrane potential, which can activate transient current. This transient Ca^{2+} conductance deactivates much more slowly than in TC neurons (Huguenard & Prince, 1992) and might take place in dendrites (Destexhe & Contreras, 1996). A similar voltage dependence of firing pattern was recorded *in vivo* (Contreras et al., 1993). According to Fuentealba et al. (2005) only 20% of all TRN the neurons are unable to generate burst firing during low membrane potentials or after prolong hyperpolarization.

Two ion channel mechanisms underlie the bursting firing in the TRN: low-voltage gated T- type Ca2+ channels (T channels) and the small-conductance Ca2+-activated type-2 K+ channel (SK2) (Fuentealba et al., 2004; Fuentealba & Steriade, 2005). Additionally, the bursts are shaped by voltage-dependent K^+ channels (Lau et al., 2000; Rudy & Mcbain, 2001; Espinosa et al., 2008), R-type channels (Randall & Tsien, 1997; Weiergräber et al., 2008; Zaman et al., 2011), sarco/endoplasmic reticulum Ca^{2+}-ATPases (Cueni et al., 2008), and Ca^{2+}-induced Ca^{2+} release via ryanodine receptors (Coulon et al., 2009).

1.12.3 Electrophysiological diversity

Previous studies, trying to differentiate neuronal classes based on their firing properties failed to find a clear outcome, but the majority managed to characterize only two types of neurons: burst firing and tonic firing neurons (Barrionuevo et al., 1981; Contreras et al., 1992; Brunton & Charpak, 1997). The latter subtype of neurons generates only tonic, single spike firing at 40 Hz with slight depolarization and 8-10 Hz firing at the resting membrane potential. For the bursting firing neurons, a depolarizing current induces tonic current at the resting or slightly depolarized membrane potential, while at hyperpolarized membrane potential more negative than -75mV generates high frequency spike bursts. The neurons, which are able to show bursting firing, possess T channels (transient calcium current), which are de-inactivated at low resting potentials, and a single excitatory stimulus is sufficient to evoke a burst in these neurons. The bursting mode of firing during high resting potential depends upon prolonged inhibitory stimulation with subsequent excitatory transient in order to generate bursts. It takes roughly 100 ms for the T channels to inactivate or de-inactivate. (Lesica et al., 2006).

Interestingly, the results from recent studies, dedicated to the TRN neuronal firing, failed to match preceding results. Lee et al. (2007), *in vitro*, showed that half of the neurons in the dorsal part of the TRN are unable to produce burst discharge, whereas up to 80% of the neurons in the ventral TRN display a stereotypical burst discharge. A decade later, Clemente-Perez et al. (2017), recording *in vitro*, did not find any location related alteration in the neuronal firing in somatostatin (SOM) and parvalbumin (PV) containing neurons, which can be qualified as representatives of majority if not all TRN neurons. Both neuronal groups were capable to show bursting and had similar biophysical properties of T-currents. However, SOM containing neurons, apparently, contained fewer dendritically located T-type calcium channels, therefore the maximal number of rebound bursts was threefold smaller in the SOM than PV neurons. Additionally, about 30% of SOM cells fired only in tonic manner, whereas all PV cells were capable of bursting and significant majority of which showed repetitive bursting (Clemente-Perez et al., 2017).

Neurons of the TRN fire in different modes depending on the current brain states. Mukhametov et al. (1970) first noticed that the same neurons fire in an irregular, tonic manner (40 Hz) during REM sleep and wakefulness, whereas during NREM sleep, neurons generated burst firing with a long interburst period. Experiments in freely moving cats (Steriade et al., 1986; Marks & Roffwarg, 1993) rats showed similar results: the TRN neurons fire in burst mode during NREM sleep and during arousal they generate tonic firing. Finally, Halassa et al., (2014) *in vivo*, targeted the dorsal parts of two distinct areas of the TRN in freely moving mice. The first was interconnected with a sensory nucleus of thalamus (LGN, visual) and a second part of the TRN was interconnected with a limbic nucleus (ATN). The neuronal firing patterns of sensory associated TRN were positively correlated with delta (1-4 Hz) and sleep spindle (8-15 Hz) oscillation, whereas the limbic associated TRN part was negatively correlated with slow wave sleep oscillations and positively correlated with arousal. This divergent electrophysiological nature of the TRN appears to be important during attention and sleep.

1.12.4 Summary of the TRN electrophysiological diversity

Clear electrophysiological heterogeneity of the TRN neurons was and is a topic of debate for over a half a century. Only recently, using genetic techniques, it was confirmed that the neuronal firing in the TRN could vary due to different neurochemical pattern or due to dissimilar afferents from thalamus, therefore the neurons in the identical nucleus can be responsible for different functions and show various firing pattern during same brain state.

1.13 Brain rhythms

1.13.1 Intrinsic TRN oscillations

The oscillatory burst discharges are an intrinsic property of the TRN neurons (Llinás & Steriade, 2006) and two mechanism of synchronization are used: GABAergic synapses and electrical coupling.

Some studies suggest that reciprocal axodendritic inhibition act as a desynchronizer (Huntsman & Huguenard, 2000). However, previous results from the same lab and a number of modeling studies found that mutual inhibition can synchronize them into spindle-like oscillations. During relatively hyperpolarised levels of slow-wave sleep, inhibitory postsynaptic potentials can be reversed and according to a modeling study, $GABA_A$-mediated depolarization can produce spindle like patterns in isolated TRN (Bazhenov et al., 1999). Although, this hypothesis never was confirmed *in vivo*.

Another, non-exclusive mechanism of spindle synchronization within the TRN nucleus is driven by gap junctions (Landisman et al., 2002). Spontaneously occuring spikelets in the TRN neurons can be recorded during sleep spindles (Fuentealba et al., 2004). Spikelets are fifty times smaller than action potentials and have different features from the excitatory postsynaptic potential (EPSP). The spikelets have significantly faster rising and decaying phases than EPSP and they never lead to an action potential. Interestingly, the halothane, gas used for anaesthesia, and at the same time a gap junction blocker, can strongly reduce the amount of the spikelets (Fuentealba et al., 2004).

1.13.2 History of EEG

In 1929, a German psychiatrist first recorded an electroencephalogram (EEG), continuous and regular potential changes in the electrode connected to the head of man (Berger, 1929). However, a few years before, Práwdicz-Neminski (1925) recorded "Elektrocerebrogamm" of mammals with two types of rhythms (9-15 Hz and 15-30 Hz), Berger was more successful in naming the new technique. Additionally, he first coined two new terms: "alpha-waves" and "beta-waves" (Berger, 1930). It took five years for Berger's work to receive the deserved recognition from scientific community (Adrian & Mattews, 1934). Soon after the recognition, the EEG became one of the most popular neuroscience techniques in Europe and the United States (Stone & Hughes, 2013).

Decades ago, Berger noticed that distinct waves are superimposed in the EEG recording, and Jasper & Andrews (1938) demonstrated that the overlaid waves can

originate from different brain areas. Diversity of the EEG rhythms were discovered quite soon: delta (1-4 Hz) and theta (4-8 Hz) oscillations were characterized by Walter (1936) and the gamma wave (30>Hz) term was first used by Jasper & Andrews (1938), but their physiological meaning remained mysterious. In the seventies, several workers started to associate distinct EEG waves with physiological processes in the brain (Başar, 1972; Freeman, 1975) and only in the nineties, when the EEG research had a renaissance, Basar could confidently state, that the EEG should not be considered as background noise, but as an important brain signal from different oscillatory systems (Başar, 1999). Therefore, the EEG in neuroscience can be perceived as relatively new technique with a deep-rooted history.

1.13.3 TRN and EEG waves

The circuits and mechanism responsible for the generation of EEG oscillations are still under active investigation. In vertebrates, sleep rhythms are characterized by frequencies lower than 15 Hz (Steriade, 2006), while awake EEG is associated with higher frequency waves, cortical desynchronization and hippocampal theta rhythms (Schwartz & Kilduff, 2015).

Slow

Slow oscillations (< 1Hz) were discovered by Wilson & Groves (1981) in the striatum of anesthetized rat, and Steriadeet al. (1993a) first characterized them in the cortex of anesthetized cat. Slow waves are generated in layer 5 of cortex (Steriade et al., 1993b; Sanchez-Vives & McCormick, 2000) during quiescent sleep and anesthesia, when the neurons of the entire neocortex undergo transition between depolarization (Up states) and hyperpolarization (Down state) in cyclical manner. Other subcortical structures such as thalamus (Contreras & Steriade, 1995), striatum (Wilson & Groves, 1981) and cerebellum (Ros et al., 2009) are involved in the global synchronized oscillation. Thalamocortical cells are important for initiation of Up state by burst firing (Contreras & Steriade, 1995), which by depolarizing TRN cells, initiates inhibition of the thalamocortical cells and prevents them from firing (Contreras & Steriade, 1995; Timofeev & Steriade, 1996). Hence, the misfiring of the TRN or thalamic neurons can significantly modulate slow oscillation (MacLean et al., 2005; David et al., 2013)

Recently, Lewis et al. (2015) reported, that local optogenetic activation of the TRN rapidly induced slow wave/delta activity resembling those seen in sleep. Additionally, animals with depolarized TRN had reduced arousal and locomotion. During natural sleep, a strong inhibition by the TRN caused during Up states is present only in the thalamic relay nuclei, whereas higher order nuclei (limbic) nuclei spike throughout the duration of the Up state (Sheroziya & Timofeev, 2014), apparently, due to fact that limbic associated neurons of the TRN exhibit low levels of activity during sleep (Halassa et al., 2014).

Early psychologists and neurophysiologists perceived sleep as a manifestation of hemispheric inhibition (Pavlov, 1923) or "abject mental annihilation" (Eccles, 1961). Nowadays, the slow wave function is still a matter of debate, but sleep appears to be very complicated. In addition to the afferent signal transmission inhibition, which disconnects brains from outside world (Steriade, 2006), there is strong evidence that slow wave sleep takes part in the elimination of weak, unnecessary synapses formed during wake (González-Rueda et al., 2018) and memory formation (Sirota & Buzsáki, 2005).

Delta

Delta oscillation (1-4 Hz) follows the deepest stages of slow-wave sleep. Thalamic and cortical neuronal circuitries generate independent delta rhythms by relaying on the intrinsic properties of their neurons. The delta waves in thalamus are produced by the rhythmical interaction between two ionic currents: leaky h-current and T current, which are activated at more negative membrane potential than required for spindle generations. Hyperpolarization activates h-current and de-inactivates T current, what leads to intracellular infusion of calcium and low threshold spike. After deactivation of the h-current and inactivate the T current by action potential, neurons are repolarized so that the h-current can begin the cycle again (McCormick & Pape, 1990; Huguenard, 1996). Thalamic clock-like delta activity is synchronized by the TRN receiving EPSPs from cortical cells. The initial thalamic hyperpolarization required for delta wave initiation is caused by a further decrease in firing of brainstem cholinergic neurons during deep slow wave sleep (Steriade et al., 1991). Delta oscillation in

cortex (~ 2 Hz) relies on a similar interaction between ionic currents and is independent of the thalamic delta wave. It can be recorded without thalamus (Steriade et al., 1993b) and can be generated during wakefulness (Petersen et al., 2003), when thalamic cells are not hyperpolarized enough to exhibit rhythmicity.

Delta oscillations are synchronized with Up states of slow waves, by the excitatory and inhibitory inputs from the corticothalamic and TRN cells, respectively (Steriade et al., 1991).

Theta

Theta oscillation (4-8 Hz) is a main characteristic of REM sleep (Jouvet, 1969) and can be increased during various locomotor activities (Vanderwolf, 1969) or mnemonic processes (Lisman & Idiart, 1995; Raghavachari et al., 2001). It is generally accepted that the rhythm is driven by pacemakers cells within hippocampus and is critical for temporal coding and decoding (Buzsáki, 2002). Subcortical structures, such as the dorsal raphe nucleus, ventral tegmental nucleus and anterior thalamic nucleus are phase locked to hippocampal theta oscillation (Vertes & Kocsis, 1997; Bland, 1986).

Alpha

Alpha oscillation (8 -13 Hz) is associated with the visual system (Mulholland, 1965), correlates with reaction time (Woodruff, 1975), is linked with long term memory (Klimesch, 1999) and is most pronounced during relaxed wakefulness (Berger, 1929; Adrian & Mattews, 1934; Hughes & Crunelli, 2005). Electrical events, which are recorded as alpha oscillations, are restricted to neocortex (Manshanden et al., 2002), while the main rhythm generator is thought to be the thalamus and its complex interactions with cortex (da Silva et al., 1973; Chatila et al., 1993; Hughes & Crunelli, 2005).

Sleep spindles

During sleep, another type of oscillation with a frequency range like alpha waves (9-15 Hz) could be recorded. Sleep spindles are brief (0.5 – 3 seconds) oscillatory events, which reoccur every 3-10 seconds during light and deep NREM sleep (Rasch & Born, 2013) and the TRN appears to be the main sleep spindle generator (Steriade et al., 1987; Fuentealba & Steriade, 2005; Halassa et al., 2011a; Kim et al., 2012).

Thalamocortical (TC) and corticothalamic (CT) feedback help the TRN synchronize and shape sleep spindles (Contreras & Steriade, 1996a; Bonjean et al., 2011). The spindles origin is during Up states of the slow oscillation, when cortical neurons fire synchronously and force TRN neurons to fire (Steriade et al., 1993). When spindles rapidly follow initial depolarisation of the Up state, a sequence known as a K – complex is formed. (Amzica & Steriade, 1997).

Spindles have a unique shape and consist of 3 phases: initiation (waxing), middle and waning phase. During the waxing phase, cortical neurons start and recruit the TRN neurons, which burst, and the inhibitory postsynaptic potentials induce rebound bursting in TC cells. The middle phase results from synchronization of TRN-TC-TRN loop, during which TC excite repeatedly both, TRN and corticothalamic neurons. In the final waning phase, both thalamic and cortical firing becomes less regular and the oscillations cease (Bal et al., 1995).

Recent studies by using high density EEG or functional magnetic resonance imaging (fMRI) techniques discovered a complex topology of sleep spindles. The frontal cortex generates 9-15 Hz spindles, whereas in parietal and central part of the brains faster spindles (13-15 Hz) dominate (Andrillon et al., 2011). Topographically distinctive spindles were identified in mice, though they had similar oscillation frequency (Kim et al., 2015). Before that, Contreras & Steriade (1996) categorized two sleep spindle types in cats in vivo: slow sleep spindles (7-8 Hz) with high amplitude and fast sleep spindles (10-20 Hz) with lower amplitude. Although, the latter result was not confirmed in the upcoming studies.

Spindles for a long time were thought to protect sleep against environmental disturbances. Individuals who generated a higher number of sleep spindles exhibited higher tolerance to external stimuli during a noisy night (Dang-Vu et al., 2010; Dang-Vu, 2012; Wimmer et al., 2012). Additionally, sleep spindles are associated with synaptic plasticity (Dan & Poo, 2004) and memory formation (Kudrimoti et al., 1999; Sirota & Csicsvari, 2003; Latchoumane et al., 2017). Abnormal spindles can be recorded during various pathological states like mental retardation (Gibbs & Gibbs,

1962), Huntington's disease (Wiegand et al., 1991), Sporadic Creutzfeldt-Jakob disease (Landolt et al., 2006), schizophrenia (Ferrarelli et al., 2007), autism and attention hyperactivity disorder (Wells et al., 2016).

Gamma/Beta

Slow globally synchronized oscillations characteristic for sleep are replaced by fast and locally synchronized oscillation like beta (15 – 30 Hz) and gamma (30 – 80 Hz) during wake. Cortical neurons located in layers 2-6 and projecting to thalamus are thought to be the best candidates to generate and synchronize beta and gamma rhythms (Steriade, 2006). Gamma oscillation is associated with sensory processing (Fries, 2009), short term memory (Tallon-Baudry et al., 1998) and conscious perception (Melloni et al., 2007). Beta waves transform into gamma oscillations under slight neuronal depolarisation (Llinás & Steriade, 2006). Unsurprisingly, they share most of their functions with gamma oscillation, and additionally, are involved in motor control (Kilner et al., 2000; Marco-Pallares et al., 2008).

It is important to note, that fast oscillations associated with wakefulness can be recorded during the Up states of the slow oscillation (Steriade & Amzica, 1996). The cortical and thalamic neurons exhibit fast oscillation under appropriate depolarization current, which is not a special quality of waking (Llinás et al., 1991; Gray & McCormick, 1996). Additionally, inhibitory interneurons in the cortex, responsible for the distribution of higher-frequency activity in cortex, are activated during Up states of the slow oscillation (Contreras et al., 1997; Hasenstaub et al., 2005). The role of the high frequency activity during sleep is still mysterious, although it could be responsible for dreaming mentation during slow wave sleep (Hobson et al., 2000).

Sharp-wave ripples

Ultra-fast (or very fast) rhythms (80–200 Hz, up to 400 Hz), also called "ripples," are superimposed over the depolarizing phase of the slow oscillation in cortex. Such ultra-fast oscillations are generated in the hippocampus and can be found in various brain areas (Chrobak & Buzsáki, 1996). Ripples are high frequency field oscillations, during which pyramidal neurons replay previous waking activity (Girardeau & Zugaro,

2011). Triple coupling, a close temporal association, between slow wave sleep, spindles and ripples, is necessary for memory consolidation (Peyrache et al., 2011; Latchoumane et al., 2017).

1.14 Functions of the TRN

Traditionally, physiological functions of the TRN were studied by using lesion, single unit recording and pharmacological approaches (Weese et al., 1999; McAlonan, 2006). However, technologies invented at the beginning of the 21st century allowed scientists to target genetically defined cells at various temporal resolutions. One of the revolutionary technologies is optogenetics (Boyden et al., 2005a). After the invention of optogenetics, neurobiological research at the neural circuit level has been drastically accelerated. First, we provide a brief history of optogenetics. Then we summarise studies on physiological functions of the TRN, with an emphasis on recent optogenetic studies.

1.14.1 History of optogenetics

At the end of the 18th century scientists were interested in the association between electricity and the nervous system. Newton thought that an electric spirit might convey sensations to the brain along the nerves and produce muscular reactions. Haller electrified people and investigated reflexes (Brewer & Porter, 2013). At the same time Luigi Galvani, professor of anatomy at Bologna, discovered so called 'animal electricity' (Galvani, 1791). Frog's leg muscles violently moved when struck by an electrical spark from a nearby electrical machine. Later Alexandro Volta proved that Galvani's assumption was wrong, but it does underestimate the importance of Galvani's discovery for the history of the electricity (Piccolino & Bresadola, 2013). After a century and half started the era of the neuroscience. Penfield and Rasmussen proved that artificial neuronal stimulation leads to sensations and movements in pre-surgery patients (Penfield & Rasmussen, 1950). Hodgkin and Huxley empowered neuroscience tools by transferring them from the field of electronics and characterized electrical transmission in nerves (Hodgkin & Huxley, 1952; Hodgkin, 1976). From that time onwards, electrophysiology remained the tool of choice for

neuronal cell manipulation over decades, although it lacked the ability to differentiate between different cell types.

Francis Crick put forward the idea that light can be used to control subtypes of neurons in 1999 (Crick, 1999). At that time optical uncaging of neurotransmitters with ultraviolet laser pulses was already a common technique, but it was not adapted to a neuro-type specific form (Callaway & Katz, 1993). Gero Miesenbock first brought to reality the main principles of optogenetics, which he named as "chARGe" due to combination of the photoreceptor of Drosophila and G protein. He was able to transmit optical signal into electrical activity in the responsive subset of neurons (Zemelman et al., 2002). That pioneering paper was a breakthrough in neuroscience. Large numbers of neurons were excited simultaneously and precisely, without undesirable excitation of functionally distinct neurons. However, due to the slow nature of the stimulation of G coupled receptors, light mediated current by "chARGe" took seconds to switch neurons off and on. In addition, the "chARGe" required simultaneous expression of two genes in a single neuron to work.

The next important step was a discovery of the light-sensitive ion channel, later named Channelorhodopsin-2 (ChR2), that drives phototaxis in the green alga *Chlamydomonas reinhardtii* (Sineshchekov et al., 2002). Nagel et al. (2003) demonstrated that ChR2 expressed in oocytes or HEK cells can depolarize them during illumination, by letting positively charged ions (such as H^+ and Na^+) into the cell. It was clear for Nagel that ChR2 is a potent tool for neuronal membrane manipulation especially in mammalian cells (Nagel et al., 2003). The idea of optogenetics as we know it today was in the air.

At the same time, post doc Karl Deisseroth and PhD student Edward Boyden understood that optogenetics is a powerful technique for future neuroscience (Boyden, 2011). Deisseroth obtained clone of ChR2 from Nagel on collaborative basis and started to race with other labs. During that time Nagel made several crucial advances in technology. He managed to fuse ChR2 with fluorescent proteins such as YFP (yellow fluorescent protein) and made a mutant of ChR2 less prone to

inactivation. Karl worked out the transfection of ChR2 to cultured hippocampal neurons and late on 4th of August Boyden patched neurons and recorded precise action potential in response to blue light activation (Boyden et al., 2005a). ChR2 appeared to be well tolerated by neurons and it did not require all-trans-retinal for functioning and could be expressed at such levels that a brief light pulse would elicit an action potential. Long repeated activation of ChR2 did not impair performance of the neurons, but they were able to spike not faster than 10 Hz. Later, Deisseroth's PhD student Feng Zhang cloned channelrhodopsin-2 into a lentiviral vector, and increased robustness ChR2 expression and activity (Boyden, 2011). At the same time Guoping Feng began to make the first transgenic mice expressing channelrhodopsin-2 (Arenkiel et al., 2007).

The term "optogenetics" was coined first in a review article written by the 'founding fathers' of this technique ; namely Deisseroth, Boyden, Miesenbock and Nagel (Deisseroth et al., 2010). In parallel, several labs published their findings of ChR2 activity in mammalian cells (Ishizuka et al., 2006; Zhang et al., 2006; Bi et al., 2006). It is important to note that Deisseroth and Boyden continued to search for new optogenetic tools for neuroscience research; for example, light-driven chloride pump halorhodopsin (NpHR) from the archaebacterium *Natronomas pharaonis* (Han & Boyden, 2007; Zhang et al., 2007). The introduction of NpHR opened up a new dimension for optogenetics. Light, in addition to activation, was also able to inhibit neurons without exogenous chemicals. Nevertheless, NpHR had a few performance limitations including the low magnitude of the current and long inactivation phase with slow recovery period. Boyden's group subsequently utilized and found the proton pump from the archaerhodopsin (Arch) class (characterized in the *H. salinarum* in the early 1970s), which was able to silence completely the neurons in awake behaving animals (Chow et al., 2010).

Just in a few years the number of available opsins used in optogenetics increased swiftly, thankfully to the successful work of Deisseroth lab. Optogenetics today is

indispensable and at the same time a relatively cheap technique for neuroscience research.

1.14.2 Physiological functions of the TRN and optogenetics

So far most of the scientific breakthroughs in biomedical sciences were accomplished due to introduction of innovative technologies. Optogenetics provided new dimension to the TRN research field, which expanded recently.

Attention

The TRN is located in a strategic position between the cortex and the thalamus and the possession of the overlapping functionally distinct sectors contributed to Francis Crick's speculative hypothesis, the searchlight hypothesis. It states that during selective attention, the TRN by intensifying corresponding TC circuits may act as the searchlight in the dusk. In other words, the TRN inhibitory projections "should be able to sample the activity in the cortex and/or the thalamus and decide where the action is" (Crick, 1984).

Several contradicting studies emerged after Crick proposed the 'searchlight' hypothesis. Unilateral lesioning of the TRN in rats introduced longer reaction to cues (Weese et al., 1999). Later, McAlonan et al. (2008) by recording from the visual TRN and lateral geniculate nucleus in attending monkeys, demonstrated that visual attention is correlated with reduced firing rate of the visual TRN. Results from Weese et al. (1999) and McAlonan (2006) supported the notion that during attention the firing rate of the TRN increases, whereas a later study by McAlonan et al. (2008) showed the opposite result.

Optogenetics helped us to understand better the association between TRN and attention. The Halassa et al. (2014) study, using an innovative custom made microdrive and optogenetics, investigated the functional role of TRN in attention in mice. During the anticipation phase of the visual task, TRN areas associated with 'vision' increased their firing rate. Optogenetic inhibition of the 'visual' TRN led to reduced reaction time in the behavioral task and light activation of the same area led mice to react more slowly. It is important to note, that the visual task score during

optogenetical interrogation was unaffected. Therefore, the reaction time change during behavior led Halassa to propose that TRN might be involved in 'arousal state'. Soon after, Ahrens et al. (2015) reported on ErbB4 deficient mice and a cross modality task. Mice lacking ErbB4 receptors in the TRN performed better in a 'within modality task' and significantly worse during a 'cross modality task'. Using optogenetics in vivo, Ahrens and colleagues discovered that the deficiency of ErbB4 produced stronger cortical output to the TRN, which introduced the behavioral phenotype. Overall, the Ahrens study showed TRN involvement in the modality 'associated' attention and top down control of the 'sensory' attention. Interestingly, the attentional deficit and hyperactivity was recorded in the animals with reduced thalamic inhibition, weakened cortical feedback (Wells et al., 2016). Therefore, the balanced cortical feedback (CT -TRN) to the thalamus is crucial for acceptable attentional state. At the same time, Halassa came up with a new study, where he incorporated a similar cross modality task together with optogenetic stimulations (Wimmer et al., 2015). Optogenetic inhibition of the PFC (prelimbic area) and activation of the sensory TRN during the anticipation phase introduced a higher percentage of errors in the task. In other words, the prelimbic area of the PFC seems to control at least sensory TRN activity.

Pain

Association of the TRN activity with pain perception is a relatively new topic. Picrotoxin, a $GABA_A$ receptor antagonist, injection into the TRN induced a "pain-like" behavior in rats (Olivéras & Montagne-Clavel, 1994). Electrophysiological data showed that noxious stimuli induce strong and short-latency depression on the TRN neuronal firing (Peschanski et al., 1980; Yen & Shaw, 2003). Liu et al. (2017) strangely started to search for the pain related cells in the rostro-dorsal sector of the TRN. They reported that selective chemogenetic (DREADD) activation in the parvalbumin containing neurons of the rostral TRN reduced thermal and mechanical nociceptive thresholds of mice, while chemogenetic inhibition of similar part of the TRN did not show any effect on sensitivity. The results seem to be unrelated to nociception propagation. Exploration of the rostral TRN connection with nociception in this study

was quite strange, because all upcoming studies investigated the centroventral part of the TRN, associated with the VB, the main thalamic nociceptive nucleus.

Recently, imaging and biochemical studies in humans revealed that neuropathic pain might be caused by decreased functions of the TRN (Henderson et al., 2013; Gustin et al., 2014; Alshelh et al., 2016; Henderson & Di Pietro, 2016). There are several studies on the way, which exploit optogenetics to gain better understanding of the TRN bursting effect on pain perception (Saab & Barrett, 2016).

Working memory

M'Harzi et al. (1991) first tried to expose the association between working memory and TRN functioning. Lesioning of the TRN in rats significantly affected their abilities to perform on radial arm tasks. Later, Wilton et al. (2001) lesioned the bilaterally rostral pole of the TRN and tested spatial and learning memory in rats. Control and lesioned animals performed without significant difference in both the radial arm maze and the Morris water maze. Controversial results might be caused by the inability to control spatial resolution during brain lesioning. Additionally, results with affected corticothalamic and thalamocortical pathways during non-specific TRN lesioning are difficult to interpret.

By combining optogenetics with a closed-loop stimulation (Latchoumane et al., 2017) approach provide evidence that the TRN has an essential role for memory consolidation during sleep through its coordinating influence on the interplay between the three rhythms: slow oscillation, sleep spindles and ripples. Optogenetically induced sleep spindles in frontal cortex during Up states of slow oscillation enhanced memory for previously learned hippocampus-dependent tasks, whereas spindles occurring in Down state did not have any effect on memory consolidation and promoted slow wave sleep incidence. Furthermore, optogenetically inhibited sleep spindles during Up state significantly lowered contextual memory recall. Spindles might be a crucial factor for synchronous occurrence of hippocampal ripples and memory replay.

Sleep

Recent experiments employing optogenetics proved that the TRN is crucial for the sleep/wake cycle. Lewis et al. (2015) noticed that optogenetically activated TRN neurons during awake and sleep partly inhibit thalamic relay neurons and induce strong delta oscillation in all cortical areas. Short optogenetic activation leads to delta power reduction during sleep only. Apparently, TRN neurons in these circumstances act as standby tool that is capable of shutting down all conscious/attentional state of the brain. Herrera et al. (2015) using optogenetics discovered the circuitry in hypothalamus controlling arousal and consciousness through TRN neurons. Short optogenetic inhibition of the rostral TRN during sleep induced relatively fast arousal.

Modulations of sleep spindle quantity have a strong effect on the quality of sleep. Mice with overexpressed SK2 channels, which underlie spindle generation, had less fragmented NREM sleep (R. Wimmer et al., 2012). Similarly, optogenetically induced sleep spindles promote NREM sleep (Kim et al., 2012; Ni et al., 2016), whereas animals with malfunctioning SK2 channel functioning and reduced sleep spindles had disrupted NREM sleep (Wimmer et al., 2012; Wells et al., 2016).

1.15 Hypothesis

As previously been described, Halassa et al. (2014) proved that the sensory and limbic associated TRN neurons act differently during the same brain states, and apparently, are responsible for different functions. We showed that the TRN is a heterogenous structure by characterizing its interconnections with thalamus, afferents from different brain areas, neurochemical diversity, morphology, electrophysiological properties and physiological functions. All the evidence shown above points out that the caudal and rostral part of the TRN are diverse in all mentioned characteristics. Additionally, it seems that sensory associated cells are found in the caudal part of TRN, whereas limbic and motor associated neurons are found in the rostral part of the TRN

Thus, the TRN heterogeneity can be described using location principles and we propose that optogenetic targeting of the TRN segments in future should be seriously considered during the design of novel optogenetic experiments. The TRN is a relatively small nucleus, but even the TRN of mouse in rostro-caudal dimension is 1 mm long. Optic fibers during surgeries are placed from the top of the nucleus and have a diameter of 0.2 mm, consequently, the optic fibers even with low numeric aperture (NA), which increases the angle of the light spread, cannot target rostral and caudal sides of the TRN simultaneously.

Considering previous optogenetic experiments, it becomes clear that during experimental design in most studies, the site of stimulation/inhibition in the TRN was chosen deliberately, but they never stressed the importance of the targeted location in the TRN. Lewis et al. (2015) optogenetically targeted the caudal part of the TRN (anteroposterior coordinate (AP): - 1.7 mm) to discover the ability of the TRN to modulate slow rhythms, while injected expressing opsins virus in both parts of the TRN (AP: -0.6 mm and AP: -1.6 mm). Latchoumane et al. (2017) targeted only rostral part of the TRN (AP: -0.6 mm) and discovered the TRN association with memory consolidation. Herrera et al. (2015) by placing optic fiber in the rostral part of the TRN (AP: -0.85 mm) studied the TRN association with rapid arousal. Only, in two separate experiments, which investigated the artificial sleep spindle activation, the TRN was optogenetically activated in the rostral part (AP -0.6 mm) (Kim et al., 2012) and caudal part (AP -1.7 mm) (Halassa et al., 2011). The approach and results in later studies were different, therefore it is difficult to compare the outcome of the rostral and caudal TRN targeting. Curiously, if the studies above targeted different parts of the TRN in their experiments, would they be able to show similar results?

Our hypothesis is following:

Caudal segment of TRN is dealing with sensory information control and rostral segment of the TRN is involved with motor and cognitive information modulation.

If the hypothesis is true, based on previous studies we can anticipate following outcomes:

1) The optogenetic inhibition of the caudal TRN should have a stronger impact on sleep spindles (alpha band) and slow/delta waves than the rostral TRN inhibition

2) The optogenetic inhibition of different parts of the TRN should have diverse effect on sleep/wake cycle

3) The rostral/caudal parts of the TRN might show dissimilar activity pattern during brain state change.

In order to test the hypothesis, we will use optogenetics with the cre-lox system, which would allow us to target only parvalbumin containing neurons in the TRN with precise spatial and temporal resolution. As previously mentioned in the introduction, about 80 percent of all cells in the TRN are parvalbumin containing. We will express light sensitive ion pumps (archaerhodopsin, Arch) and chloride channel (halorhodopsin, NpHR) in the parvalbumin neurons by injecting the virus in the rostral TRN (AP -0.8 mm) or caudal TRN (AP-1.5 mm) area of the genetically modified mice, containing Cre recombinase protein only in the parvalbumin expressing neurons. The delivery of the light will be performed by intracranial introduction of an optic fiber probe. Activation of the proton pumps/channel by light will hyperpolarize the neurons, and thus will inhibit the neuronal feedback from the TRN to the interconnected thalamic nuclei. The EMG and EEG recordings will be used to assess the effect of the various TRN inhibition in freely moving animals.

Chapter 2: Materials and Methods

2.1 Animals

Animal procedures were reviewed and approved by the University of Stratchlyde Ethical Review Committee and performed under license in accordance with UK legislation as defined in Animals (Scientific Procedures) Act 1986. Both sexes (5 females) C57BL/6 background mice, expressing Cre recombinase in the parvalbumin containing neurons(10 - 16-week-old) were used in the experiments (n=25).

2.2 Viral vector and injections

The adeno-associated viruses (AAV-2) of archaerhodopsin (pAAV-Ef1a-DIO-eArch3.0-EYFP), halorhodopsin (pAAV-Ef1a-DIO-eNpHR3.0-EYFP) and YFP only (pAAV-Ef1a-DIO- EYFP) (Vector Core, University of North Carolina) were used for stereotaxic injections. To enable selective targeting of the TRN, we used mice that expressed Cre recombinase (Cre) under the parvalbumin promoter. Titers of this vector was around $10^{6.7}$ cfu/ml. AAV vectors (200 – 600 nl) were injected bilaterally into the TRN of mice using a Nanoliter (WPI). Rostral injection coordinates: anteroposterior (AP): - 0.8 mm; ± mediolateral (ML): 1.4 mm; dorsoventral (DV): -3.2mm, -3.5 mm, -3.8 mm. Caudal injection coordinates: AP: - 1.6 mm; ± ML: 2.2 mm; DV: -3.2mm, -3.5 mm, -3.8 mm). Mice were given at least 4 weeks of recovery following surgery to allow gene expression.

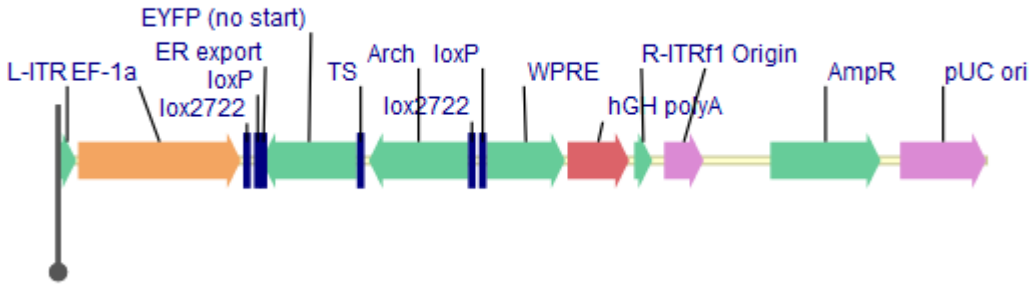

Figure 2.1 Example of vector map of the virus (pAAV-Ef1a-DIO eArch 3.0-EYFP). This vector allows optical inhibition with enhanced proton pumps, Archaerhodopsin from *H. sodomense*, which was modified for mammalian expression with ER export and trafficking signals resulting in 3-5-fold increase in originally reported currents and stable in vivo expression (From Everyvector.com 2009).

2.2.1 Viral vector design

Genetic techniques allow targeting genetically defined populations of cells. Small ChR2 gene, less than 1 kb long, can be tagged to a fluorescent marker YFP or mCherry without affecting photosensitivity and delivered to a specific population of neuron through viral delivery, electroporation or creation of transgenic lines. Generally, viral expression targets small volume of cells (< 1 mm^3) (Powell et al., 2015).

Lentivirus and adeno-associated virus (AAV) are used for expression of the exogenous opsins. They provide easy production of high-titer vector, convenient and stable long term expression of the opsin. (Zhang et al., 2006). In addition, gutted version of both vectors are less toxic, as they express no viral genes (Davidson & Breakefield, 2003).

Adeno-associated virus is prone to infect neurons, through the interaction of AVV2 capsid protein with heparin sulphate proteoglycan (HSPG) found on the cell surface. It seems to infect different classes of neurons unequally, but with a specific promoter, AAV produce high levels of sustained expression in the targeted neurons (Davidson & Breakefield, 2003). Retrograde transport through neuronal processes of AVV2 is limited. AAV vectors are highly effective for gene delivery with titter capacity at 10^{13} and particle size at 20-30 nm but have relatively small transgene capacity (4-5 kb). According to Zhang et al., (2007) AAV-mediated expression may be relatively less stable to lentiviral expression due to smaller percentage of virus integration (less than 1%) (Zhang, Aravanis, et al., 2007). Nowadays, the most commonly used serotype of AAV is 5. Type of the serotype is responsible for the spread of the virus in the brain tissue, therefore in choosing the serotype following should be considered: the brain area, cells targeted, the amount of spread needed and the time of expression desired.

In order to target distinct population of neurons, promoters have to be incorporated in the AAV vector (See figure 2.1). The central polypurine tract (cPPT), derived from wild-type human immunodeficiency virus-1 (HIV-1), is required for transduction into non-dividing neurons (Zennou et al., 2001). Woodchuck hepatitis B virus post-transcriptional regulatory element (WPRE) is a common microbiological tool used to increase expression genes delivered by viral vector. Rev response element (RRE) is

required for mRNA transfer from nucleus to cytoplasm. Psi promotes gene insertion into the mammalian cell. EF-α1 abbreviation is also commonly found on vectors and stands for elongation factor. It is responsible for enzymatic delivery of tRNA to ribosome. Cre dependent viruses' vector, as used in my study, use doubly floxed inverted opsin (loxP sites), which enables cell-specific gene expression (See figure 2.1).

2.3 Fabrication of optic fiber implants

We used the methods described previously (Sparta et al., 2012). Briefly, a small drop of prepared epoxy glue (F123, Thorlabs) was applied on the flat surface of ferrule (CFLC230, Thorlabs). The stripped side of the optic fiber (NA = 0.39) with 200 µm diameter (FT200UMT, Thorlabs) was inserted through the flat surface of the ferrule (CFLC230, Thorlabs), cured with a heat gun for several minutes (150 ^{o}C) and left for 24 hours at room temperature. The optic fiber was cut on the convex side of the ferrule using a diamond knife (S90R, Thorlabs). Then, the convex side was polished with decreasing sizes of polishing paper (6 µm (LF6D),3 µm (LF3D),1 µm (LF1D),0.3 µm (LFCD), Thorlabs). A small cut was made on the surface of remaining optic fiber at the desired length and broken by pulling. During optic fiber testing, light output should not decrease more than 70% to the original light intensity output coming from the light source.

2.4 Stereotaxic surgery

Transgenic mice containing Cre recombinase in parvalbumin expressing cells, were used in the experiment. Firstly, animals were weighed and placed in the anesthesia chamber. An oxygen pressure meter was set to 1 l/min and anesthesia was induced by 5% (isoflurane). After sedation anesthesia was reduced to 1.5-2%. Five minutes later, the mouse was transferred to the stereotaxic frame where it was maintained on the heating pad (RS Components). The head was shaved, and eye lubricant was applied to the eyes, to prevent corneal dehydration. Hair removal cream was used to remove the fur from the head. In order to minimize the risk of infection, the surgical area was wiped with betadine. Lidocaine (50 µl) was applied to the incision area. The incision was made using scissors. The skin was pulled to ensure a large working

surgical area. To clean the skull ethanol (100%) and hydrogen peroxidase (3%) were used. The dorsoventral coordinates of Bregma and Lambda were measured in order to establish proper skull position. Screws used for EEG recording were placed in the

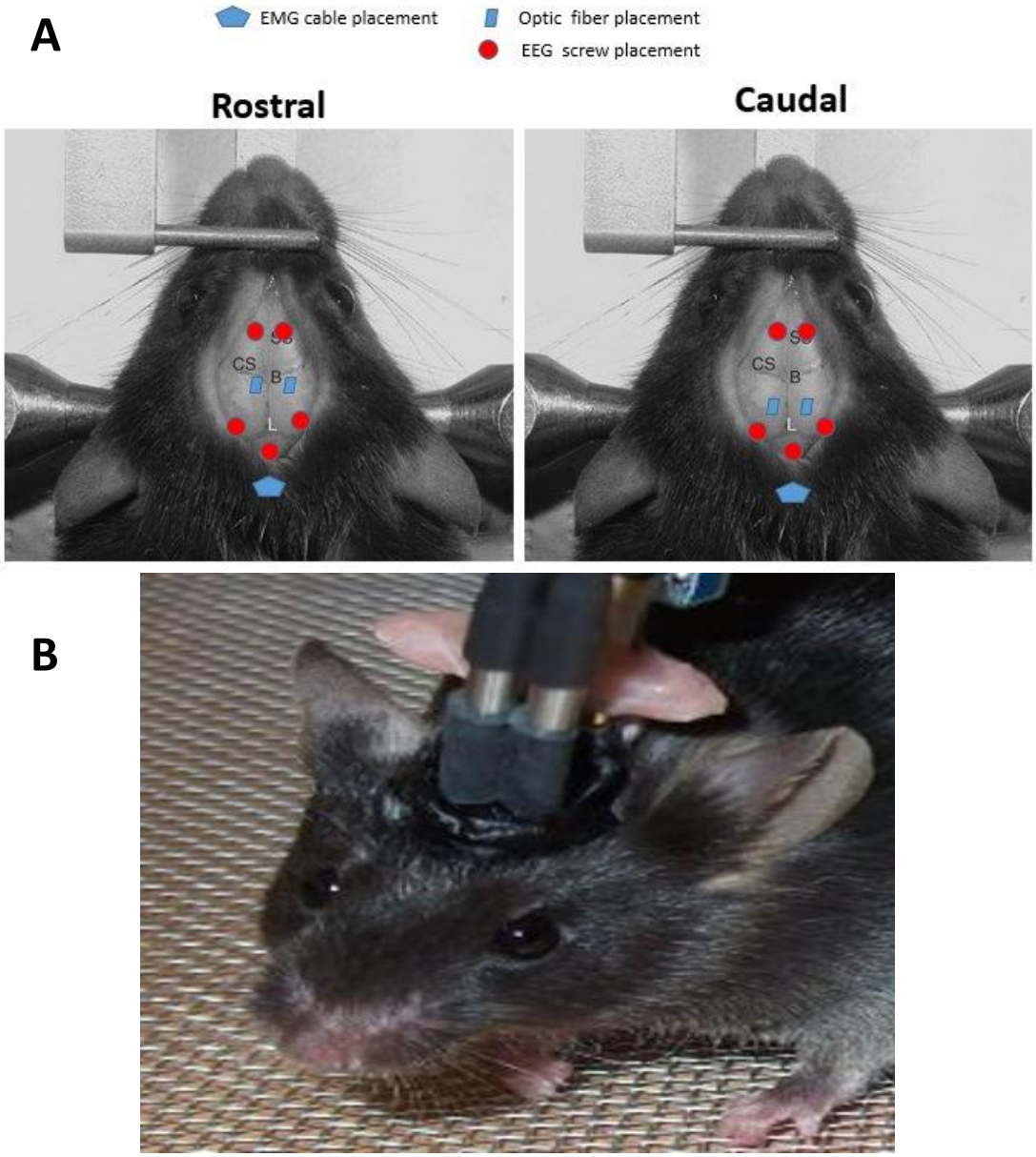

Figure 2.2 A Location of the sites used for EEG screws, EMG cable and optic probe implantation in the rostrally and caudally injected mice. Skull screws (red circles) were placed in the frontal cortex, auditory cortex and cerebellum. EMG cable (blue pentagon) were placed in the neck muscle of the mouse. Optic fibers (blue rectangles) were placed rostrally (AP: -0.8 mm) in the rostrally injected mice and caudally (AP: -1.6 mm) in the caudally injected mice. **B** Post surgery mouse with connected optic fibers and EEG/EMG cables. Stimulation light did not propagate through colored cement and light leaking between optic fiber and optic probe connection were covered with black rubber ferrules. B – bregma, L – lambda, CS – central suture.

frontal (anteroposterior (AP): + 2.00 mm; mediolateral (ML): 1 mm) and parietal (AP: - 3.00; ML: 4 mm) parts of the skull. A ground screw was fixed in the cerebellum area. The screws were wired to the connectors which were fixed to the skull later using dental cement. The EMG wire soldered to the connector was placed in the neck muscle. Appropriate coordinates for virus injection were marked with a pencil on the skull and drilled until the dura as reached. The dura was pierced using 25-gauge needle. Coordinates used for rostral TRN targeting (AP: -0.8 mm; ML: 1.4 mm) dorsoventral (DV): 3.8/3.5/3.2 mm) and caudal TRN targeting (AP: -1.6; ML: 1.4; DV: 3.8/3.5/3.2 mm; See Figure 2.2). A pipette filled with virus was lowered at the rate of 500-1000 µm/min. The virus was injected at the rate of 25-50 nl per minute using Nanoliter (WPI). The virus injection was performed in three coordinates of dorsoventral axis. After each injection, the pipette remained in the brains at least for 5 minutes to ensure diffusion into the target area. Then two optic fiber implants were placed in the brain at the depth of 2.7 mm. Kwik-Sil (WPI) was used to cover an interface between open brain area and the skull. Then, the dental cement was applied in order to hold the optic fiber implants stable. Several layers of super glue were applied to make stronger connection between fiber and dental cement. To cover the light propagation through pink cement, several layers of the cement mixed with black ink were applied. After the cement application, the skin around the incision was wiped with betadine and then washed with autoclaved saline. Anesthesia was withdrawn, and the mouse was removed from the stereotaxic frame. Dust caps were fitted on the fiber implants. Lastly, 50 µl of buprenorphine was subcutaneously injected. The mouse remained on the heating pad until it showed signs of recovery from anesthesia. After surgery, the mouse was transferred to the special recovery cage with soft food. After a 24 hours period the animal was returned to the old cage with other mice.

2.5 Optical stimulation

All photostimulation experiments were conducted bilaterally. archaerhodopsin/halorhodopsin expressing neurons were activated using Plexon LED Modules (Plexon, USA) with a wavelength of 525 nm (green). Control of the light pulse trains were carried by USB-6210 (National Instruments) connected to the PlexBright LD-1 Single Channel LED Driver (Plexon, USA). Signal for the light pulse train was programmed with LabVIEW software (National Instruments). The light intensity at the tip of the optic fiber was ~ 3 mW for all recordings. Simulations for the transmission of light through tissue were performed using the calculator developed by the Deisseroth lab (http://web.stanford.edu/group/dlab/cgi-bin/graph/chart.php). Stimulation protocol was cyclic and consisted of 30 seconds of tonic light stimulation followed by 60-90 seconds of no light stimulation. Light intensity was maintained at constant levels throughout a single 30 s period.

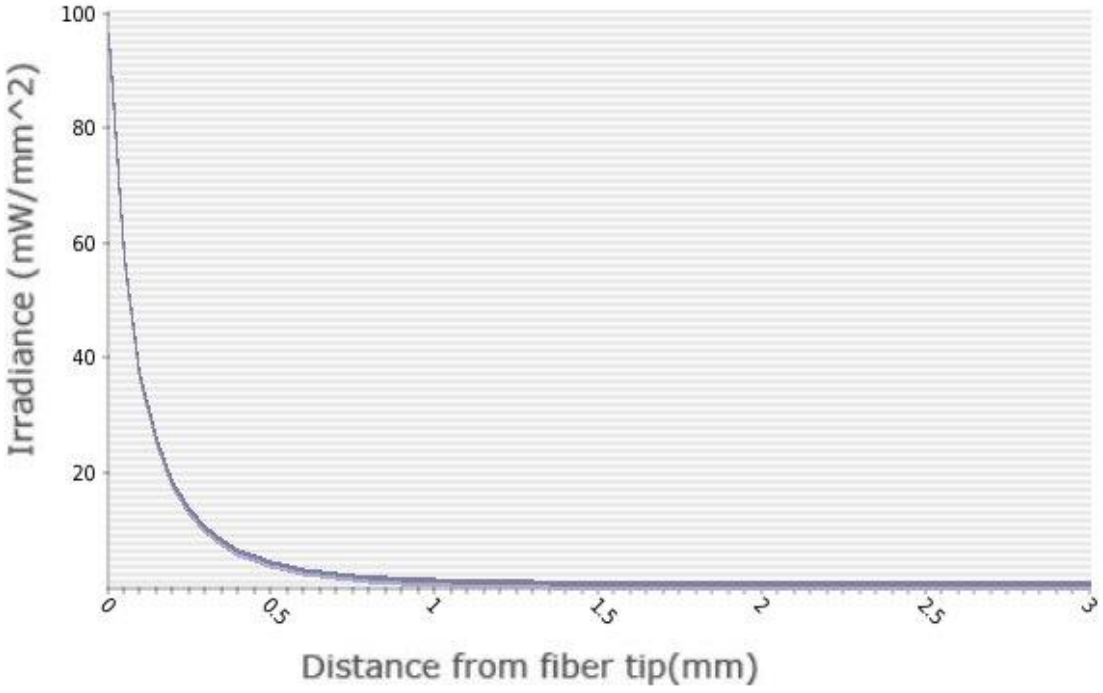

Figure 2.3 Relationship between irradiance level and the distance from fiber tip. Light wavelength = 560 nm. Fiber numerical aperture (NA) = 0.39. Light power from fiber tip = 3 mW. Fiber core radius = 0.1 mm. Irradiance at the tip of the fiber = 95 mW/mm^2. Irradiance at 0.5 mm depth = 3.9 mW/mm^2. Irradiance at 0.9 mm depth = 1 mW/mm^2. Graph generated in http://web.stanford.edu/group/dlab/cgi-bin/graph/chart.php

Halorhodopsin light stimulation had gradual ramping of the light intensity at the end of the signal, to exclude electrophysiological artifact induced by chloride pump after sharp deactivation. Recording sessions were limited to no more than 60 stimulation trials to prevent habituation effects. Below, technical details are described and considered with respect to the characterization of inhibitory opsins, heating effects and light propagation inside the brain.

2.5.1 Archaerhodopsin characterization

According to Chow et al., (2010) archaerhodopsin (Arch) enables near 100% silence of the neurons. Working wavelength: yellow-green light (590-520 nm). Activation kinetics (light on): 8.8 ± 1.8 ms. Deactivation kinetics during light cessation 19.3 ± 2.9 ms. Under continuous 15 seconds illumination photocurrent declines to 70 % of starting illumination and requires at least a minute to recover to fully.

Neurons got back up system which allows them to deal with excessive silencing, therefore Arch is safe to use. Within one second of green light illumination, intracellular pH changed from 7.31 to 7.43, plateauing rapidly. After 60 seconds of illumination pH increased till 7.46. Observed changes in pH are comparable to ChR2 neurons during illumination. Arch expression itself did not affect resting potential, membrane capacitance and resistance of the neurons. In vivo illumination of Arch expressed neurons can decrease spiking rate at least by 95 % with latency of onset near to 0 ms and with recovery latency of 0.3 ± 0.5 ms.

2.5.2 Halorhodopsin characterization

Working wavelength: yellow light. During light activation Halorhodopsin pumps Cl^- ions inside the cell and produce current of 88.7 ± 32.8 pA, which is capable to hyperpolarise hippocampal neurons by 32.9 ± 14.4 mV (Han & Boyden, 2007). Current deactivation and activation kinetics are ~ 10-15 ms, whereas neuronal voltage onset and offset times are 68 ± 57 ms and 73± 39 ms, respectively. Light intensity of 21.7 mW/mm^2 capable to inhibit 98.2 ± 3.7 % of the spikes (Zhang et al., 2007). NpHR is structurally similar to ChR2 and is well tolerated by mammalian cells. Resting membrane resistance of the neurons are not affected by expression of the Halo. Yellow light activated opsin activity seems to be compromised during longer

activation. After 15 second continuous light stimulation the photocurrent declines to 70% of starting value prior to stimulation, due to entering into inactivation phase. A brief pulse of blue light can restore Halo to its active state. A few years after the discovery of NpHR, its photocurrent was increased by enhanced expression (eNpHR) on the cell membrane (Gradinaru et al., 2008).

2.5.3 Heat as a byproduct of optical stimulation

Richard Fork, using blue laser beam decades before optogenetics birth, stimulated neurons of the marine mollusc Aplysia californica (Fork, 1971). In his case, neuronal firing occurred as a rebound to turning the laser beam off, whereas an addition of ouabain to the bath synchronized neuronal firing with laser application. Laser appeared to "cause the changes through some mechanism other than damage".

Later, it became clear that temperature changes induced by light stimulations are sufficient to alter both neural and hemodynamic activity (Liao et al., 2013; Rabbitt et al., 2016) . It is well known, that temperature has an effect on synaptic transmission, action potentials and axonal conductance (Yu et al., 2012) . Lowering temperature *in vitro* results in increased membrane resistance, slower and reshaped action potentials, due to altered ion channel activity and showed ability of neurons to buffer $Ca2^{+}$ (Thompson et al., 1985; Volgushev et al., 2000). Conversely, the

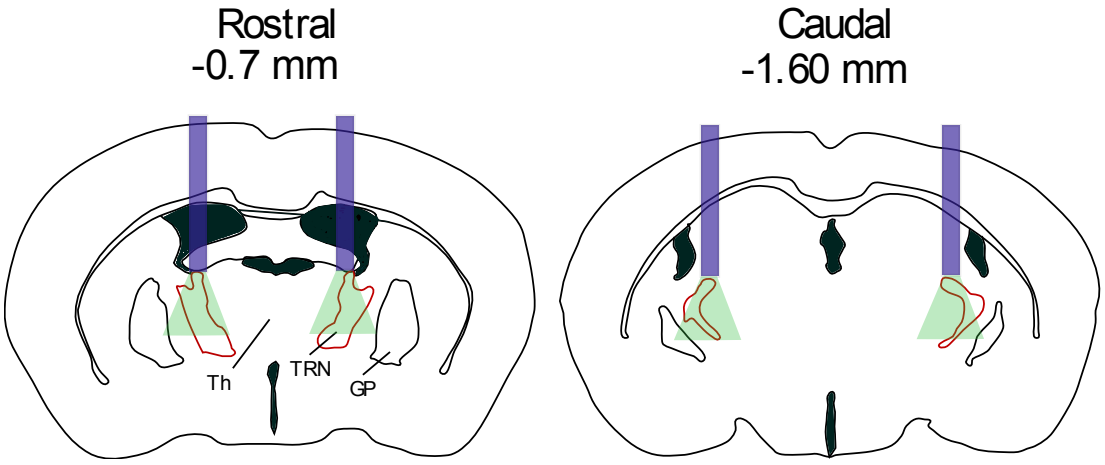

Figure 2.4 Modeling of the light spread over 1 mm depth. Left, the light spread in the rostrally targeted TRN (AP coordinates = -0.7 mm). Right, the light spread in the caudally inhibited TRN (AP coordinates = - 1.6 mm). Globus pallidus neurons received almost no light. Irradiance level reached 1 mm depth was close to 0.75 mW/mm^2.

temperature rise *in vitro* reduces membrane resistance, depolarise, the membrane and causes spontaneous action potentials (Kim & Mccormick, 1998).

The same rules apply to *in vivo* experiments. Light produced tissue heating to cause physiological (Moser, 1993) and behavioural (Long & Fee, 2008) effects. As previously mentioned, heat from a strong laser alone can cause neuronal cells to fire (Fork, 1971). In addition, the metal recording electrode heated with strong laser light is capable to activate neurons without opsins (Han, 2012). Therefore, all in vivo optogenetic experiments require control experiments, where all methodological steps including illumination conditions are repeated, excluding opsin expression. Nonetheless, whenever possible, the light power should be limited to the safe physiological levels.

In general, heat effect on neurons is still a mysterious field and accepted levels of light powers used in optogenetics are still questionable. According to Han (2012), few hundred mW/mm^2 of irradiance or few mW at the optic fiber tip are not supposed to produce detrimental damaging effects. Whereas (Stujenske et al., 2015) modelling and experimental data suggests, that the tissue, which is 400 µm below the optic fiber, will experience a steady build up temperature at continuous 10 mW stimulation over 60 seconds, with a plateau at an average increase of 2.2^{o} C (532 nm wavelength) . Stimulation power reduction to 5 mW and 1 mW would result in a decrease of peak temperature to 1^{o} C and 0.2^{o} C, respectively. Interestingly, that at mentioned tissue depth, 80% temperature change is reached within 5 s of light onset and 90% of it in 14 seconds.

As mentioned previously, temperature produced during the optogenetic experiments can significantly affect neuronal firing rate (Reig et al., 2010). At a depth of 400 µm, commonly used intensities of 5mW and 10 mW light illumination are able to increase firing rates above 30% and 40% of basal level, respectively. Generally, the light illumination capable of increasing the temperature to > 1^{o} C, leading to a substantial increase in neuronal firing. that the heating effect on the neuronal firing is . However, Gordon claimed, that the the heat suseptibility of the neuronal cells

depends of the brain state. Neuronal firing rate during resting state were strongly dependant of light intensity, whereas neuronal firing of the another mice, engaged in a prefrontal-dependent spatial working memory task in their previous study, did not corellate with light intensity (Spellman et al., 2015). Though, state dependance cannot be excluded. Overall, the temperature induced during optogenetic stimulation seems to have an effect on neuronal firing and during long continuous stimulation the light power should be kept at 1-3 mW.

Low power stimulation would lead to low volume propagation, which is undesirable during illumination of various brain areas. In order to overcome heating issues and the same time to be able to stimulate deeply located areas, a few additional steps should be taken. Firstly, large diameter fibers are less likely to produce temperature triggered artefacts without substantial difference in the illumination volume (Stujenske et al., 2015). Secondly,a lower NA (numeric aperture) of the fiber would lead to a more focused narrower light beam, which would propagate to the deeper structures. Lastly, dynamic light delivery is an effective strategy to reduce heating, while achieving volumetric coverage of high light intensities (Znamenskiy & Zador, 2013). For example, a 1ms light pulse of 50 mW presented every 10 ms (duty cycle of 10%) would produce as much heating as continuous 1 ms pulse of 5 mW (Znamenskiy & Zador, 2013).

The number of studies trying to understand heat effects on neuronal activity *in vivo* is limited, whereas optogenetic research is showing exponential growth. That imbalance can significantly reduce the quality of upcoming optogenetic studies. Light produced heating does have significant effect on neuronal firing, and it is imperative to dissociate heat stimulation from optogenetical stimulation.

2.5.4 Light propagation inside the brain

According to *in vitro* work, blue light intensity should be > 1 mW/mm^2 to achieve spiking in ChR2 expressing cells (Zhang & Oertner, 2007; Boyden et al., 2005b; Li et al., 2005). For that reason, knowledge related to light transmission in the brain is also vital for successful optogenetic experiments *in vivo*. The Diesseroth group found that

total transmitted light power was reduced by 50% after passing through 100 µm of cortical tissue and by 90% at 1 mm depth (Aravanis et al., 2007). The conical spread of light, determined by numeric aperture of the fiber (NA), decrease a light intensity. In addition to that the reduction is caused by absorption and scattering. For example, NA of 0.39 would spread the light with conical angle at about 34^{o}. The findings led Diesseroth group to the conclusion, that at known ChR2 activation intensity, a light intensity of 20 mW would be capable to evoke spiking at about of 1.4 mm depth in vivo. We also modelled the light spread over 1 mm depth (See figure 2.3).

2.6 Electrophysiology

After four weeks required for virus expression, the mice were transferred daily to the recording chamber to acclimate. Recording chambers consisted of the plastic, black box inserted in the custom-made Faraday cage. During the habituation session, a mouse was connected to the EEG-EMG cable. Cables were flexible and the mouse was able to move around the recording chamber. Each chamber contained material for nest building. The recording chamber was located inside a grounded faraday cage to minimize electrical noise. Electrophysiological recording sessions lasted on average 2 hours. The connectors on the skull were connected through a custom-made adaptor to an Intan Technologies amplifier RHD 2132 board which amplified 1000 times the signal incoming from the brain. The amplified signal was sent to the Intan evaluation board where it was further processed. RHD2000 Interface software installed on the computer was used to monitor and store recorded EEG/EMG signals. The EEG and EMG data was acquired with 1 kHz sampling rate.

Data analysis

2.6.1 Sleep state classification

All data was analysied in the ofline environment. Intan provided MATLAB function, which converted Intan files into MATLAB files. Behavioral states were characterized before EEG analysis. We classified EEG traces into two states: wake and sleep (majority of which was expected to consist of slow-wave-sleep) using EMG recording. Sleep scoring algorithm was adopted from Halassa et al. (2014). EMG data were filtered from 60 – 200 Hz and threshold were applied (See Figure 2.5). The algorithm,

by going through the EEG/EMG data in 5 seconds steps, detected brain state for each step. Minimum criteria for wake and sleep was at least 10 seconds. Threshold was detected by visual examination and was identical (3) to the threshold used by the Halassa et al. (2014) The wake trace was identified by higher value than the threshold and sleep trace had lower values than imposed EMG threshold. Visual inspection was used to discard putative sleeping trials with low slow/delta oscillation, non-characteristic for slow wave oscillation. Proportionally, a small number of the time segments not related to sleep or wake states were not used in the analysis. A small number of animals (2-3) with noisy EEG had problem with brain state characterization. The sleep scoring was done in a semiautomatic way using custom-written MATLAB algorithms.

2.6.2 Spectral EEG analysis

Before spectral analysis each trace was filtered from the artifacts. If the EEG trace contained a peak higher or lower than 800 μV, it was discarded. Spectrum analysis was computed similarly. Spectra was computed for each EEG trace with the Chronux toolbox (http://chronux.org/) using 19 tapers over 5 or 10 second windows. Mean spectra were computed by averaging all single trial spectra. Mean spectrograms were computed by averaging single trial spectrograms with 5 tapers in 5 seconds sliding window with 1 second steps.

2.6.3 Statistical analysis

In order to assess the effects of optogenetic stimulation on brain oscillations, each trial data from a 5-10 sec period of stimulation was compared to that of 5-10 sec pre-stimulation for each experimental group using Student's paired *t*-test.

To compare differences between animal groups (Archaerhodopsin, Halorhodopsin and Controls (YFP)), two-sample t-test, ANOVA and effect size measurement with confidence intervals were employed. Measure effect size computed using MATLAB was useful to quantify the difference between two groups and it is not dependent on sample size as other employed statistical tests. The averaged differences of the oscillation caused by the TRN light stimulation for each animal was used in Chapter 3.

2.6.4 Sleep/wake cycle analysis

To quantify the effect of the green light stimulation on the sleep/wake cycle two terms were used: latency and the ratio of wake/sleep. The latency is a period from light stimulation starting point untill the brain state change. The ratio of short sleep was calculated the following way: the number of stimulation trial with sleep episodes shorter than 80 seconds were divided on sum of the trial numbers with short (< 80 sec) and long (> 80 sec) sleeping episodes.

2.7 Immunohistochemistry

Perfusion. To reach terminal anesthesia pentobarbital/lidocaine mixture (50/50) was injected intraperitoneally. After complete loss of reflexes, the mouse was attached to a board and the ribcage was opened. It was intracardially perfused using 25 ml of PBS and 25 ml 4% PFA. Brains were removed and placed in the 4% PFA for 24 hours. On the next day the brains were moved to a 30% sucrose in PBS for at least 48 hours before sectioning.

Slicing and staining. Sucrose cryoprotected brains were placed in the microtome Leica where they were frozen using dry ice. The brains were cut into 50 µm sections and placed in wells filled with PBS. After 3 washes (10 minutes each) with PBS the incubation was performed at room temperature in PBS containing 0.3% Triton X-100 and 1-2% normal donkey serum (PBSX solution). Primary antibody against PV (P-3088; Sigma) was diluted at 1/2500 with PBSX solution and applied to brain slices. Well plates were left on the shaker overnight. After several washes with PBS, the sections were incubated for 2-4 hours with a mixture of secondary antibody (Alexa Fluor 594; A-11005; Invitrogen; 1:200) with PBSX solution. Sections were mounted on the glass slides covered by Vectashield Hard Set (Vector Labs) and a cover slip placed on them.

Microscopy. The sections were observed using an upright epifluorescent microscope (Nikon, Eclipse E600). The digital images were captured using MetaMorph.

Quantification of virus spread. As expected parvalbumin-positive neurons were expressed all over the TRN. Although, the rostrally injected virus had expression

mostly in the rostral and middle part of the TRN, and vice versa the caudally injected virus was expressed only in the caudal and middle part of the TRN. The opsin expression diagrams were used to summarize opsin expression in the caudally and rostrally injected animal groups (Archaerhodopsin, Halorhodopsin and Control) (See figures 2.6 – 2.9). Pictures and diagrams of the TRN from single animals used in the construction of the summary diagrams can be found in the Appendix (See figures 8.1 – 8.25).

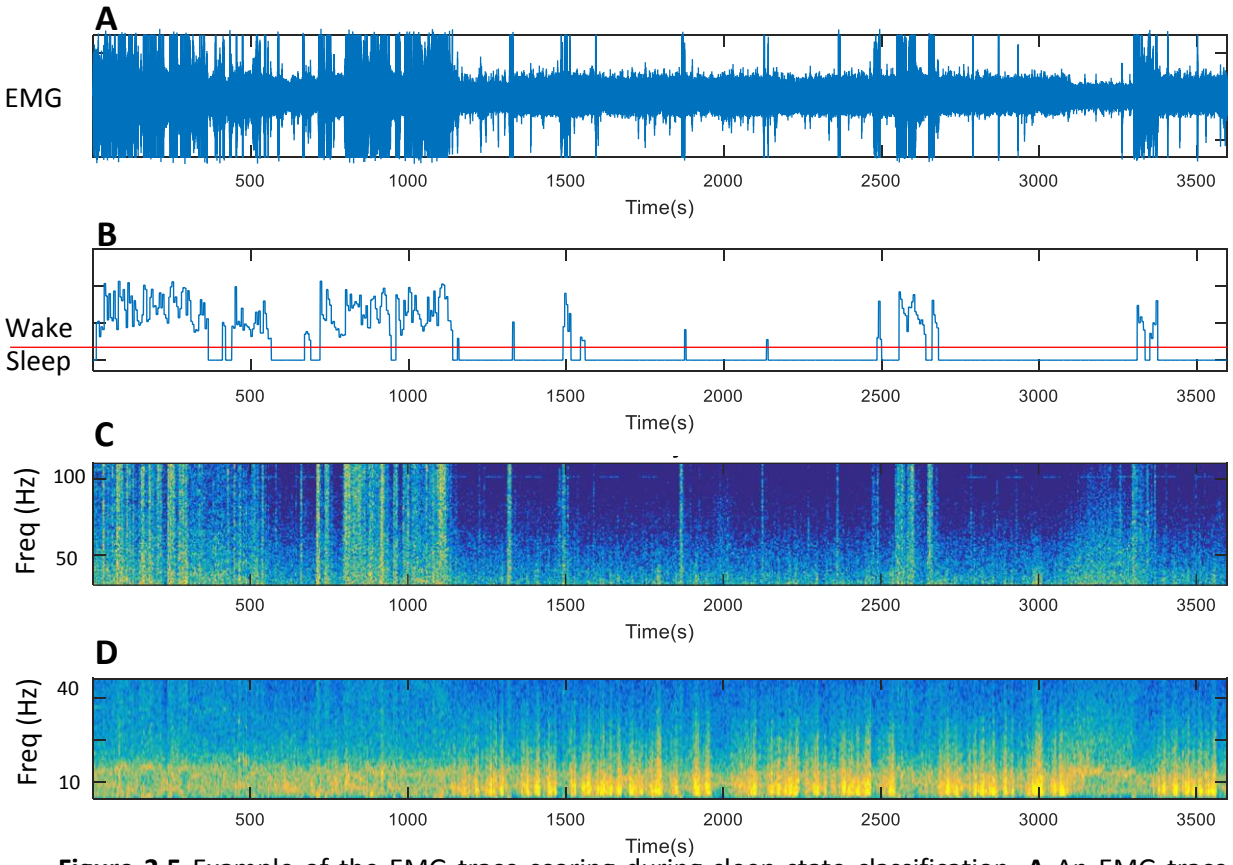

Figure 2.5 Example of the EMG trace scoring during sleep state classification. **A** An EMG trace recorded during one of the session from a freely moving mouse. **B** The EMG trace after 60 – 200 Hz filtration and threshold application. The red line is used only for demonstration purpose. The algorithm used for sleep scoring is explained above. **C** Low frequency spectrogram (0 – 40 Hz). **D** High frequency spectrogram (40 – 100 Hz).

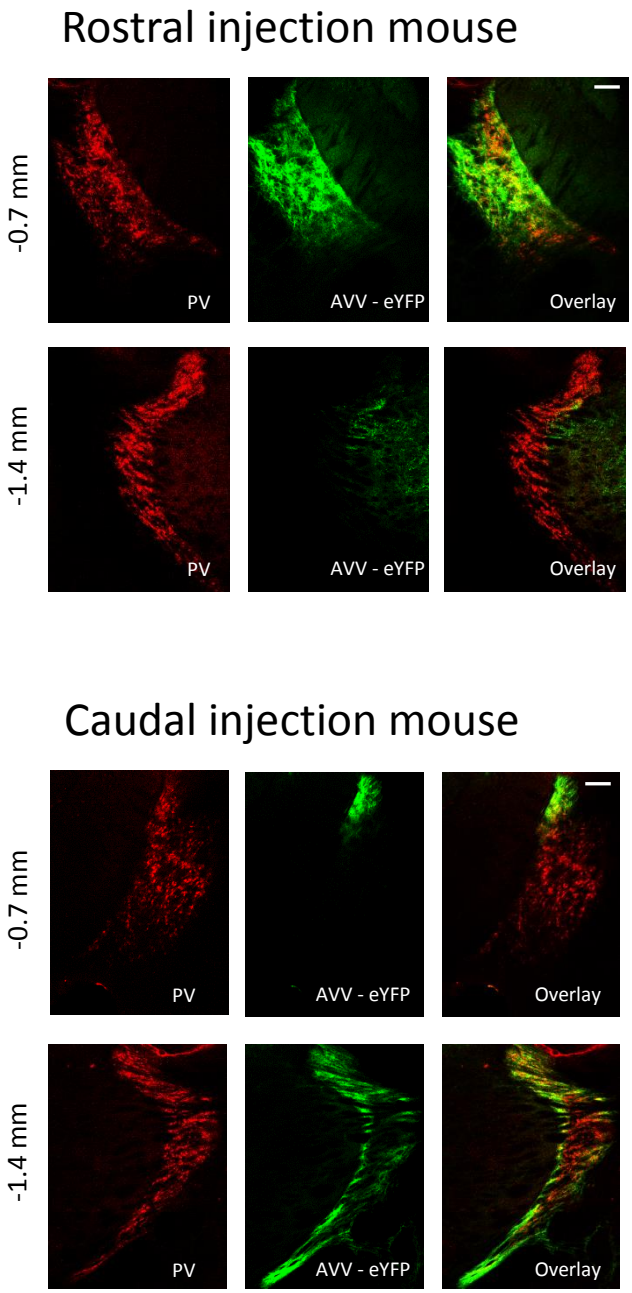

Figure 2.6 Expression pattern of Arch-FYP after bilateral rostral or caudal injection of AAV in mice. Photograph of PV (parvalbumin, red) and eYFP (green) expression in the rostral (top) and caudal (bottom) TRN. Scale bar, 250 µm.

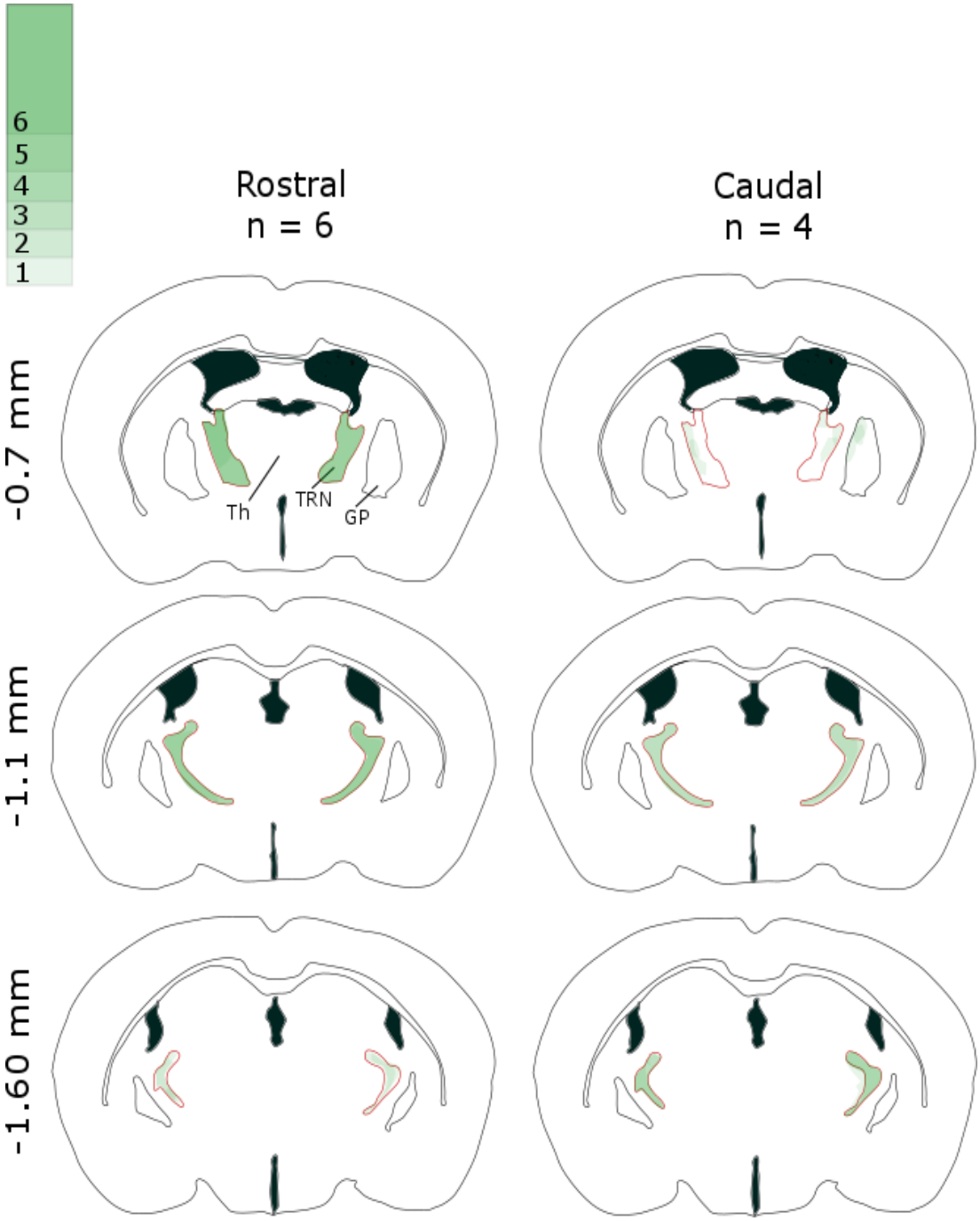

Figure 2.7 Summary diagram of the halorhodopsin expression pattern in the caudally and rostrally injected mice. Schematic drawings of coronal sections at three anteroposterior coordinates. The virus expression is marked by green shading. Virus expression in the same area for several animals is shown in darker green colour. Colour bar on the left top corner explains the relationship between the darker shading and the number of animals with coexpressed areas. In most of the animals the rostral virus injection expressed halorhodopsin in the rostral and middle part of the TRN, and the caudal virus injection expressed opsin in the caudal and middle part of the TRN. The red boundary highlights the TRN. Th – thalamus, GP – globus pallidus.

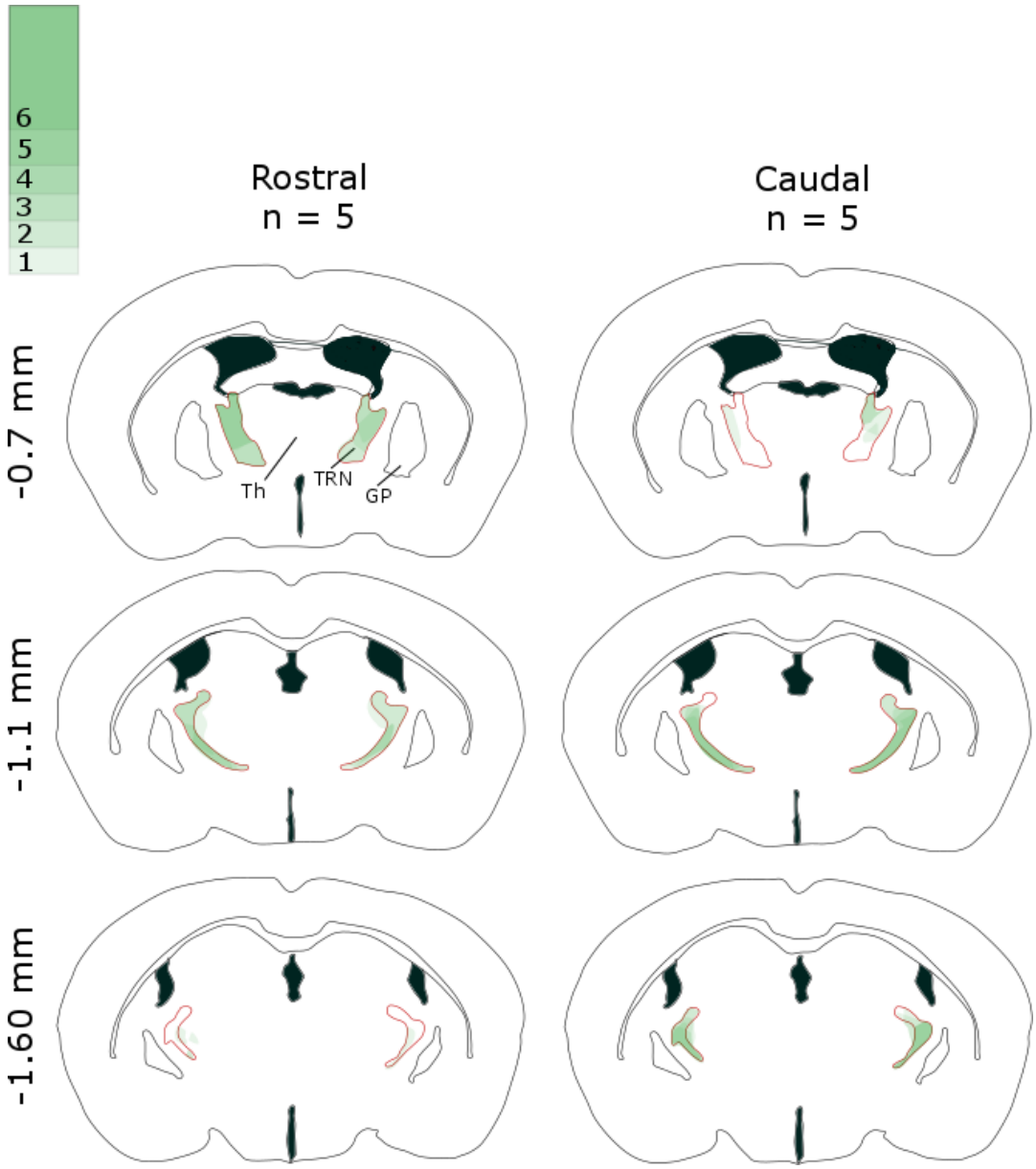

Figure 2.8 Summary diagram of the archaerhodopsin expression pattern in the caudally and rostrally injected mice. Schematic drawings of coronal sections at three anteroposterior coordinates. The virus expression is marked by green shading. Virus expression in the same area for several animals is shown in darker green colour. Colour bar on the left top corner explains the relationship between the darker shading and the number of animals with coexpressed areas. In most of the mice the rostral virus injection expressed archaerhodopsin in the rostral and middle part of the TRN, and caudal virus injection expressed opsin in the caudal and middle part of the TRN. The red boundary highlights the TRN. Th – thalamus, GP – globus pallidus.

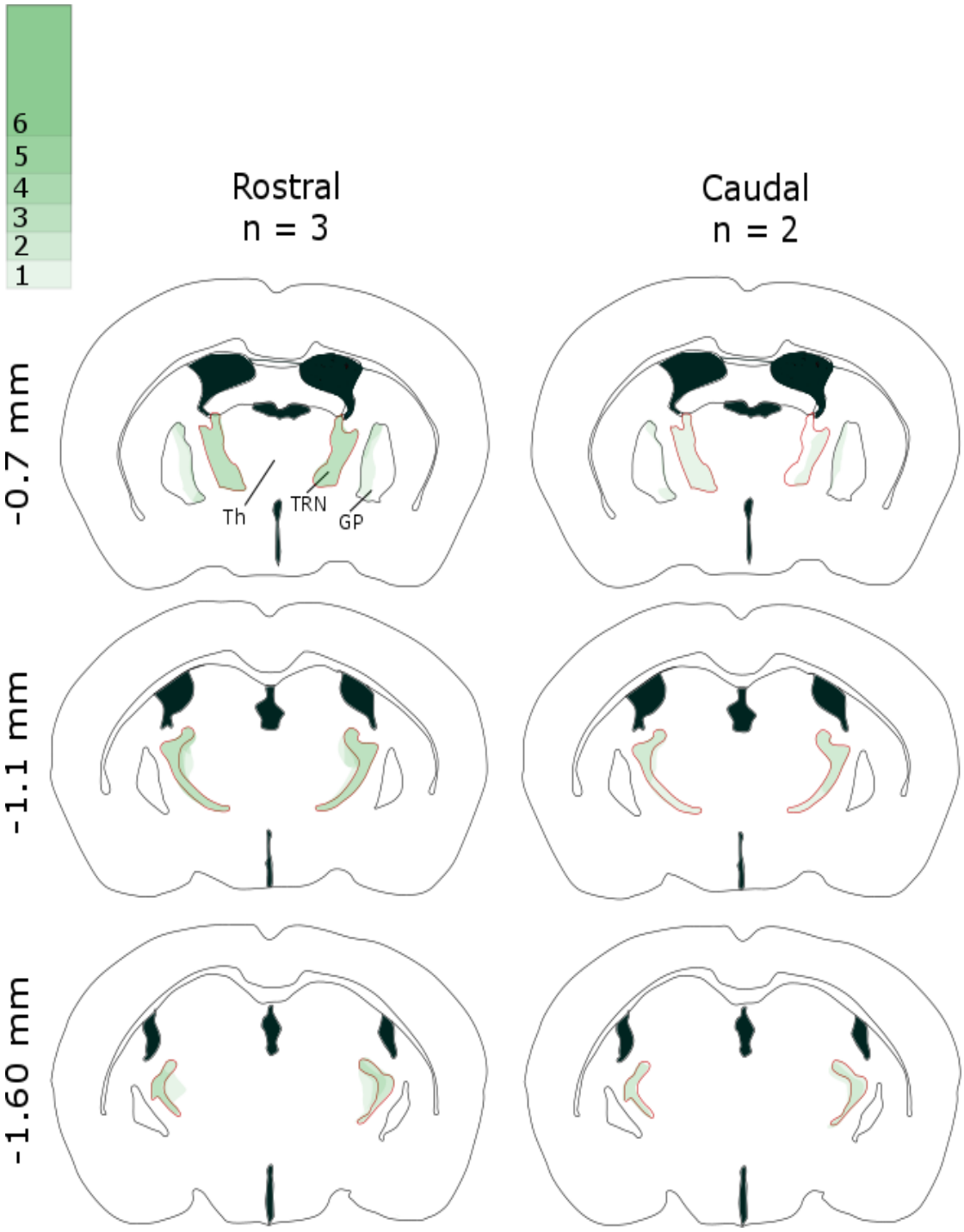

Figure 2.9 Summary diagram of the YFP (Control) expression pattern in the caudally and rostrally injected mice. Schematic drawings of coronal sections at three anteroposterior coordinates. The virus expression is marked by green shading. Virus expression in the same area for several animals is shown in darker green colour. Colour bar on the left top corner explains the relationship between the darker shading and the number of animals with coexpressed areas. The rostral and caudal virus injection expressed YFP in the all part of the TRN. The red boundary highlights the TRN. Th – thalamus, GP – globus pallidus.

Chapter 3: Differential effect of rostral and caudal optogenetic inhibition of the TRN upon EEG oscillation.

3.1 Introduction

Virtually all sensory information from the outside world propagates to the cortex through the thalamus (Jones, 1985), and this is considered important in our perceptual experiences. Nevertheless, perception is not simply based on the propagation of signals encoded from external stimuli. Distinct cortical processing modes are crucial for functional connection between the thalamus and the cortex (Zagha & McCormick, 2014). Internally generated brain states by exploiting identical neuronal networks can facilitate vigilance or disconnect brains from the outside world. Vigilance states, such as arousal, attention and rapid eye movement (REM) sleep are characterized by desynchronized neuronal activity (Saper et al., 2011; Harris & Thiele, 2011). In contrast, during non-rapid eye movement (NREM) sleep and under anesthesia, large populations of cortical neurons fire in a synchronous mode, but do not transmit sensory information and, are putatively, involved in consolidation of memory functions (Steriadeet al., 1993a; Contreras & Steriade, 1996b; Sirota & Buzsáki, 2005).

The electroencephalogram (EEG) of the mammalian brain during NREM sleep is characterized by a few dominant oscillations: slow wave (< 1Hz), delta oscillation (1-4 Hz) and spindles (11 -15 Hz) (Steriade, 1994a). Slow wave oscillations reflect slow and synchronous changes of membrane potential in cortical neurons that shift between depolarized (UP) and hyperpolarized (DOWN) states. Apart from slow wave oscillations, which presumably, originate from cortical neurons (Sakata & Harris, 2009; Sanchez-Vives & McCormick, 2000; Timofeev & Chauvette, 2011), delta oscillation and sleep spindles are orchestrated by thalamocortical (TC), corticothalamic (CT) and thalamic reticular (TRN) neurons (David et al., 2013).

The thalamic reticular nucleus is a non-characteristic nucleus of the thalamus, with two unusual features: it does not propagate signals directly to the cortex (Jones, 1975), and it contains inhibitory (GABA) neurons, which send inhibitory feedback to all nuclei of the dorsal thalamus (Pinault, 2004). It has been hypothesized that this

strategic location allows it to act as a 'gatekeeper' and control/modulate the upcoming thalamic inputs to the cortex (Crick, 1984).

The TRN neurons as a consequence of the high expression of T-type (Albéri et al., 2013), small-conductance (SK)-type (Pape et al., 2004), Kv3 channels (Espinosa et al., 2008) and possession of modulatory afferents from the locus coeruleus (Morrison & Foote, 1986; Funke & Eysel, 1993), basal forebrain (Bickford et al., 1994; Ni et al., 2016b), hypothalamus (Herrera et al., 2015b) and zona incertia (Cavdar et al., 2006), can bidirectionally switch excitability due to brain state change or behavioural demands. Therefore, neurons in the TRN can discharge action potentials in two distinct modes (Bal & McCormick, 1993). During drowsiness and NREM sleep they fire in bursts, while during wakefulness they exhibit tonic firing (Fuentealba & Steriade, 2005). The afferents from CT and TC neuronal branches and the dense innervation of the dorsal thalamic nuclei are organized in a topographical manner allowing TRN neurons to effect state-dependent processing in distinct thalamocortical loops (Pinault & Deschênes, 1998).

The functional characteristics of the TRN are diverse. During awake states the TRN has been implicated in sensory processing (Hartings et al., 2003) and attentional gating (McAlonan, 2006; Lewis et al., 2015), whereas during sleep the TRN is thought to promote memory formation (Latchoumane et al., 2017), modulate sleep states (McCormick & Bal, 1997) and has even been implicated in consciousness (Min, 2010). Many sedative and anaesthetic drugs by acting on GABAergic synaptic transmission (Brown et al., 2015) can potentiate TRN activity and induce unconscious states (Brown et al., 2011). For further details of the role of the TRN see Chapter 1.

The features of sleep EEG waves are strongly associated with neuronal firing of the TRN cells. A subset of the TRN neurons, during bursting firing mode, generate sleep spindles (Steriade et al., 1987). Brief optogenetic activation of the TRN neurons induced artificial sleep spindles (Halassa et al., 2011). Interestingly, the density of sleep spindles correlates with the amount of NREM sleep (Kim et al., 2012).

Additionally, neurons, responsible for sleep spindle production are linked with delta oscillation (Halassa et al., 2014). Tonic activation of the TRN cells using excitatory opsin during sleep and awake states leads to the increase of delta power oscillation, whereas short tonic inhibition during sleep produce modest decrease of the delta oscillation and promotes arousal (Lewis et al., 2015; Herrera et al., 2015).

Relatively recently Halassa et al. (2011) established that the TRN nucleus consists of distinct subnetworks which are responsible for different physiological functions and levels of activity during same brain states. Differences arise due to the fact, that the thalamus can be dissociated into two types of thalamic nuclei: first order (relay) nuclei, which receive sensory information and are responsible for propagation of sensory information to the cortex, and higher order (association or limbic) nuclei, which do not deal with sensory information and act as a communicator/facilitator between corticocortical and cortico-subcortical areas (Guillery, 1995; Schmitt et al., 2017). Halassa's lab showed that TRN neurons, projecting to the sensory thalamic nucleus (lateral geniculate nucleus), behave differently to TRN neurons projecting to higher order nucleus (anterior thalamic nucleus). Sensory projecting TRN neurons during the awake state are responsible for activating (disinhibition) of modality specific corticothalamic loops, which results in attention/arousal, while during sleep the same neurons, by production of sleep spindles and modulation of slow wave activity, apparently, facilitate sensory pathway inhibition. Interestingly, the limbic projection neurons of the TRN show little activity during sleep and this may facilitate memory construction and other offline limbic processes.

Halassa argues that this type architecture of the small, but important modulatory part of the brain might be a determinant of cognitive function. Basically, the TRN by receiving conscious/unconscious orders from the cortical areas, might act as a switcher between externally stimuli and internally generated information.

Based on the thalamic/TRN nuclei tracing studies (Ohara & Lieberman, 1985; Shosaku, 1985; Thompson & Robertson, 1987; Rodrigo-Angulo & Reinoso-Suárez, 1988; Crabtree & Killackey, 1989; Velayos et al., 1989; Cornwall et al., 1990c; Hazrati

& Parent, 1991; Shibata, 1992; Lozsádi, 1994; Lozsádi, 1995; Gonzalo-Ruiz & Lieberman, 1995; Tai et al., 1995; Pinault & Deschênes, 1998a), it is evident that the sensory projecting TRN neurons are located mostly in the caudal part of the TRN, whereas the limbic (or higher order) projecting TRN neurons are found predominantly in the rostral part of the TRN. Therefore, we hypothesized that optogenetic inhibition of the caudal part during sleeping states should lead to a reduction in oscillations associated with sensory TRN neurons, namely delta oscillations and alpha oscillation (sleep spindles). Optogenetic inhibition of the rostral TRN, based on the hypothesis, should have smaller or no impact on the delta and alpha oscillation (sleep spindles). To test the hypothesis, we combined optogenetic and electrophysiological approaches in freely moving mice and investigated EEG oscillations modulated by optogenetic stimulations in different parts of the TRN.

3.2 Methods

To investigate the role of the caudal and rostral TRN neurons in sleep/wake conditions, neurons in these segments of the nucleus have to be targeted precisely. Parvalbumin expressing (PV) neurons, which are found in abundance in the TRN (up to 80%) and are absent in thalamus, can act as the differentiating factor between the TRN and other thalamic nuclei (Clemente-Perez et al., 2017). Two inhibitory opsins Halorhodopsin (NpHR), Archaerhodopsin (Arch) and YFP (Control) were expressed specifically in anterior or posterior part of the TRN in parvalbumin (PV)-Cre mice using adeno-associated viral vectors (NpHR, n = 10; Arch, n=10 and YFP (Controls), n =5). The effects of optical stimulation on cortical EEGs were assessed by delivering tonic green light (~ 3 mW) through chronically implanted optic fibers over 30 second periods in freely behaving animals. Optogenetic inhibition of the TRN neuronal activity may produce varied outcomes depending on ongoing behavioural states. Therefore, before analysis we classified behavioural epochs into two states: wake and slow-wave sleep (SWS), using simultaneously recorded EMG. Rapid eye movement (REM) sleep classification was omitted in our analysis due to negligible time spent in this state (5%-10% of sleep) (Brankačk et al., 2010). An EEG trace was included for data analysis, if the mouse remained in one of the states (SWS or wake) for 90

seconds (See Figure 3.1). Two statistical approaches were used to describe the effect of the light stimulation on the TRN. In order to assess the effects of optogenetic inhibition on brain oscillations, **each trial** data from a 5-10 sec period of stimulation was compared to that of 5-10 sec pre-stimulation for each experimental group using a student paired t test. To compare differences between viral groups and controls, ANOVA and measure effect size (MES, Hedge's *g*) with confidence intervals (CI, 95%) were employed. Averaged differences of the oscillation caused by TRN light stimulation for **each animal** was used in this analysis. For full details of the surgical and experimental methods and the location of the viral expression patterns see Chapter 2.

3.3 Results

3.3.1 Sleeping Data analysis

Delta oscillation (1-4 Hz)

EEG was recording from auditory right (AR) channel, placed in the auditory cortex and frontal right (FR) channel, placed in the frontal cortex, were used in the analysis since these recording was consistent and reliable during experiments. Tonic light stimulation (optogenetic inhibition) of the TRN in Arch and NpHR expressing animals led to a modest reduction of the delta oscillation power in all cortex areas during the first 5 seconds of stimulation as compared to pre-stimulation values (See Figure 3.2 and Figure 3.3. Arch: 316 traces; 10 mice; NpHR: 221 traces, 9 mice). In Arch animals, delta oscillation power reduction was not significant ($p = 0.10$, Student paired t-test), while the reduction of the delta oscillation in NpHR animals was relatively greater and significant ($p < 0.01$, Student paired test). The delta band power reduction in Arch and NpHR animals apparently took place only during 5 seconds of stimulation. Control animals, expressing only YFP in the different parts of the TRN, during similar light stimulation over 5 seconds showed an apparent increase in delta oscillation power compared to pre-stimulation values (See Figure 3.4. Control: 161 traces, 5 mice, p =

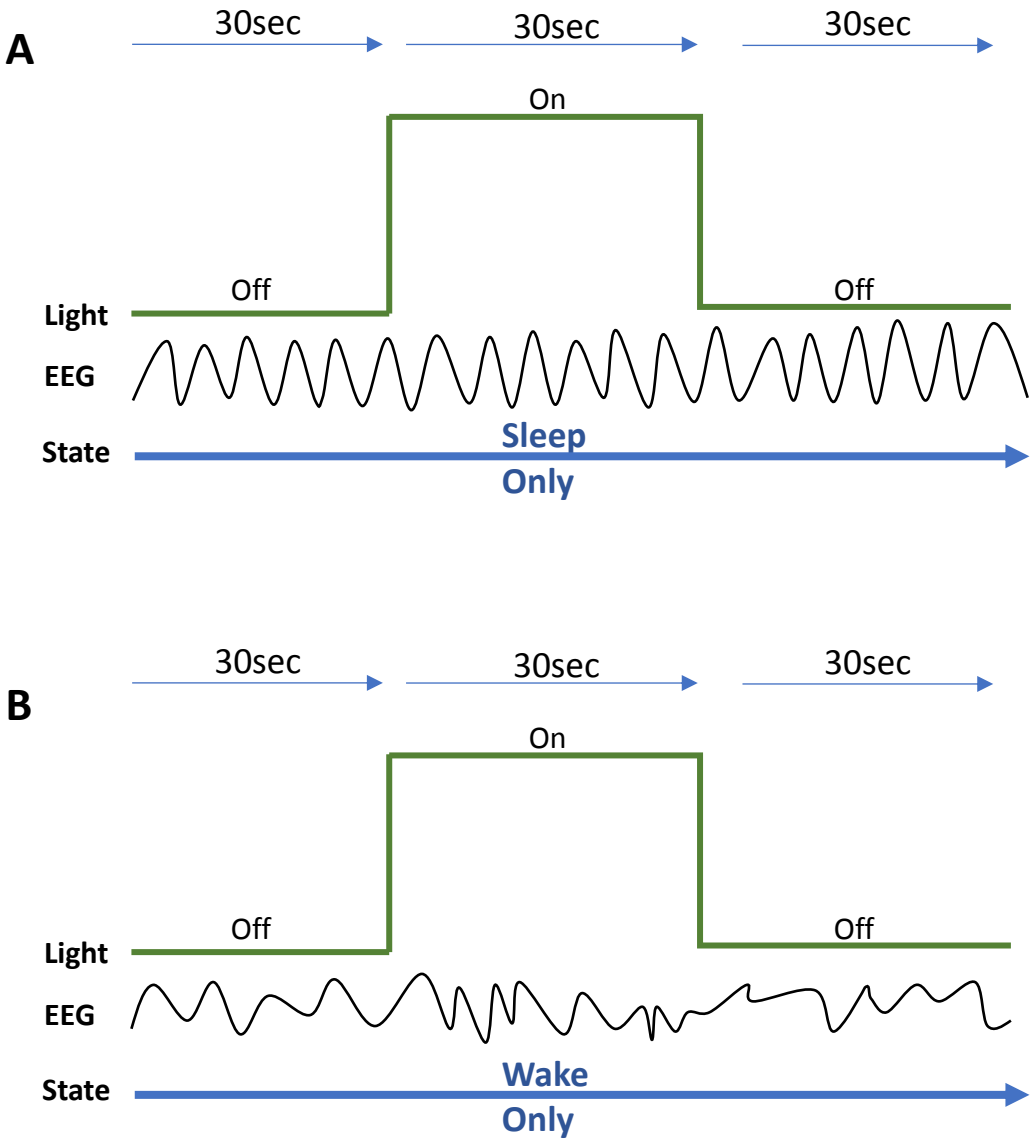

Figure 3.1 Data inclusion criteria for the analysis of results in Chapter 3. **A** Sleeping only traces. Trace was included in analysis, if animal was asleep for at least 90 seconds: 30 seconds before stimulation, 30 seconds during stimulation and 30 seconds after stimulation. **B** Wake only traces. Trace was included in analysis, if animal was awake for at least 90 seconds: 30 seconds before stimulation, 30 seconds during stimulation and 30 seconds after stimulation.

0.08, Student paired test). Nevertheless, the modest increase in delta power was maintained throughout 30 seconds of stimulation ($p < 0.01$, Student paired test. See Figure 3.4 A).

The averaged difference in delta band power of 5 seconds before and 5 seconds during stimulation was used to quantify the difference between viral groups (See Figure 3.5). A similar pattern of results was found in the recordings from AR and FR. In Arch animals, the delta power was decreased by 0.50 dB/0.59 dB (AR/FR) and in NpHR mice delta power was reduced by 0.66 dB/0.62 dB (AR/FR) (See Figure 3.5). In contrast, an equivalent stimulation in the control animals produced a modest delta power increase by 0.38 dB/ 0.32 dB (AR/FR). The delta power change in mice expressing inhibitory opsins was significantly different from control mice. Two different result sets for AR and FR channels were produced. (Results for AR channel: NpHR = 8 mice; Arch = 8 mice; Control = 5 mice. Measure effect between Arch and Control groups: Arch/measure effect size (MES) = 1.34, CI (confidence interval) = 2.57/0.11; Measure effect between NpHR and control groups: NpHR/MES = 2.17, CI = 3.56/0.77. Results of ANOVA statistics for Arch, NpHR and Control animals: ANOVA $F = 5.21$, $p = 0.016$; post-hoc Tukey HSD $p<0.05$. Identical results for frontal right channel, FR: NpHR = 9 mice; Arch = 10 mice; Control = 5 mice. Arch/MES = 1.35, CI = 2.53/0.18; NpHR/MES = 2.37, CI = 3.77/0.96; ANOVA $F = 5.51$, $p = 0.012$; post-hoc Tukey HSD $p<0.05$).

Our goal was to explore and compare the rostral and caudal neuronal activity of the TRN. All animals expressing inhibitory opsins in the rostral part of the TRN (rostral Arch and rostral NpHR mice) were combined in the Rostral group, whereas all animals with caudally expressed opsins were treated as Caudal group members. Animals expressing different inhibitory opsins with similar functions were combined to increase N number, required for ANOVA statistics (See Figure 3.6). Rostrally and caudally stimulated control animals were not dissociated for the same reason. Color coding was used to show the tendency of rostrally (red) and caudally (blue) stimulated control animals.

Using the same approach as in the distinct viral groups, the averaged change in delta band power of 5 seconds before and 5 seconds during stimulation was used to quantify the difference between the stimulated location (caudal/rostral) groups (See Figure 3.6). Caudal and rostral TNR optogenetic inhibition led to a reduction of delta oscillation. Caudally stimulated animals showed larger delta power decrease of 0.66 dB/0.67 dB (AR/FR), relative to rostrally stimulated animals 0.50dB/0.41 dB (AR/FR). In recordings from the caudal and rostral AR, the reductions in delta oscillations were significantly different from the control group. In contrast, in recordings from the FR channel, delta oscillations in the caudal but not the rostral group were different from the control group. (AR: Caudal = 8 mice; Rostral = 8 mice; Control Caudal = 2 mice, Control Rostral = 3 mice. Caudal/ MES = 1.64, CI = 2.93/0.36; Rostral/MES = 1.69, CI = 2.94/0.43. ANOVA $F = 5.22$, $p = 0.016$; post-hoc Tukey HSD $p<0.05$. FR: Caudal = 10 mice; Rostral = 10 mice; Control Caudal = 2 mice, Control Rostral = 3 mice; Caudal/ MES = 1.59, CI = 2.81/0.38; Rostral/MES = 1.32, CI = 2.50/0.15; ANOVA $F = 4.74$, $p = 0.019$; post-hoc Tukey HSD $p<0.05$).

The lack of effect in the FR channel may relate to the low n number in the rostral group. Measure effect size of the rostrally stimulated animals relatively to control animals was quite high and with positive confidence interval (MES = 1.32, CI = 2.50/0.15). There was a modest increase in delta power in both, rostrally and caudally stimulated control mice, during the first 5 second of light stimulation.

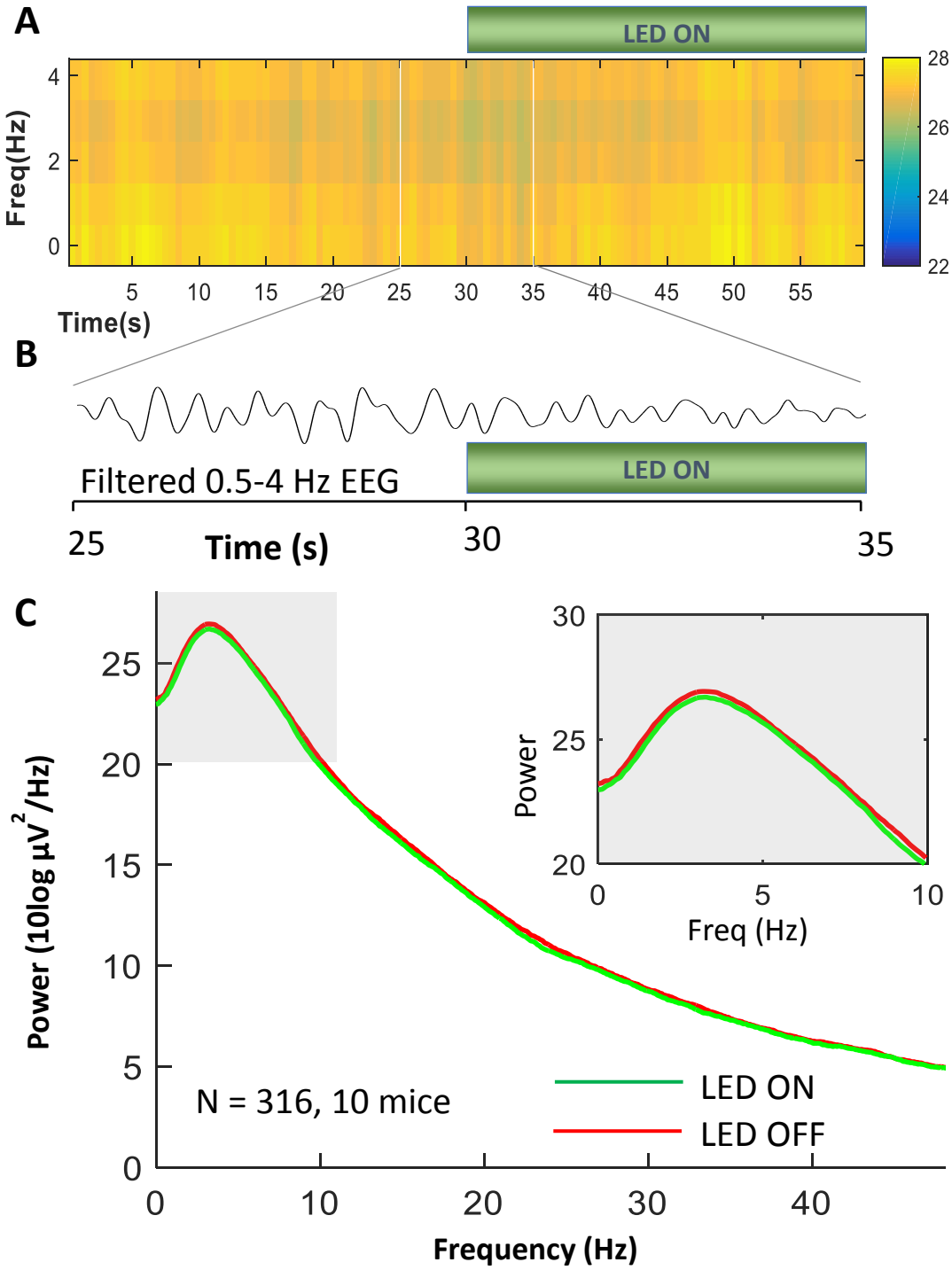

Figure 3.2 Light stimulation effect on delta oscillation in Archaerhodopsin expressing mice during sleep. **A** Mean spectrogram of 0 - 4 Hz over 60 seconds. Green bar (LED ON) portrays light stimulation, which starts at 30 seconds. **B** Magnified and 0.5-4 Hz filtered EEG trace over 10 seconds. Light stimulation starts at 30 seconds. **C** The power spectrum of 5 seconds before (red) and 5 seconds during (green) light stimulation. Delta power was reduced slightly but not significantly during light activation over 5 seconds (N = 316, 10 mice, p= 0.10; Student paired test. Frontal right channel (FR) was used for analysis).

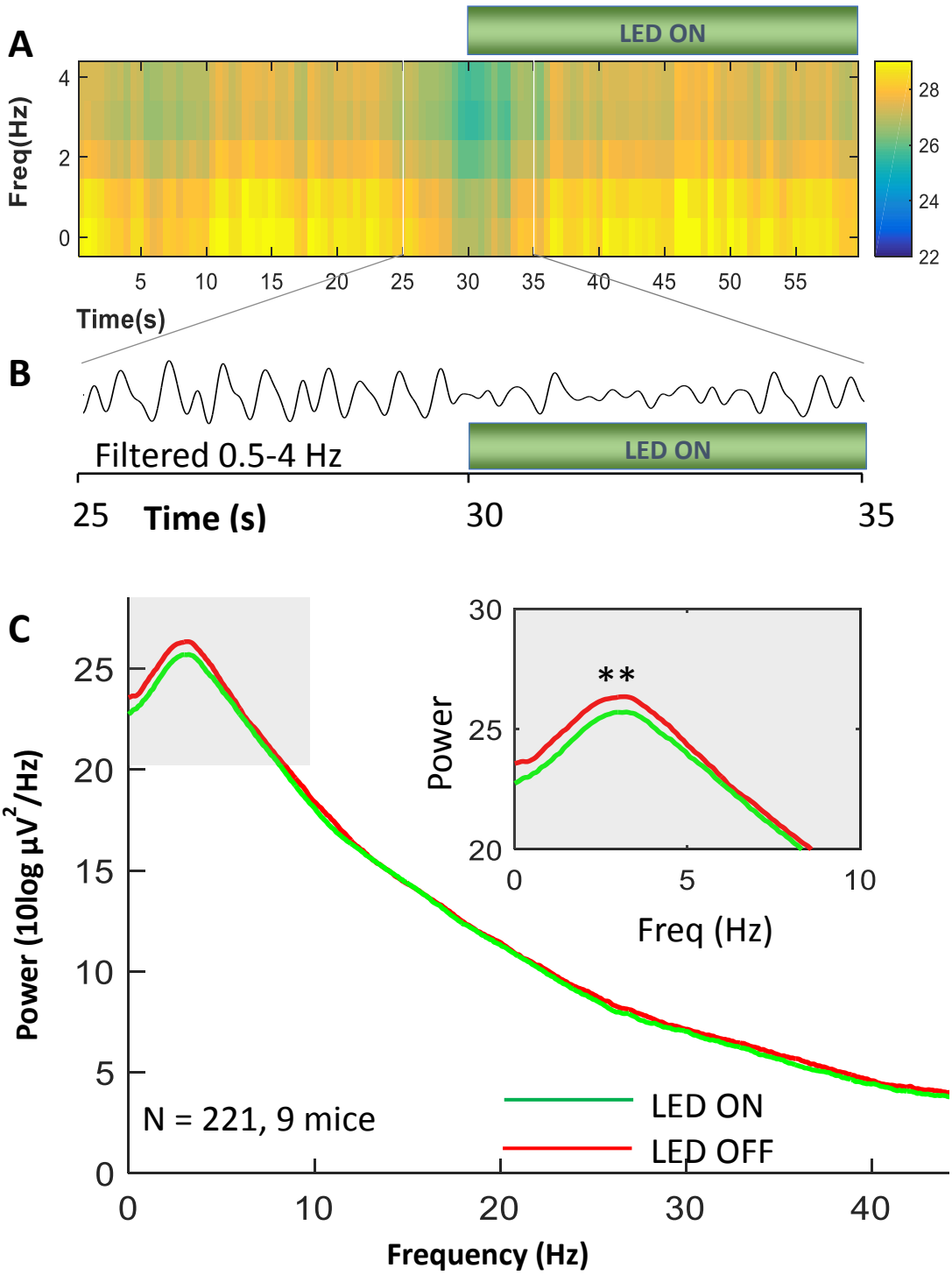

Figure 3.3 Light stimulation effect on delta oscillation in Halorhodopsin expressing mice during sleep. **A** Mean spectrogram of 0 - 4 Hz over 60 seconds. Green bar (LED ON) portrays light stimulation, which starts at 30 seconds. **B** Magnified and 0.5-4 Hz filtered EEG trace over 10 seconds. Light stimulation starts at 30 seconds. **C** The power spectrum of 5 seconds before (red) and 5 seconds during (green) light stimulation. Delta power was reduced slightly and significantly during light activation over 5 seconds (N = 221, 9 mice, $^{**}p < 0.01$; Student paired test. Frontal right channel (FR) was used for analysis).

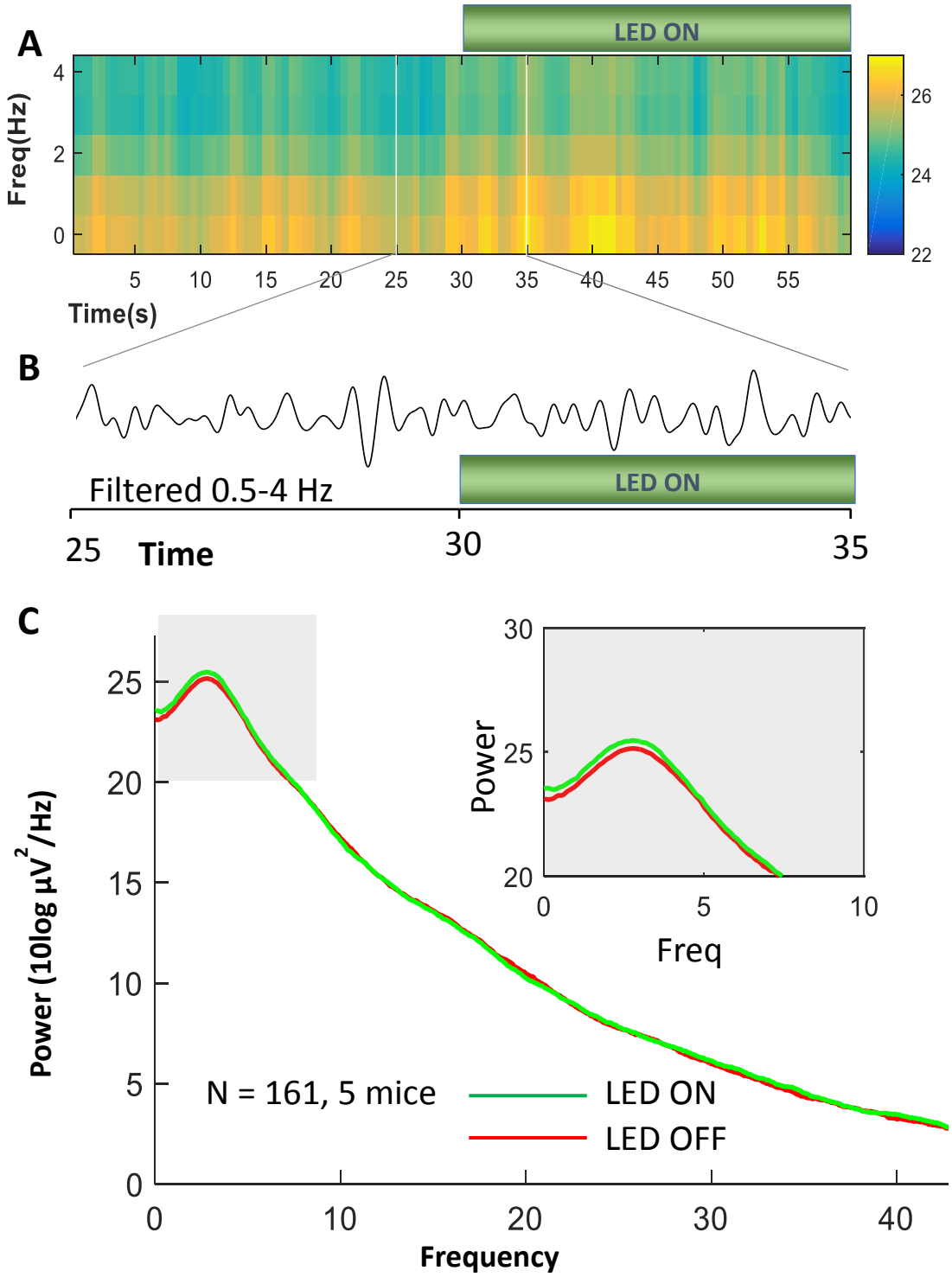

Figure 3.4 Light stimulation effect on delta oscillation in YFP only (Control) expressing mice during sleep. **A** Mean spectrogram of 0 - 4 Hz over 60 seconds. Green bar (LED ON) portrays light stimulation, which starts at 30 seconds. **B** Magnified and 0.5-4 Hz filtered EEG trace over 10 seconds. Light stimulation starts at 30 seconds. **C** The power spectrum of 5 seconds before (red) and 5 seconds during (green) light stimulation. Delta power was increased during light activation over 5 second without statistical significance (N = 161, 5 mice, p = 0.08; Student paired test. Frontal right channel (FR) was used for analysis).

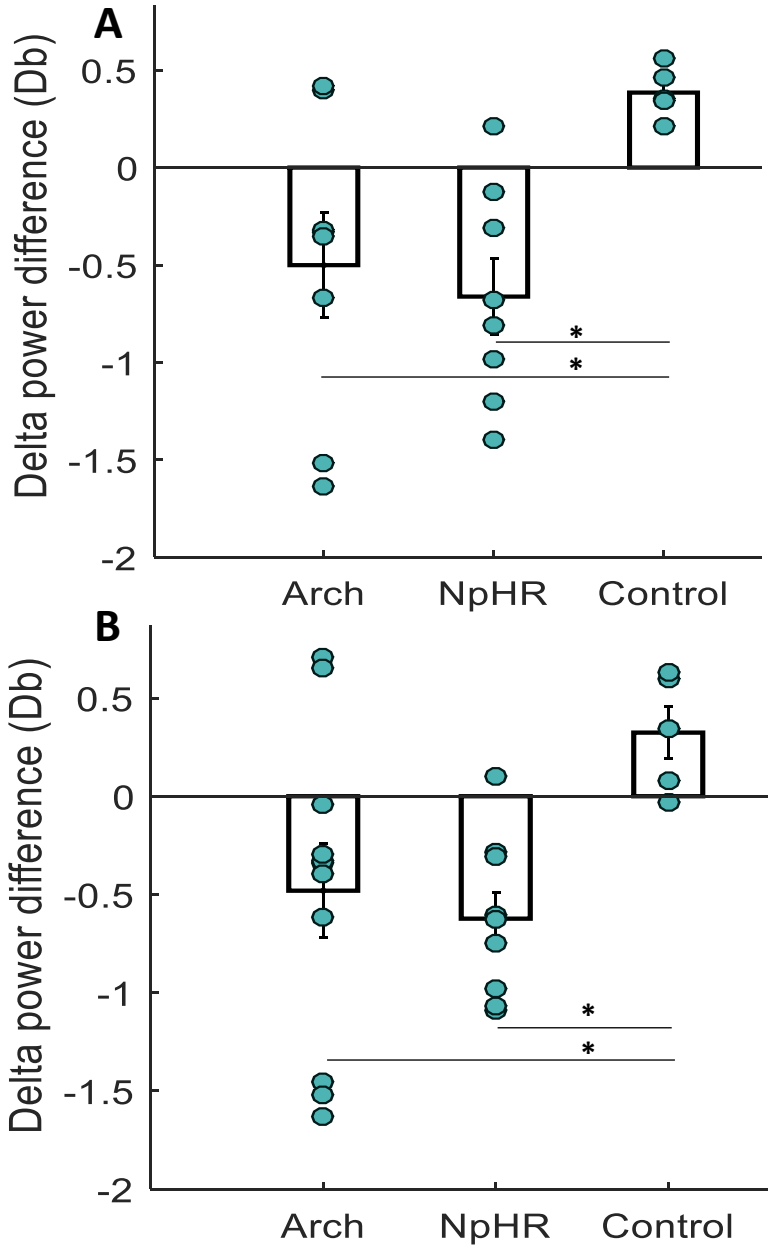

Figure 3.5 Summary of delta oscillation change caused by TRN light stimulation (optogenetic inhibition) over 5 seconds during sleep in mice expressing Archaerhodopsin (Arch), Halorhodopsin (NpHR) and YFP (Control). EEG was recorded from auditory right (A) and frontal right (B) channels. Each green dot represents a result from a single animal. Green light significantly reduced delta power in Arch and NpHR mice compared to control animals. Light activation in control mice, led to a modest increase in delta power. The delta power change in the mice expressing opsins is significantly different in both AR and FR channels. (**AR**: NpHR = 8 mice; Arch = 8 mice; Control = 5 mice. Arch/MES = 1.34, CI = 2.57/0.11; NpHR/MES = 2.17, CI = 3.56/0.77. ANOVA F =5.21, p = 0.016; post-hoc Tukey HSD *p<0.05. **FR:** NpHR = 9 mice; Arch = 10 mice; Control = 5 mice. Arch/MES = 1.35, CI = 2.53/0.18; NpHR/MES = 2.37, CI = 3.77/0.96; ANOVA F =5.51, p = 0.012; post-hoc Tukey HSD *p<0.05. Data expressed as mean ± S.E.M. Db - decibels).

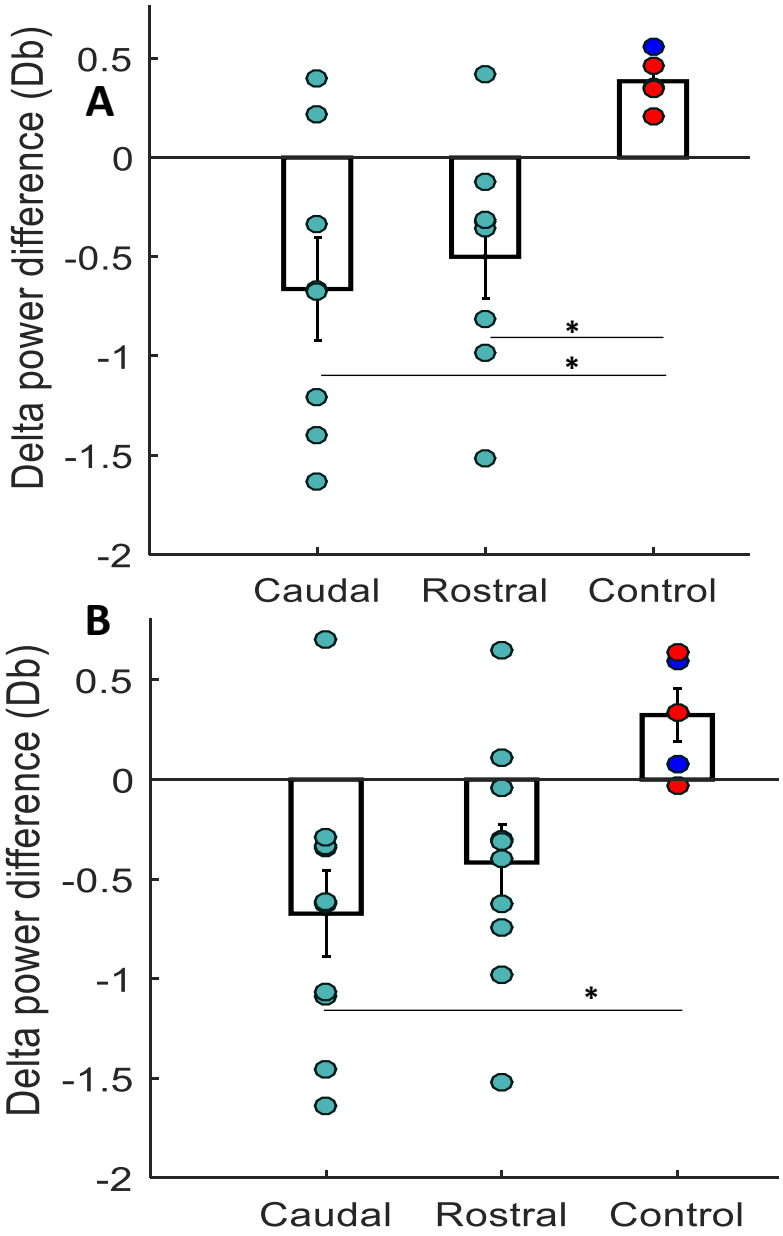

Figure 3.6 Summary of delta oscillation change caused by light stimulation (optogenetic inhibition) of rostral and caudal part of the TRN. EEG was recorded from auditory right (A) and frontal right (B) channels. Results from caudal Arch and caudal NpHR animals are combined in Caudal, and the results from rostrally injected animals are assigned as Rostral. Each green dot represents a result from a single animal. Rostrally injected control mice (red) are dissociated from caudally injected mice (blue) by color coding. Caudal and rostral TRN stimulation over 5 seconds led to significant reduction of the delta oscillation power compared to the control group. (**AR**: Caudal = 8 mice; Rostral = 8 mice; Control Caudal = 2 mice, Control Rostral = 3 mice. Caudal/ MES = 1.64, CI = 2.93/0.36; Rostral/MES = 1.69, CI = 2.94/0.43. ANOVA F =5.22, p = 0.016; post-hoc Tukey HSD *p<0.05. **FR**: Caudal = 10 mice; Rostral = 10 mice; Control Caudal = 2 mice, Control Rostral = 3 mice; Caudal/ MES = 1.59, CI = 2.81/0.38; Rostral/MES = 1.32, CI = 2.50/0.15; ANOVA F =4.74, p = 0.019; post-hoc Tukey HSD *p<0.05. Data expressed as mean ± S.E.M. Db - decibel).

Theta oscillation results (5-8 Hz)

The TRN light stimulation (inhibition) over 5 second did not have a dramatic effect on theta oscillation. There was a tendency for a reduction of theta oscillation power in most of Arch and NpHR animals, but this did not reach statistical significance (See Figure 3.7). (AR: NpHR = 8 mice; Arch = 8 mice; Control = 5 mice. Arch/MES = 1.23, CI = 2.44/-0.02; NpHR/MES = 0.42, CI = 1.51/-0.66. ANOVA F =1.52, p = 0.24. FR: NpHR = 9 mice; Arch = 11 mice; Control = 5 mice. Arch/MES = 0.75, CI = 1.84/-0.34; NpHR/MES = 0.98, CI = 2.13/-0.17; ANOVA F =1.3, p = 0.29).

Similar results were found in caudal and rostral animal's groups. Caudally inhibited animals produced a stronger mean decrease in theta oscillation relatively to rostrally stimulated animals, nonetheless the difference was not significant (See Figure 3.8). Rostral and caudal stimulation in the control animal did not produce any positive or negative tendency. (AR: Caudal = 8 mice; Rostral = 8 mice; Control Caudal = 2 mice, Control Rostral = 3 mice. Caudal/ MES = 0.79, CI = 1.95/-0.37; Rostral/MES = 1.52, CI = 1.52/-0.72. ANOVA F =1.39, p = 0.27. FR: Caudal = 10 mice; Rostral = 10 mice; Control Caudal = 2 mice, Control Rostral = 3 mice; Caudal/ MES = 0.94, CI = 2.07/-0.18; Rostral/MES = 0.42, CI = 1.93/-0.29; ANOVA F =1.72, p = 0.2).

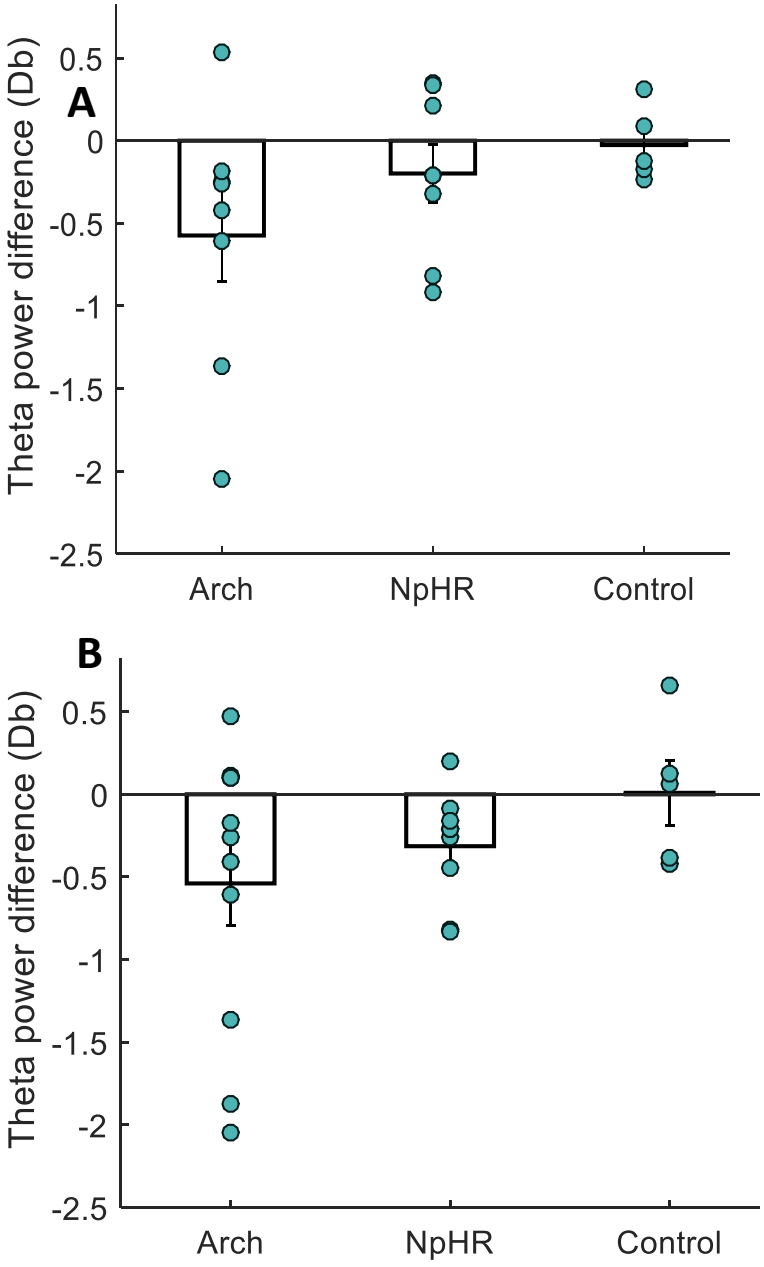

Figure 3.7 Summary of theta oscillation difference caused by the TRN light stimulations (optogenetic inhibition) over 5 seconds in mice expressing Archaerhodopsin (Arch), Halorhodopsin (NpHR) and YFP (Control). EEG was recorded from auditory right (AR) and frontal right (FR) channels. Each green dot represents single animal result. Green light stimulation did not have significant effect on theta oscillation in both AR and FR channels. (**AR**: NpHR = 8 mice; Arch = 8 mice; Control = 5 mice. Arch/MES = 1.23, CI = 2.44/-0.02; NpHR/MES = 0.42, CI = 1.51/-0.66. ANOVA F =1.52, p = 0.24. **FR:** NpHR = 9 mice; Arch = 11 mice; Control = 5 mice. Arch/MES = 0.75, CI = 1.84/-0.34; NpHR/MES = 0.98, CI = 2.13/-0.17; ANOVA F =1.3, p = 0.29. Data expressed as mean ± S.E.M. Db - decibels).

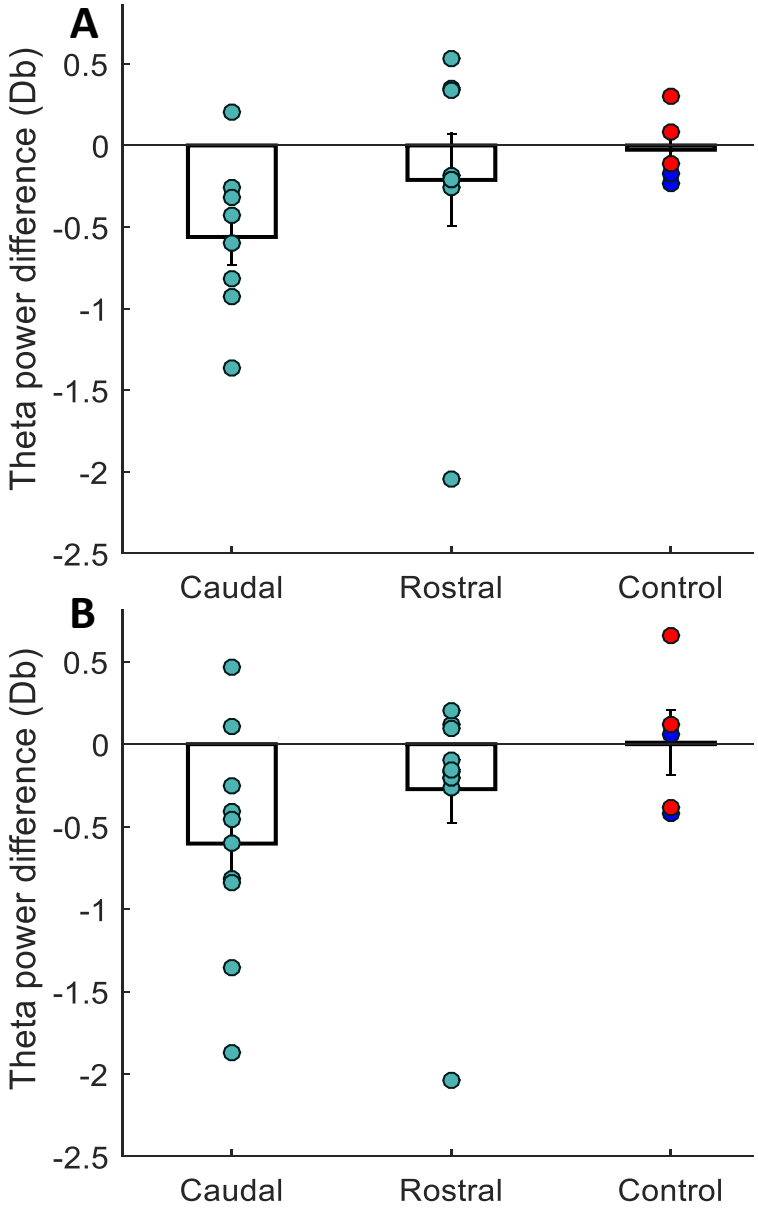

Figure 3.8 Summary of theta oscillation change caused by light stimulation (optogenetic inhibition) of rostral and caudal part of the TRN. EEG was recorded from auditory right (A) and frontal right (B) channels. Results from caudal Arch and caudal NpHR animals are combined in Caudal, and the results from rostrally injected animals are assigned as Rostral. Each green dot represents single animal result. Rostrally injected control mice (red) are dissociated from caudally injected mice (blue) by color coding. Caudal and rostral TRN stimulation did not have significant effect on theta oscillation power. (**AR**: Caudal = 8 mice; Rostral = 8 mice; Control Caudal = 2 mice, Control Rostral = 3 mice. Caudal/ MES = 0.79, CI = 1.95/-0.37; Rostral/MES = 1.52, CI = 1.52/-0.72. ANOVA F =1.39, p = 0.27. **FR**: Caudal = 10 mice; Rostral = 10 mice; Control Caudal = 2 mice, Control Rostral = 3 mice; Caudal/ MES = 0.94, CI = 2.07/-0.18; Rostral/MES = 0.42, CI = 1.93/-0.29; ANOVA F =1.72, p = 0.2. Data expressed as mean ± S.E.M. Db - decibels).

Alpha oscillation (spindle oscillation, 9 – 16 Hz)

In this study, we measured alpha oscillations from 9-16Hz, which is a slightly wider frequency range than that typically measured (8-14Hz), but a range that is acceptable for sleep spindle oscillations. (Clayton et al., 2015). Tonic light stimulation (inhibition) of the caudally stimulated TRN during the first 10 seconds resulted in a significant reduction of the alpha oscillation (See Figure 3.9, 170 traces, 10 mice; $p < 0.05$, Student paired test). Identical stimulation in the animals, expressing inhibitory opsins in the rostral TRN, did not show any effect on alpha oscillation (See Figure 3.10; 347 traces, 10 mice; $p = 0.27$, Student paired test). Light stimulations of control animals did not produce any decrease on the alpha oscillation during first 10 seconds, as well. (See Figure 3.11; 161 traces, 5 mice; $p = 0.56$; Student test).

Next, we compared the mean reduction of the alpha band power between animal groups in auditory right and auditory left EEG channels (See Figure 3.12; AR and FR). During evaluation of the changes caused by the TRN light stimulation (inhibition) in virus group animals (Arch, NpHR and YFP) no significant difference was found in either EEG channels. Arch and NpHR exhibited a weak tendency to reduce alpha oscillations in the frontal right channel (AR: NpHR = 8 mice; Arch = 8 mice; Control = 5 mice. Arch/MES = 0.73, CI = 1.88/-0.42; NpHR/MES = 0.39, CI = 1.51/-0.74. ANOVA F =0.40, p = 0.71. FR: NpHR = 9 mice; Arch = 11 mice; Control = 5 mice. Arch/MES = 0.83, CI = 1.92/-0.27; NpHR/MES = 0.90, CI = 2.04/-0.25; ANOVA F =2.35, p = 0.11).

The comparison of groups divided by the location of light stimulation showed contrasting results. Although, the power of the alpha oscillation from the auditory right EEG channel was similar in all groups, the data from the frontal channel displayed significance (See Figure 3.13, FR). Optogenetic deactivation of the caudal TRN for 10 seconds led to a significant reduction of the alpha oscillation by 0.53 dB, while rostral TRN optogenetic inhibition for 10 seconds did not produce any effect (AR: Caudal = 8 mice, Rostral = 8 mice; Control Caudal = 2 mice, Control Rostral = 3 mice. Caudal/ MES = 0.28, CI = 1.40/-0.84; Rostral/MES = 0.59, CI = 1.73/-0.55. ANOVA F =0.36, p = 0.70. FR: Caudal = 10 mice; Rostral = 10 mice; Control Caudal = 2 mice,

Control Rostral = 3 mice; Caudal/ MES = 1.25, CI = 2.41/0.09; Rostral/MES = 1.13, CI = 2.27/-0.02; ANOVA F =5.12, p = 0.014; post-hoc Tukey HSD $p<0.05$). Rostral stimulations in control animals showed a tendency for a modest increase in alpha oscillation (See Figure 3.13, red dots), in contrast to caudally stimulated control mice, which did not display any noticeable difference in the first 10 seconds of stimulation (blue dots).

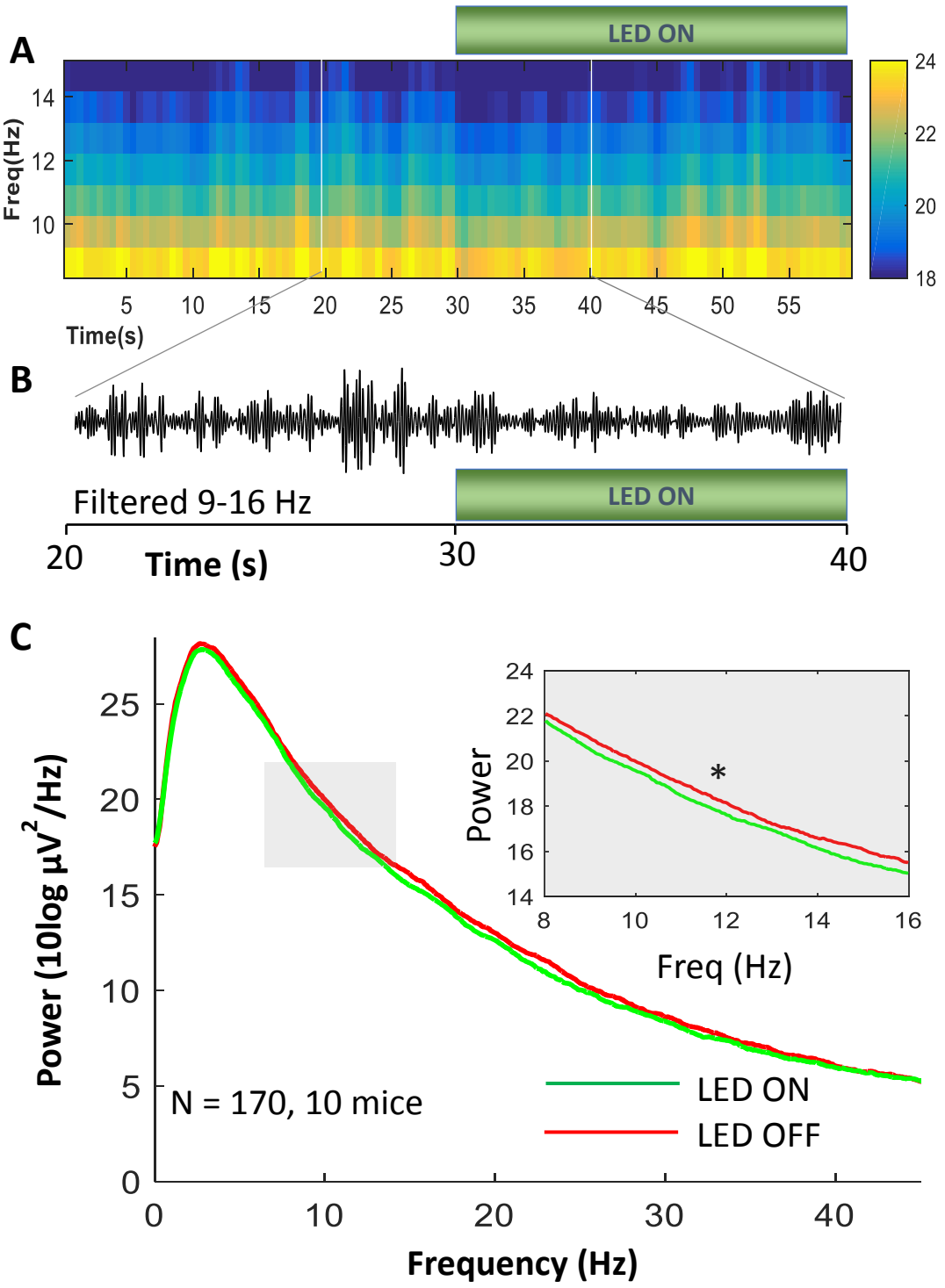

Figure 3.9 Light stimulation effect on alpha oscillation power in caudally stimulated TRN mice (NpHR + Arch) during sleep. **A** Mean spectrogram of 9 - 16 Hz over 60 seconds. Green bar (LED ON) portrays light stimulation, which starts at 30 seconds. **B** Magnified and 9-16 Hz filtered EEG trace over 10 seconds. Light stimulation starts at 30 seconds. **C** The power spectrum of 10 seconds before (red) and 10 seconds during (green) light stimulation. Alpha power was reduced significantly during light activation over 10 second (N =170, 10 mice, *p < 0.05; Student paired test. Frontal right channel (FR) was used for analysis).

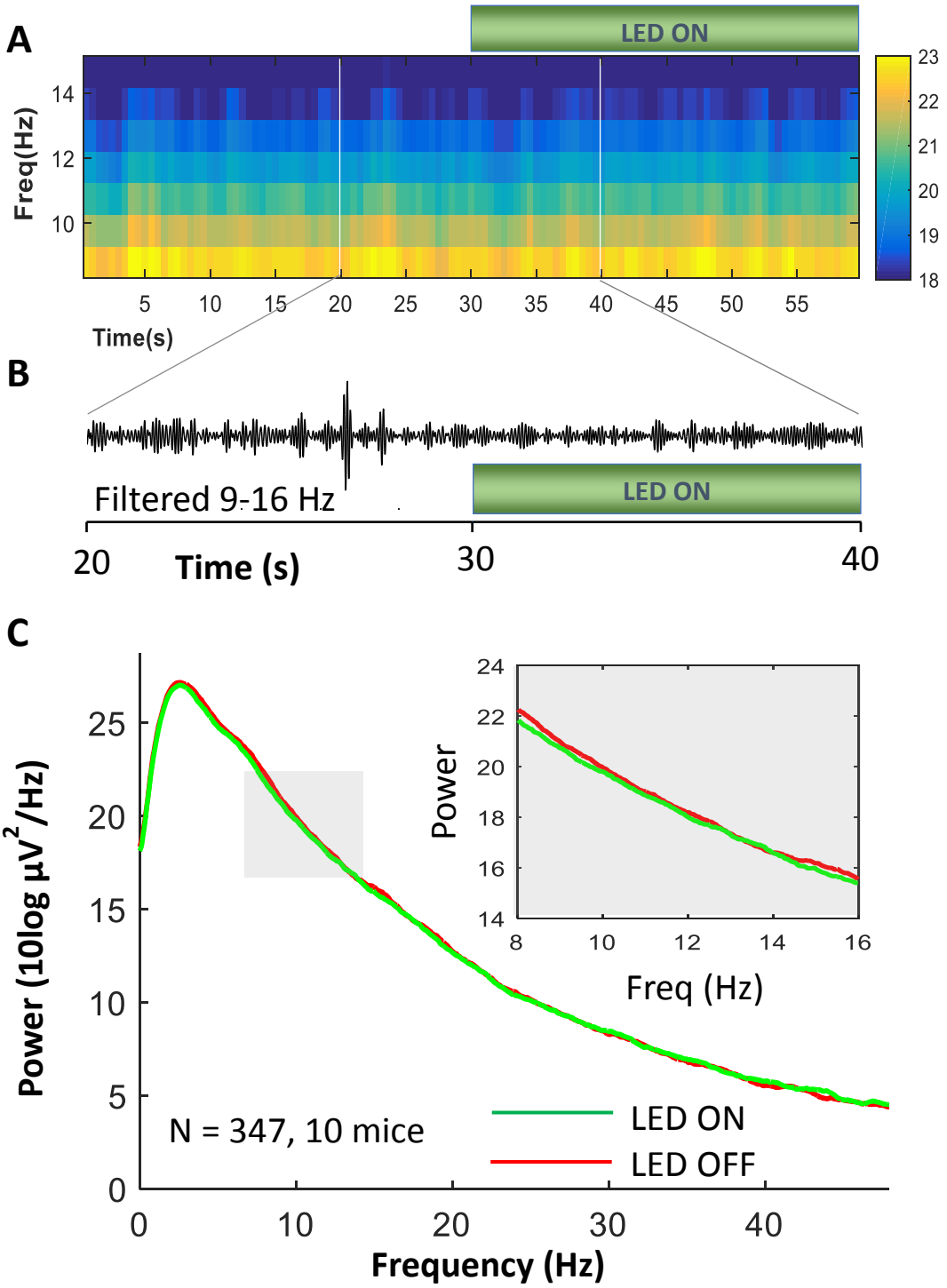

Figure 3.10 Light stimulation effect on alpha oscillation power in rostrally stimulated TRN mice (NpHR + Arch) during sleep. **A** Mean spectrogram of 9 - 16 Hz over 60 seconds. Green bar (LED ON) portrays light stimulation, which starts at 30 seconds. **B** Magnified and 9-16 Hz filtered EEG trace over 10 seconds. Light stimulation starts at 30 seconds. **C** The power spectrum of 10 seconds before (red) and 10 seconds after (green) light stimulation. Alpha power was not affected during light activation over 10 second (N =347, 10 mice, p = 0.27; Student paired test. Frontal right channel (FR) was used for analysis).

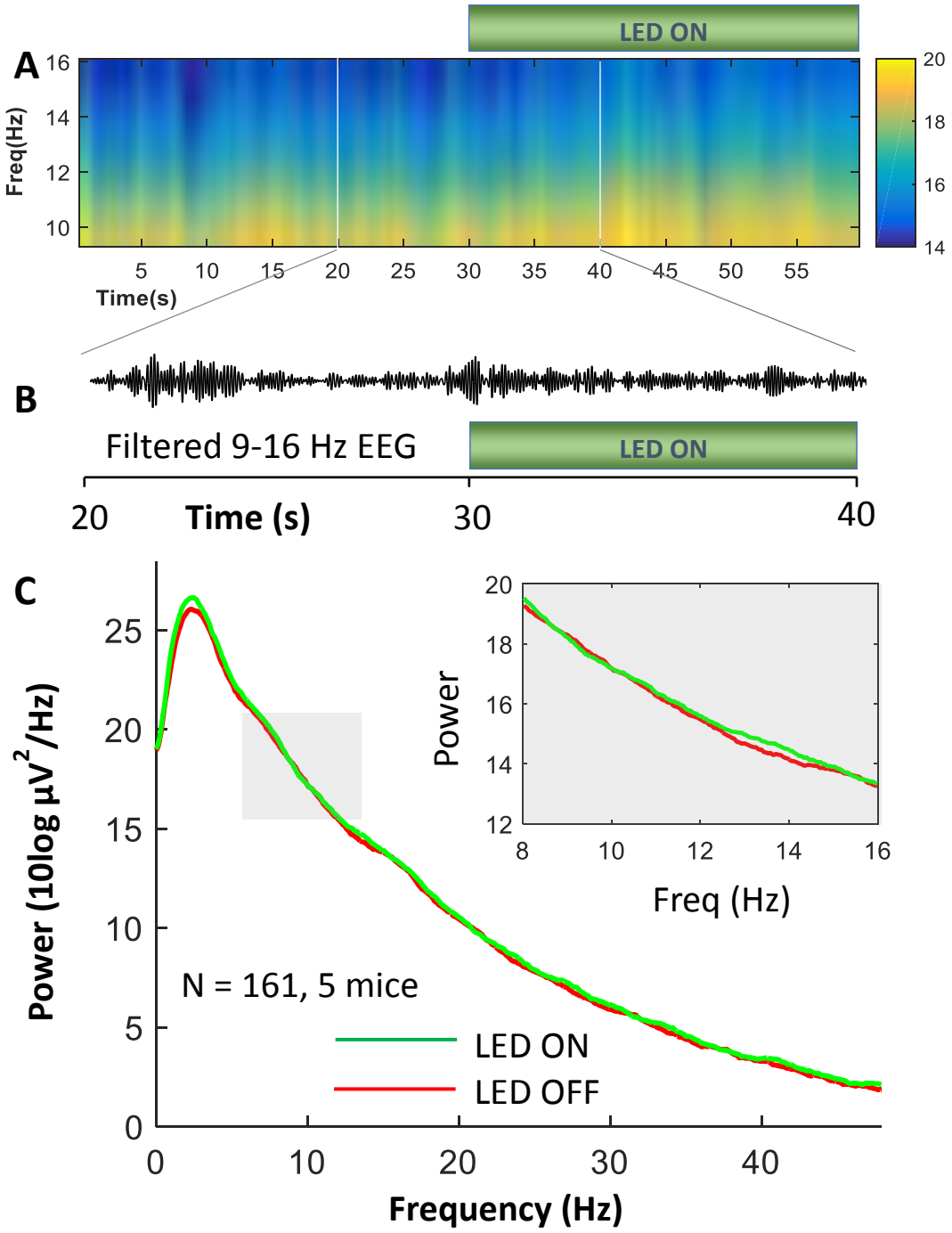

Figure 3.11 Light stimulation effect on alpha oscillation power in control (YFP) mice (Rostral + Caudal) during sleep. **A** Mean spectrogram of 9 - 16 Hz over 60 seconds. Green bar (LED ON) portrays light stimulation, which starts at 30 seconds. **B** Magnified and 9-16 Hz filtered EEG trace over 10 seconds. Light stimulation starts at 30 seconds. **C** The power spectrum of 10 seconds before (red) and 10 seconds after (green) light stimulation. Alpha power was not affected during light activation over 10 second (N =161, 5 mice, p = 0.56; Student paired test. Frontal right channel (FR) was used for analysis).

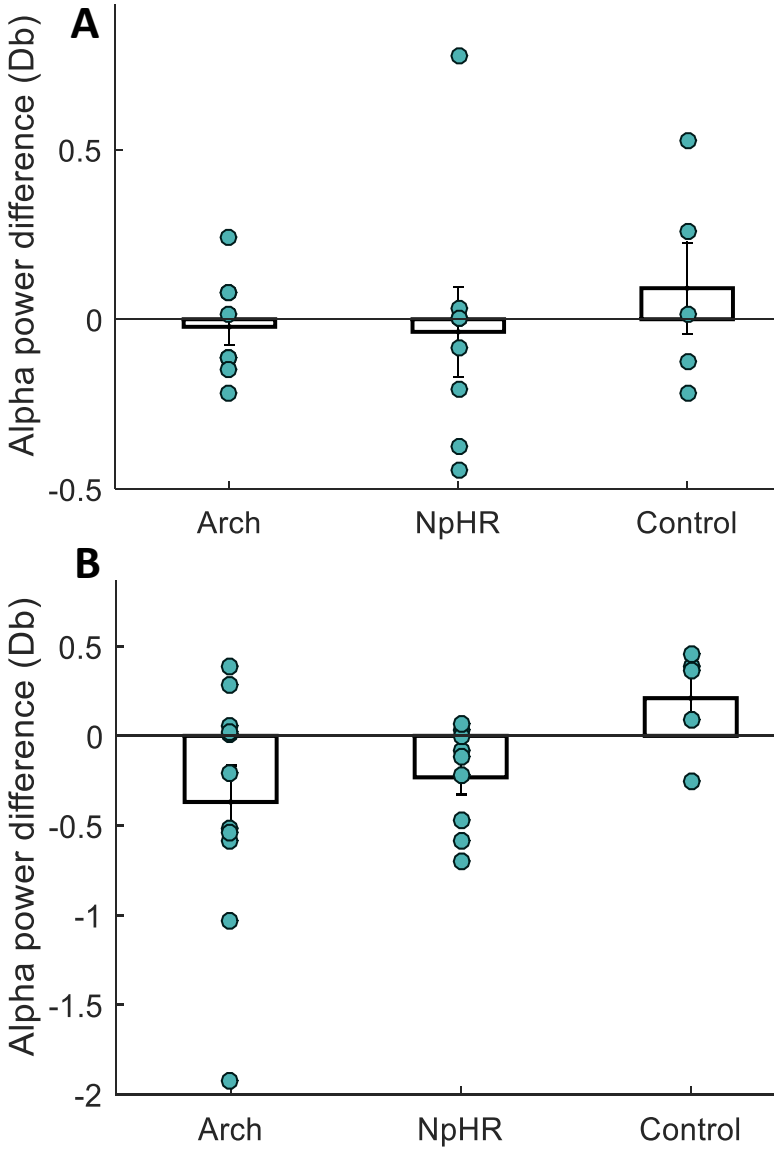

Figure 3.12 Summary of alpha oscillation difference caused by the TRN light stimulations (optogenetic inhibition) over 10 seconds in mice expressing Archaerhodopsin (Arch), Halorhodopsin (NpHR) and YFP (Control). EEG was recorded from auditory right (A) and frontal right (B) channels. Each green dot represents a single animal result. Green light stimulation did not have significant effect on alpha oscillation power in both AR and FR channels. (**AR**: NpHR = 8 mice; Arch = 8 mice; Control = 5 mice. Arch/MES = 0.73, CI = 1.88/-0.42; NpHR/MES = 0.39, CI = 1.51/-0.74. ANOVA F =0.40, p = 0.71. **FR:** NpHR = 9 mice; Arch = 11 mice; Control = 5 mice. Arch/MES = 0.83, CI = 1.92/-0.27; NpHR/MES = 0.90, CI = 2.04/-0.25; ANOVA F =2.35, p = 0.11. Data expressed as mean ± S.E.M. Db - decibels).

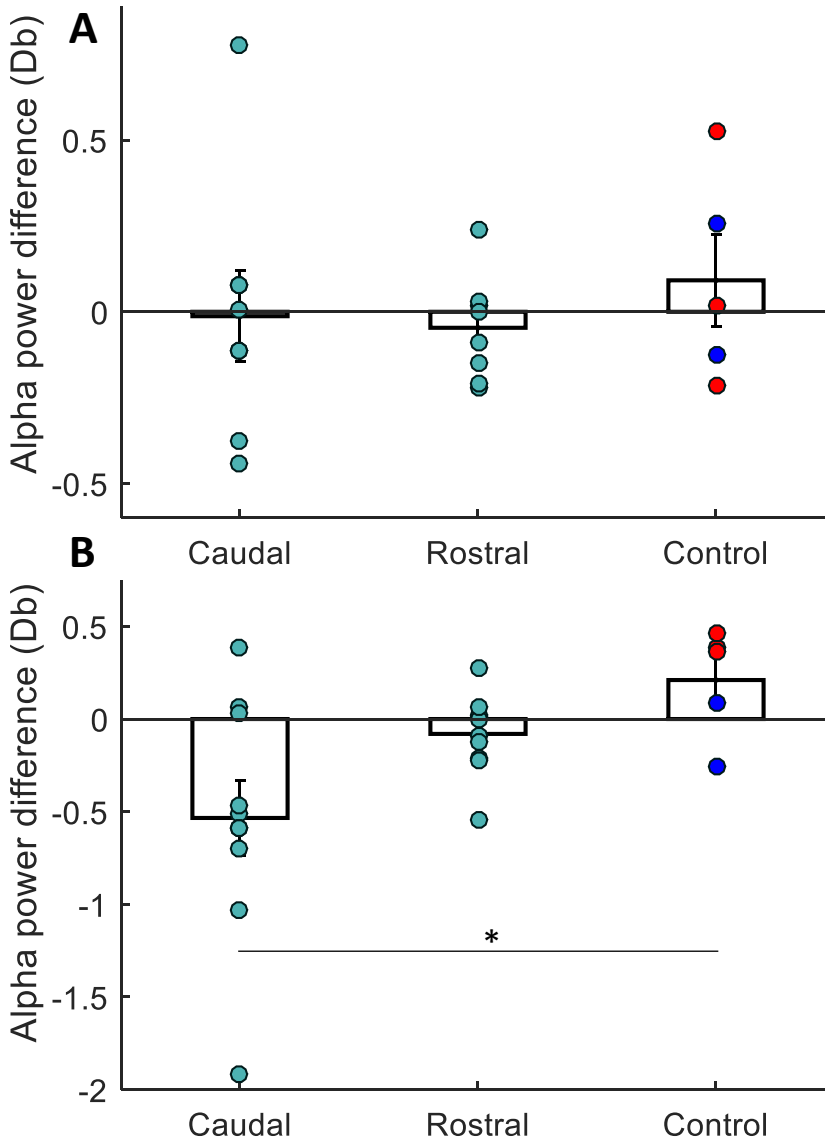

Figure 3.13 Summary of alpha oscillation change caused by light stimulation (optogenetic inhibition) of rostral and caudal part of the TRN. EEG was recorded from auditory right (AR) and frontal right (FR) channels. Results from caudal Arch and caudal NpHR animals are combined in Caudal, and the results from rostrally injected animals are assigned as Rostral. Each green dot represents single animal result. Rostrally injected control mice (red) are dissociated from caudally injected mice (blue) by color coding. Caudal TRN stimulation for 10 seconds led to significant reduction of the alpha oscillation power in FR channel only. (**AR**: Caudal = 8 mice; Rostral = 8 mice; Control Caudal = 2 mice, Control Rostral = 3 mice. Caudal/ MES = 0.28, CI = 1.40/-0.84; Rostral/MES = 0.59, CI = 1.73/-0.55. ANOVA F =0.36, p = 0.70. **FR**: Caudal = 10 mice; Rostral = 10 mice; Control Caudal = 2 mice, Control Rostral = 3 mice; Caudal/ MES = 1.25, CI = 2.41/0.09; Rostral/MES = 1.13, CI = 2.27/-0.02; ANOVA F =5.12, p = 0.014; post-hoc Tukey HSD *p<0.05. Data expressed as mean ± S.E.M. Db - decibels).

Beta oscillations (16 - 29 Hz)

Similar to the data obtained for alpha oscillations, light stimulation over 10 seconds led to a significant reduction of the beta band oscillation in caudally stimulated animals (See Figure 3.14, 170 traces, 10 mice; $p < 0.05$, Student paired test). Identical stimulations in the rostral TRN nuclei did not produce any effect on beta oscillation (See Figure 3.15, 10 mice; $p = 0.58$, Student paired test). The outcome of the YFP expressing TRN light stimulation (control), was similar to the rostral TRN inhibition, it did not exhibit any significant reduction or increase (See Figure 3.16, 5 mice, $p = 0.40$).

Next, we compared an averaged change in beta oscillation of the different viral groups (Arch, NpHR and YFP animals). Irrespective of the expressed virus and EEG channels, there was no significant change detected in the beta oscillation. (See Figure 3.17; AR: NpHR = 8 mice; Arch = 8 mice; Control = 5 mice. Arch/MES = 0.31, CI = 1.44/-0.81; NpHR/MES = 0.11, CI = 1.23/-1.01. ANOVA F =0.33, p = 0.72. FR: NpHR = 9 mice; Arch = 11 mice; Control = 5 mice. Arch/MES = 0.71, CI = 1.79/-0.38; NpHR/MES = 0.73, CI = 1.86/-0.39; ANOVA F =1.16, p = 0.33).

A comparison of the results from the same animals, but in this case grouped by their stimulation location, clarified the light stimulation effect on beta oscillation (See Figure 3.18). Similar to the alpha oscillation results, beta oscillation power in the auditory right channel was unchanged during the first 10 seconds of the TRN stimulation in all three groups of animals (caudal, rostral and control). EEG recorded from the frontal cortex showed opposing effects of optogenetic inhibition depending on the anatomical location. The beta oscillation power of animals with a caudally inhibited TRN showed a significant reduction of 0.36 dB, whereas animals with a rostrally inhibited TRN and control animals displayed a rise in beta oscillation by 0.12 dB and 0.18 dB, respectively. Interestingly, the beta oscillation change of caudally stimulated animals was significantly different from rostrally stimulated and control animals. AR: Caudal = 8 mice; Rostral = 8 mice; Control Caudal = 2 mice, Control Rostral = 3 mice. Caudal/ MES = 0.37, CI = 1.49/-0.76; Rostral/MES = 0.04, CI = 1.16/-1.08. ANOVA F =0.46, p = 0.63. FR: Caudal = 10 mice; Rostral = 10 mice; Control

Caudal = 2 mice, Control Rostral = 3 mice; Caudal/ MES = 1.38, CI = 2.41/0.20; Rostral/MES = 0.18, CI = 2.27/-0.90; ANOVA F =7.09, p = 0.004; post-hoc Tukey HSD Rostral/Caudal $p<0.01$, Caudal/Control $p<0.05$). The opposing direction of effects of rostral and caudal stimulation in control animals raises doubts about the significant decrease of caudal Arch and NpHR stimulation compared to controls. Hence, the 3 rostrally stimulated control animals (see Figure 3.18, red dots) showed an apparent increase in beta power oscillation during 10 seconds of stimulation, whereas the 2 control animals with caudally stimulated TRN (See Figure 3.18, blue dots) had reduced beta power.

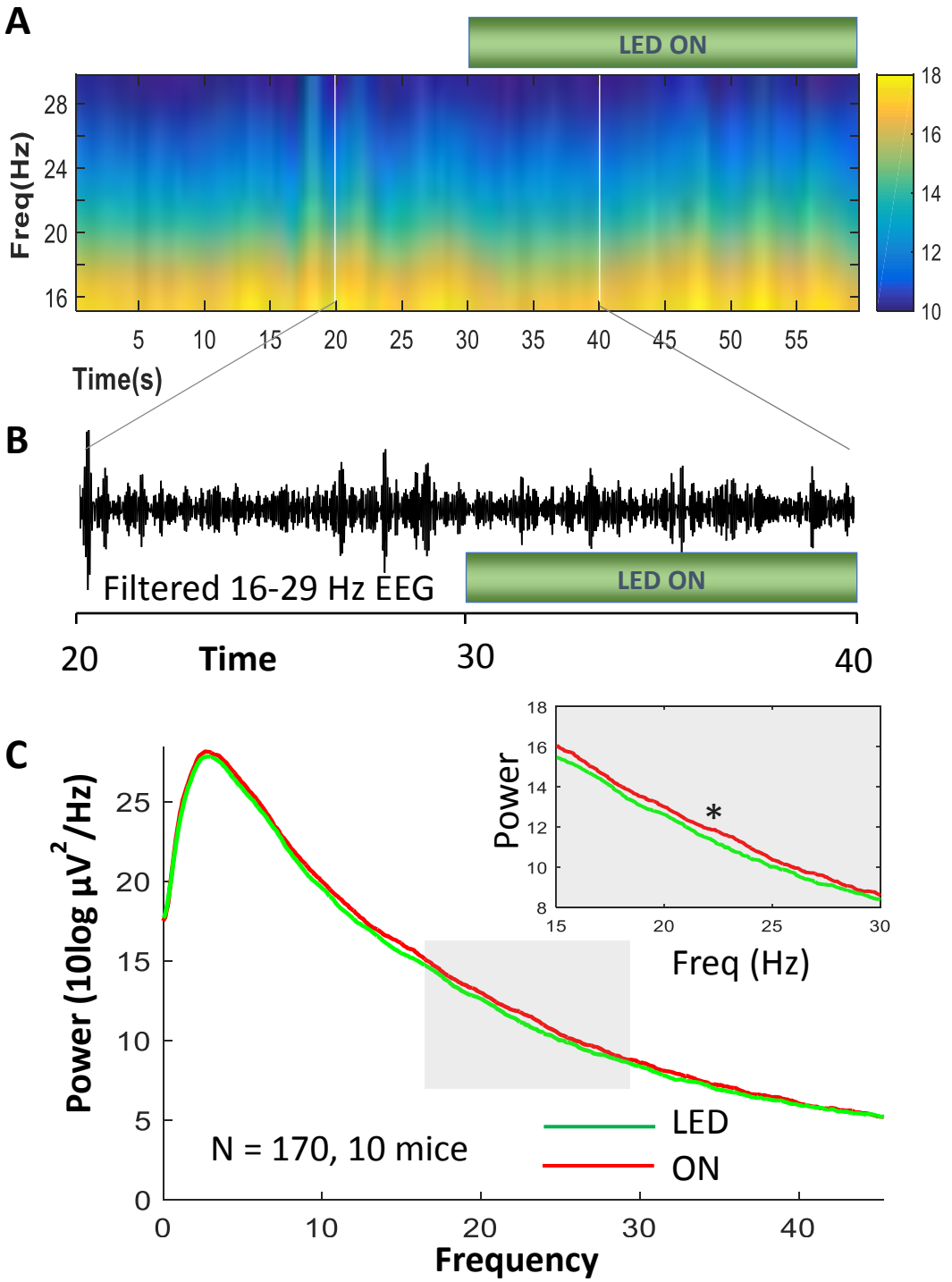

Figure 3.14 Light stimulation effect on beta oscillation power in caudally stimulated TRN mice (NpHR + Arch) during sleep. **A** Mean spectrogram of 16 - 29 Hz over 60 seconds. Green bar (LED ON) portrays light stimulation, which starts at 30 seconds. **B** Magnified and 16-29 Hz filtered EEG trace over 10 seconds. Light stimulation starts at 30 seconds. **C** The power spectrum of 10 seconds before (red) and 10 seconds during (green) light stimulation. Beta power was reduced significantly during light activation over 10 second (N =170, 10 mice, *p < 0.05; Student paired test. Frontal right channel (FR) was used for analysis).

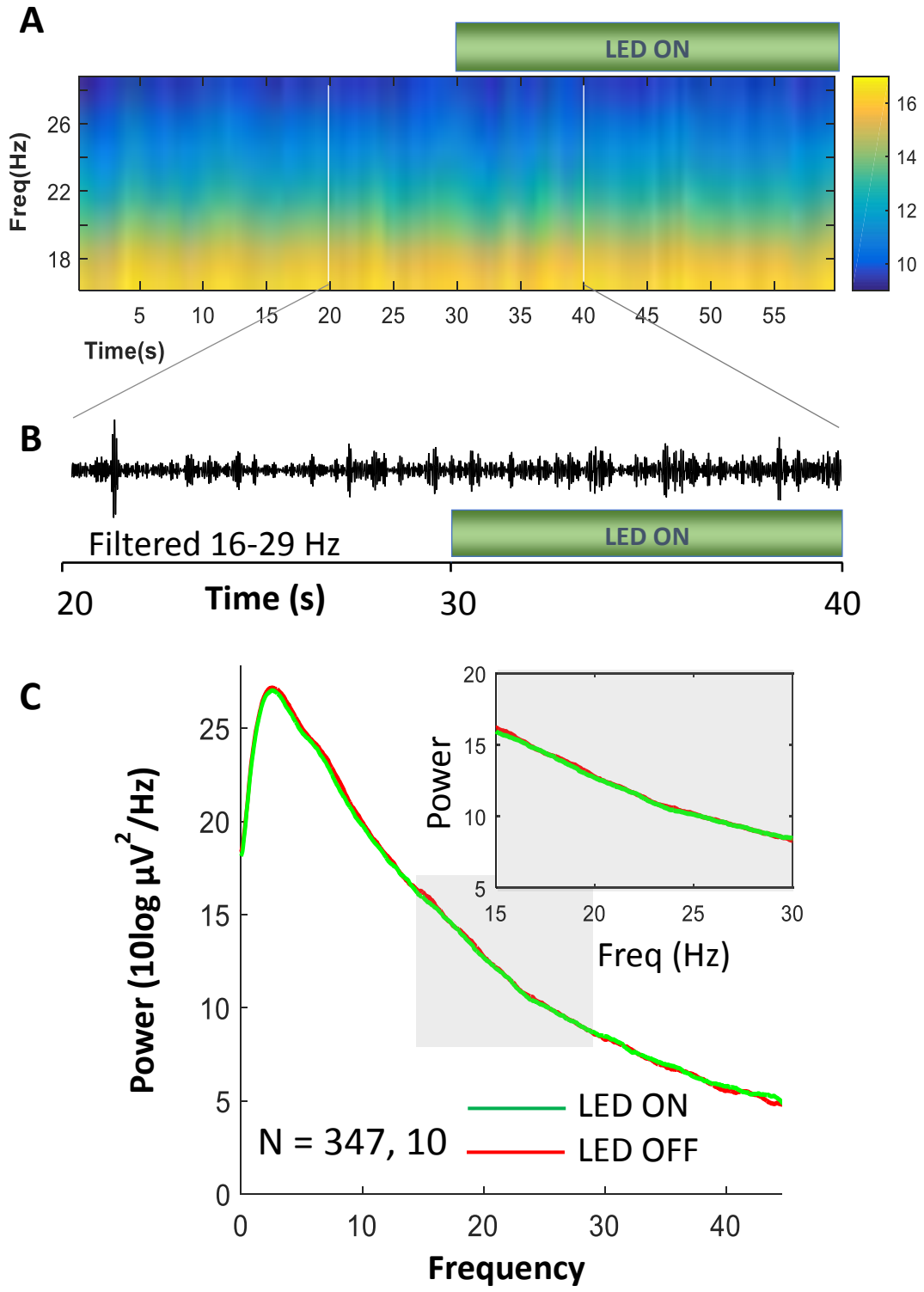

Figure 3.15 Light stimulation effect on beta oscillation power in rostrally stimulated TRN mice (NpHR + Arch) during sleep. **A** Mean spectrogram of 16 - 29 Hz over 60 seconds. Green bar (LED ON) portrays light stimulation, which starts at 30 seconds. **B** Magnified and 16-29 Hz filtered EEG trace over 10 seconds. Light stimulation starts at 30 seconds. **C** The power spectrum of 10 seconds before (red) and 10 seconds during (green) light stimulation. Beta power was not affected during light activation over 10 second (N =347, 10 mice, p = 0.58; Student paired test. Frontal right channel (FR) was used for analysis.

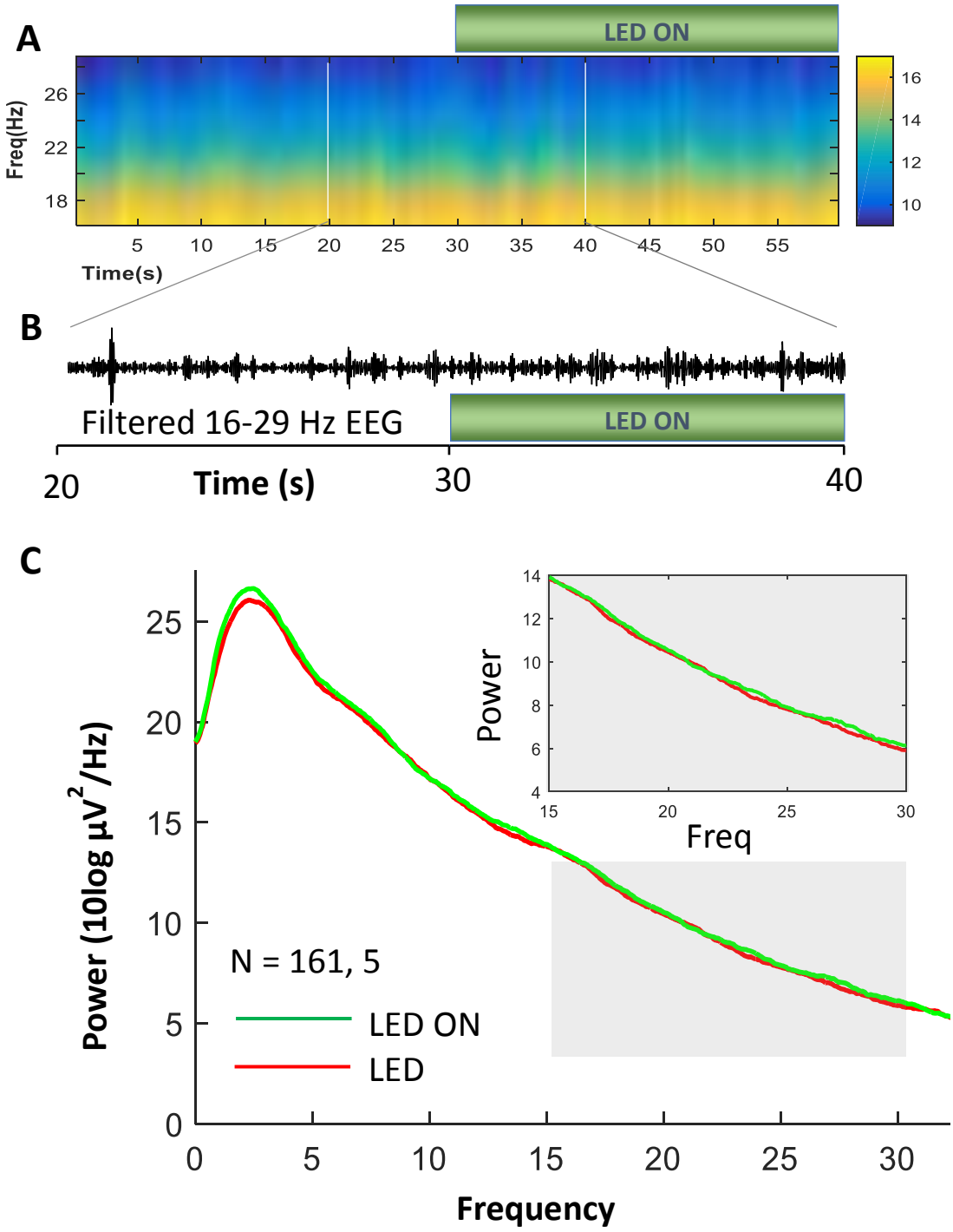

Figure 3.16 Light stimulation effect on beta oscillation power in control (YFP) mice (Rostral + Caudal) during sleep. **A** Mean spectrogram of 16 - 29 Hz over 60 seconds. Green bar (LED ON) portrays light stimulation, which starts at 30 seconds. **B** Magnified and 16-29 Hz filtered EEG trace over 10 seconds. Light stimulation starts at 30 seconds. **C** The power spectrum of 10 seconds before (red) and 10 seconds during (green) light stimulation. Beta power was not affected during light activation over 10 second (N =161, 5 mice, p = 0.40; Student paired test. Frontal right channel (FR) was used for analysis).

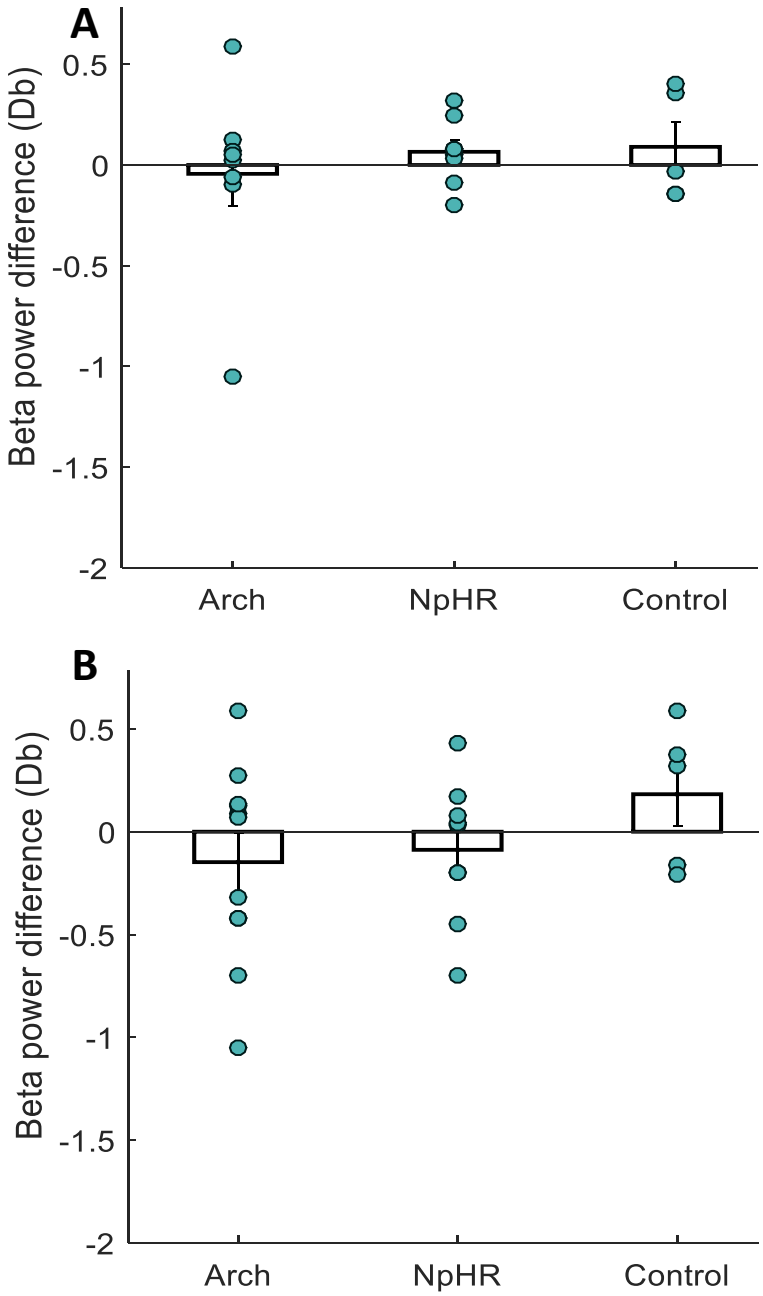

Figure 3.17 Summary of Beta oscillation difference caused by the TRN light stimulations (inhibition) over 10 seconds in mice expressing Archaerhodopsin (Arch), Halorhodopsin (NpHR) and YFP (Control). EEG was recorded from auditory right (A) and frontal right (B) channels. Each green dot represents single animal result. Green light stimulation did not have significant effect on beta oscillation power in both AR and FR channels. (**AR**: NpHR = 8 mice; Arch = 8 mice; Control = 5 mice. Arch/MES = 0.31, CI = 1.44/-0.81; NpHR/MES = 0.11, CI = 1.23/-1.01. ANOVA F =0.33, p = 0.72. **FR:** NpHR = 9 mice; Arch = 11 mice; Control = 5 mice. Arch/MES = 0.71, CI = 1.79/-0.38; NpHR/MES = 0.73, CI = 1.86/-0.39; ANOVA F =1.16, p = 0.33. Data expressed as mean ± S.E.M. Db - decibels).

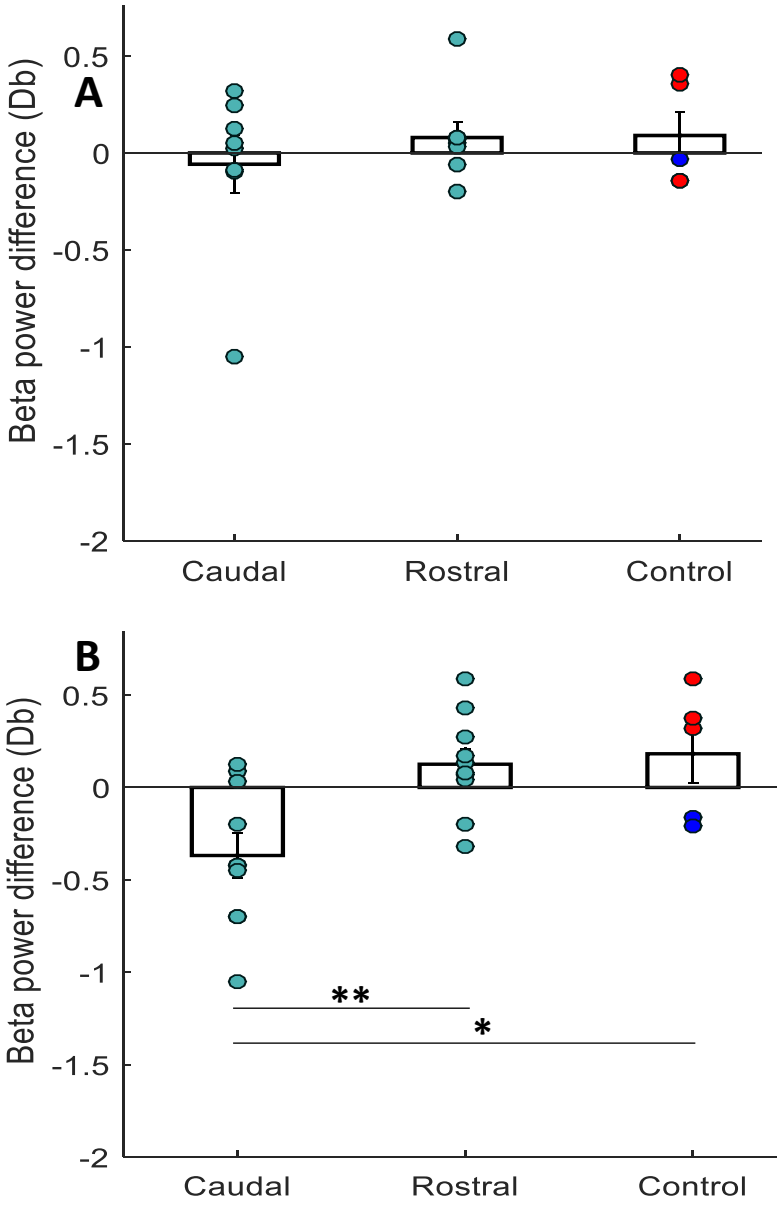

Figure 3.18 Summary of Beta oscillation change caused by light stimulation (optogenetic inhibition) of rostral and caudal part of the TRN. EEG was recorded from auditory right (A) and frontal right (B) channels. Results from caudal Arch and caudal NpHR animals are combined in Caudal, and the results from rostrally injected animals are assigned as Rostral. Each green dot represents single animal result. Rostrally injected control mice (red) are dissociated from caudally injected mice (blue) by colour coding. Caudal TRN stimulation for 10 seconds led to significant reduction of beta oscillation power in FR channel relatively to rostrally stimulated and control animals. (**AR**: Caudal = 8 mice; Rostral = 8 mice; Control Caudal = 2 mice, Control Rostral = 3 mice. Caudal/ MES = 0.37, CI = 1.49/-0.76; Rostral/MES = 0.04, CI = 1.16/-1.08. ANOVA F =0.46, p = 0.63. **FR**: Caudal = 10 mice; Rostral = 10 mice; Control Caudal = 2 mice, Control Rostral = 3 mice; Caudal/ MES = 1.38, CI = 2.41/0.20; Rostral/MES = 0.18, CI = 2.27/-0.90; ANOVA F =7.09, p = 0.004; post-hoc Tukey HSD **p<0.01, *p<0.05. Data expressed as mean ± S.E.M. Db - decibels).

Gamma Oscillation (30 - 50 Hz)

Next, we assessed the effect of TRN optogenetic inhibition on gamma oscillation. Results from the auditory right channels did not reveal any clear effects in virus infected animals (See Figure 3.19 AR). Frontal right channel EEG showed more consistent changes for animals expressing NpHR (See Figure 3.19 FR). Gamma oscillation power during the first 5 seconds of TRN stimulation (optogenetic inhibition) was reduced by 0.19 dB in these animals, whereas gamma power of Arch mice declined only by 0.07 dB and was not as consistent as in the case of NpHR animals. YFP expressing mice, showed a rise in gamma band power by 0.7 dB. The apparent reduction in gamma oscillation in halorhodopsin treated mice, was not however significant using ANOVA (AR: NpHR = 8 mice; Arch = 8 mice; Control = 5 mice. Arch/MES = 0.22, CI = 0.91/-1.34; NpHR/MES = 0.03, CI = 1.15/-1.09. ANOVA F =0.18, p = 0.82. FR: NpHR = 9 mice; Arch = 11 mice; Control = 5 mice. Arch/MES = 0.47, CI = 1.54/-0.60; NpHR/MES = 2.09, CI = 3.43/0.75; ANOVA F =1.84, p = 0.18). Nevertheless, measure effect size for NpHR mice relatively to control mice showed a significant difference (MES = 2.09, Confidence interval = 3.43/0.75).The gamma oscillation data for groups with different stimulation sites showed relative similar effects in all virus animal groups. The EEG results from the auditory right channel had varying results for all groups, whereas EEG data from the FR channel had more consistent outcomes with few outliers in both caudal and rostral groups (See Figure 3.20 FR). Inhibition of rostral and caudal TRN reduced gamma oscillation power by 0.16 dB and 0.10 dB, respectively. Light stimulation of control mice increased gamma band power by 0.07 dB. Although the results for both caudal and rostral groups were moderately consistent, they failed to reach significance in both tests: ANOVA and measure effect size (AR: Caudal = 8 mice; Rostral = 8 mice; Control Caudal = 2 mice, Control Rostral = 3 mice. Caudal/ MES = 0.31, CI = 0.82/-1.43; Rostral/MES = 0.06, CI = 1.18/-1.06. ANOVA F =0.30, p = 0.74. FR: Caudal = 10 mice; Rostral = 10 mice; Control Caudal = 2 mice, Control Rostral =3 mice; Caudal/ MES = 0.94, CI = 2.06/-0.19; Rostral/MES = 0.66, CI = 1.75/-0.44; ANOVA F =1.43, p = 0.26). Control caudal stimulation and

control rostral stimulation of the TRN did not exhibit any tendency for change in the gamma oscillation power (See Figure 3.20) blue and red dots).

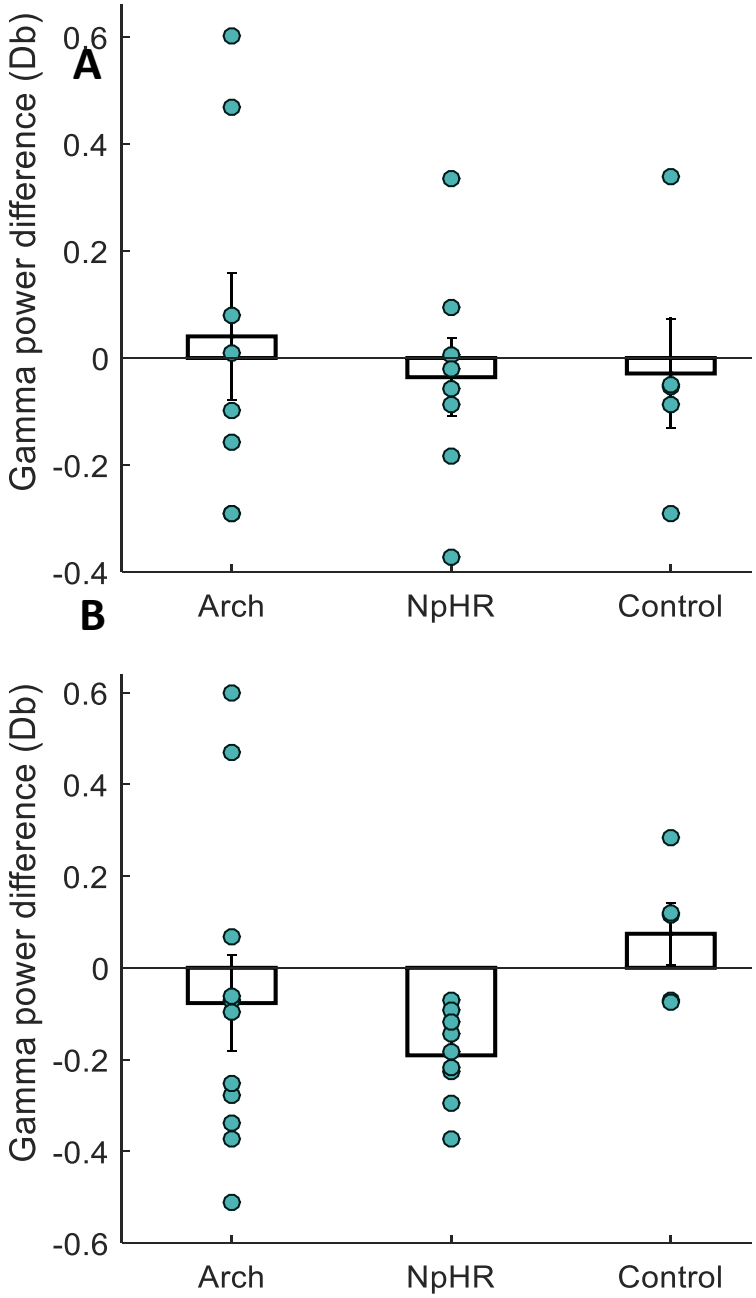

Figure 3.19 Summary of gamma oscillation change caused by the TRN light stimulations (inhibition) over 5 seconds during sleep in mice expressing Archaerhodopsin (Arch), Halorhodopsin (NpHR) and YFP (Control). EEG was recorded from auditory right (A) and frontal right (B) channels. Each green dot represents single animal result. Green light stimulation did not have significant effect on gamma oscillation power in both AR and FR channels. (**AR**: NpHR = 8 mice; Arch = 8 mice; Control = 5 mice. Arch/MES = 0.22, CI = 0.91/-1.34; NpHR/MES = 0.03, CI = 1.15/-1.09. ANOVA F =0.18, p = 0.82. **FR:** NpHR = 9 mice; Arch = 11 mice; Control = 5 mice. Arch/MES = 0.47, CI = 1.54/-0.60; NpHR/MES = 2.09, CI = 3.43/0.75; ANOVA F =1.84, p = 0.18. Error bars = SEM. Db - decibels).

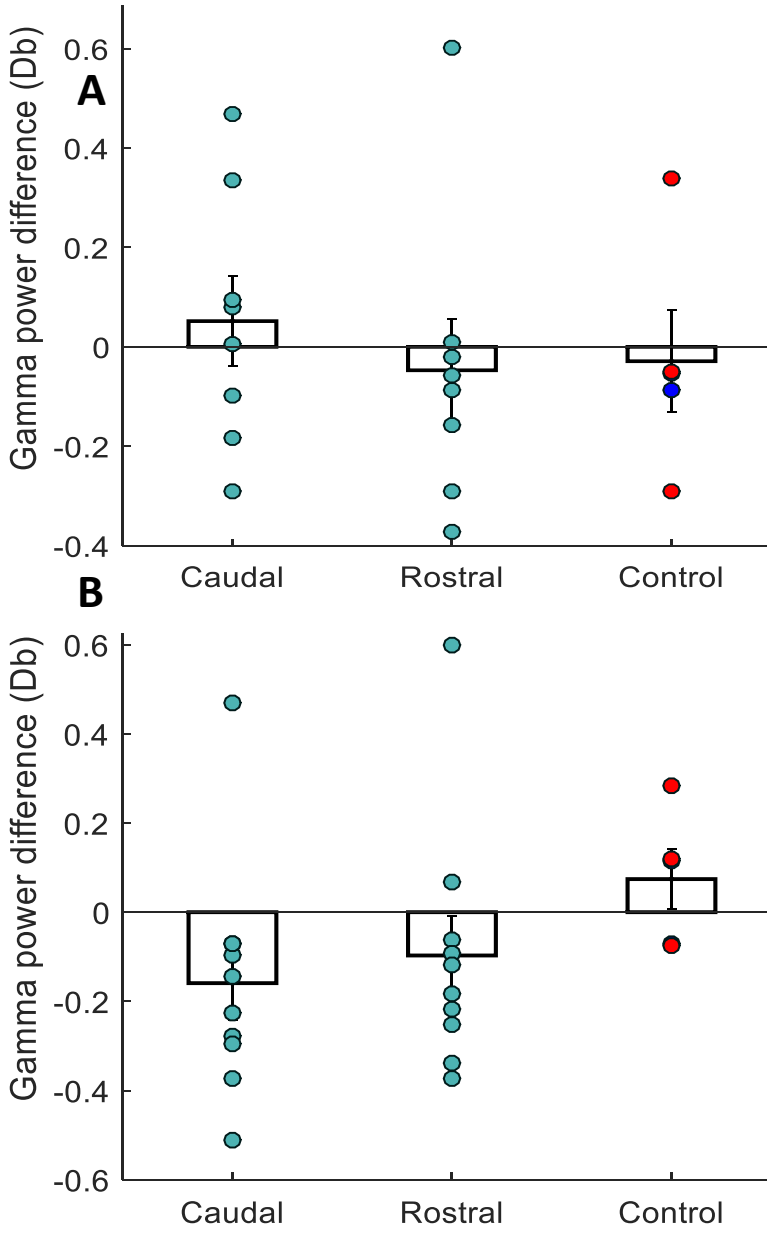

Figure 3.20 Summary of gamma oscillation change caused by light stimulation (optogenetic inhibition) of rostral and caudal part of the TRN. EEG was recorded from auditory right (A) and frontal right (B) channels. Results from caudal Arch and caudal NpHR animals are combined in Caudal, and the results from rostrally injected animals are assigned as Rostral. Each green dot represents single animal result. Rostrally injected control mice (red) are dissociated from caudally injected mice (blue) by color coding. Green light stimulation did not have significant effect on gamma oscillation power in both AR and FR channels. (**AR**: Caudal = 8 mice; Rostral = 8 mice; Control Caudal = 2 mice, Control Rostral = 3 mice. Caudal/ MES = 0.31, CI = 0.82/-1.43; Rostral/MES = 0.06, CI = 1.18/-1.06. ANOVA F =0.30, p = 0.74. **FR**: Caudal = 10 mice; Rostral = 10 mice; Control Caudal = 2 mice, Control Rostral = 3 mice; Caudal/ MES = 0.94, CI = 2.06/-0.19; Rostral/MES = 0.66, CI = 1.75/-0.44; ANOVA F =1.43, p = 0.26. Error bars = SEM. Db - decibels).

High Gamma oscillation (50-80 Hz)

Likewise, with the previous oscillation bands, we assessed the effect of TRN optogenetic inhibition on high gamma oscillation. During sleep, the optogenetic inhibition of the TRN in Arch, NpHR and YFP expressing animals did not generate any consistent changes in the high gamma band. (See Figure 3.21 AR: NpHR = 8 mice; Arch = 8 mice; Control = 5 mice. Arch/MES = 0.32, CI = 1.44/-0.8; NpHR/MES = 0.45, CI = 1.59/-0.68. ANOVA F =0.27, p = 0.76. FR: NpHR = 9 mice; Arch = 11 mice; Control = 5 mice. Arch/MES = 0.16, CI = 1.22/-0.89; NpHR/MES = 0.3, CI = 1.40/-0.80; ANOVA F =0.10, p = 0.90).

Localized stimulation (optogenetic inhibition) of the TRN did not result in any changes in high gamma oscillation (See Figure 3.22). Control caudal and control rostral light modulation had similar, non-consistent effects on high gamma band power (AR: Caudal = 8 mice; Rostral = 8 mice; Control Caudal = 2 mice, Control Rostral = 3 mice. Caudal/ MES = 0.38, CI = 1.51/-0.75; Rostral/MES = 0.35, CI = 1.48/-0.77. ANOVA F =0.27, p = 0.76. FR: Caudal = 10 mice; Rostral = 10 mice; Control Caudal = 2 mice, Control Rostral = 3 mice; Caudal/ MES = 0.30, CI = 1.38/0.78; Rostral/MES = 0.14, CI = 1.22/-0.93; ANOVA F =0.11, p = 0.89).

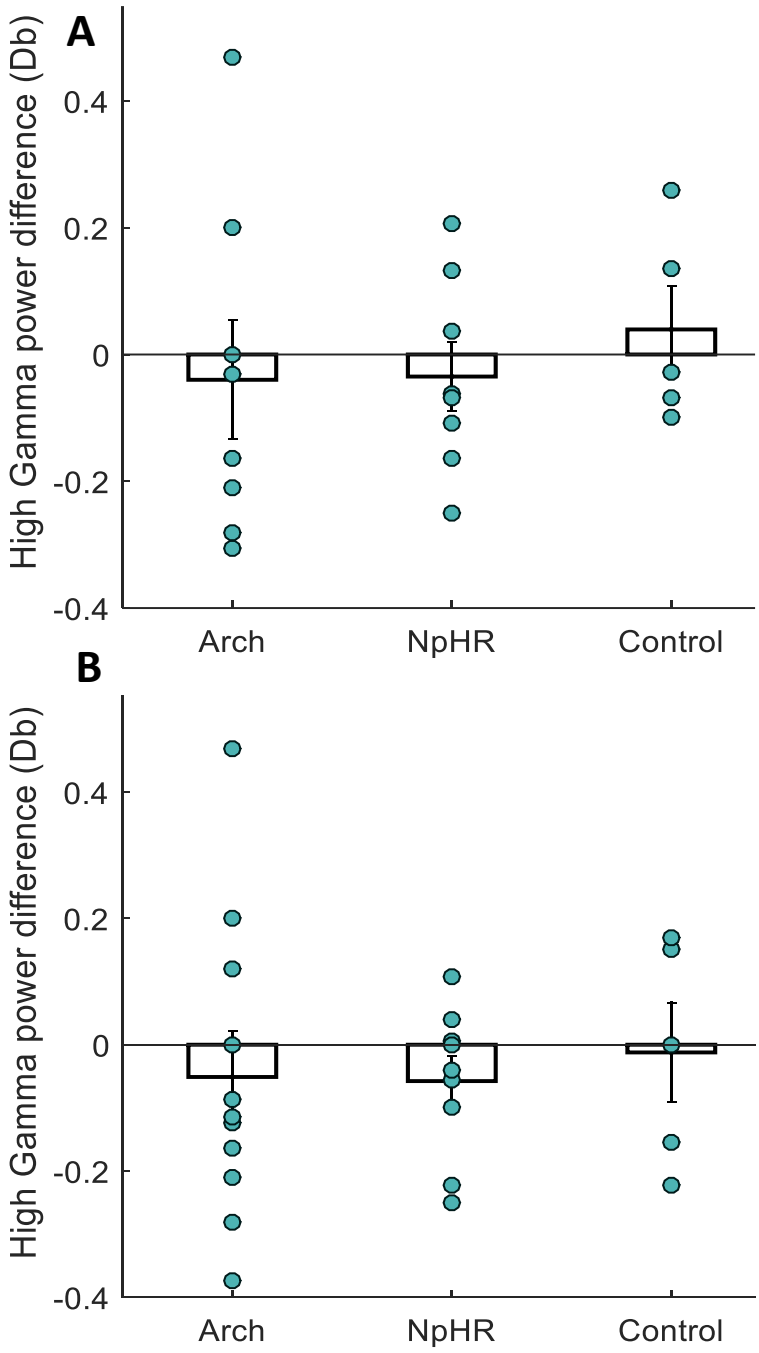

Figure 3.21 Summary of high gamma oscillation differences caused by the TRN light stimulations over 5 seconds during sleep in mice expressing Archaerhodopsin (Arch), Halorhodopsin (NpHR) and YFP (Control). EEG was recorded from auditory right (A) and frontal right (B) channels. Each green dot represents single animal result. Green light stimulation did not have significant effect on high gamma oscillation power in both AR and FR channels. (**AR**: NpHR = 8 mice; Arch = 8 mice; Control = 5 mice. Arch/MES = 0.32, CI = 1.44/-0.8; NpHR/MES = 0.45, CI = 1.59/-0.68. ANOVA F =0.27, p = 0.76. **FR:** NpHR = 9 mice; Arch = 11 mice; Control = 5 mice. Arch/MES = 0.16, CI = 1.22/-0.89; NpHR/MES = 0.3, CI = 1.40/-0.80; ANOVA F =0.10, p = 0.90. Error bars = SEM. Db - decibels).

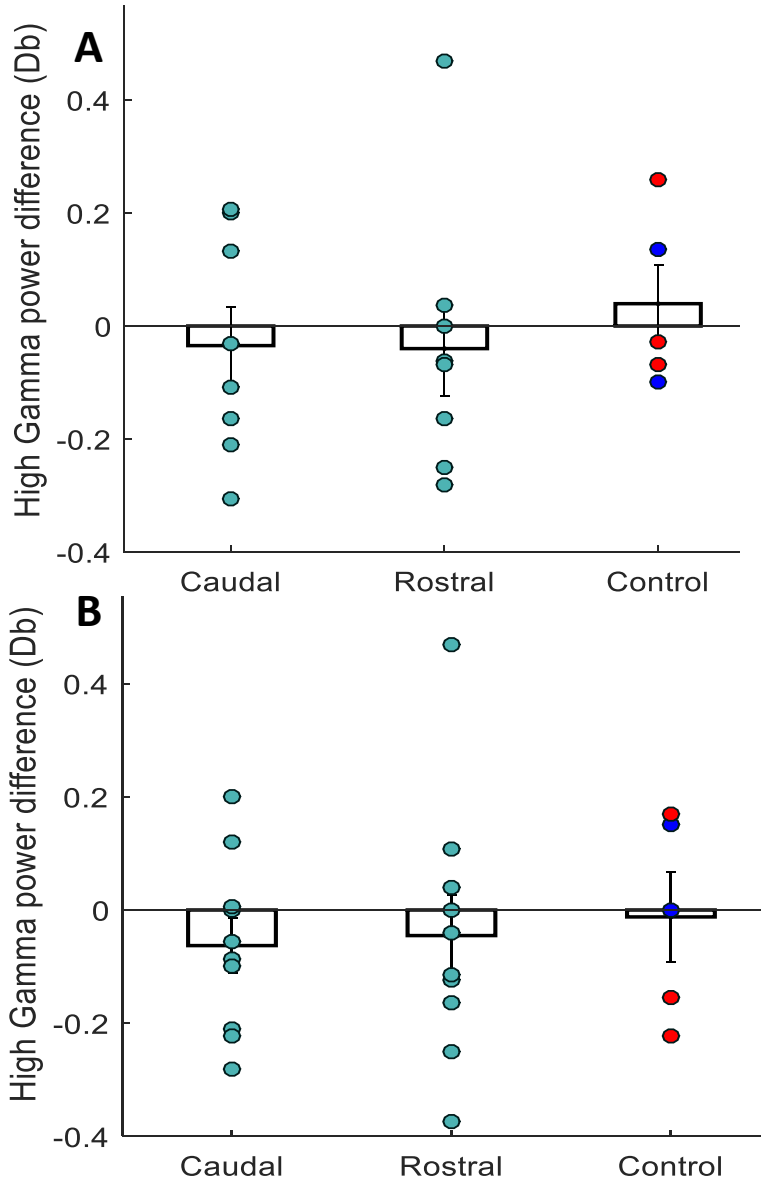

Figure 3.22 Summary of high gamma oscillation change caused by light stimulation (optogenetic inhibition) of rostral and caudal part of the TRN. EEG was recorded from auditory right (A) and frontal right (B) channels. Results from caudal Arch and caudal NpHR animals are combined in Caudal, and the results from rostrally injected animals are assigned as Rostral. Each green dot represents single animal result. Rostrally injected control mice (red) are dissociated from caudally injected mice (blue) by color coding. Green light stimulation did not have significant effect on high hamma oscillation power in both AR and FR channels. (**AR**: Caudal = 8 mice; Rostral = 8 mice; Control Caudal = 2 mice, Control Rostral = 3 mice. Caudal/ MES = 0.38, CI = 1.51/-0.75; Rostral/MES = 0.35, CI = 1.48/-0.77. ANOVA F =0.27, p = 0.76. **FR**: Caudal = 10 mice; Rostral = 10 mice; Control Caudal = 2 mice, Control Rostral = 3 mice; Caudal/ MES = 0.30, CI = 1.38/0.78; Rostral/MES = 0.14, CI = 1.22/-0.93; ANOVA F =0.11, p = 0.89. Error bars = SEM. Db - decibels).

3.3.2 Wake data analysis

All previous analysis was dedicated to the data recorded during sleep. The TRN is well known for its state dependent activity (Halassa et al., 2014), therefore we expected to see different results of TRN light stimulation during the awake state.

Despite expression of the Arch, NpHR and YFP in the rostral and caudal TRN, simulation (optogenetic inhibition) of the TRN during the awake state did not affect any of the tested EEG oscillations. Interestingly, the robust changes in the power of alpha and delta bands caused by the first 5 seconds of stimulation during sleep, were not apparent during awake state stimulations (See Figure 3.23 and 3.24). Delta band power was similar in all three animal groups during awake state stimulations (Virus groups ANOVA, $F = 0.11$, $p = 0.88$ and stimulation of location groups ANOVA, $F = 0.02$, $p = 0.97$; Sleep: NpHR = 9 mice, Arch = 11 mice, Control = 5 mice. Wake: NpHR = 8 mice; Arch = 6 mice; Control = 4 mice). Similar to the delta oscillation results, alpha oscillation during awake TRN stimulations was also unchanged (Virus group ANOVA, $F = 0.10$, $p = 0.90$ and stimulation location group ANOVA, $F = 1.16$, $p = 0.34$; Sleep: NpHR = 9 mice, Arch = 11 mice, Control = 5 mice. Wake: NpHR = 8 mice; Arch = 6 mice; Control = 4 mice). Theta, beta, gamma and high gamma results were also unaffected by green light stimulation during wake state.

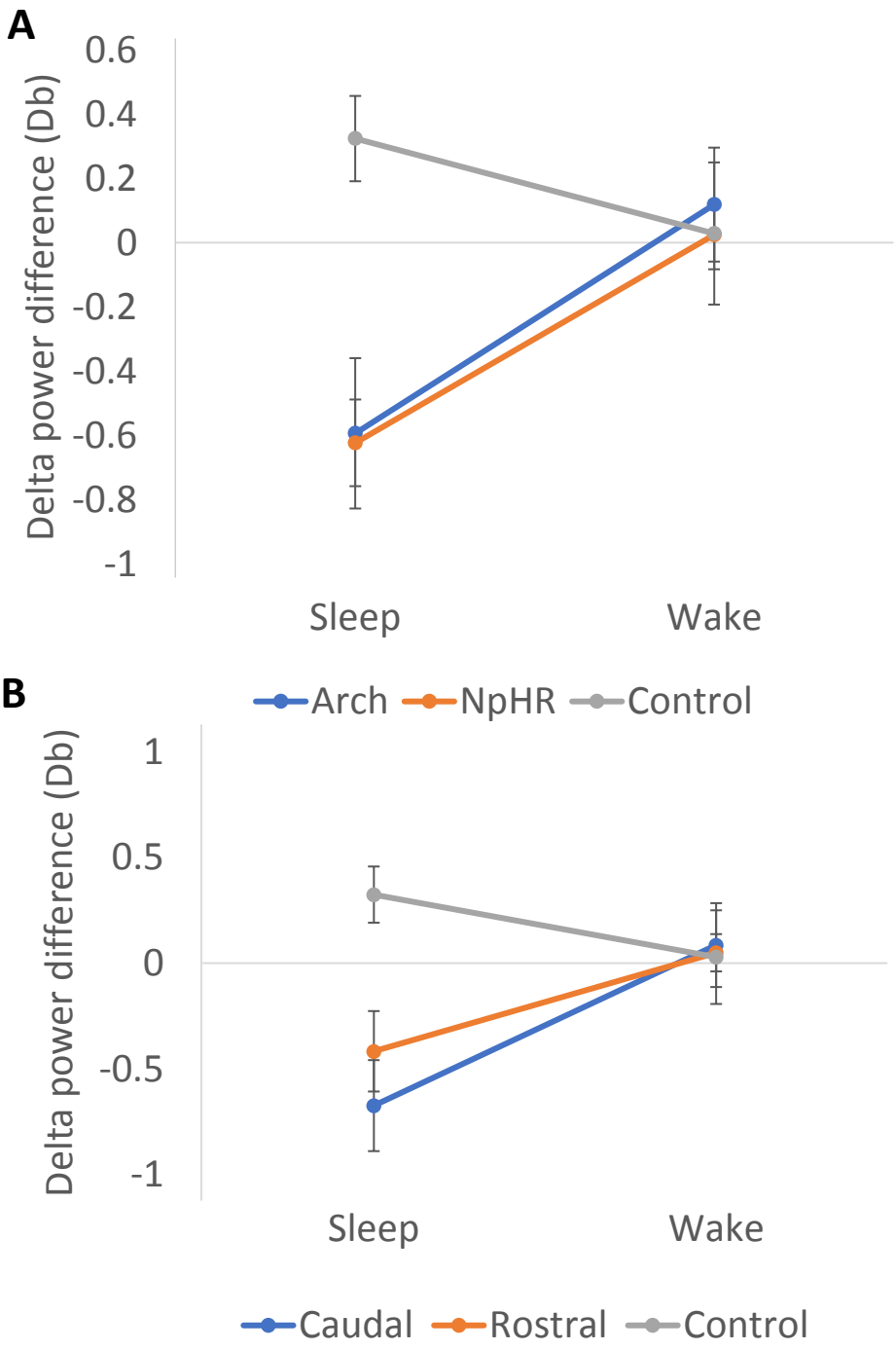

Figure 3.23 State dependent effect of TRN light stimulation (optogenetic inhibition). **A** Reduction of delta oscillation power, associated with TRN light stimulation, is state dependant. During 5 seconds of the TRN stimulation, delta oscillation was reduced in Arch and NpHR expressing animals, while it was slightly increased in Control (YFP) animals during sleep. Similar stimulations had no effect on delta oscillation of awake animals. ANOVA, F = 0.11, p = 0.88. **B** Delta reduction effect caused by light stimulation (optogenetic inhibition) of the rostral and caudal TRN was pronounced only during sleeping state. Similar stimulations during awake state produced uniform results for all mice. ANOVA, F = 0.02, p = 0.97. Sleep**:** NpHR = 9 mice, Arch = 11 mice, Control = 5 mice. Wake: NpHR = 8 mice; Arch = 6 mice; Control = 4 mice. Error bars = SEM. FR channel was used for analysis.

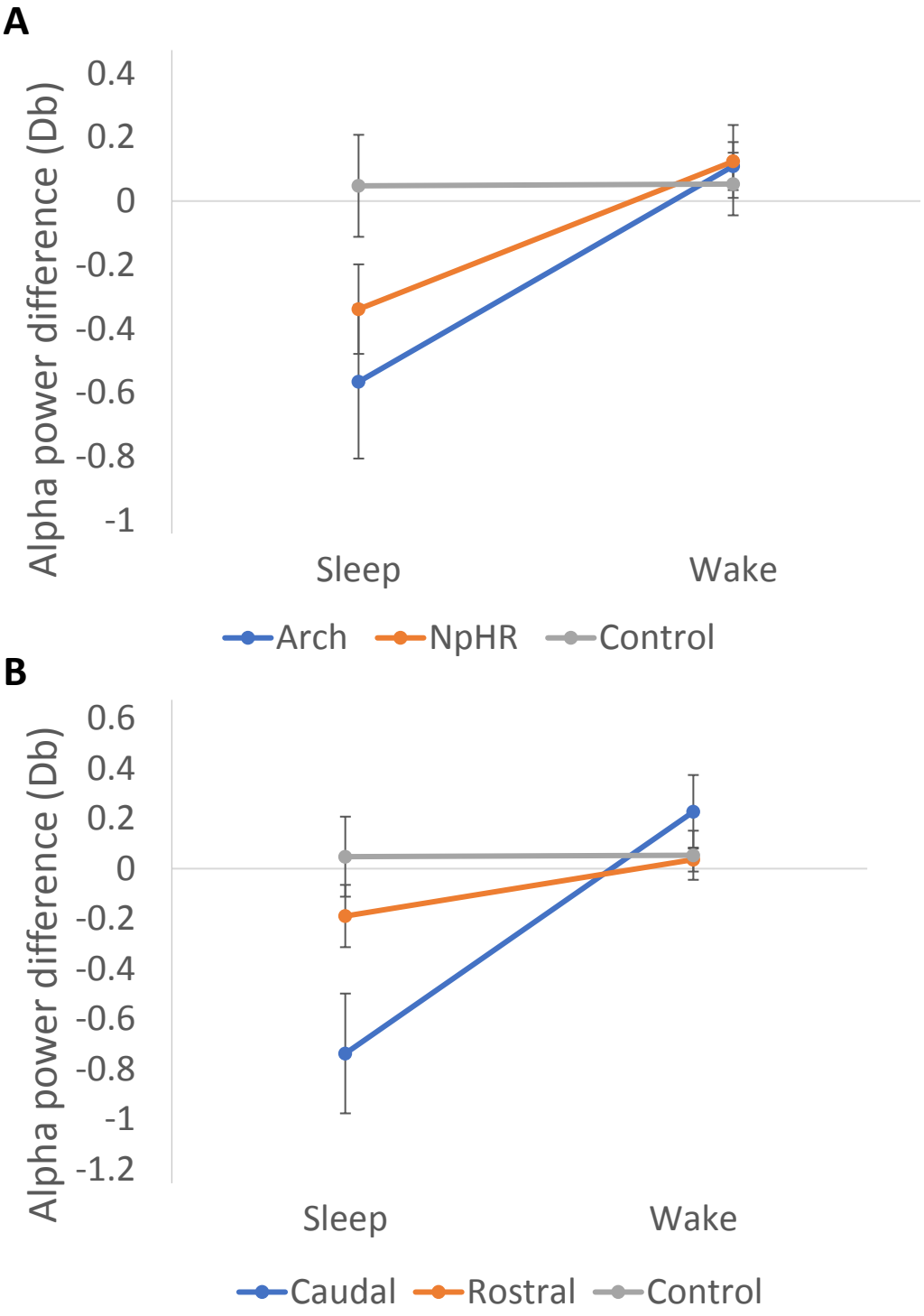

Figure 3.24 State dependent effect of TRN light stimulation (optogenetic inhibition). **A** The reduction of alpha oscillation power, associated with TRN light stimulation, is state dependant. Similar stimulations had no effect on alpha oscillation of awake animals. ANOVA, F=0.10, p = 0.90 **B** Alpha reduction effect caused by light stimulation (optogenetic inhibition) of the caudal TRN was pronounced only during sleeping states. Similar stimulations during awake state produced uniform results for all mice. ANOVA, F=1.16, p = 0.34. Sleep**:** NpHR = 9 mice, Arch = 11 mice, Control = 5 mice. Wake: NpHR = 8 mice; Arch = 6 mice; Control = 4 mice. Error bars = SEM. FR channel was used for analysis.

3.3.3 Effect of the continuous and recurring light stimulation

Tonic light stimulation to the TRN was delivered repeatedly. Light stimulation of 30 seconds was followed by an off-light period, which lasted typically for 60 seconds. A single recording session lasted on average two hours and contained nearly 60 stimulations. In order to understand if the continuous and recurrent light stimulation had an effect on the produced results, graphs portraying the relationship between the number of stimulations and changes in oscillation bands were generated (See Figures 3.24 - 3.28).

During the awake state, no significant correlations were detected between stimulation number and oscillation change in all animal groups (Arch, Halo, Control, Caudal, Rostral).

During sleep, diverse effects of repeated stimulation on oscillation bands were apparent. Caudally stimulated animals showed a slight, but significant negative correlation between alpha/beta oscillation change and continued stimulation. Alpha band correlation coefficient was equal to -0.2 and Beta band correlation coefficient was equal to -0.17 (See Figure 3.25, $n = 6$, $p < 0.05$). Alpha and beta oscillation powers showed a stronger reduction at the end of the stimulation session. In contrast, EEG changes for 5 seconds caused by rostral stimulation were not dependent on stimulation number (See Figure 3.26, $n = 6$).

Light stimulations of the rostral and caudal part of the TRN in animals expressing YFP (control), did not have any relationship between the number of stimulations and oscillatory band change as expected (See Figure 3.27 and Figure 3.28). However, rostrally stimulated animals showed a slight negative correlation (correlation coefficient = -0.22, $n = 3$, $p < 0.05$) between high gamma band changes caused by 5 second stimulations and the number of stimulations. These results suggest that light stimulation on its own (without inhibitory opsin expression) might influence animal's EEG and consequently their behavior.

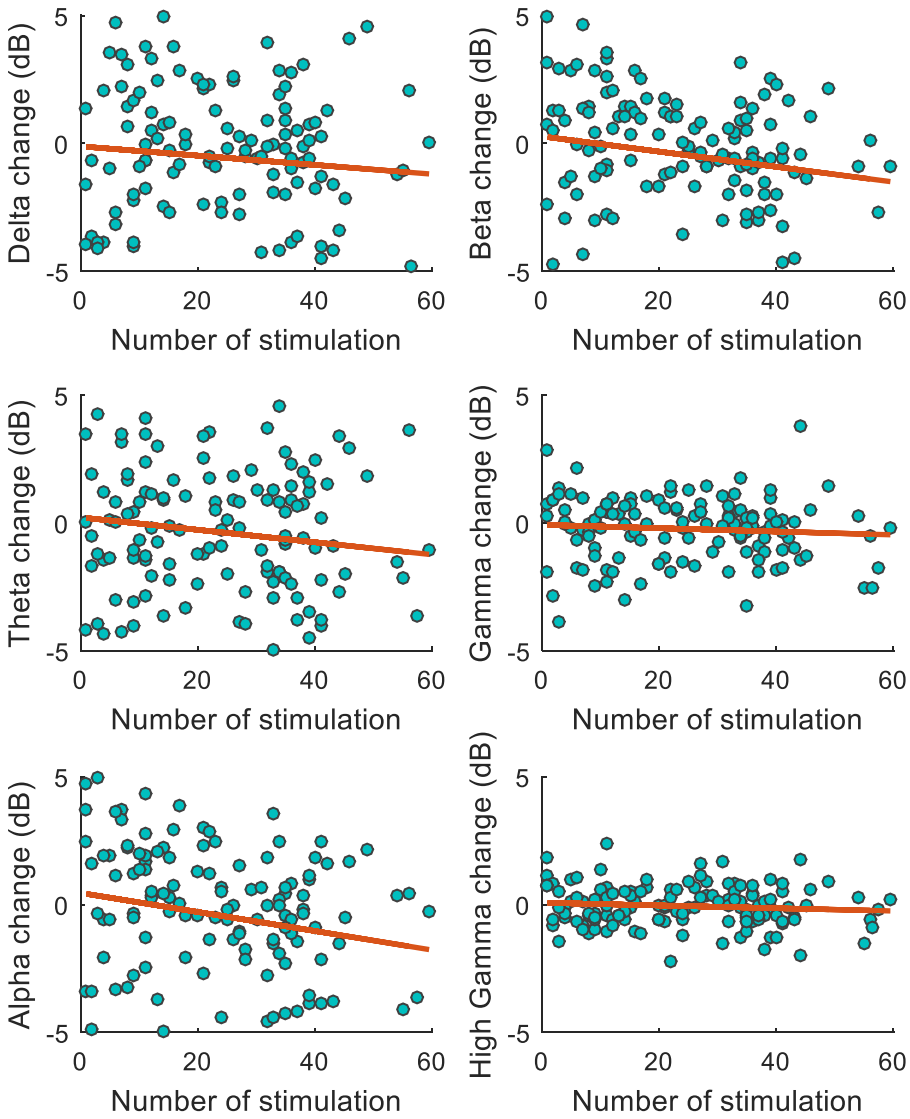

Figure 3.25 Relationship between the change in oscillation power resulting from 5 seconds of optogenetic inhibition and the number of stimulations in caudally stimulated animals expressing opsins. All shown stimulations were performed during the sleeping state. There was a moderate negative correlation between the differences of alpha and beta oscillations and the number of stimulations (n=6). The frontal right channel was used for analysis. Each green dot represents a power change during a single trial. Red line equates to a line of best fit'. n – number of mice.

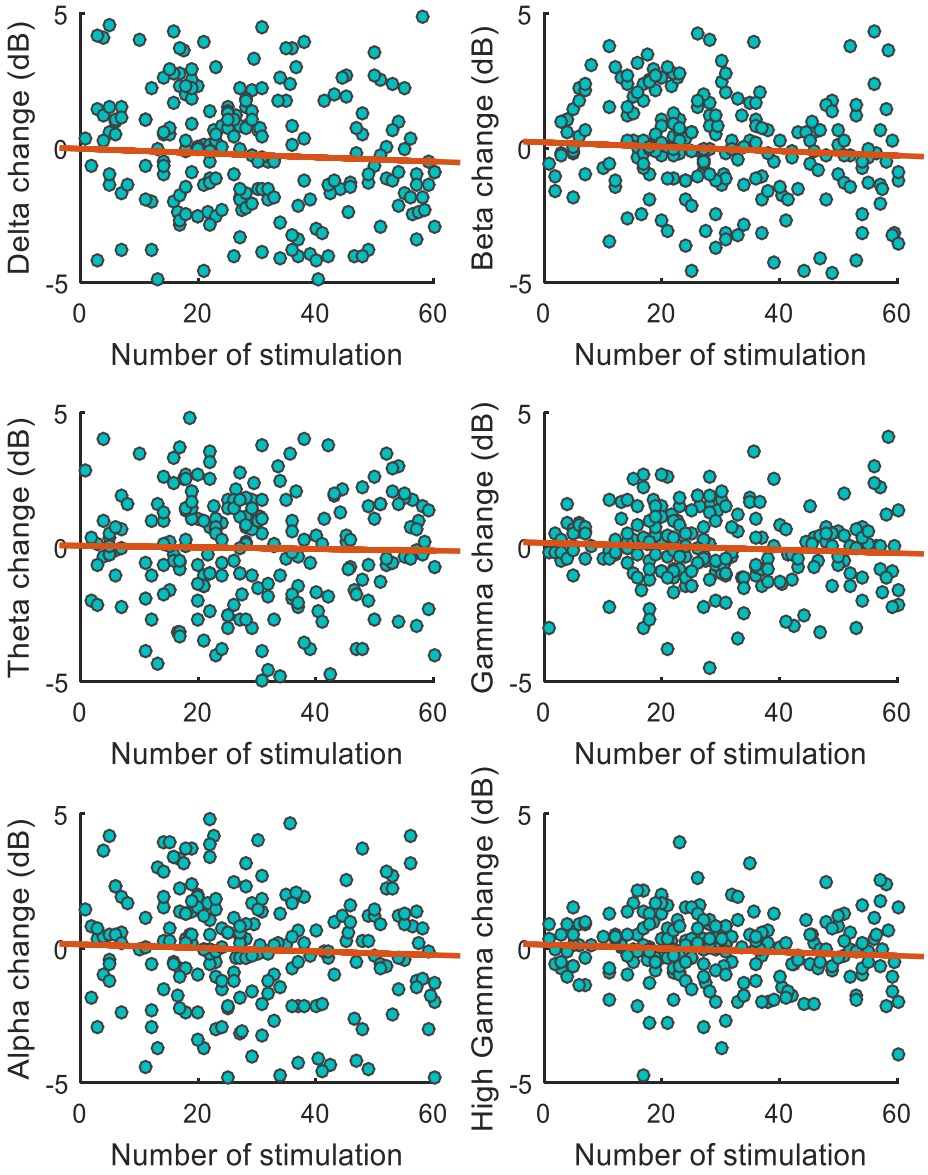

Figure 3.26 Relationship between the change in oscillation power resulting from 5 seconds of optogenetic inhibition and the number of stimulations in rostrally stimulated animals expressing opsins. Rostrally stimulated animals did not display any relationship between oscillation power change and number of stimulations. (n = 6)**.** Frontal right channel was used for analysis. Each green dot represents a power change during single trial. Red line – a line of best fit. n – number of mice.

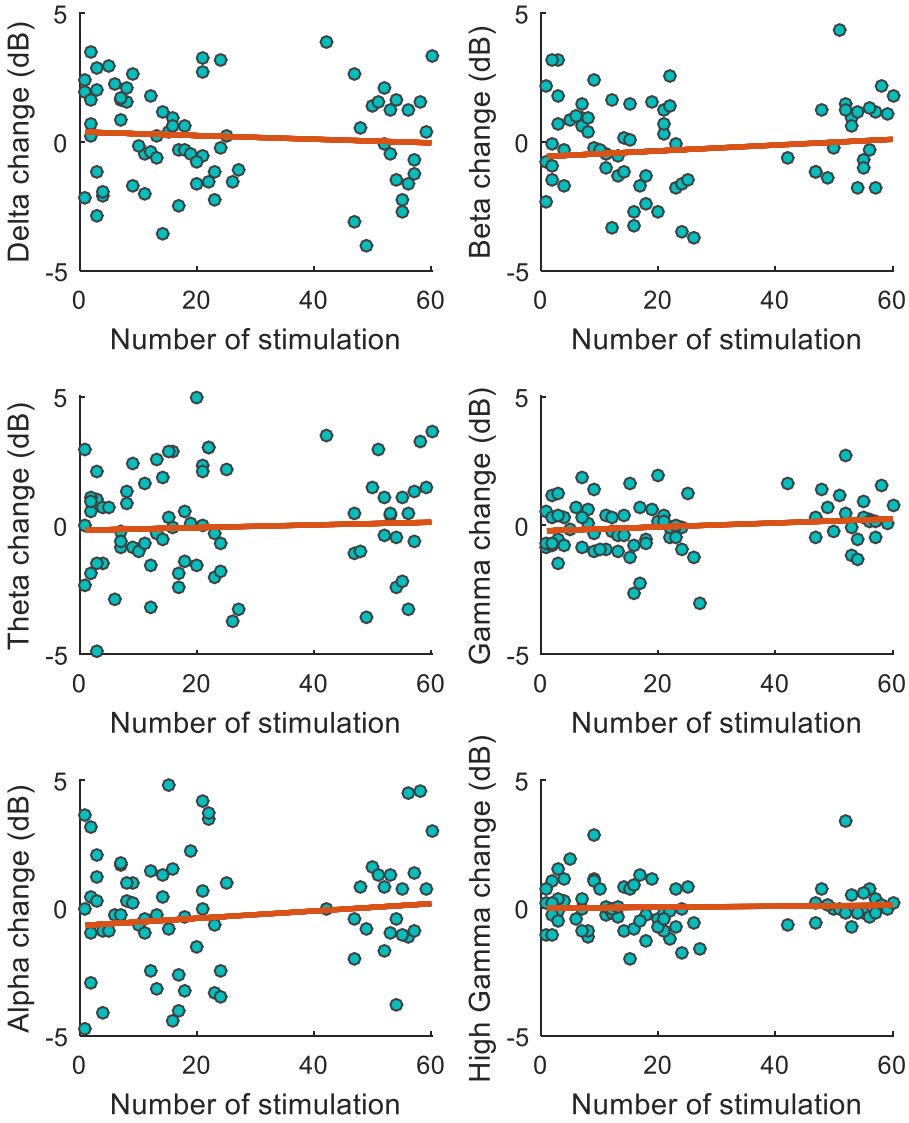

Figure 3.27 Relationship between the change in oscillation power resulting from 5 seconds of optogenetic inhibition and the number of stimulations in caudally stimulated animals expressing YFP (control). All shown stimulation were performed during sleeping state. Large number light stimulations in caudally stimulated control animals did not have any effect on oscillation frequency change (n = 2)**.** Frontal right channel was used for analysis. Each green dot represents a power change during single trial. Red line – a line of best fit. n – number of mice.

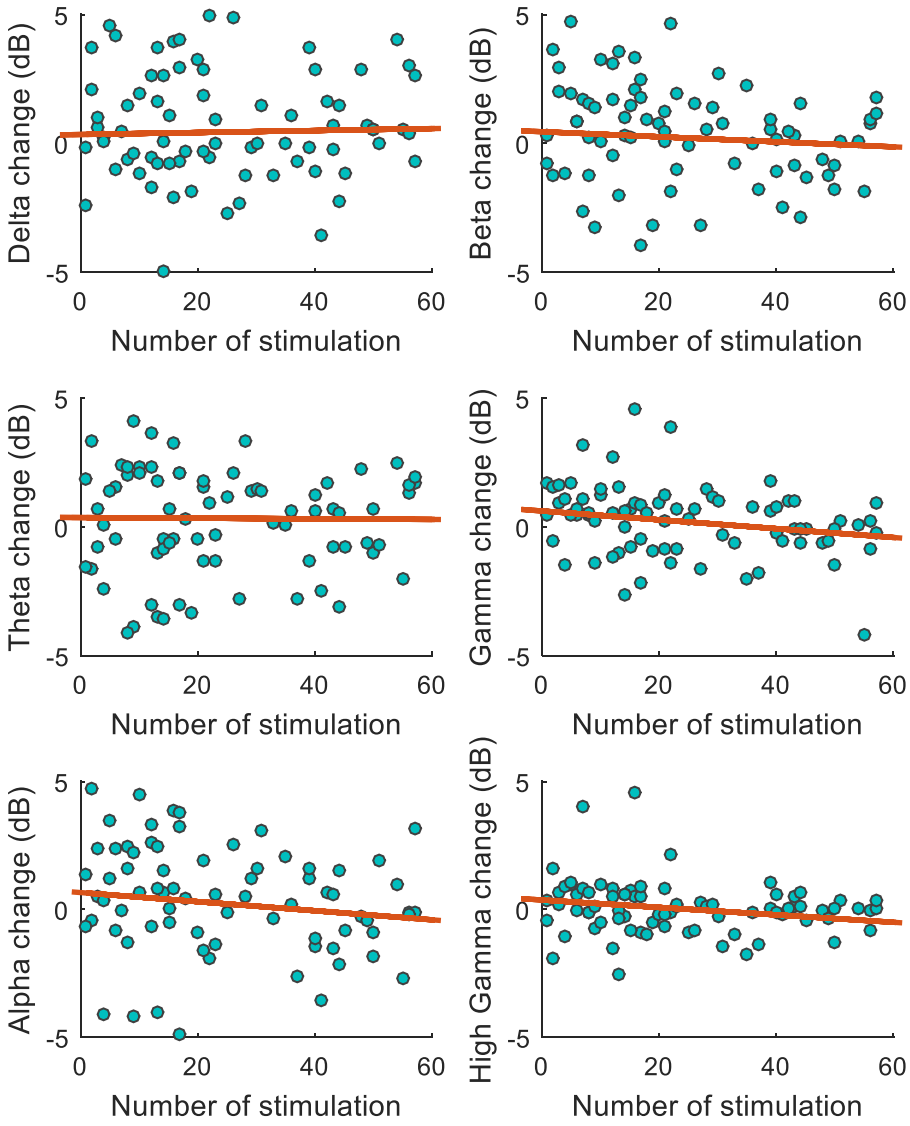

Figure 3.28. Relationship between oscillation power change in 5 seconds of light stimulation and number of stimulations in rostrally stimulated animals expressing YFP. Slight negative correlation between high gamma frequency and numbers of stimulation was detected (n = 3)**.** Frontal right channel was used for analysis. Each green dot represents a power change during single trial. Red line – a line of best fit. n – number of mice.

3.4 Discussion

To examine site-specific effects of optogenetic TRN inhibition on cortical EEGs, we compared cortical EEGs across different frequency bands before and after the onset of optical stimulation, by classifying data according to ongoing behavioural states (NREM sleep or wakefulness). During sleep, delta oscillations can be reduced by optogenetic inhibition in either the rostral or caudal TRN and that the reduction can be observed in both frontal and sensory cortical areas. On the other hand, alpha waves were modulated only by caudal TRN stimulation and the reduction in alpha power was observed only in the frontal cortical area. Additionally, beta waves showed opposite tendencies to change during optogenetic modulations of the rostral and caudal TRN. These effects were not observed when optical stimulation was applied during wakefulness. Therefore, the effect of optogenetic TRN inhibition on cortical EEGs depend on stimulation sites, cortical areas, oscillatory frequencies and ongoing behavioural states.

3.4.1 Slow/Delta oscillation is controlled by entire TRN

Optogenetic inhibition of the rostral and caudal TRN significantly reduced delta oscillation in recorded cortical areas for 5 seconds of stimulation during sleep. Caudal TRN inhibition expectedly showed a stronger reduction. The significant reduction in delta wave oscillation during rostrally stimulated (inhibited) TRN can be explained by the relatively crude targeting of the rostral TRN, during which the nuclei responsible for motor and sensory information coordination still can be reached by virus and light. In future, the retrogradely expressing opsins could be injected in the limbic part of the TRN to confirm the hypothesis (Halassa et al., 2011; Halassa et al., 2014). Right now, we cannot exclude the idea, that some of the thalamic limbic (cognitive) nuclei might take part in the slow/delta oscillation generation. Higher order nuclei (Sheroziya & Timofeev, 2014) and rostral TRN (Halassa et al., 2014) spike throughout the slow/delta oscillation, thereby hyperpolarisation of the TRN neurons, could affect the thalamic nuclei membrane potential and consequently, related oscillations.

Previously, sub-second optogenetic modulation in the rostral TRN had a strong effect on slow wave oscillations (Latchoumane et al., 2017)

Control stimulation of the TRN induced a long lasting slow/delta wave increase. A consistent increase in oscillations can be caused by heating effect induced by light activation and result in neuronal spiking. Lewis et al. (2015) using optogenetic activation induced strong and long lasting slow/delta wave increase during wake and sleep, although, control experiments were omitted. Our control results did not produce an increase in the delta oscillation during wake , what could be caused by the state dependent neuronal sensitivity to heat (Stujenske et al., 2015) or by insufficient neuronal activation (Znamenskiy & Zador, 2013).

3.4.2 Spindle oscillation is a characteristic for the caudal TRN only

Alpha waves in the frontal cortex were decreased for 10 seconds by the optogenetic inhibition of the caudal TRN, while rostral TRN light stimulation had no effect on spindle oscillations during sleep. These data suggest that the caudal TRN is responsible for the generation of spindle oscillations during sleep. Halassa et al. (2014) also demonstrated that the firing of the TRN neurons associated with sensory thalamus are correlated with sleep spindles. So, the modulation of the spindle oscillation during optogenetic inhibition of the caudal TRN and numerous tracing studies (See Chapter 1 – Topographical organization of the TRN) add weight to the idea that the so called 'sensory TRN' is found only in the caudal part of the TRN.

According to Halassa et al. (2014), sensory associated neurons show correlated firing in both oscillations: delta and sleep spindle, therefore we may have predicted a reduction of both waves in the caudally targeted TRN and no effect in the rostral TRN. Caudal TRN inhibition showed a perfect match to our expectations, whereas rostral TRN optogenetic inhibition also reduced delta oscillation significantly. Neurons of the rostral TRN are associated with the motor thalamus and might be linked only with delta oscillation or some of the higher thalamic nuclei could be inhibited during sleep similarly to relay nuclei.

It is important to note, that the recorded alpha oscillation can act as reflection of sleep spindles, but it does not try to replace spindle scoring, which reliability is also a matter of debate. Although, sleep spindles show similar frequency, they last no longer than 3 seconds and fire at least once in 10 seconds during NREM sleep (Fuentealba et al., 2005).

The alpha oscillation reduction was recorded in the frontal cortex only. Knowing that mice cortex can generate topographically distinctive spindles allows us to propose, that the caudal TRN is responsible for the generation of the frontal sleep spindles, but putatively, this is not the case. Previous sleep spindle scoring results and anatomical distance between caudal TRN and frontal cortex support the idea that optogenetic inhibition of the caudal TRN affected global sleep spindles. The expected reduction of the sleep spindle in the auditory cortex, apparently, was hidden by the heating effect on the non-PV cells or through other unknown mechanism (Stujenske et al., 2015).

One Korean lab persistently targets the rostral TRN for optogenetic sleep spindle activation and inhibition (Kim et al., 2012; Latchoumane et al., 2017). That lab induced spindles in the wake/sleep animals at a higher success relatively to Halassa et al. (2011) and managed to associate rostrally activated spindles with ripples and memory consolidation. Seemingly, they are dealing with frontal spindles, which are responsible for different functions (Kim et al., 2015).

3.4.3 Diverse modulation of beta wave of the distinct parts of the TRN

Optogenetic inhibition of the caudal TRN showed strong and significant reduction of the beta oscillation, whereas the same stimulation in the rostral TRN moderately increased power of the beta waves over 10 seconds of stimulation (Fig 3.18). This is the first evidence of opposite band modulation due to different stimulation location of the TRN. Perhaps, the heterogenous nature of the connections between the TRN and subcortical afferent play an important role in this modulation (See chapter 1). Basal forebrain, globus pallidus and brainstem send their axons to the TRN and are closely associated with beta oscillation (Brown et al., 2012).

Although, sample sizes were small, control stimulations of the different segments of the TRN showed a similar response. Light stimulation of the caudal TRN showed a tendency to reduce power and a similar stimulation of the rostral TRN expressing YFP showed an increase in the beta oscillation. However, the number of control samples is too low for statistical analysis, and hence the given beta wave data should be treated with caution. Although, the beta power reduction in control animals was smaller than in the animals expressing inhibitory opsins in the caudal TRN. Once again, this beta modulation during rostral and caudal control stimulation might be caused by heating effect, which depolarized TRN neurons or incoming axons. Lewis et al. (2015) reported that during optogenetic activation of the caudal part of the TRN, the beta power was moderately reduced relative to non-stimulated EEG. Overall, an increased number of control stimulations is required to understand better the association between beta wave and the segments of the TRN.

Beta oscillations have not previously been a focus of TRN related research and are generally perceived as a slow gamma or a subharmonic of ongoing gamma oscillations due to spiking imbalance of inhibitory and excitatory neurons (Brown et al., 2012). During anaesthesia induction of gamma frequency is reduced to the beta range as sedation develops and ends up in the alpha range during the unconscious state (Scheib, 2017). Additionally, a mouse model of Downs syndrome (Dp16) showed disrupted NREM associated with reduced delta oscillations and increased alpha/beta oscillations (Levenga et al., 2018). Therefore, affiliated oscillations are associated with arousal/consciousness and it could be expected that beta/alpha and delta power reduction in caudally stimulated animals could result in disrupted sleep as well.

3.4.4 TRN state dependent control of the cortical EEG

We provide evidence that delta/alpha/beta oscillations reductions by optogenetic inhibition are state dependent and are pronounced only during sleep. Lewis et al. (2015) first showed that optogenetic inhibition of the TRN with halorhodopsin during sleep induced slow wave reduction, while identical stimulation during the awake state did not produce any significant effect. TRN oscillation control during sleep, is possible, due to sensitivity of the hyperpolarized thalamocortical neurons (Steriade

et al., 1991). Activation of the TRN neurons induce, a strong hyperpolarization on the thalamic neurons, which results in a rapid increase of slow/delta oscillation (Lewis et al., 2015), whereas the reduced neuronal burst firing of the TRN neurons during optogenetic inhibition might lead to a more depolarized membrane potential of the thalamus. During the wake state, thalamic neurons have higher membrane potential levels and the TRN neurons exhibit weaker inhibitory control, fire tonically and can only amplify chosen cortical inputs without modulation of their content (Halassa & Acsády, 2016). Thus, the optogenetic inhibition of the TRN during the awake state does not have a pronounced effect on the EEG oscillations, but still has obvious consequences on behaviour (Halassa et al., 2014; Clemente-perez et al., 2017).

3.4.5 Repeated optogenetic inhibition (light stimulation) effect on TRN

The number of tonic and repeated light stimulations (optogenetic inhibition) of the caudal TRN had a minor negative correlation with alpha and beta power reduction over 5 seconds. Light stimulations did not produce consistent alpha and beta oscillation reductions and at the beginning of the stimulations an increase of alpha/beta power was recorded in various trials. The reduction of alpha/beta power was recorded more often with an increased number of stimulations. Similar slight negative correlations between high gamma change and the number of stimulations was found in the control animals with rostrally stimulated TRN. This slight correlation might be caused by the ionic mechanisms linked with optogenetics or heating. Interestingly, that EEG bands linked to the slight correlation in the caudal and rostral TRN did not match. However, all mentioned correlations were relatively small (~ -0.2, $p < 0.05$), and may not be a robust effect.

3.4.6 Off target stimulations

In order to minimize the risk of off-target stimulation we used optogenetics with the cre-lox system, which allowed us to target only parvalbumin (PV) containing neurons. Up to 80% of neurons in the TRN express PV and none are found in the thalamus (Pritz & Stritzel, 1993; Arai et al., 1994), therefore parvalbumin sensitive expression acts as an exceptional tool for optogenetic differentiation between the TRN and thalamus. Although, the failure to target precisely the TRN with viral infection in a

few mice resulted in green fluorescence in the thalamic cell area. We can exclude thalamic optogenetic inhibition for two reasons: firstly, our results match with previous TRN modulations outcomes (Halassa et al., 2014; Lewis et al., 2015; Latchoumane et al., 2017) and secondly, the optogenetic inhibition of the thalamic cells would induce opposite results: further hyperpolarize the cells and a consequent delta band power increase.

Another adjacent nucleus to the TRN, the globus pallidus (GP), contains an abundant number of neurons expressing parvalbumin (Jaeger & Kita, 2011). In a few of the caudally and rostrally targeted mice, a small inner part of the GP expressed the virus (See Method, figures 2.5 – 2.7 and Appendix, figures 8.1 – 8.25). Additionally, the globus pallidus sends axons to the rostral/central part of the TRN in rodents (Asanuma & Porter, 1990; Cornwall et al., 1990d; Gandia et al., 1993). Although, the light beam did not propagate to the GP neurons, we can expect that the low number of synapses from the GP in the TRN expressed inhibitory opsins. Recently, Spellman et al. (2015) by targeting the axonal terminals with optogenetic inhibition managed to moderately inhibit them (30-50%). So, we can expect moderate inhibition of a small number of GP terminals in the TRN together with PV neurons. This additional GP terminal inhibition did not affect results significantly. The GP cell do not fire frequently during NREM sleep (Lazarus et al., 2013) and the inhibition or activation of the GP during anesthesia does not modify the burst firing of the TRN neurons (Villalobos et al., 2016). Moreover, partial inhibition of several GABAergic terminals on already hyperpolarized neurons are not expected to produce an additional effect.

The zona incerta, located directly under the TRN, sends axons to the middle and rostral part of the TRN and contains a large number of parvalbumin expressing cells (Cavdar et al., 2006; Watson et al., 2014). Histological examination revealed that zone incerta did not express the virus (See Appendix, figures 8.1 – 8.25). Even if it did, the irradiance of green light was extremely low and would not be predicted to reach the deep nucleus (See figure 2.4) as the zona incerta is located 1,5 mm away from the tip

of the fibre. Therefore, we can exclude a contribution of the zone incerta to the results.

3.4.7 Timing of the optogenetic modulation explained

Tonic light was presented for 30 seconds in each trace but the modulation of the oscillations of interest lasted only 5 or 10 seconds. The short timescale of the reductions of the oscillations can be explained by the photocurrent decline characteristics for Arch and NpHR opsins. After 15 second of continuous light stimulation photocurrent declines to 70% of starting stimulation, due to inactivation phase of ion channels after prolonged light stimulation (Gradinaru et al., 2008). The intensity of the light stimulation was quite low (3 mW), but we still cannot exclude the heating effect on non-PV cells, which could also help to decrease the time of modulation. Interestingly, the significant delta band reduction lasted for about 5 seconds, whereas the alpha/beta band effect was longer. During delta oscillations, thalamic cells should be more hyperpolarized than during sleep spindle generation (Huguenard, 1996). Putatively, after 5 seconds optogenetic inhibition, the photocurrent gradually was reducing, heating was at maximum and the light caused inhibition of the TRN were becoming not effective enough to keep all neurons silent and subsequently, the thalamic cells gradually hyperpolarized back to lower membrane potential with the help of brainstem firing.

3.4.8 Missing data for confirmation of optogenetic inhibition

Although, our results are consistent with previous findings (Halassa et al., 2014; Lewis et al., 2015), we still require data from single unit firing to confirm that the light caused inhibition of the TRN neurons. The TRN is not a simple structure for electrophysiological characterization. When Lewis et al. (2015) activated TRN neurons with tonic light most of the thalamic neurons were hyperpolarized, but only a quarter of the TRN neurons had increased spike rate, whereas most of the TRN neurons had reduced firing rate. A similar heterogenous electrophysiological firing is expected during TRN during optogenetic inhibition.

3.4.9 Summary

Tonic stimulations of the TRN during awake states did not produce any significant change in EEGs, whereas stimulations during sleep decreased delta power during 5 seconds of stimulation in all opsin expressing animals. Light stimulation of the caudal part of the TRN decreased alpha band oscillations for 10 seconds, whereas animals with rostrally stimulated TRN did not have any significant effect on alpha oscillation. Additionally, rostrally and caudally stimulated animals had opposing effects on beta oscillations during 10 seconds of stimulation. Although, it was a relatively crude way to test the hypothesis, we concluded that rostral and caudal TRN consist of the distinct subnetworks which have different activity levels during sleep. The caudal TRN is responsible for the modulation of the alpha and beta oscillations, whereas both parts of the TRN can control the delta oscillation.

Chapter 4: Effect of TRN optogenetic inhibition upon the sleep/wake cycle

4.1 Introduction

Abnormal sleep is a common feature of most diseases. Diabetes, obesity (Nedeltcheva & Scheer, 2014), chronic pain (Choy, 2015), neuropsychiatric disorders (Jagannath et al., 2013), gastrointestinal disorders (Ali et al., 2013) and many more are caused or are associated with abnormal sleep. Sleep disorders are a global issue, but their causes and consequences are not well understood.

Neurobiology relevant sleep research started in the 1930s, when Bremer, by trisecting brainstem between the pons and midbrain, induced chronic drowsiness in the cat (Bremer, 1935), whereas a similar transection of the pons rostral to the trigeminal nerve induced constant wakefulness (Batini et al., 1958). In addition, Moruzzi & Magoun (1949) confirmed that wakefulness is correlated with a tonic barrage of impulses from the midbrain reticular formation, which desynchronise cortical oscillations. Experiments mentioned above suggested that both the “sleep centre” and “wake centre” neurons are found in the brainstem and that sleep, apparently, is caused by the inhibition of neurons of the wakefulness “centre” in the rostral pons.

Wakefulness is maintained by tonic activation of the ascending reticular activation system (ARAS) (Schwartz & Kilduff, 2015). ARAS is comprised of noradrenergic locus coeruleus (LC), serotonergic (5-HT) raphe nuclei, dopaminergic ventral tegmental area (VTA), GABAergic and dopaminergic substantia nigra (SN), cholinergic laterodorsal and pedunculopontine tegmentum (LDT/PPT), cholinergic parabrachial nucleus and periaqueductal gray matter (Brown et al., 2012). Neurons in the ASAR directly and indirectly (via thalamus, hypothalamus and basal forebrain) activate cortical neurons (Jones, 2005; Carter et al., 2010; Ito et al., 2013). Some difficulties were encountered during identification of the sleep promoting “centre”. The solitary nucleus has sleep active neurons and for a long time were accounted for as a “sleep centre” (Eguchi & Satoh, 1980). Recent chemo- and optogenetic studies showed that, the medullary parafacial zone (PZ) by inhibiting parabrachial neurons projecting to

basal forebrain, promote NREM sleep at the expense of wakefulness and REM sleep (Anaclet et al., 2015).

Although, the brainstem is crucial for wakefulness and sleep state generation, areas such as the hypothalamus and basal forebrain are also important for sleep and wakefulness regulation. The hypothalamus contains arousal active neurons (Herrera et al., 2015) and sleep active neurons in in the ventrolateral preoptic nucleus (VLPO) (Alam et al., 2014). VLPO neurons project heavily to nuclei of the ARAS (Sherin et al., 1998) and its neurotoxic lesioning decrease delta power and NREM sleep time in the rat (Lu et al., 2000). The basal forebrain comprises several circuits that promote REM and NREM sleep (Xu et al., 2015) and damage of the preoptic area of the basal forebrain results in persistent insomnia (McGinty & Sterman, 1968).

The sleep process would be too simple if it was dependant on a few brain structures. Synchronized EEG oscillations of the cortex during NREM sleep, which, putatively, dissociate the forebrain from outside world (Steriade, 2006), is possibly due to the progressive reduction in firing of neurons in the ARAS and is orchestrated by well-known intrinsic modulators: cortex, thalamus and thalamic reticular nucleus (TRN) (Paré & Steriade, 1993; Steriade, 1994b; Crunelli & Hughes, 2010). Thus, the malfunction of any modulator can influence the sleep quality and quantity.

Due to original anatomical and neurochemical features, TRN is capable of controlling and influencing thalamocortical and corticothalamic cell firing (Crandall et al., 2015; Deleuze & Huguenard, 2016). Additionally, the TRN receives inputs from all brainstem nuclei included in the ARAS (Kolmac & Mitrofanis, 1998), hypothalamic wake correlated circuitries (Herrera et al., 2015), basal forebrain (Cornwall et al., 1990e) and from sleep active nuclei: solitary nucleus (Nanobashvili et al., 2009) and zona incerta (Cavdar et al., 2006). The capability of the TRN to influence NREM sleep oscillations (Halassa et al., 2011; Lewis et al., 2015) and the existence of inputs from the subcortical areas controlling global brain state allows the TRN to act as an important regulator of the sleep/wake cycle.

Local cortical slow wave oscillation (< 4 Hz), sleep spindles (9-15 Hz) and brain state modulation are functionally interconnected and are rapidly controlled by the TRN (Halassa et al., 2011; Lewis et al., 2015; Herrera et al., 2015). Tonic optogenetic activation of the TRN neurons induces an increase in the slow/delta oscillation during wake and sleep, while tonic optogenetic inhibition leads to a reduction in delta oscillation in the sleeping state only (Lewis et al., 2015). Tonic activation of the TRN produces a sleep like state, characterized by increased delta oscillation and reduced locomotion, during awake (Lewis et al., 2015) and short tonic inhibition of the TRN results in arousal (Herrera et al., 2015). Additionally, artificially induced sleep spindles by optogenetic activation can increase the time spent in NREM sleep (Kim et al., 2012; Ni et al., 2016), and vice versa the mice with reduced number or quality of sleep spindles show shorter NREM sleep episodes (Wimmer et al., 2012; Wells et al., 2016). Potentially, the cortex or brainstem depending on the brain state exploit the TRN like a controlling device, which through modulation of the thalamic neurons can control local cortical oscillations and alertness of the forebrain.

According to Halassa et al. (2014) the TRN is a heterogenous structure, where neurons associated with sensory thalamic cells demonstrate correlated firing with delta and sleep spindle oscillations during sleep, whereas neurons connected with limbic thalamic cells show correlated spiking with arousal. We, by reviewing the TRN interconnections with the thalamus, afferents from different brain areas, neurochemical diversity, morphology, electrophysiological properties and physiological functions (Chapter 1), portrayed that the dissociation between the sensory and limbic TRN can be based on the anatomical location. Caudal TRN has sensory features and rostral TRN mostly responsible for limbic (cognitive) modulations. In Chapter 3, it was demonstrated that the caudal TRN is responsible for modulation of sleep spindles and beta oscillations. Therefore, we can expect that the optogenetic inhibition of the different parts of the TRN may have diverse effects on the sleep/wake cycle.

Tonic optogenetic inhibition of the caudal TRN, which facilitates sensory pathway inhibition during sleep, will reduce the number of sleep spindle oscillations stabilizing sleep and consequently, should shorten NREM sleep episodes. Reduction of rostral TRN firing, correlated with arousal (Halassa et al., 2014), might prolong NREM sleep episodes. Consequently, analogous modulation of the neuronal activity in the different parts of the nucleus should produce contrasting outcomes on the sleep/wake cycle.

4.2 Methods

To investigate the effect of caudal and rostral TRN modulation on the sleep/wake cycle, we combined optogenetic and electrophysiological approaches in freely moving mice. Two inhibitory opsins Halorhodopsin (NpHR), Archaerhodopsin (Arch) and YFP (Control) were expressed specifically in anterior or posterior part of the TRN in parvalbumin (PV)-Cre mice using adeno-associated viral vectors (NpHR, n = 8; Arch, n = 6 and YFP (Controls), n = 5). Virus was injected caudally (AP, -1.6 mm) in the caudally targeted TRN and rostrally (AP, -0.8) in the rostrally targeted TRN. Similar coordinates were used for chronic optic fibre placement. We found restricted expression patterns of Arch and Halo in PV-positive neurons of the TRN depending on injection sites (See Figure 2.3-2.5). The effect of optical stimulation on the brain state was assessed using simultaneously recorded EMG. We classified behavioural epochs into two states: wake and slow-wave sleep (SWS). Rapid eye movement sleep (REM) classification was omitted in our analysis due to negligible time spent in this state (5%-10% of sleep) (Brankačk et al., 2010). Additionally, previous TRN optogenetic modulations showed no effect on REM sleep oscillations (Herrera et al., 2015). To compare differences between viral groups and controls, ANOVA, two sample paired test and measure effect size (MES, Hedges) with confidence intervals (CI) were employed. For full details of the surgical and experimental methods and the location of the viral expression patterns see Chapter 2.

4.3 Results

4.3.1 Sleep/wake cycle during No Stim and Stim sessions

Sleep pattern before and during light stimulation

In order to compare the sleep pattern before and during TRN light stimulation, several (1-3) recordings in freely moving mice were performed without optic fibre cable attachment to the optic probes on the mice head (See figure 4.1). Initially, each mouse was habituated to the open field environment and had an attached EEG/EMG cable for at least 5 days. As soon as the mouse felt asleep, the first control recording session was introduced. During the control recording session (No Stim) optic cable fibres were located outside the black box and the TRN was not stimulated. After the first control (No stim) session, several stimulation sessions (Stim) followed, during which optic fibres were connected to chronically implanted optic probes on the mouse head. The stimulation protocol was cyclic and consisted of 30 seconds of tonic green light stimulation followed by 60-90 seconds of no light stimulation. The protocol was analogous for Stim and No Stim sessions. After several Stim sessions, another No Stim session was introduced. In total, only two No Stim sessions were performed, whereas the number of Stim sessions was dependant on the sleeping

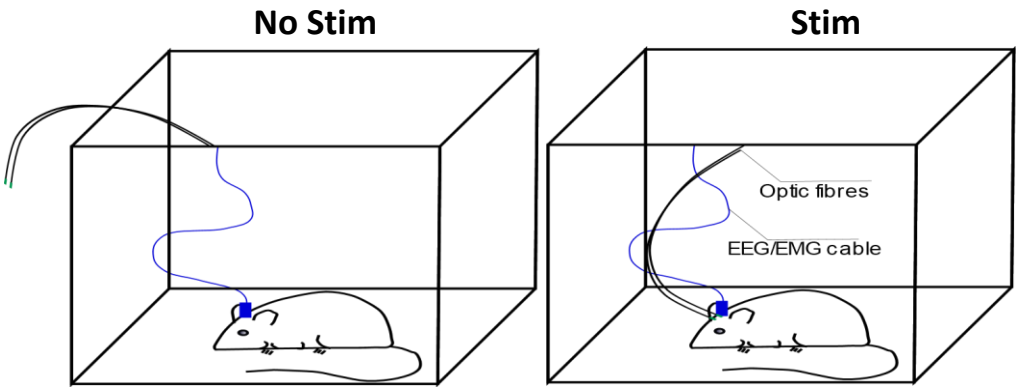

Figure 4.1 Picture explains two types of recording/light stimulations employed for the same mouse. During Non-Stim recording, EMG/EEG channels were attached to the head of the mouse, but optic fibers were not connected. During Stim recording, both optic fibers and EMG/EEG cable were attached to the connectors located on the head of the mouse. All mice expressed inhibitory opsin in the TRN.

behaviour of the mice. Those mice which did not sleep or slept periods shorter than 10 minutes were excluded from the analysis.

A mouse expressing Arch in the rostral part of the TRN showed a similar sleep pattern during No Stim and Stim recording sessions (See Figure 4.2). Its' sleep scoring/brain state lines (See Figure 4.2, B), derived from high frequency filtered and thresholder EMG, were almost identical and spectrograms (See Figure 4.2, C) showed no visible difference. The mouse expressing Arch in the caudal part of the TRN, during Stim and No Stim session showed diverse results (see Figure 4.3). The caudally stimulated mouse during No Stim session, slept similarly to rostrally stimulated mouse, whereas during the Stim session, when tonic optogenetic inhibition of the caudal TRN was introduced, its sleep became discontinuous and it had shorter sleep episodes (See Figure 4.2, Stim).

General characterization of the wake/sleep cycle

To quantify the sleep/wake cycle changes before and during optogenetic inhibition of the TRN, we recorded the average time slept during 30 seconds light activation for each animal (See Figure 4.4 A). Additionally, we counted the numbers of sleeping traces, wake traces and mixed state traces. A trace was counted as a sleep trace if an animal was asleep during the 30 seconds of light stimulation. An awake trace was coined if the animal showed 0 seconds of sleep during the 30 seconds of light stimulation and a mixed state trace was documented if an animal changed behavioural state during light activation. The numbers of sleep, wake and mixed traces were used to count the ratio of mixed state/sleep, ratio of sleep/wake, ratio of sleep and ratio of wake (See Figure 4.4 B), which were used to characterize the sleep/wake cycle. The given ratios allow us to understand, which brain state (sleep, wake or transition phase) were affected by the TRN stimulation. The averaged time slept during 30 seconds light stimulation and the various ratios were recorded for

each animal. The mean group results were derived using averaged results from each animal.

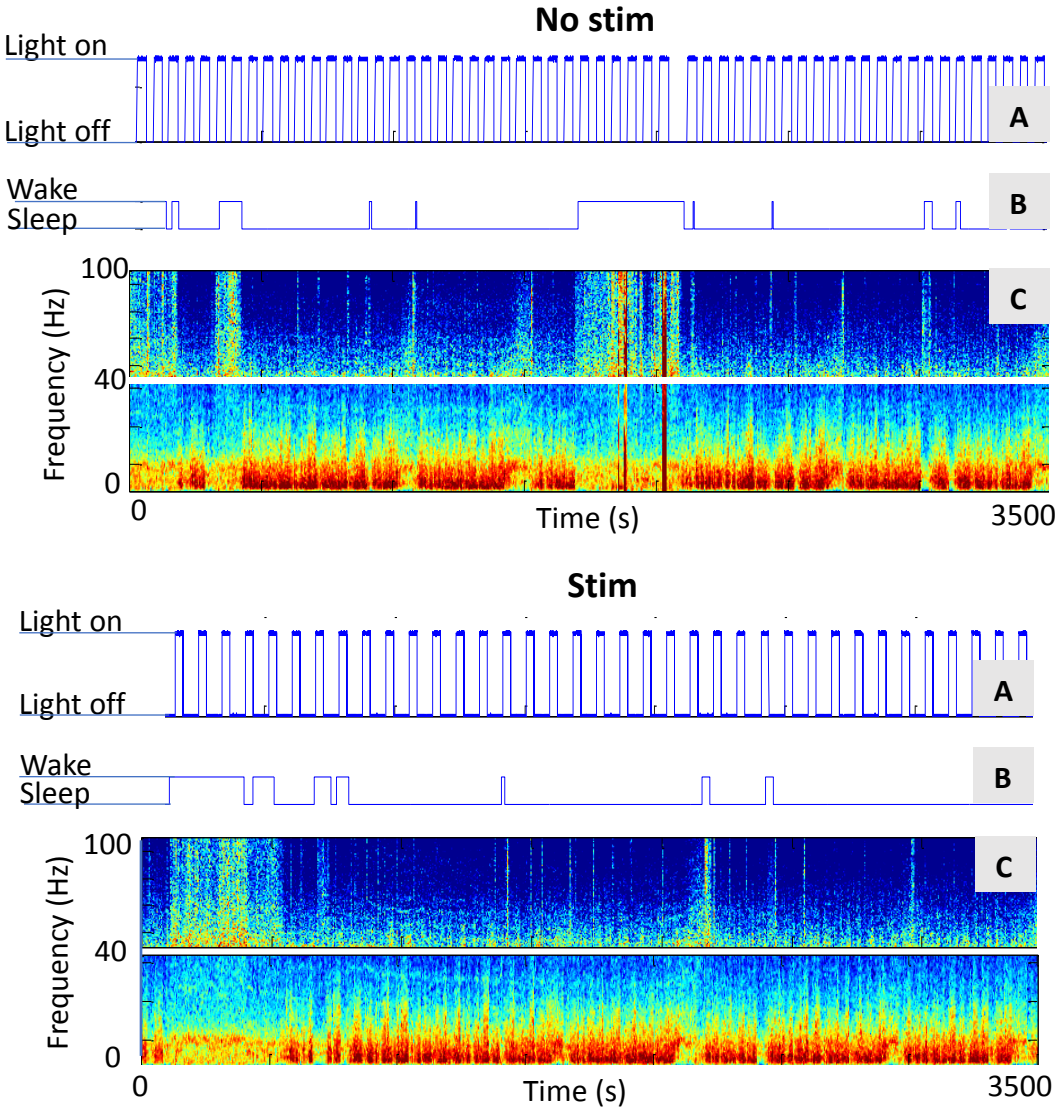

Figure 4.2 Example of the two traces recorded from the same animal expressing Arch in the rostral part of the TRN. Top trace, **No stim**, is recorded without attaching optic fibres. Bottom trace, **Stim**, was recorded with optic fibers connected to the optic probes on the mouse head and the rostral part of the TRN received light stimulation. **A** Blue line shows light stimulation pattern. Light On was at the top position of the line and at the bottom level line symbolize period without light stimulation. **B** Another blue line portrays pattern of the brain state change. This detecting line was derived from recorded EMG data. Horizontal line on the top display wake and horizontal line on the bottom symbolize sleeping. **C** Two spectrograms show frequency of the trace from 0 to 100 Hz. During sleep the lower frequencies of EEG are at the maximum (red) and higher frequencies are at the lowest (blue) powers. The trace with rostrally stimulated (optogenetically inhibited) TRN (Stim) is visibly comparable to the trace without the TRN light stimulation (Non-stim).

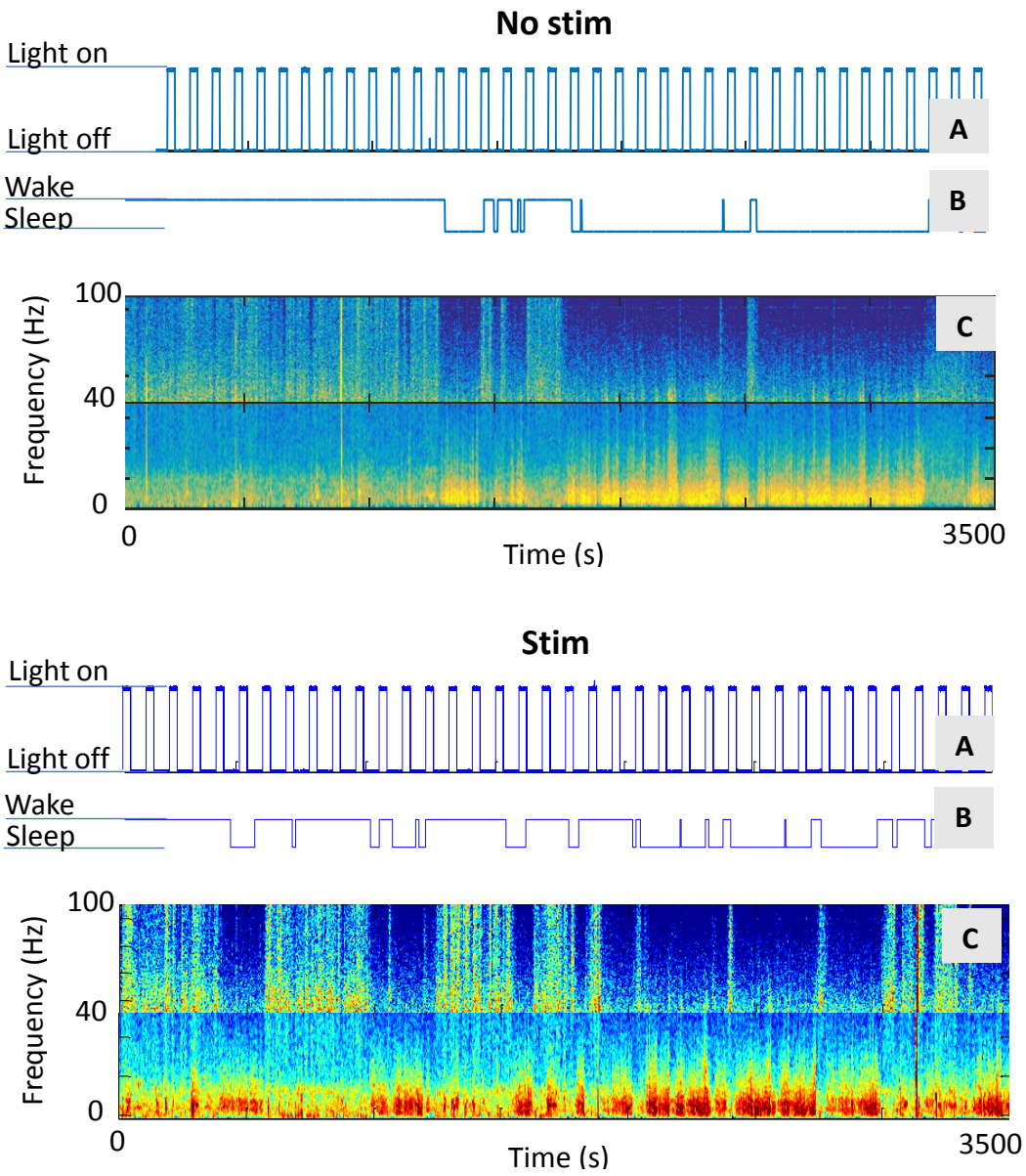

Figure 4.3 Example of the two traces recorded from the same animal expressing Arch in the caudal part of the TRN. Top trace, **No stim**, is recorded without attaching optic fibres. Bottom trace, **Stim**, was recorded with optic fibers connected to the optic probes on the mouse head and the rostral part of the TRN received light stimulation. **A** Blue line shows light stimulation pattern. Light On was at the top position of the line and at the bottom level line symbolize light off. **B** Another blue line portrays pattern of the brain state change. This detecting line was derived from recorded EMG data. Horizontal line on the top is detected wake state and horizontal line on the bottom symbolize a sleeping state. **C** Two spectrograms show frequency of the trace from 0 to 100 Hz. During sleep the lower frequencies of EEG are at the maximum (red) and higher frequencies are at the lowest (blue) powers. The trace with caudally stimulated (optogenetically inhibited) TRN (Stim) is visibly different from the trace without the TRN light stimulation (Non-stim).

A

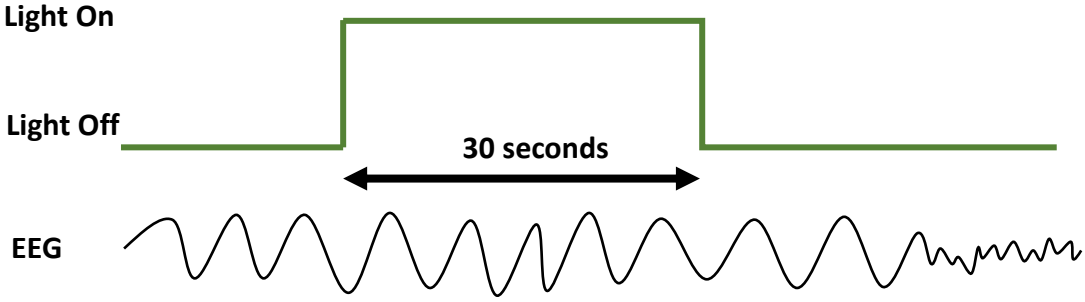

Sleep trace = 30 seconds of sleep during stimulation
Wake trace = 0 seconds of sleep during stimulation
Mixed state trace = animal slept longer than 0 second and shorter than 30 sec.

B

$$\text{Ratio of mixed states/sleep} = \frac{\text{Number (N) of mixed states}}{\text{N of sleep traces} + \text{N of mixed states}}$$

$$\text{Ratio of sleep/wake} = \frac{\text{Number of sleep traces}}{\text{N of wake traces} + \text{N of sleep traces}}$$

$$\text{Ratio of sleep} = \frac{\text{Number of sleep}}{\text{Sum of sleep, wake and mixed states}}$$

$$\text{Ratio of wake} = \frac{\text{Number of wake}}{\text{Sum of sleep, wake and mixed states}}$$

Figure 4.4 Schematic representation of the quantification approach used to characterize sleep/wake cycle in all mice. **A** Stimulation protocol was cyclic and consisted of tonic, 30 seconds long light stimulation followed by 60-90 seconds of no light stimulation. Traces recorded during light stimulations (30 seconds) were used to quantify the average sleeping time during light stimulation. Additionally, same traces were separated into numbers of sleeping, wake and mixed state traces, according to the time spent on sleep. **B** Formulas used to derive ratios from numbers of sleeping, wake and mixed state traces. Ratio of mixed states/sleep, ratio of sleep/wake, ratio of sleep and ratio of wake, were used to characterize sleep/wake cycle during light stimulation.

Effects of rostral and caudal TRN optogenetic inhibition on the sleep/wake cycle

All mice, which underwent No Stim and Stim recordings sessions expressed Arch either in the rostral or caudal part of the TRN. Initially, we were interested in the effect of local TRN inhibition on sleep. Both mice groups spent relatively similar time in sleep before and during TRN stimulation. (See figure 4.5 **a**. Caudal mice, n = 3; paired t test, p = 0.57; MES = 0.4, CI = -1.21/2.02. Rostral mice, n =3; paired t test, p = 0.95; MES = 0.04, Cl = -1.75/1.83). Caudally stimulated mice showed a slight tendency for a reduction of average sleeping time during Stim sessions. As expected, a similar graph was produced when the sleep ratio of both groups was compared. The ratio of sleep of caudally and rostrally stimulated animals was identical during No Stim sessions, whereas during Stim sessions animals with caudally stimulated TRN showed a slight tendency for a reduction in the sleep ratio. In rostrally stimulated animals, the sleep ratio remained the same during both recording conditions (See figure 4.5 **b**. Stim session, two sample t test, p = 0.15/ measure effect size, hedges (MES) = -0.87, confidence interval = -2.54/0.81. No Stim session, two sample t test, p = 0.88/ MES = -0.11, CI = -1.90/1.68; rostral mice, n = 3; caudal mice, n = 3). Analysis of the wake ratio showed analogous results in both animal groups before and during TRN light stimulation (See figure 4.5 **c**. Stim session, two sample t test, p = 0.85; MES = 0.12, CI = -1.67/1.91. No Stim session, two sample t test, p = 0.64; MES = 0.33, CI = -1.28/1.94; rostral mice, n = 3; caudal mice, n = 3). Similarly, the sleep to wake ratio analysis was not affected (See figure 4.5 **d**. Stim session, two sample t test, p = 0.89; MES = - 0.10, CI = -1.89/1.61. No Stim session, two sample t test, p = 0.47; MES = -0.52, CI = -2.15/1.10; rostral mice, n = 3; caudal mice, n = 3). We can conclude that optogenetic inhibition of rostral and caudal TRN during 30 seconds did not have an effect on the average time of sleep and the proportion of sleep and wake states. It is important to note that the same analysis was performed on the traces after light stimulation (30 seconds) and reproduced similar non-significant outcome. Although, The ratio of mixed states/sleep was identical for caudal and rostral animals without TRN stimulation, during TRN stimulation, rostrally and caudally stimulated animals showed a significantly different ratio. Notably, rostrally stimulated animals tended to

change state more rarely whereas caudally stimulated animals changed brain state more frequently during stimulation (See figure 4.5 **e**. Stim session, two sample t test, p = 0.03; MES = 2.16, CI = 0.14/4.17; No Stim session, two sample t test, p = 0.85; MES = - 0.14, CI = -1.93/1.65; rostral mice, n = 3; caudal mice, n = 3). Hence, identical modulation (optogenetic inhibition) of the rostral and caudal TRN elicited the tendency to the opposite results. The increased/ reduced ratio of the mixed state could be caused by frequent/rare awaking and falling into sleep. It follows therefore to next investigate which behavioural state change, awakening or falling asleep, was exaggerated by TRN optogenetic inhibition.

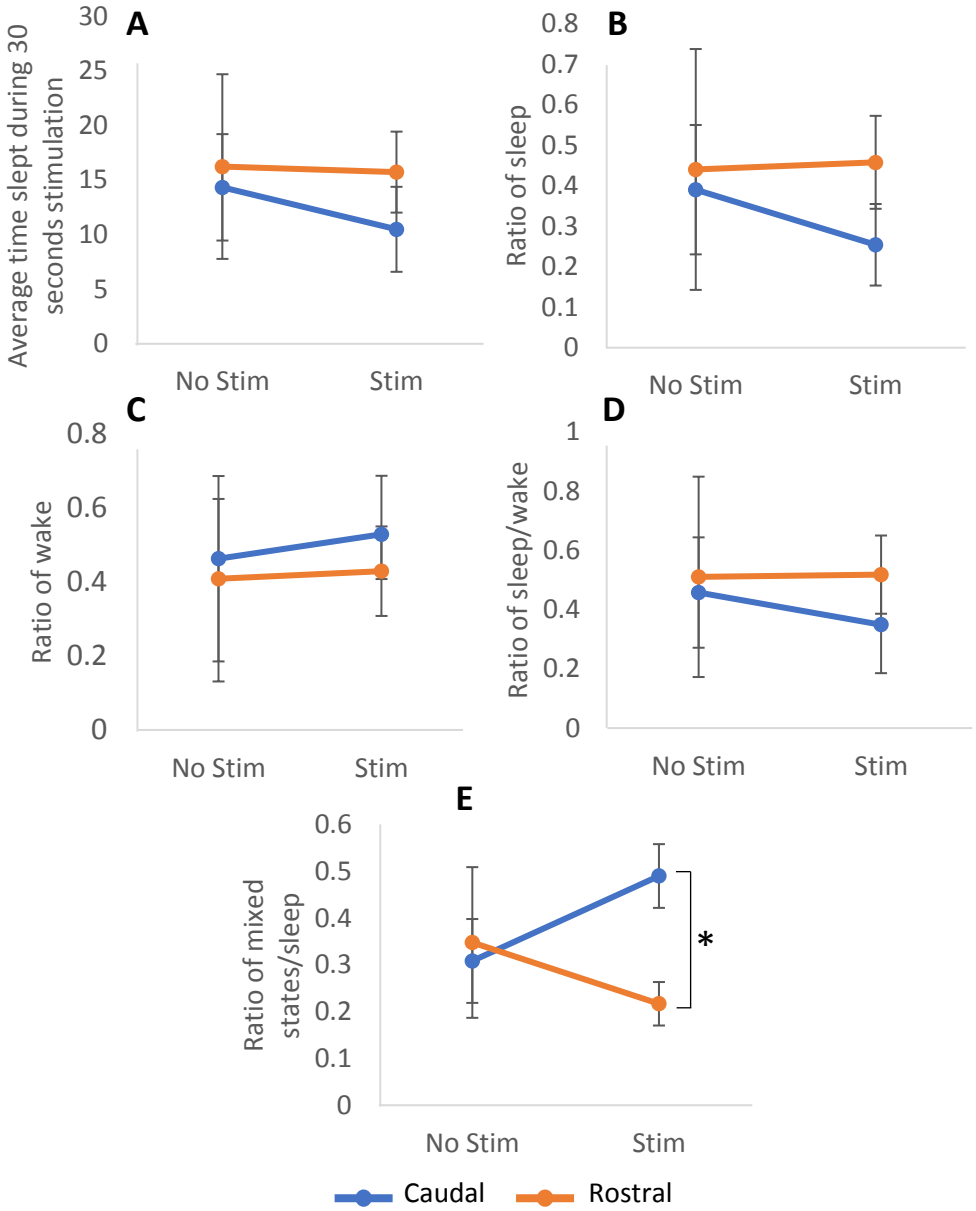

Figure 4.5 Graphs portray how the optogenetic modulation of the rostral and caudal TRN affects sleep/wake cycle in mice. Inhibitory opsin, archaerhodopsin, was expressed specifically in caudal (blue, n = 3) and rostral (orange, n = 3) TRN. Sleep/wake cycle was investigated without TRN light stimulation (No Stim) and during TRN stimulation (Stim). **A** An average time slept during 30 seconds of light stimulation. **B** Proportion of sleep before and during TRN light stimulation. **C** Proportion of wake before and during TRN light stimulation. **D** Ratio of sleep to wake before and during TRN optogenetic inhibition. **E** A proportion of mixed state traces to the sleep only traces with and without TRN optogenetic inhibition. The proportion of sleep and wakefulness was not affected by the TRN light stimulation, but the brain states of the caudally/rostrally stimulated animals changed more frequently/rarely. Two sample t test, * $p < 0.05$. Error bars – SEM.

Effects of TRN light stimulation (optogenetic inhibition) on arousal

A new inclusion criterion for data analysis was introduced to investigate the relationship between optogenetic inhibition of the TRN and awaking (See Figure 4.6 **A**). To better characterize the awaking effect, we introduced two new values: latency and ratio. The **latency,** period between the start of the light stimulation period and the animal waking up, characterized the speed of waking up, putatively caused by the TRN optogenetic inhibition. Herrera et al. (2015) reported that 5 second short tonic optogenetic inhibition of the rostral TRN during sleep resulted in a short latency to wake up. We did not include latencies longer than 80 seconds for analysis, because the 30 seconds long light stimulations were introduced every 90 seconds in our study. Additionally, we introduced a **ratio**, which defined the proportion of the short sleep episodes (See Figure 4.6, **B**). Previous studies have shown that a reduction in sleep spindles resulted in shorter NREM sleep episodes (Wimmer et al. 2012; Wells et al. 2016). Sleep shorter than 80 seconds was qualified as a short sleep and sleep longer than 80 seconds was referred to as a long sleep. Once again, an 80 seconds time point was selected, due to the frequency of the light stimulation used.

The latency was not affected in both animal groups before and during light stimulation, although rostral TRN stimulations showed a tendency for a slight prolongation of the latency. Low n number does not allow us to state significance in this case (See Figure 4.7, A. Caudal mice, n = 3; paired t test, p = 0.39; Measure effect size, hedges (MES) = -0.58, confidence interval (CI) = -2.21/1.05. Rostral mice, n = 3; paired t test, p = 0.26; MES = -2.08, (CI) = - 4.06/-0.09). Figure displaying total and averaged proportion of short sleep episodes (See figure 4.7 A) appeared to be similar to the figures portraying the proportion of total and averaged numbers of mixed state (See figure 4.5 E). Before light stimulation the rostral and caudal stimulated mice had similar averaged proportion of short sleep episodes, whereas during light stimulations the short sleep bouts proportion doubled in caudal stimulated mice but was reduced in the rostral mice. The proportions of short sleep episodes in caudal

and rostral-stimulated mice were significantly different during light stimulation (See figure 4.7 B. No Stim, two sample t test, p = 0.68; Measure effect size, hedges (MES) = -0.3, confidence interval (CI) = -2.10/1.50. Stim, two sample t test, p = 0.03; MES = 2.22, (CI) = 0.18/4.25. Caudal mice, n = 3. Rostral mice, n = 3).

Hence it appears that caudal TRN optogenetic inhibition results in the increased proportion of short sleep episodes, which were potentially caused by abnormally frequent arousal. The rostral TRN optogenetic inhibition resulted in a reduction in the ratio of short sleep episodes and a tendency for an increase in the latency. Therefore, rostral TRN inhibition showed a tendency for the prolongation of sleep episodes. Hence, distinct optogenetic modulation of the rostral and caudal TRN showed distinct effect on the duration of sleep episodes and consequently, on waking.

A

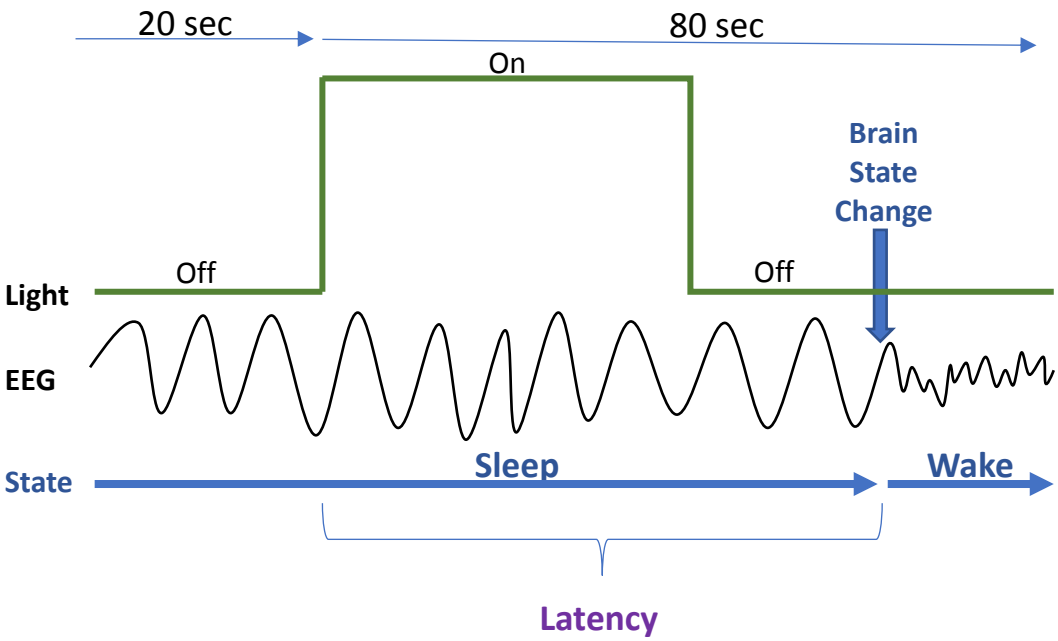

B

$$\text{Ratio} = \frac{\text{Number (N) of short sleep episodes (< 80 sec)}}{\text{N of long sleep (> 80 sec)} \; + \; \text{N of short sleep (< 80 sec)}}$$

Figure 4.6 Data inclusion criteria for analysis of data investigating the relationship between optogenetic inhibition of the TRN and awaking. Two values (purple) were introduced: latency and ratio. **A** Inclusions criteria for latency collection. Data was included if the animal slept at least 20 seconds before the start of the light stimulation and woke up within 80 seconds after the beginning of the light stimulation. **B** Calculation of the ratio. The ratio shows the proportion of short sleep episodes during sleep. Sleep is stated as 'short sleep' if it lasted less than 80 seconds. Sleep lasting longer than 80 seconds is referred to as 'long sleep'. The ratio was calculated by dividing the number of 'short sleep ' episodes to the number of all sleep episodes.

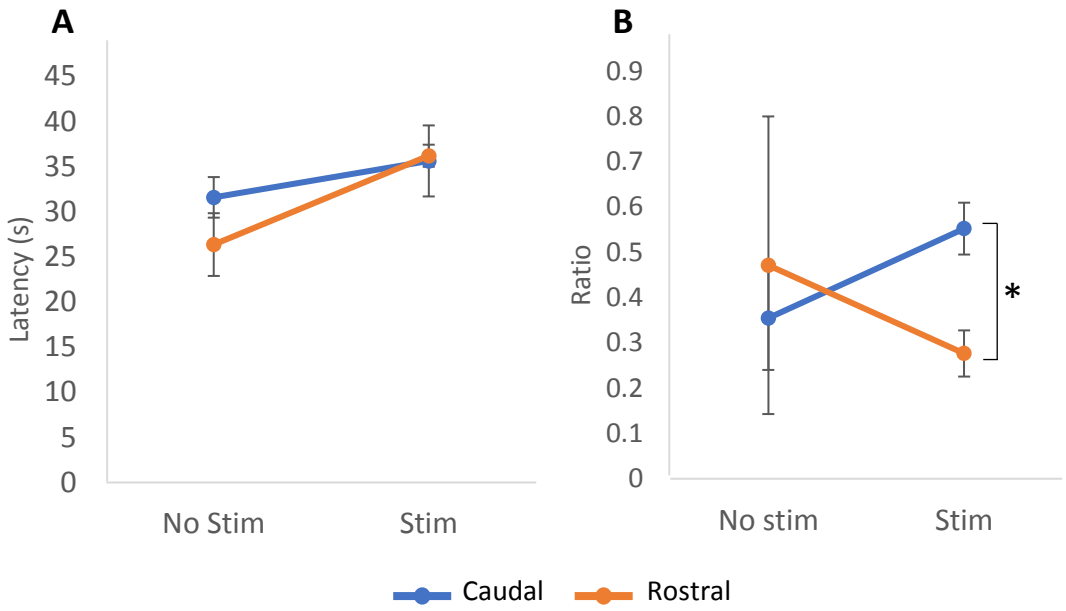

Figure 4.7 Figure characterize the effect of TRN light stimulation (optogenetic inhibition) on arousal. Sleep/wake cycle was investigated without TRN light stimulation (No Stim) and during TRN stimulation (Stim). **A** Latency, a period between light stimulation start and wake up, before and during TRN light simulation in caudally and rostrally stimulated mice. **B** The averaged proportions of short sleep bouts. The caudal TRN inhibition resulted in the increased proportion of short sleep episodes, whereas the rostral TRN inhibition showed opposite result and reduced the proportion of short sleep episodes. Two sample t test, * $p < 0.05$. Error bars – SEM.

Effect of TRN light stimulation (optogenetic inhibition) on falling asleep

Altered inclusion criteria for data analysis were introduced to investigate the relationship between optogenetic inhibition of the TRN and falling asleep (See Figure 4.8, A). To characterize falling asleep better, we introduced same parameters as previously: latency and ratio. Only in this case, **latency,** was a period between light stimulation and sleep onset and the **ratio** defined the proportion of the short wake episodes (See Figure 4.8, B). A wake episode shorter than 80 seconds was qualified as a short wake and a wake episode longer than 80 seconds was referred to as a long wake.

Animals with expressed inhibitory opsins in the caudal and rostral TRN did not show any visible reduction in the proportion of short wake and long wake episodes. The latency to sleep onset was not affected in animal group before and during light stimulation (See figure 4.9, A. No Stim, two sample t test, p = 0.17; Measure effect size, hedges (MES) = -1.82, confidence interval (CI) = -3.72/0.08. Stim, two sample t test, p = 0.65; MES = - 0.33, (CI) = - 2.13/1.47. Caudal mice, n = 3. Rostral mice, n = 3 Additionally, the averaged short wake proportion was not changed significantly before and during TRN light stimulation (See figure 4.9 B. No Stim, two sample t test, p = 0.39; Measure effect size, hedges (MES) = 0.63, confidence interval (CI) = -2.27/1.01. Stim, two sample t test, p = 0.57; MES = 0.4, (CI) = - 1.22/2.01. Caudal mice, n = 3. Rostral mice, n = 3).

In general, we did not find any evidence that rostral or caudal TRN inhibition has any effect on faster or slower sleep onset. So, it appears that the tonic inhibition of the caudal TRN by induction of abnormal arousal, increases the proportion of short sleep episodes, while rostral TRN tonic inhibition, which tends to reduce the proportion of short sleep episodes, somehow delays the arousal.

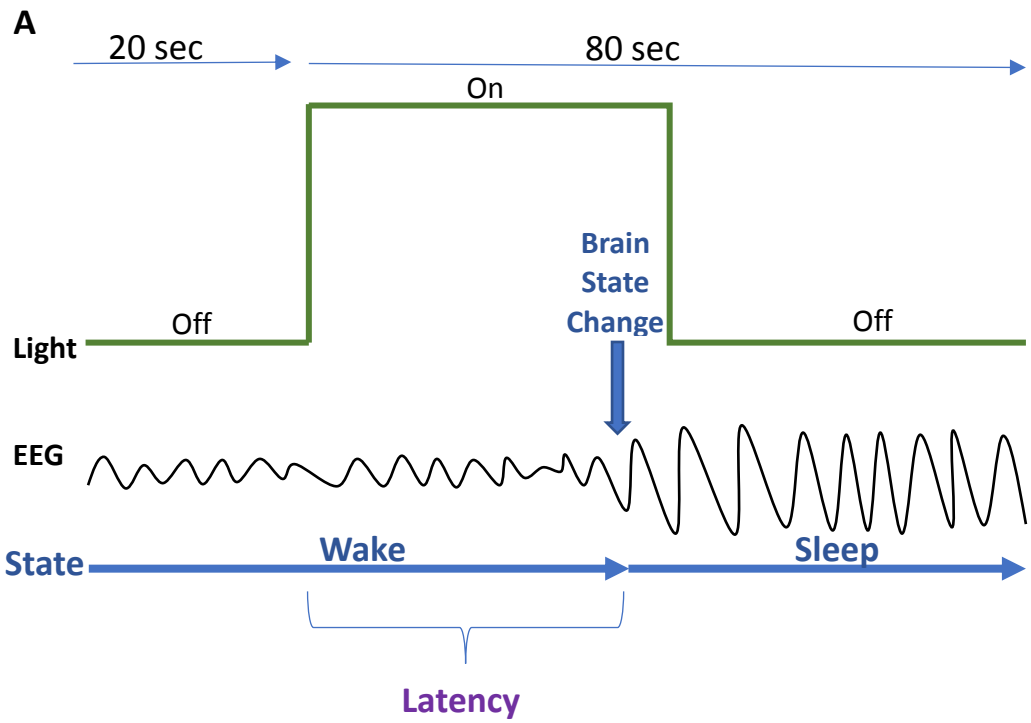

B

$$\text{Ratio} = \frac{\text{Short wake (< 80 sec)}}{\text{Long wake (> 80 sec)} + \text{Short wake (< 80 sec)}}$$

Figure 4.8 Data inclusion criteria for analysis of data investigating the relationship between optogenetic inhibition of the TRN and falling asleep. Two values (purple) were introduced: latency and ratio. **A** Inclusions criteria for latency collection. Data was included if the animal was awake for at least 20 seconds before the start of light stimulation and fell asleep within 80 seconds after the beginning of the light stimulation. **B** Calculation of the ratio. The ratio shows the proportion of short wake episodes during wake state. Wake is stated as a 'short wake' if it lasted no longer than 80 seconds. Wake lasting longer than 80 seconds is referred as 'long wake'. The ratio was calculated by dividing the number of 'short wake' episode to the number of all wake episodes.

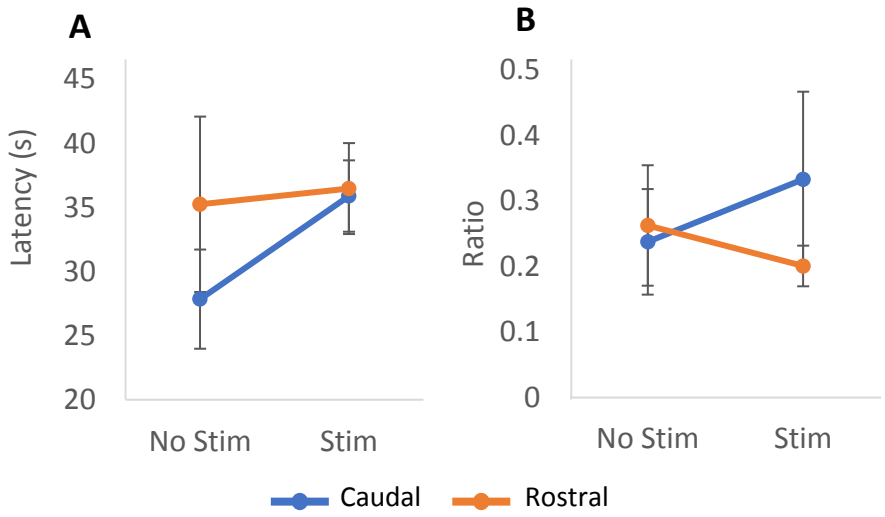

Figure 4.9 Figure characterize the effect of TRN light stimulation (optogenetic inhibition) on falling asleep. Sleep/wake cycle was investigated without TRN light stimulation (No Stim) and during TRN stimulation (Stim). **A**, Latency, a period between light stimulation and falling asleep, before and during TRN light simulation in caudally and rostrally stimulated mice. **D**, The averaged proportions of short wake bouts. Caudal and rostral TRN inhibition did not produce any significant effect on the latency and the proportion of the short wake episodes. Error bars – SEM.

4.3.2 Sleep/wake cycle in mice expressing Arch, NpHR and YFP

Next, we aimed to compare results of TRN optogenetic inhibition using another opsin halorhodopsin (rostral mice, n =4; caudal mice, n =4). Additionally, as a control YFP (yellow fluorescent protein) was expressed in the rostral (n = 3) and caudal (n =2) TRN to address the possibility that a heating effect contributed to the results of optogenetic stimulation. No Stim sessions were excluded in the experimental protocol and all further analysis was done during TRN light stimulation.

Once again, we started by quantification of the sleep/wake cycle changes caused by optogenetic inhibition (See Figure 4.4). The 'averaged' duration of sleep during 30 seconds of light stimulation was similar in caudally and rostrally targeted animals expressing Arch, NpHR and YFP (control). Animals expressing inhibitory opsins in the rostral TRN had slightly longer sleep during light stimulation (See figure 4.10 A. Arch, two sample t test, p = 0.38; measure effect size, hedges (MES) = 0.63, confidence interval (CI) = -2.27/1.01. NpHR, two sample t test, p = 0.55; MES = 0.39, CI = -1.9/1.12. Control, two sample t test, p = 0.84; MES = 0.15, Cl = -1.65/1.94). Even when we combined the results from both inhibitory opsins to increase the sample number, the difference between averaged sleeping time of caudally and rostrally stimulated animals remained similar (See figure 4.11 A. Opsin = Arch + NpHR; two sample t test, p = 0.11; MES = 0.84, CI = -1.94/0.25).

Next, we tested the proportion of sleep during 30 seconds stimulation in mice expressing Arch, NpHR and YFP. The method of the ratio calculation can be found in the earlier figure (See figure 4.4, B). The sleep proportion graphwas similar to the averaged sleeping time graph. Rostral and caudal mice had equal proportions of sleep independent of the type of virus expression (See figure 4.10 B. Arch, two sample t test, p = 0.25; measure effect size, hedges (MES) = 0.87, confidence interval (CI) = -2.54/0.81. NpHR, two sample t test, p = 0.37; MES = 0.59, CI = -2.01/0.83. Control, two sample t test, p = 0.2; MES = 0.2, Cl = -1.99/1.99). The sample number increase by the summation of the results of Arch and NpHR mice did not reveal a significant

difference between the rostral and caudal stimulated mice (See figure 4.11 B. Opsin, two sample t test, p = 0.25; MES = 0.6, CI = -1.67/0.47).

The analysis of wake ratio showed analogous results in all mice groups. The wake ratio was identical in the rostral and caudal mice expressing Arch, NpHR and YFP in the TRN (See figure 4.10 C. Arch, two sample t test, p = 0.64; measure effect size, hedges (MES) = 0.33, confidence interval (CI) = -1.28/1.94. NpHR, two sample t test, p = 0.91; MES = 0.07, CI = -1.32/1.46. Control, two sample t test, p = 0.87; MES = 0.11, CI = -1.90/1.68). No difference in the proportion of wake was found between mice expressing inhibitory opsins in the caudal and rostral TRN (See figure 4.11 C. Opsin, two sample t test, p = 0.7; MES = 0.21, CI = -1.15/1.56).

Lastly, we compared the proportion of the mixed state traces to sleep traces. Mice expressing inhibitory opsins in the caudal and rostral TRN produced significantly different proportions. Caudally stimulated mice changed brain state twice more often than rostrally stimulated ones. Control mice, expressing YFP, did not reproduce that result. (See figure 4.10 D. Arch, two sample t test, p = 0.03; measure effect size, hedges (MES) = 2.16, confidence interval (CI) = 0.14/4.17. NpHR, two sample t test, p = 0.04; MES = 1.65, CI = 0.04/3.25. Control, two sample t test, p = 0.17; MES = 0.17, CI = -1.62/0.37. Caudal Arch, n = 7. Rostral opsin, n = 7). The addition of the results from mice with caudally and rostrally expressed inhibitory opsins, increased n number, allowed us to test results using 2-way ANOVA test (See figure 4.11 D. Opsin, 2-way ANOVA, F = 3.8, p = 0.07; post-hoc Tukey HSD, p = 0.03. two sample t test, p = 0.001; MES = 2.1, CI = 0.79/3.40. Caudal Arch, n = 3; rostral Arch, n = 3; caudal NpHR, n = 4; rostral NpHR, n = 4; caudal control, n = 2; rostral control, n = 3). Additionally, we were able to compare the proportion of mixed states between rostral control and rostral opsin mice. Rostral TRN inhibition significantly reduced the proportion of the mixed states relative to control light stimulation (See figure 4.11 D. Opsin, two sample t test, p = 0.02; MES = 1.7, CI = 2.92/0.48. Rostral control, n = 3; rostral opsin, n = 7).

In summary, the outcomes from halorhodopsin and YFP expressing mice are in agreement with our previous results derived from archaerhodopsin expressing mice.

Tonic optogenetic inhibition of the caudal TRN resulted in frequent brain state changes, while the same modulation in the rostral TRN induced rare sleep state changes. Compared to control mice, rostral light stimulations in mice expressing opsins, changed the brain state less often. However, this comparison was not made in caudally stimulated mice because of the small sample size of control mice expressing YFP (n = 2).

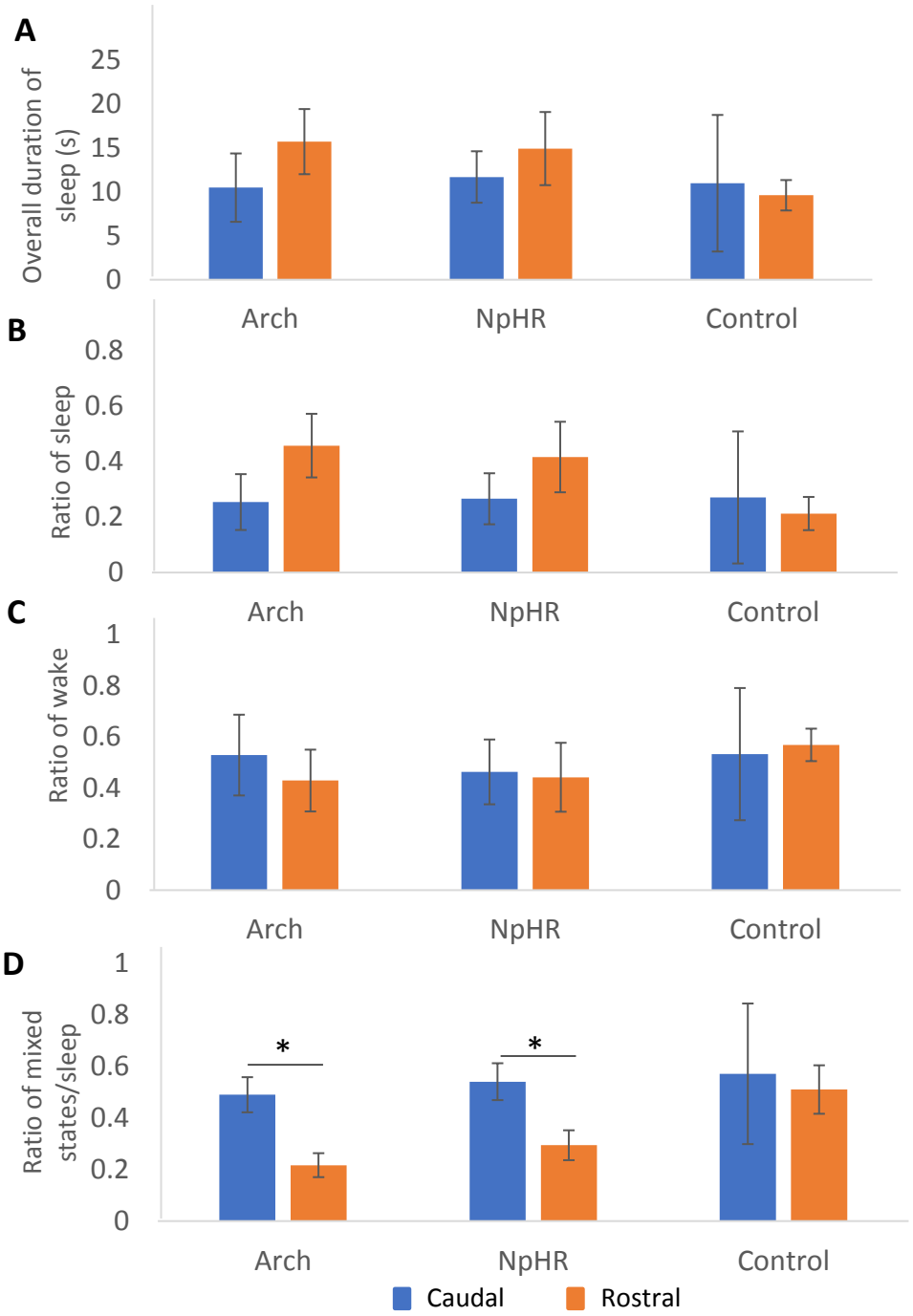

Figure 4.10 Graphs portray how the optogenetic modulation of the rostral and caudal TRN affects sleep/wake cycle in mice. Inhibitory opsins, archaerhodopsin (Arch) and halorhodopsin (NpHR), and YFP (control) were expressed specifically in the caudal (blue, Arch = 3, NpHR = 4, YFP = 2) and rostral (yellow, Arch = 3, NpHR = 4, YFP = 3) TRN. The sleep/wake cycle was investigated during TRN light stimulation. **A** An average time slept during 30 seconds of light stimulation. **B** Proportions of sleep during TRN light stimulation. **C** Proportions of wake during TRN light stimulation. **D** Proportions of mixed state traces during TRN light stimulation. The brain states of the caudally/rostrally stimulated animals changed more frequently/rarely. Two sample t test, * $p < 0.05$. Error bars – SEM.

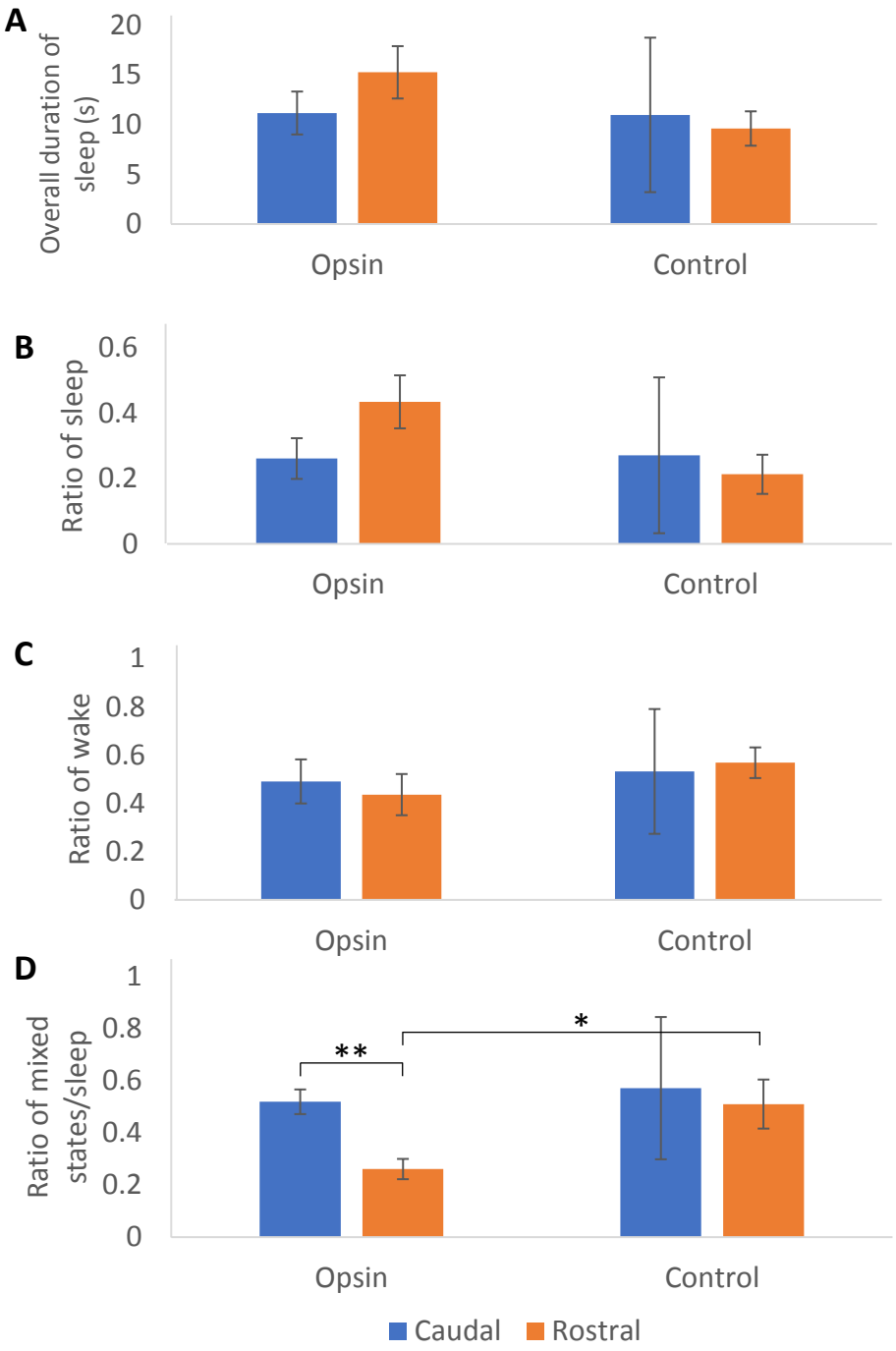

Figure 4.11 Graphs portray how the optogenetic modulation of the rostral and caudal TRN affects sleep/wake cycle in mice. Inhibitory opsins, (Opsin = Arch + NpHR) and YFP (control) were expressed specifically in caudal (blue, Opsin = 7, YFP = 2) and rostral (yellow, Opsin = 7, YFP = 3) TRN. **A** An average time slept during 30 seconds of light stimulation. **B** Proportions of sleep during TRN light stimulation. **C** Proportions of wake during TRN light stimulation. **D** Relationships between mixed state and sleep only traces during TRN light stimulation. The brain states of the caudally/rostrally stimulated animals changed more frequently/rarely. Two sample t test, * $p < 0.05$. Error bars – SEM.

Falling asleep during TRN light stimulation in mice expressing Arch, NpHR and YFP

New inclusion criteria for data analysis were introduced above (See Figure 4.8, **A**). To characterize the effect of falling asleep better, we introduced two values: latency and ratio. The **latency,** period between light stimulation and sleep onset, characterized the speed of falling asleep, putatively, caused by the TRN optogenetic inhibition. Additionally, we introduced the **ratio**, value which defined the proportion of the short wake episodes (See Figure 4.6, **B**). The wake episode shorter than 80 seconds was qualified as a short wake and the wake episode longer than 80 seconds was referred to as a long wake.

Analysis of the latency to fall asleep after light stimulation, did not reveal any significant differences between groups. Rostrally and caudally stimulated mice spent a similar time awake before falling asleep (See figure 4.12. Caudal mice: ANOVA, F = 0.08, p = 0.92; Arch = 64 traces (used in the analysis), 3 mice; NpHR = 60 traces, 4 mice; Control = 21 traces, 2 mice. Rostral mice: ANOVA, F = 0.49, p = 0.61; Arch = 45 traces, 3 mice; NpHR = 38 traces, 4 mice; Control = 79 traces, 3 mice). The latency difference between mice groups was so low, that we refrained to combine and compare the inhibitory opsin group to control group.

Lastly, we examined the effect of TRN light stimulation on the ratio of short wakes in all mice groups. Rostrally stimulated mice displayed the tendency for a reduction of the short wake ratio relatively to caudally stimulated mice. However, this trend was not statistically significant (See figure 4.13, A. Arch, two sample t test, p = 0.37; Measure effect size, hedges (MES) = 0.65, confidence interval (CI) = -0.99/2.99. NpHR, two sample t test, p = 0.65; MES = 0.29, CI = -1.1/1.69. Control, two sample t test, p = 0.53; MES = 0.47, CI = -1.35/228). In order to increase the n number, we clustered the results of the Arch and NpHR mice into Opsin groups. However, despite increasing the n number the results remained statistically insignificant. Hence, TRN optogenetic inhibition did not modulate the proportion of short sleep episodes (See figure 4.13, B. 2-way ANOVA, F = 1.44, p = 0.25. Opsin, two sample t test, p = 0.33; MES = 0.44, CI = -0.93/1.81).

Considering previous Stim/No Stim results and the results above we can conclude, that TRN optogenetic inhibition during the awake state does not change the parameters of the sleep wake cycle and does not modify the ability of the mice to fall asleep.

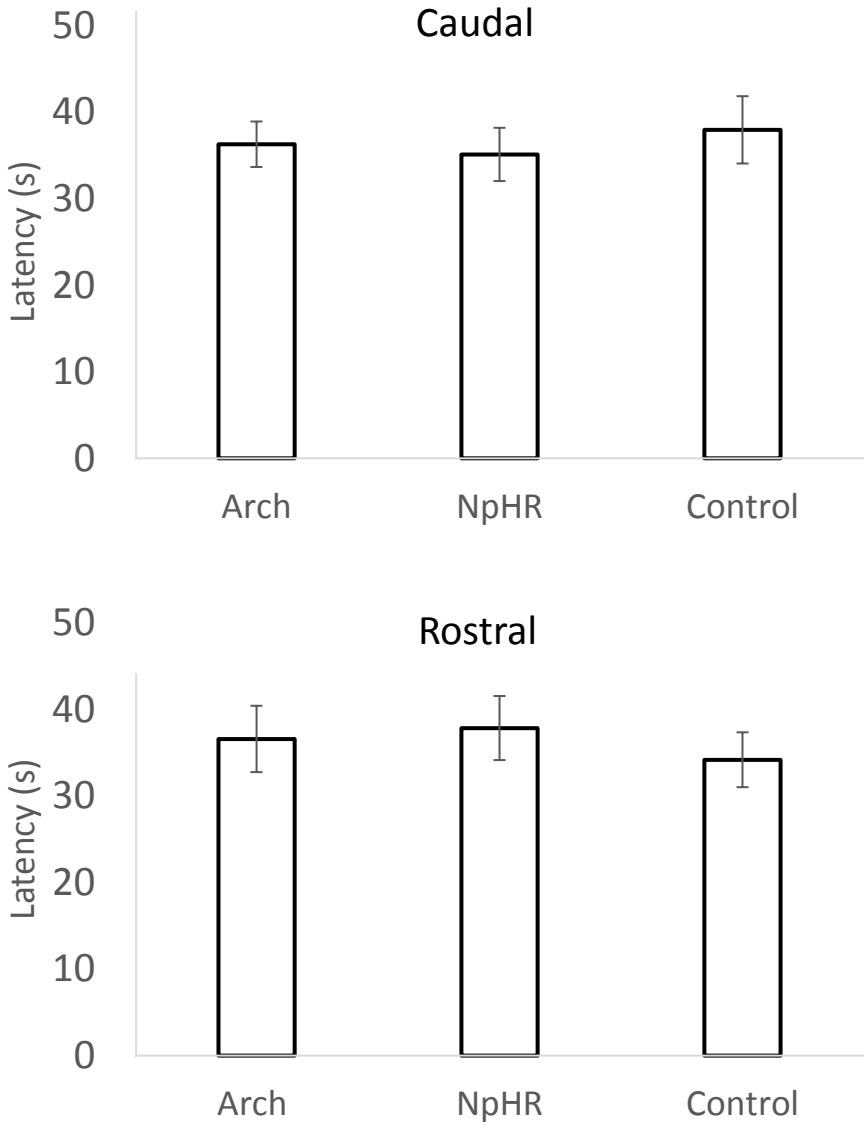

Figure 4.12 Graphs demonstrate the effect of the caudal and rostral TRN light stimulation on the latency of animals expressing Arch, NpHR and YFP (control). The latency is a period between light activation and falling asleep. Top graph displays the averaged latency change between caudally stimulated mice. Bottom graph shows the differences in the latencies in the rostrally stimulated animals. Rostral and caudal TRN stimulation resulted in similar latencies in all animal groups. Caudal mice: ANOVA, F = 0.08, p = 0.92; Arch = 64 traces (used in the analysis), 3 mice; NpHR = 60 traces, 4 mice; Control = 21 traces, 2 mice. Rostral mice: ANOVA, F = 0.49, p = 0.61; Arch = 45 traces, 3 mice; NpHR = 38 traces, 4 mice; Control = 79 traces, 3 mice. Error bars – SEM.

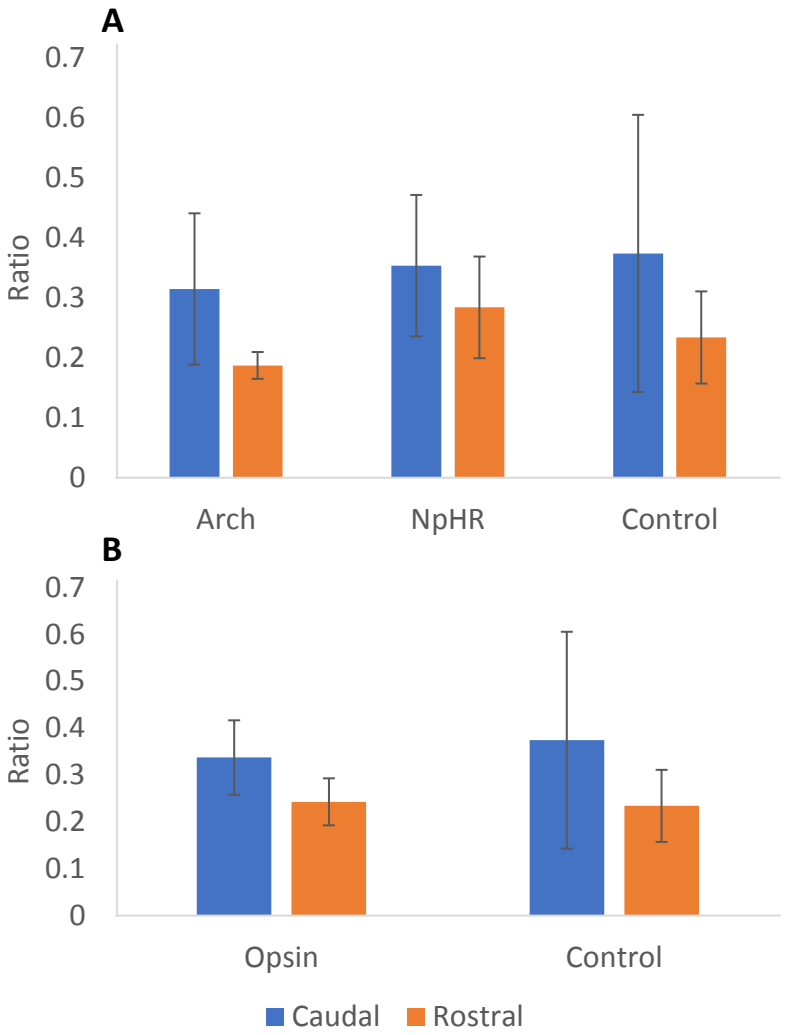

Figure 4.13 Figure characterizing the effect of TRN light stimulation on the ratio of 'short wake' episodes. Wake episode less than 80 seconds were considered a 'short wake' and those longer than 80 seconds were referred to as a 'long wake' episode. The ratio was calculated by division of 'short wake' episodes by the number of all wake episodes. **A** Ratio change of the short wake episodes during caudal (blue) and rostral (yellow) TRN light stimulation in mice expressing Arch, NpHR and YFP (control). **B** The 'short wake' ratio changes in mice expressing inhibitory opsins (Opsin = Arch + NpHR) and YFP. The caudal and rostral TRN optogenetic inhibition did not modulate the proportion of short wake episodes. Error bars – SEM.

Arousal linked light stimulation in mice expressing Arch, NpHR and YFP

New inclusion criteria for data analysis were introduced above (See Figure 4.6, **A**). To characterize the arousal effect better, we introduced two values: latency and ratio. The **latency,** period between light stimulation and wake up, characterized the speed of waking up, putatively, caused by the TRN optogenetic inhibition. Additionally, we introduced the **ratio**, value which defined the proportion of the short sleep episodes (See Figure 4.6, **B**). The sleep episode shorter than 80 seconds was qualified as a short sleep and the sleep episode longer than 80 seconds was referred to as a long wake.

Previously, we compared the latency of arousal in the Stim/No Stim studies between mice with rostral and caudal TRN modulation (See figure 4.7, b) and did not find a significant difference. During this set of experiments, we also concluded that there is no difference between control, rostral and caudal stimulated mice (See Appendix, figure 8.26. Caudal Opsin, two sample t test, p = 0.26. Rostral Opsin, two sample t test, p = 0.43). However, if the inclusion criteria are modified to include mice that slept only 10 seconds before stimulation there was a significant reduction in the latency period between light stimulation and waking up in mice expressing inhibitory opsins relatively to control (YFP) mice (See figure 4.14). This effect of sleeping length before light stimulation will be explored further in Chapter 5.

Caudally stimulated Arch and NpHR mice showed a reduced latency period relative to control mice, whereas rostrally inhibited TRN did not (See figure 4.14, top row. *Caudal:* ANOVA, F = 3.18, p = 0.04. Arch vs Control: post-hoc Tukey HSD, p = 0.26; Measure effect size, hedges (MES) = 0.34, Confidence interval (CI) = -0.79/0.1. NpHR vs Control: post-hoc Tukey HSD, p = 0.04; MES = 0.59, CI = 1.03/0.14. Arch = 64 traces, n = 3. NpHR = 71 traces, n = 4. Control = 28 traces, n = 2. *Rostral:* ANOVA, F = 0.8, p = 0.45. Arch vs Control: post-hoc Tukey HSD, p = 0.89; Measure effect size, hedges (MES) = 0.04, Confidence interval (CI) = -0.44/0.35. NpHR vs Control: post-hoc Tukey HSD, p = 0.49; MES = -0.29, CI = -0.68/0.18. Arch = 63 traces, n = 3. NpHR = 45 traces, n = 4. Control = 40 traces, n = 3). This effect was significant in NpHR mice and when

the results from animals expressing both inhibitory opsins, Arch and NpHR were combined. During light stimulation, mice expressing inhibitory opsins in the caudal TRN had a faster arousal latency than control mice. Rostrally stimulated mice expressing inhibitory opsins and YFP (control) displayed a similar latency (See figure 4.14, bottom row. *Caudal:* two sample t test, p = 0.03; Measure effect size, hedges (MES) = 0.46, Confidence interval (CI) = -0.87/-0.05. Opsin = 135 traces, n = 7. Control = 28 traces, n = 2. *Rostral:* two sample t test, p = 0.49; (MES) = - 0.13, (CI) = -0.49/0.24. Opsin = 108 traces, n = 7. Control = 40 traces, n = 3).

Finally, we wanted to understand how the tonic inhibition in NpHR mice and light stimulation in control mice would affect the ratio of short sleep episodes. In the study employing only Arch expressing mice (Stim/No Stim) optogenetic inhibition of the caudal TRN increased the amount of short sleep episodes, while rostral TRN inhibition led to the opposite results (See Figure 4.5). Mice expressing NpHR in rostral and caudal TRN displayed identical results, whereas mice expressing YFP did not show any difference in the short sleep proportion between rostral and caudal stimulations (See figure 4.15, A. Arch: two sample t test, p = 0.03; MES = 2.22. CI = 0.18/4.25. NpHR: two sample t test, p = 0.04; MES = 1.59, CI = 0.00/3.18. Control: two sample t test, p = 0.67; MES = - 0.31, CI = - 2.11/1.49. Arch = 3 caudal/ 3 rostral mice. NpHR = 4/4 mice. Control = 2/3 mice). Arch and NpHR mice results were combined into the Opsin group to increase the n number. Both opsins are inhibitory and predicted to inhibit TRN cells during light stimulation. The increase in n number resulted in a highly significant difference between rostrally and caudally stimulated mice for the proportion of short sleep episodes. Additionally, the rostrally stimulated opsin mice produced a smaller proportion of short sleep episodes than rostrally stimulated control mice which approached statistical difference (p = 0.06). A comparison between caudal opsin and caudal control mice was not conducted because of the small sample size. (See figure 4.15 B. 2-way ANOVA, F = 5.96, p = 0.03. Opsin: post-hoc Tukey HSD, p = 0.004; two sample t test, p = 0.002; MES = 1.99, CI = 0.71/3.27. Rostral opsin vs Rostral control, two sample t test, p = 0.06; MES = - 1.38, CI = -2.86/0.10).

On average, the inhibition of the caudal TRN produced sleep, where 60% of all sleeping episodes were shorter than 100 seconds (the latency + 20 seconds of pre-stimulation sleep), while sleep during rostral inhibition of the TRN contained only 30% of short sleep episodes. The sleep of caudal and rostral control mice during light stimulation contained about 40% of short sleep episodes. The weak point of the analysis was that we did not quantify the long sleep episodes.

The reduced latency of arousal and the increased proportion of the short sleep episodes during sleep allows us to suggest, that caudal TRN tonic inhibition induces arousal, which results in discontinued sleep.

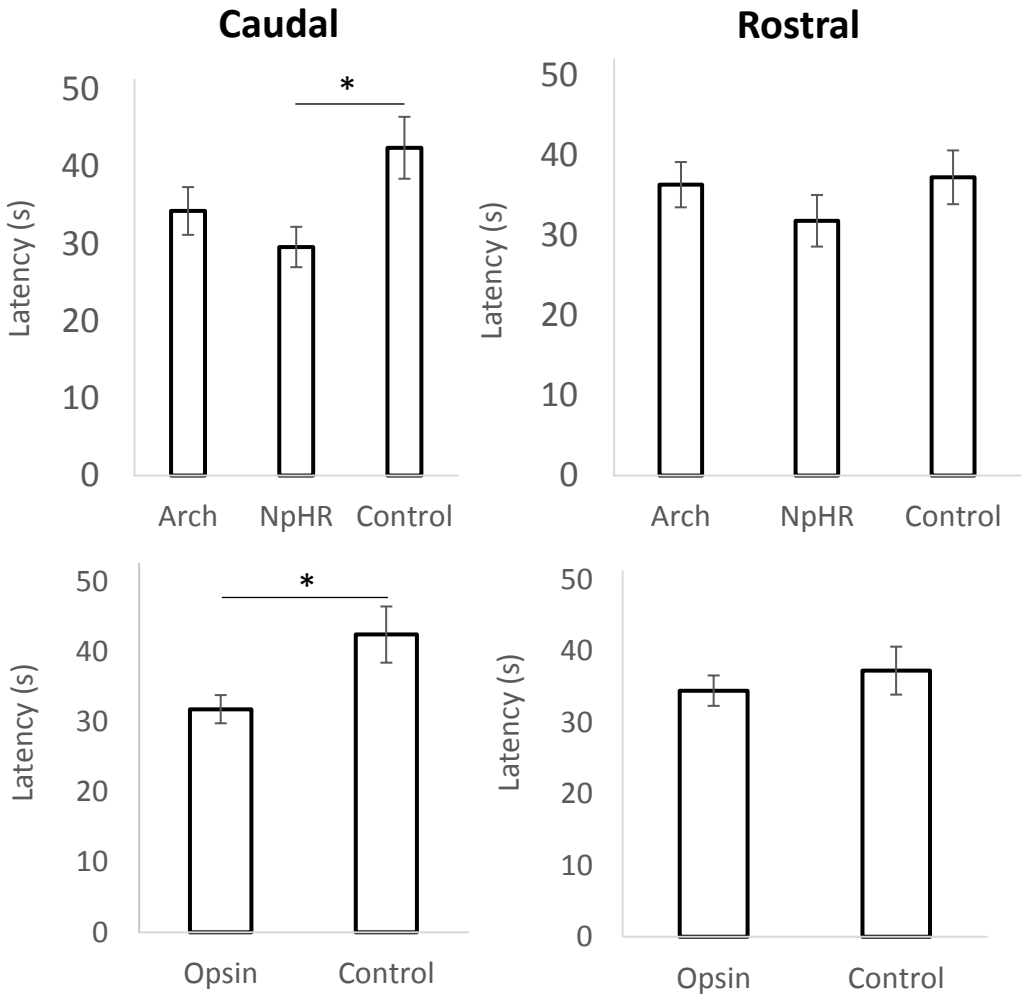

Figure 4.14 Graphs demonstrate the effect of the caudal and rostral TRN light stimulation on the latency in animals expressing Arch, NpHR and YFP (control). Mice slept at least 10 seconds before stimulation. The latency is a period between light activation and arousal. Top graphs display the average latency change between Arch, NpHR and YFP (control) mice. Bottom graphs shows the differences in the latencies between mice with inhibitory opsins (Arch + NpHR) and control mice. The latency of the caudally stimulated mice expressing inhibitory opsin was significantly shorter than the latency of the control mice with the same stimulation. * $p < 0.05$. Error bars – SEM.

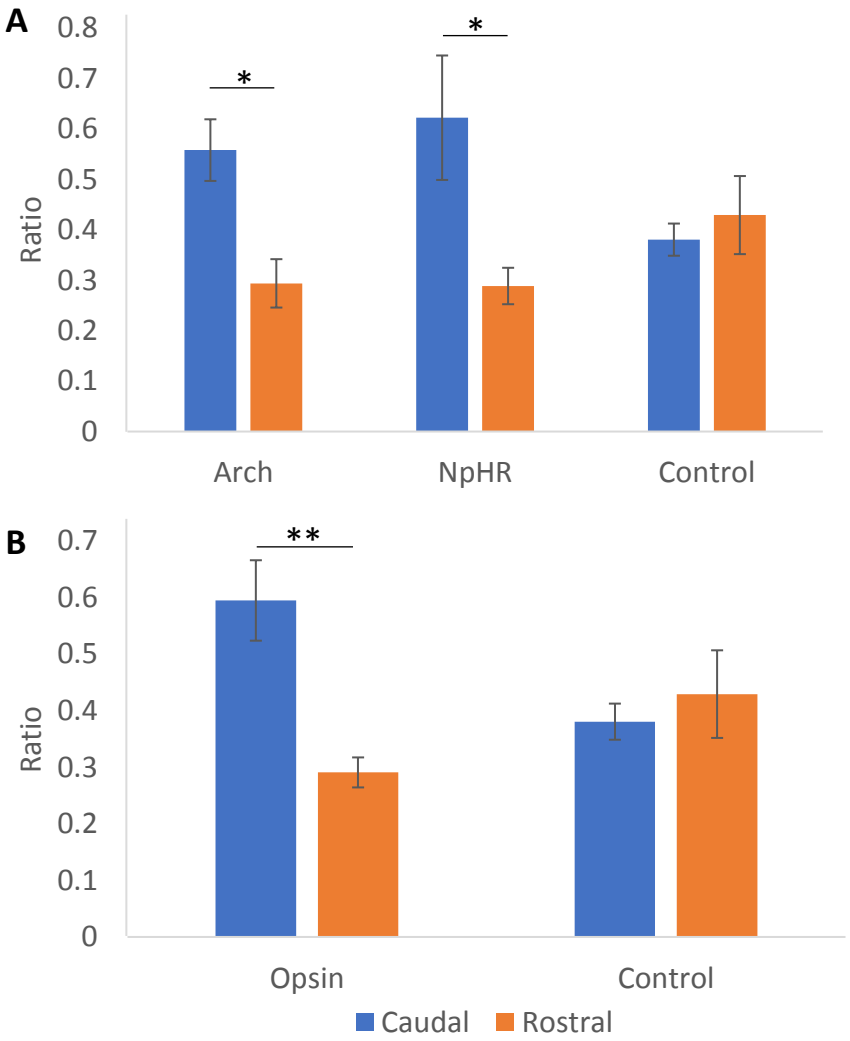

Figure 4.15 Figure characterize the effect of the TRN light stimulation on the ratio of short sleep episodes. Sleep episode shorter than 80 seconds was qualified as a short sleep and sleep episode longer than 80 seconds was referred as a long sleep. Ratio was calculated by division of the number of short sleep episodes by the number of all sleep episodes. **A** The ratio changes of short sleep episodes during caudal (blue) and rostral (orange) TRN light stimulation in mice expressing Arch, NpHR and YFP (control). **B** The short sleep ratio changes in mice expressing inhibitory opsins (Opsin = Arch + NpHR) and YFP. The caudal TRN optogenetic inhibition increased the proportion of short sleep episode during sleep and the rostral TRN inhibition generated contrary result. * $p < 0.05$. ** $p < 0.01$. Error bars – SEM.

4.3.3 The effect of the continuous and recurrent light stimulation

Tonic light delivery to the TRN was conducted in a repeated manner. Light stimulation of 30 seconds was followed by an off-light period, which lasted typically for 60 seconds. A single recording session on average lasted two hours and contained nearly 50 stimulations. In order, to understand the effect of the continuous and recurrent light stimulation on the speed of brain state change, graphs portraying the relationship between the number of stimulation and the latencies were generated (See figures 4.18 – 4.21). Arch expressing mice did not have any significant correlation between both types of latencies (arousal and falling asleep) and order of stimulation (See figure 4.18. *Sleep:* Caudal Arch = 64 traces. Rostral Arch = 63 traces. *Wake:* Caudal Arch = 70 traces. Rostral Arch = 41 trace. Caudal Arch = 3 mice. Rostral Arch = 3 mice). Likewise, the correlation between the various latencies and the order of stimulation was not found in the NpHR expressing animals (See figure 4.19. *Sleep:* Caudal NpHR = 71 traces. Rostral NpHR = 45 traces. *Wake:* Caudal NpHR = 63 traces. Rostral NpHR = 32 trace. Caudal NpHR = 4 mice. Rostral NpHR = 4 mice). By contrast, control animals expressing YFP in the caudal and rostral TRN did show a tendency for a correlation between the latency to arousal and the order of the stimulation. In the rostrally stimulated animals it was positive (correlation coefficient = 0.3, $p = 0.06$) and in the caudally stimulated mice the correlation was negative (correlation coefficient = - 0.29, $p = 0.11$). The latencies during awake did not have any correlation with the number of stimulations (See figure 4.20. *Sleep:* Caudal Control = 30 traces. Rostral Control = 40 traces. *Wake:* Caudal Control = 32 traces. Rostral Control = 40 trace. Caudal Control = 3 mice. Rostral Control = 2 mice). Finally, we analysed the correlation between the latencies and numbers of stimulations in the Arch mice during Non-Stim session (without optic cable attachment). The correlation was not found during these recordings (See figure 4.21. *Sleep:* Caudal Non-Stim = 25 traces. Rostral Non-Stim = 11 traces. *Wake:* Caudal Non-Stim = 16 traces. Rostral Non-Stim = 7 trace. Caudal Arch= 3 mice. Rostral Arch = 2 mice).

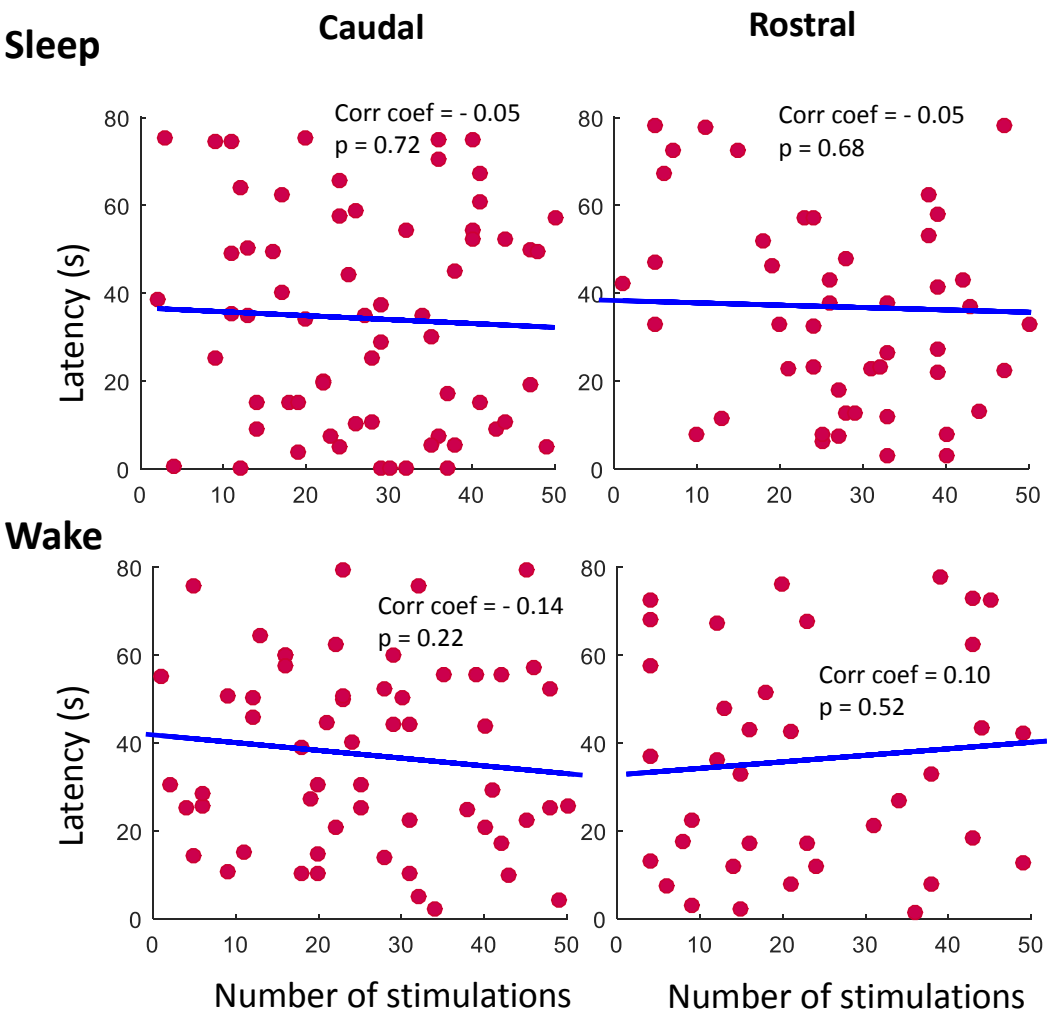

Figure 4.18 Relationship between the latencies and the number of stimulations in Arch expressing mice. Top row (sleep) is dedicated to the latency of arousal, period between the light stimulation beginning and the arousal. Bottom row (wake) is showing the relationship of the latency between the light stimulation and falling asleep. There was no correlation between the latencies and the number of stimulations. Sleep: Caudal Arch = 64 traces. Rostral Arch = 63 traces. Wake: Caudal Arch = 70 traces. Rostral Arch = 41 trace. Caudal Arch = 3 mice. Rostral Arch = 3 mice. Corr_coef - correlation coefficient. Each red dot represents single trace. Blue line – a line of best fit.

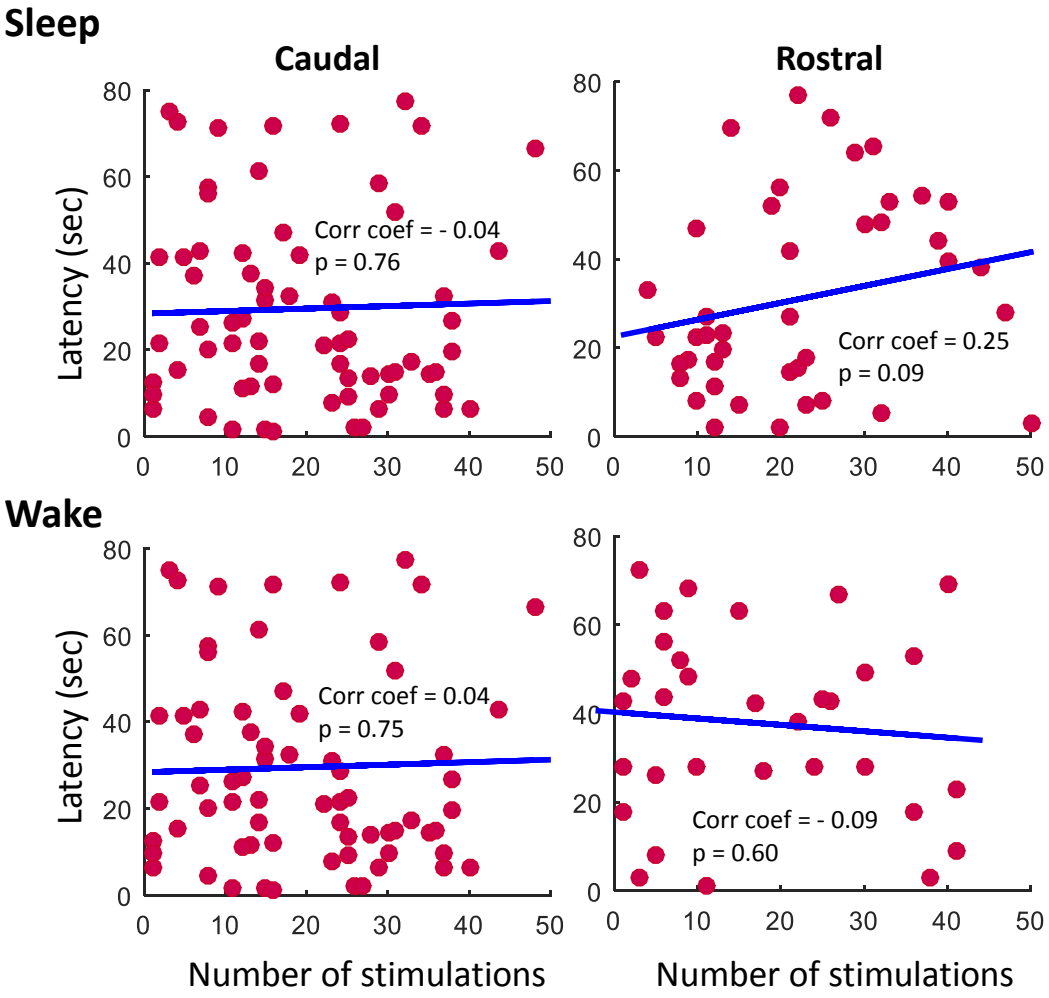

Figure 4.19 Relationship between the latencies and the number of stimulations in NpHR expressing mice. Top row (sleep) is dedicated to the latency of arousal, period between the light stimulation beginning and the arousal. Bottom row (wake) is showing the relationship of the latency between the light stimulation and falling asleep. There was no correlation between the latencies and the number of stimulations. Sleep: Caudal NpHR = 71 traces. Rostral NpHR = 45 traces. Wake: Caudal NpHR = 63 traces. Rostral NpHR = 32 trace. Caudal NpHR = 4 mice. Rostral NpHR = 4 mice. Corr_coef - correlation coefficient. Each red dot represents single trace. Blue line – a line of best fit.

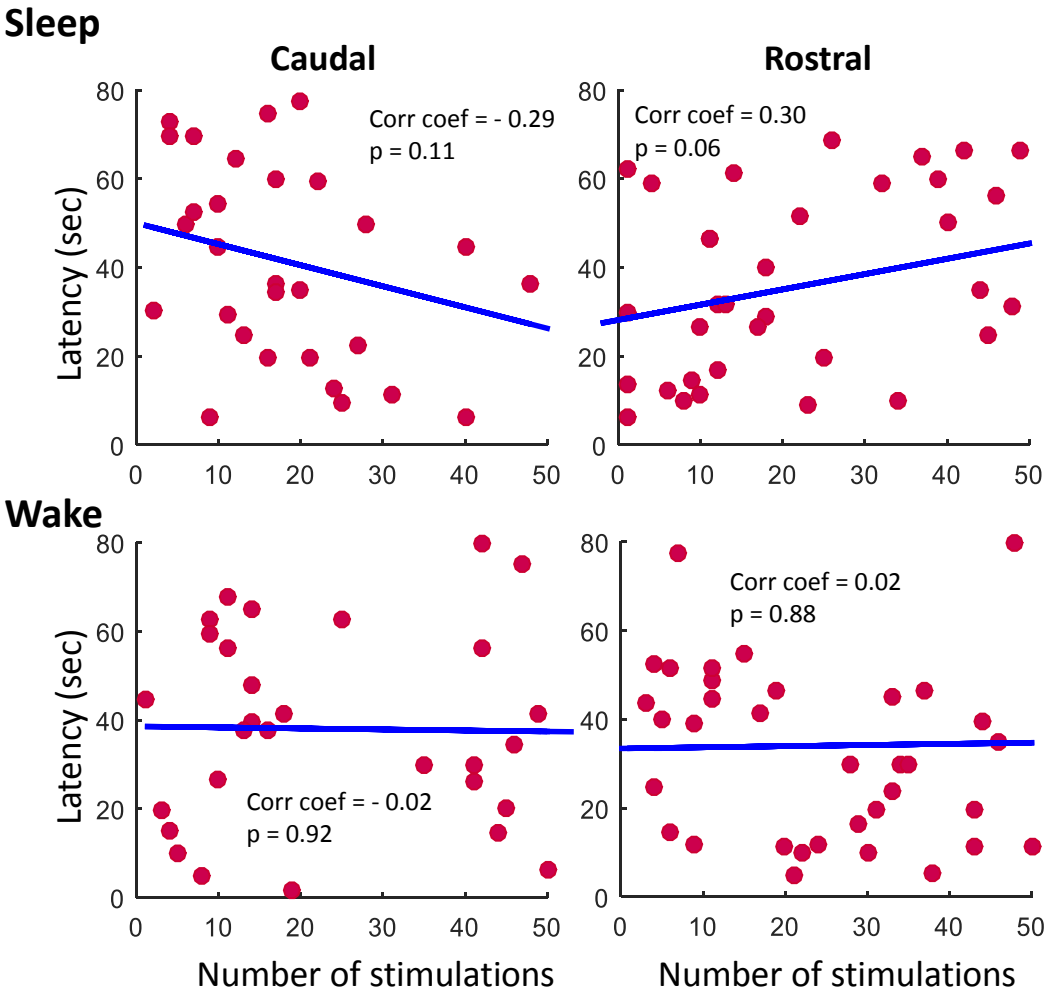

Figure 4.20 Relationship between the latencies and the number of stimulations in YFP (control) expressing mice. Top row (sleep) is dedicated to the latency of arousal, period between the light stimulation beginning and the arousal. Bottom row (wake) is showing the relationship of the latency between the light stimulation and falling asleep. There was no correlation between the latencies and the number of stimulations. Although, the latency of the arousal during caudal and rostral light stimulation show the tendency to the significance. Caudal Control = 30 traces. Rostral Control = 40 traces. Wake: Caudal Control = 32 traces. Rostral Control = 40 trace. Caudal Control = 3 mice. Rostral Control = 2 mice. Corr_coef - correlation coefficient. Each red dot represents single trace. Blue line – a line of best fit.

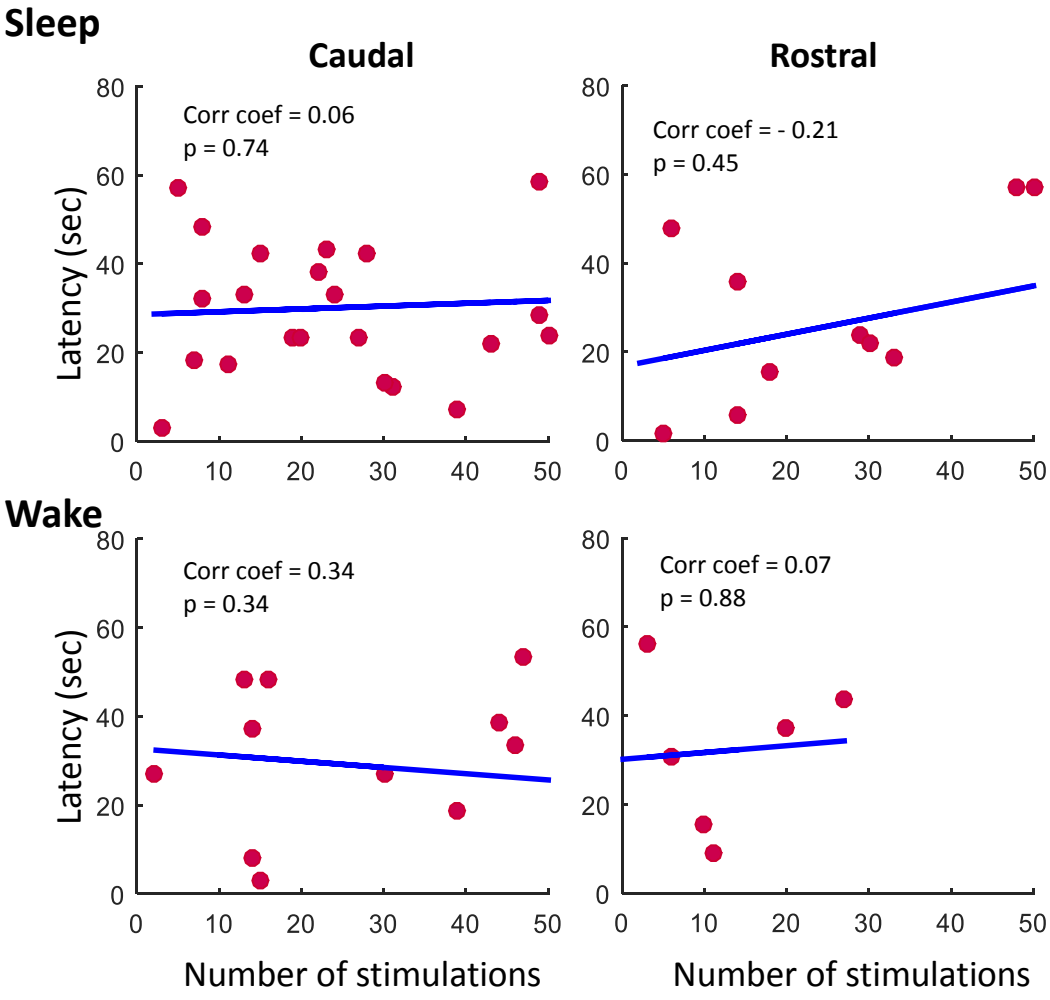

Figure 4.21 Relationship between the latencies and the number of stimulations in Arch mice without TRN light stimulation (optic fibers were not attached to the head of the mouse). Top row (sleep) is dedicated to the latency of arousal, period between the light stimulation beginning and the arousal. Bottom row (wake) is showing the relationship of the latency between the light stimulation and falling asleep. There was no significant relationship between the latencies and the number of stimulations. Sleep: Caudal Non-Stim = 25 traces. Rostral Non-Stim = 11 traces. Wake: Caudal Non-Stim = 16 traces. Rostral Non-Stim = 7 trace. Caudal Arch= 3 mice. Rostral Arch = 2 mice. Corr_coef - correlation coefficient. Each red dot represents single trace. Blue line – a line of best fit.

4.4 Discussion

4.4.1 Sleep/wake cycle during caudal TRN inhibition

According to previous studies we hypothesized that the caudal TRN is linked to sensory thalamic nuclei and that during sleep it is responsible for sensory pathway inhibition (See chapter 1). Halassa et al. (2014) reported that the TRN neurons linked to sensory thalamic nuclei are responsible for sleep spindles. The malfunctioned sleep spindles oddly affects the architecture of the sleep: total sleeping time is not changed, but the time of sleeping bouts is reduced (Wells et al., 2016). Sleep spindles are well known for the stabilization of the sleep architecture (Wimmer et al., 2012; Kim et al., 2012). The results of the present study of caudal TRN optogenetic inhibition, are in line with these earlier findings. The optogenetic inhibition of the sensory TRN led to the reduction of sleep spindle oscillations (See Chapter 3) and consequently, the sleep became less stable, discontinuous and contained a larger number of the short sleeping episodes. Additionally, the shortened latency to arousal was characteristic only for caudal TRN. Herrera et al. (2015) demonstrated, that short tonic inhibition of the rostral TRN neurons led to the shortened latency of arousal. They associated the latency reduction with hypothalamic-TRN circuitry, but the TRN modulation according to our results is more complicated (See chapter 5).

4.4.2 Sleep/wake cycle during rostral TRN inhibition

As mentioned before, several laboratories have published high impact papers based only on rostral TRN modulation (Kim et al., 2012; Ni et al., 2016). Halassa et al. (2014) using electrophysiology *in vivo* proved the heterogenous nature of the TRN and confirmed that the TRN neurons associated with limbic thalamic nuclei fire differently during sleep. These neurons are not responsible for sleep spindle production during sleep and are arousal correlated. Collected results from previous tracing, neuroanatomical, electrophysiological and behavioural studies allowed us to hypothesize that most of the rostral TRN is dedicated to the cognitive ('limbic') functions. Consequently, we expected that the optogenetic inhibition of the cognitive part of the TRN would not have an effect on sleep spindle oscillation (See Chapter 3) and that inhibition of arousal correlated cells should prolong sleep. Basically, the

modulation of the same nucleus would produce opposite results. In this study we demonstrated that the rostrally inhibited animals had a tendency for longer sleep and had a reduced proportion of the short sleep episodes relative to the caudally stimulated and control animals. Although, quantification of the long sleep episodes is missing to strengthen the results and clarify the sleep/wake cycle pattern and should be a subject of future analysis.

4.4.3 Contradicting results from previous studies

Some might think that the results from Herrera et al. (2015) , where they demonstrated that the short tonic inhibition of the rostral TRN neurons reduced the latency of arousal, might contradict with our results. The delicate approach to the results allows to undersdstand that both results are possible and can be explained. Firstly, in the study by Herrera et al. the inclusion criteria for NREM stimulation was 10 seconds of NREM sleep (20 seconds in our case). The sleep length before stimulation is crucial (See Chapter 5), as the TRN appears to be sensitive not just to the initial state, but might act as a tumbler used for the state change (Kim et al., 2012; Wimmer et al., 2012). Secondly, the light stimulation lasted no longer than 5 seconds and the light-induced heating effect was not involved. Lastly, Herrera et al. targeted all GABAergic neurons, whereas our optogenetic inhibition was concentrated only on parvalbumin containing neurons. According to our findings, Herrera could shorten the reported latency during stimulation even further by selecting the caudal part of the TRN for stimulation, instead of the rostral part.

Two similar studies, which activated the rostral TRN, showed an increased number of artificial sleep spindles and prolonged NREM sleep (Kim et al., 2012; Ni et al., 2016).. In this case, it seems, that we are dealing with different mechanisms of NREM sleep prolongation. In order to induce sleep spindles both studies activated the TRN with 8 Hz light stimulations followed by 6-7 seconds of a quiescence interval. These activations were able to produce spindles even in the wake state. It is important to note, that mentioned optogenetic stimulations with lower frequencies did not produce any significant effects. Additionally, the NREM increase was associated with

frequent transitions between NREM-REM and REM-NREM, whereas in our study these transitions were not visible on the generated spectrograms.

4.4.4 Summary

In the present study, experiments were performed on the same animals before and during light stimulation to exclude the effect of the sleeping architecture of individual mice. Control mice expressing YFP (no opsin) were employed, to eliminate the light stimulation effect during optogenetic modulation. The influence of the circadian rhythm did not appear to affect the outcomes. Some of the animals were tested in different times of the day, and at the final stages of the study the caudally and rostrally stimulated mice were tested simultaneously in the separate boxes.

The finding of the opposite effect of rostral and caudal optogenetic inhibition on sleep architecture supports the concept of the nucleus functioning during sleep as suggested by Halassa et al., (2014), where the sleep sensory (caudal) TRN actively inhibits sensory input to the brain, while limbic (rostral) TRN has reduced activity and perhaps facilitates offline processing. Thereby, the present EEG and sleep/wake cycle results strongly support the hypothesis that TRN heterogenous circuitries, sensory and cognitive (limbic) could be roughly differentiated based on the anteroposterior coordinates.

It could be argued that the optogenetic inhibition of the silent (reduced activity) rostral TRN during sleep should produce no effect. The expounding answer is simple, sleep as a process and the TRN as a structure possess similar features, both are non-homogenous. The detailed explanation of the rostral and caudal TRN activity during sleep will be covered in Chapter 5.

Chapter 5: Evaluation of the involvement of the TRN in brain state transition

5.1 Introduction

Sleep is a non-homogenous process, which consists of interchanging intervals of non-rapid eye movement (NREM) and rapid eye movement (REM) sleep. In humans, NREM sleep makes up for ~80% of normal night's sleep, during which slow wave activity dominates and typically lasts for 40 - 60 minutes. In rodents, the entire phase of NREM sleep is shorter with each episode lasting 3-5 minutes, although occasionally they can extend up to 20 minutes (Saper et al., 2011). The NREM sleep is further divided into another three stages: N1, N2 and N3. During N1 or drowsiness, EEG frequency is slowed down with strong alpha activity appearing at posterior sites and theta activity at anterior sites. Sleep spindles and K-complexes are prevalent during N2 stage, light sleep, whereas during the last NREM stage, deep sleep, the slow wave sleep amplitude is increased (Vyazovskiy & Delogu, 2014). In mice, NREM sleep is not divided into stages, which is unusual, as the core physiological mechanism controlling sleep is common to most mammalian species and contain slight evolutionary modifications (Phillips et al., 2010). REM sleep, which is localised between N2, or N1 stage (Vyazovskiy & Delogu, 2014), is characterized by a wake like EEG frequency with a strong synchronous theta range, generated by the hippocampus (Brown et al., 2012).

The processes of the transition between the brain states is quite common, but the mechanism is largely unknown (Phillips et al., 2010). These 'transition' changes in rodents lasts over few seconds, but in humans may take 10 seconds and up to a minute (Wright et al., 1995; Takahashi et al., 2010a). The transition between sleep and wakefulness typically takes less than 1% of the average NREM bout duration. Interestingly, the duration of the NREM sleep bouts during sleep follow an exponential distribution (Lo et al., 2004). Similarly, transitions of a few seconds occur during NREM sleep transformation into REM sleep and are characterized by lower voltage and higher frequency activity (Saper et al., 2011).

The suspected brain structures underlying the state transitions, unsurprisingly, are also involved in the sleep/wake cycle regulation and are rested on three regions

implicated in sleep: brainstem, basal forebrain and hypothalamus. A Viennese neurologist, Baron Constantin von Economo described encephalitis lethargic and noticed, that the prolonged state characteristic for the infection, was caused by damage to the posterior hypothalamus and rostral midbrain. Based on these observations, von Economo predicted that the hypothalamus near the optic chiasm contains sleep promoting neurons, whereas the posterior hypothalamus contains neurons that promote wakefulness (von Economo, 1930). More than 70 years later Saper et al. (2001) proposed a "flip-flop" hypothesis, which stated, that sleep-promoting neurons in the ventrolateral preoptic nucleus (hypothalamus) and wake-promoting neurons in the tuberomammillary nucleus (hypothalamus) and locus coeruleus (brainstem) constitute the mutually inhibitory circuit which ensures rapid, stable and complete state transition. Slow behavioural transition latencies (up to several seconds) might be explained by the fact, that the neuronal population requires time to overcome the resistance of an antagonistic neuronal population (Saper et al., 2011). Additionally, the speed of the state change varies with the size and complexity of the mammalian species brain (Phillips et al., 2010).

The thalamic nuclei are the most important and abundant source of subcortical afferents to the cerebral cortex, but previous studies failed to provide evidence that these inputs might play a major role in wakefulness. Thalamic lesion in rats had no effect on wakefulness or EEG waveform, apart from sleep spindle elimination (Vanderwolf & Stewart, 1988; Buzsaki et al., 1988). Additionally, patients with bilateral thalamic damage end up in a vegetative state, with preserved wake-sleep cycles (Kinney & Samuels, 1994). Although, the latest studies point out that several higher order thalamic nuclei can modulate brain-wide cortical activity during sleep and provides dual control of sleep–wake states (Gent et al., 2018).

Additionally, the TRN has the ability to modulate thalamocortical transmission and is critical for selective attention and arousal (McAlonan et al., 2008; Herrera et al., 2015). The TRN receives inputs from all major sleep/wake cycle centres: the arousal brainstem nuclei (Kolmac & Mitrofanis, 1998), hypothalamus (Herrera et al., 2015),

basal forebrain (Cornwall et al., 1990e), tractus solitarius (Nanobashvili et al., 2009) and zone incerta (Cavdar et al., 2006). Moreover, the GABAergic inputs from the basal forebrain and hypothalamus are involved in the inhibition of the TRN cells during arousal (Buzsaki et al., 1988; Herrera et al., 2015). Therefore, the TRN is an effective modulatory tool of the thalamo-cortical circuitry through which the brainstem, hypothalamus and basal forebrain can control the forebrain state.

Previous studies have shown that TRN activity increases during brain state change and can be a crucial part of the state transition mechanism. Vyazovskiy et al. (2004) first noticed that sleep spindles (~ 11 Hz) in the frontal cortex were most prominent during NREM sleep and increased before NREM-REM transition. The sleep spindles increased concomitantly with the beginning of the NREM sleep episode. The introduction of transgenic techniques has produced an abundant number of mice types with abnormal sleep spindles. Surprisingly, most of these mice had unaffected sleep/wake cycle with normal EEG oscillations, but the timing and oscillations linked to the brain state transition were abnormal. For example, the transgenic mice lacking $Ca_V3.3^{-/-}$ (calcium channels), which are expressed abundantly in the TRN and underlie sleep spindle firing, had significantly reduced alpha oscillations 30 seconds before REM sleep onset (Astori et al., 2011). Mice with overexpressed Ca^{2+} dependent small-conductance-type 2 (SK2) potassium channels, had decreased delta power and protracted alpha oscillation peak power between NREM-REM transition and the NREM required longer transition time. Additionally, the NREM sleep episodes were increased, REM episodes slightly reduced and a similar prolongation of the alpha power change was found in the transition from NREM into waking (Wimmer et al., 2012). Frequent artificial sleep spindles in the rostral TRN generated longer NREM sleep episodes and significantly increased the number of the NREM-REM and REM-NREM transitions (Kim et al., 2012). Hence, the sleep spindles generated in the specific pre-brain state period, might act as a key for the brain state change.

A better understanding of the brain state transmission process by the TRN is provided by Winsky-Sommerer et al. (2008), where they tested mice lacking the α3 $GABA_A$

subunit, which is highly expressed in the TRN and cortical layer VI $GABA_A$ receptors. This study aimed to discover an additional phenotype of epilepsy but failed to find even minor changes in the sleep/wake cycle. The paper mainly stressed the negative results, although it mentioned that these mice showed significantly lower alpha oscillations (10-15 Hz) during NREM-REM sleep transitions. Additionally, wild type mice showed peak alpha oscillations during wake-NREM transition, whereas the mutant mice lacked this peak, although the difference failed to reach significance. The mutant mice had slightly larger power in the frontal cortex in the 11-13-Hz band during transition from sleep to wake (Winsky-Sommerer et al., 2008). We are of the view, that Winsky-Sommerer et al. (2008) unintentionally showed the first evidence of the two types of sleep spindles in mice, fast and slow, and that each is responsible for different functions. It would appear that the fast sleep spindles (10-15 Hz) maybe important for wake-NREM and NREM-REM transitions, whereas the frontally located slow sleep spindles (11-13 Hz), probably, are taking part in NREM – wake transition.

Kim et al. (2015) discovered topographically distinctive spindles in mice, though they failed to find differences in frequency between them. Perhaps, the mice brain size does not allow us to distinguish the difference between slow and fast oscillations. In humans, slow sleep spindles were identified in the frontal cortical areas (~12 Hz), whereas the fast sleep spindles were found mainly in the parietal zones (~14 Hz) (Andrillon et al., 2011). Interestingly, the depth EEG recordings from epileptic patients found a sharp border between slow and fast spindles in the supplementary motor area.

Knowing that the border between the sensory and limbic (cognitive) TRN is located on the motor TRN (See figure 1.3) we can hypothesize that the fast spindles in mice are mostly produced in the caudal TRN and that the slow spindles are generated in the rostral TRN. According to the results from Winsky-Sommerer et al. (2008), the fast spindles (alpha oscillation) are generated at the early sleep stages to promote the transition between wake to NREM, therefore the optogenetic inhibition of the caudal TRN during early sleep might results in rapid arousal. Additionally, the

inhibition of the rostral TRN during same period should not produce any significant effect on arousal. The inhibition of the slow sleep spindles, putatively, promoting NREM-wake transition in the rostral TRN should result in the prolonged NREM sleep intervals.

5.2 Methods

To investigate the effect of the caudal and rostral TRN modulation on sleep transition, we combined optogenetic and electrophysiological approaches in freely moving mice. Two inhibitory opsins Halorhodopsin (NpHR), Archaerhodopsin (Arch) and YFP (Control) were expressed specifically in anterior or posterior part of the TRN in parvalbumin (PV)-Cre mice using adeno-associated viral vectors (NpHR, n = 8; Arch, n = 6 and YFP (Controls), n = 5). Virus was injected caudally (AP, -1.6 mm) in the caudally targeted TRN and rostrally (AP, -0.8) in the rostrally targeted TRN. Similar coordinates were used for chronic optic fibre placement. We found restricted expression patterns of Arch and Halo in PV-positive neurons of the TRN depending on injection sites (See Figure 2.3-2.5). The effect of optical stimulation on the brain state was assessed using simultaneously recorded EMG. We classified behavioural epochs into two states: wake and slow-wave sleep (SWS). To compare differences between viral groups and controls, ANOVA, two sample paired test and measure effect size (MES, Hedges) with confidence intervals (CI) were employed. For full details of the surgical and experimental methods and the location of the viral expression patterns see Chapter 2.

5.3 Results

5.3.1 The TRN involvement in the wake – NREM sleep transition

Caudal TRN inhibition during early sleep stage led to rapid arousal

We introduced new inclusion criteria for the data to investigate the relationship between the TRN activity and wake – NREM sleep transition (See figure 5.1). These criteria were that mice were asleep at least 10 seconds and no more than 20 seconds, before the start of the light stimulation and woke up during an 80 second period after the start of the stimulation. Additionally, a new value was introduced, **latency,** this is the period between the start of the light stimulation and arousal, which characterized the speed of waking up, putatively, caused by the TRN optogenetic inhibition. We did not include the latencies longer than 80 seconds for analysis, because the 30 seconds long light stimulations were introduced every 90 seconds in our study.

First, we tested the latency changes induced by light stimulation during the wake-NREM transition. The mice expressing Arch and NpHR during caudal TRN light stimulation had significantly smaller averaged latencies than control mice with the same stimulation (See figure 5.2 a. ANOVA, F = 3.3, p = 0.04. Arch vs control, post-hoc Tukey HSD, p = 0.004; Measure effect size (MES) = - 0.87, confidence interval (CI) = - 1.76/0.02. NpHR vs control, post-hoc Tukey HSD, p = 0.11; MES = - 0.8, CI = - 1.60/0.00. Arch = 13 traces, NpHR = 22 traces, Control = 9 traces). Although, the averaged latencies of the rostrally light stimulated Arch and NpHR mice were higher than in control mice, they failed to reach statistical significance (See figure 5.2 b. ANOVA, F = 1.5, p = 0.25. Arch vs control, post-hoc Tukey HSD, p = 0.32; Measure effect size (MES) = 1.47, confidence interval (CI) = - 0.01/2.95. NpHR vs control, post-hoc Tukey HSD, p = 0.33; MES = 0.84, CI = - 1.60/0.00. Arch = 4 traces, NpHR = 5 traces, Control = 5 traces). The combination of the results in the Opsin groups from the mice expressing Arch and NpHR allowed us to increase the n number for statistical analysis. Caudally stimulated mice expressing inhibitory opsins woke up much faster than control mice (See figure 5.2 c. Two sample t test, p = 0.02; MES = 0.91, CI = 1.66/0.15). The graph showing the latencies of the rostrally stimulated mice

reminded a mirror image of the caudally stimulated mice. In the case of the rostrally targeted TRN, the latency of the control animals was much smaller than the latency of the opsin expressing animals, but the difference between two remained insignificant (See figure 5.2, d. Two sample t test, p = 0.09; MES = 0.95, CI = - 0.2/2.1).

These results suggest that only caudal TRN optogenetic inhibition during early sleep stages lead to rapid arousal. Additionally, the rapid arousal was induced by the rostral stimulations of the mice expressing YFP. Potentially, the rostral TRN heat-activated neurons induce a similar effect on the latency period as caudal TRN inhibition during the early sleep stages.

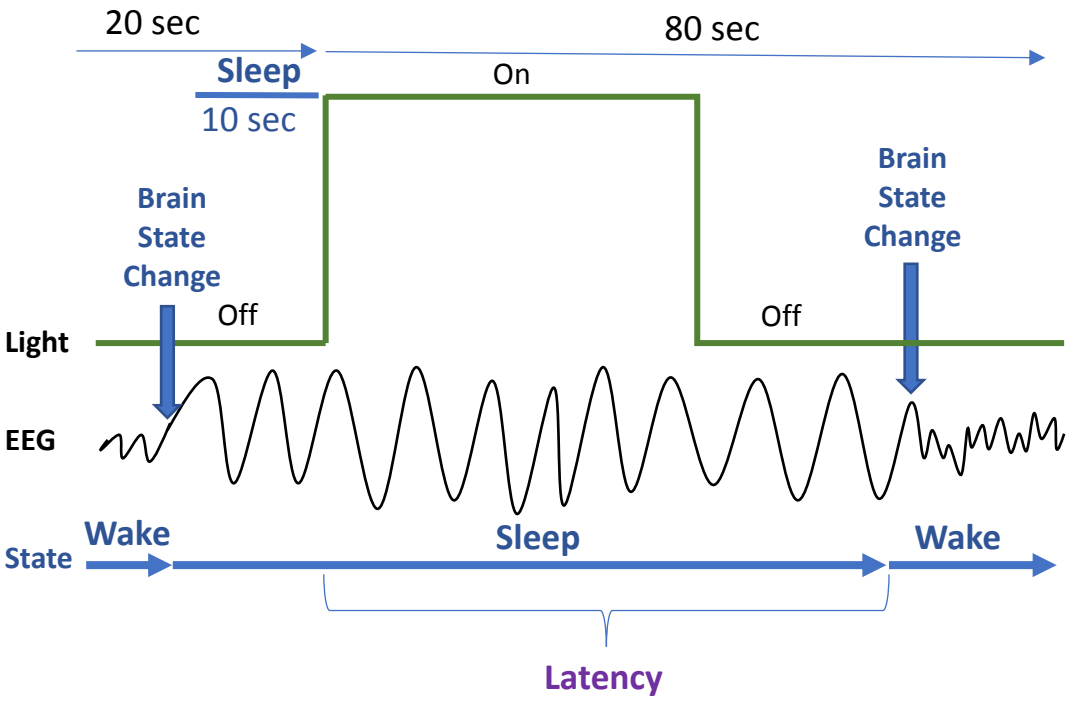

Figure 5.1 Inclusion criteria for data analysis to investigate the relationship between optogenetic inhibition of the TRN and wake-NREM transition. The latency period was determined in animals that were asleep greater than/equal to 10 sec but less than 20 sec before the start of the light stimulation and woke up during 80secs after the beginning of the light stimulation'

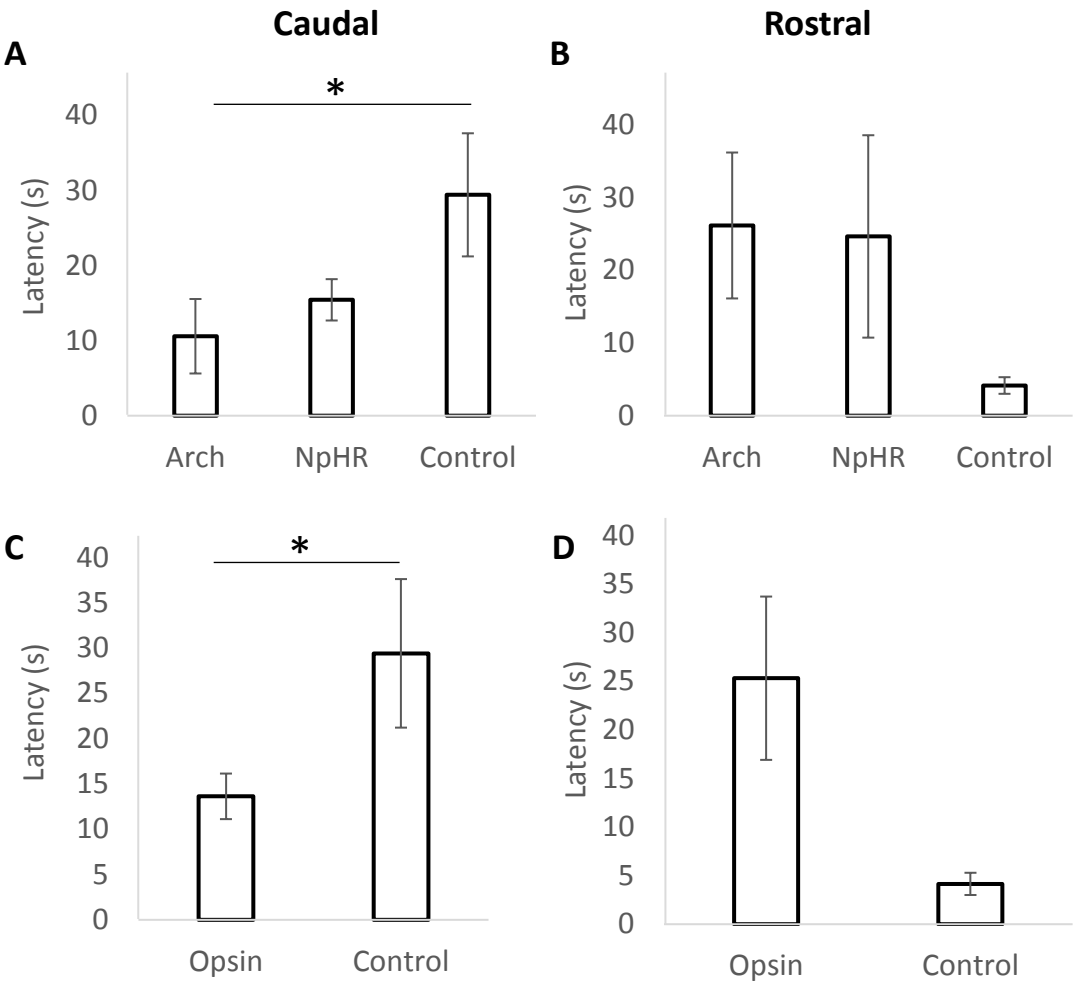

Figure 5.2 The effect of caudal and rostral TRN light stimulation on the latency period (speed of waking up) in animals expressing Arch, NpHR and Control (YFP). Top graphs (**A, B**) display the average latency change between mice with Arch, NpHR and YFP (control) expression. Bottom graphs (**C, D**) shows the differences in the latencies between mice with inhibitory opsins (Arch + NpHR) and control mice. The averaged latency of the caudally stimulated mice expressing inhibitory opsin (Arch on top and opsin in bottom) was significantly shorter than the latency of the control mice with the same stimulation. Interestingly, the rostrally stimulated control mice had a very short average latency, although this was not significantly different from experimental mice. * $p < 0.05$. Error bars – SEM.

TRN modulated rapid arousal is only characteristic for early sleep stages

Generally, it is believed that mice do not have stage 1 and stage 2 of NREM sleep and that the transition phase between wake-NREM sleep occurs over several seconds (less than 1% of average NREM sleep bout) (Takahashi et al., 2010b). Although, we showed above, that the early sleep stage crucially affects TRN mediated arousal. We decided to investigate the relationships between the latencies to arousal induced by TRN inhibition and the sleep stages during which the light stimulation occurred.

The latency to arousal in chapter 4 were calculated when the animal was sleeping for at least 20 seconds before light stimulation (See figure 4.6). Above, we calculated the latencies of the same mice, which slept for at least 10 seconds and less than 20 seconds (See figure 5.1). The latencies of 10 and 20 seconds sleep periods were compared to understand how the sleep stage might affect the latencies of arousal produced by caudal and rostral TRN tonic inhibition.

Arch and NpHR expressing mice showed almost identical relationships between the latency and sleep stage changes. Both, rostrally and caudally stimulated animals had shorter latencies when they had 10 seconds of sleep before light stimulation than 20 seconds of sleep, but this effect was only significant in caudally stimulated animals (See figure 5.3 a, b. *Arch:* 2-way ANOVA, F = 5.99, p = 0.01. Caudal, post-hoc Tukey HSD, p = 0.004; Measure effect size (MES) = 0.99; CI = 0.37/1.60. 20 sec = 64 traces, 10 sec = 13 traces. Rostral, post-hoc Tukey HSD p = 0.83; MES = 0.45; CI = - 0.56/1.46. 20 sec = 63 traces, 10 sec = 4 traces. *NpHR:* 2-way ANOVA, F = 3.64, p = 0.05. Caudal, post-hoc Tukey HSD, p = 0.03; Measure effect size (MES) = 0.69; CI = 0.20/1.18. 20 sec = 71 traces, 10 sec = 22 traces. Rostral, post-hoc Tukey HSD p = 0.88; MES = 0.31; CI = - 0.61/1.24. 20 sec = 45 traces, 10 sec = 5 traces). The summation of the Arch and NpHR mice results into the Opsin group, increased n number for ANOVA analysis but did not influence previous tendencies. The caudal Opsin latencies showed a similar pattern of results and the rostral Opsin group had statistically similar latencies at both sleeping stages (See figure 5.3 c, Opsin: 2-way ANOVA, F = 9.79, p = 0.001. Caudal, post-hoc Tukey HSD, p = 0.0001; Measure effect size (MES) = 0.83; CI = 0.44/1.21. 20 sec = 135 traces, 10 sec = 35 traces. Rostral, post-hoc Tukey HSD p =

0.63; MES = 0.41; CI = - 0.28/1.09. 20 sec = 108 traces, 10 sec = 9 traces). Interestingly, the control mice results shown similar latency change dynamics influenced by the light stimulation stage, but the affected side of the stimulation was more apparent in rostrally stimulated mice. The rostrally stimulated mice showed strong and significant latency change, whereas caudally stimulated control mice displayed similar latencies during both sleep stages (See figure 5.3, d. Control: 2-way ANOVA, F = 12.92, p = 0.0006. Caudal, post-hoc Tukey HSD, p = 0.38; Measure effect size (MES) = 0.43; CI = - 0.37/1.22. 20 sec = 27 traces, 10 sec = 8 traces. Rostral, post-hoc Tukey HSD p = 0.008; MES = 1.61; CI = 0.62/2.59. 20 sec = 40 traces, 10 sec = 5 traces). So, the caudal inhibition of the TRN in Arch and NpHR mice and the light stimulation of the rostral TRN in control mice produced similar and significant latency change dynamics (See figure 5.3, e). Rostrally inhibited NpHR and Arch mice and the light stimulation of the caudal TRN, did not reproduce the latency change due to sleep depth (See figure 5.3, f).

Additionally, another inclusion criteria was employed to assess the effect of TRN inhibition on arousal; mice, which slept more than 20 seconds and less than 30 seconds before stimulation. These data showed that the latency period was similar to that in mice which slept more than 20 seconds before optogenetic stimulation (Data not shown, p >0.05).

In summary, rostral TRN inhibition produced equal latencies independent of the timing of the sleep stage inhibition, whereas caudal TRN inhibition generated significantly different latencies depending on the timing of the inhibition. It was only during the early sleep stages, that the optogenetic inhibition of the caudal TRN lead to the rapid arousal. Thereby, the caudal TRN activity seems to be crucial for sleep initiation or for so called wake – NREM sleep transition. The rostral TRN light stimulation effect in control mice, which is similar to caudal TRN inhibition should be investigated further in future.

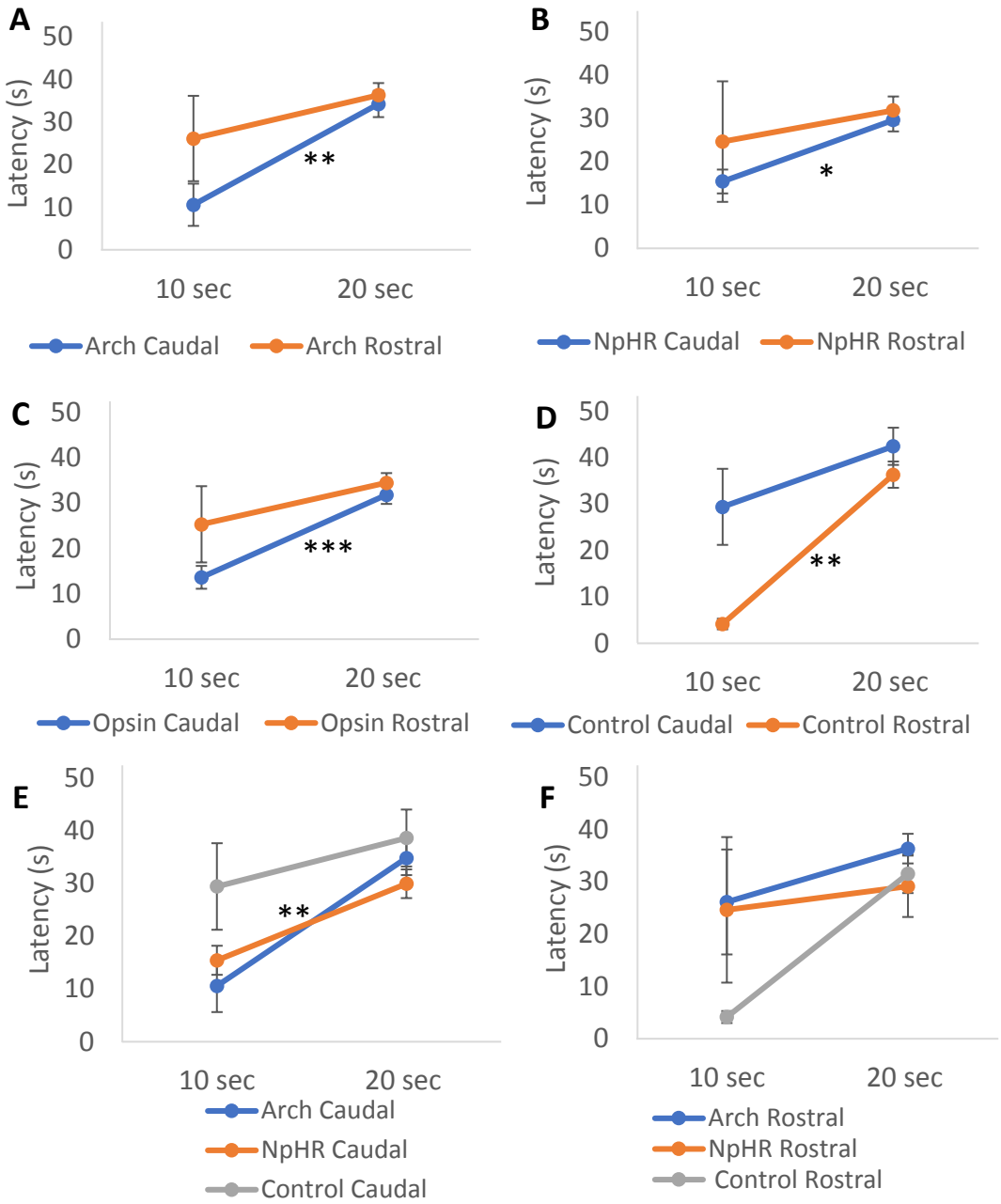

Figure 5.3 Graph portrays the change of the relationship between the latency and sleep stage during, which the TRN inhibition occurred. The latency, period between the light activation and arousal. Inhibitory opsins were expressed specifically in the caudal (blue) and rostral (yellow) TRN (excluding figure 5.3 d). 10 sec – symbolize early sleep stage, where the mice had to sleep at least 10 seconds but no more than 20 seconds before light activation. 20 sec – symbolize sleep stage, where same mice had to sleep at least 20 seconds before light stimulation. **A** Latencies induced during different sleep stages in Arch expressing mice. **B** Latencies induced during different sleep stages in NpHR expressing mice. **C** Latencies induced during different sleep stages in Opsin (NpHR + Arch) expressing mice. **D** Latencies induced during different sleep stages in YFP (control) expressing mice. **E** and **F** The comparison of the latency dynamics in the mice expressing various opsins. * $p < 0.05$. ** $p < 0.01$. *** $p < 0.001$. Error bars – standard error of the mean.

Relationship between the sleeping time before light activation and latency

Optogenetic inhibition of the caudal TRN during various sleeping periods had a different effect on the latency. In order to explore the relationship between the sleeping time before light stimulation and the sleeping time after light stimulation (latency) we constructed several scatter plots for mice expressing various opsins. At the beginning, we tested the relationship between these two-time intervals in the Arch mice before and during stimulations (No Stim and Stim sessions, see figure 4.1). Before stimulation caudal and rostral mice did not show any significant correlation, whereas during light stimulation the caudal animals demonstrated significant positive correlation between the sleeping time before stimulation and the latency. If the caudally stimulated mice slept less than 20 seconds before the start of stimulation, they woke up in most cases faster than 5 seconds after stimulation, whereas if mice slept longer than 25 seconds before stimulation, the latency was close to 60 seconds (See figure 5.4 a,b. Caudal Stim: Correlation coefficient (Corr coef) = 0.61, p = 0.0008. Caudal Arch No Stim = 6 traces, caudal Arch Stim = 26 traces. Rostral Stim: Corr coef = 0.12, p = 0.69. Rostral Arch No Stim = 4 traces, rostral Arch Stim = 13 traces). No relationship between the latency and the sleeping period before stimulation were found in the rostrally stimulated mice expressing Arch (See figure 5.4, c). Additionally, there was no relationship found in the NpHR expressing animals. Most of the caudally stimulated mice expressing NpHR woke up during the first 20 seconds independent of the sleeping period before stimulation (See figure 5.4, d. Caudal NpHR: Corr coef = 0.24, p = 0.13. Rostral NpHR: Corr coef = 0.12, p = 0.7. Caudal NpHR = 41 trace, rostral NpHR = 11 traces). Interestingly, a similar relationship between the latency and the sleeping time before light stimulation was found in the rostrally stimulated mice expressing YFP (control) (See figure 5.4, e. Caudal Control: Corr coef = 0.63, p = 0.04. Rostral Control: Corr coef = 0.48, p = 0.09. Caudal control = 13 traces, rostral control = 11 traces).

The results above suggest that early sleep periods (up to 20 seconds) are quite sensitive to TRN inhibition. Putatively, sleep spindle inhibition in the caudal TRN leads to rapid arousal (up to 5-10 seconds).

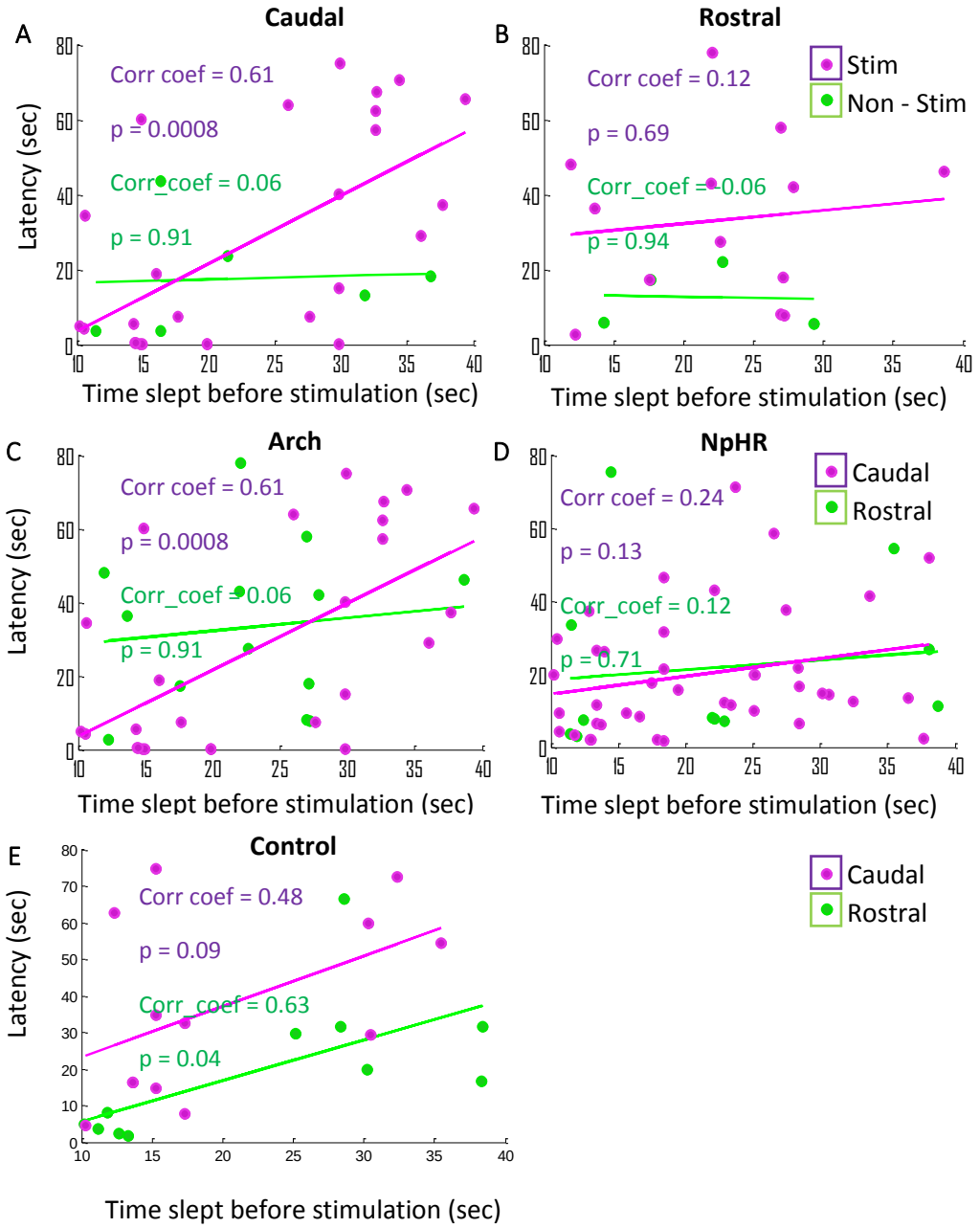

Figure 5.4 Scatter plots portray the relationship between the sleeping time before light stimulation start and the sleeping time after light stimulation start (latency). **A, B** Relationship between the latency and the sleeping time before stimulation in the caudally and rostrally stimulated mice expressing Arch before (No Stim, green) and during light stimulation (Stim, magenta). **C, D, E** Relationship between the latency and the sleeping time before stimulation in the caudally (magenta) and rostrally stimulated (green) mice expressing Arch, NpHR and YFP (control). Corr_Coef - Correlation coefficient. Green or magenta line – a line of best fit.

5.3.2 TRN inhibition does not influence the sleep onset time.

We introduced another inclusion criteria for the data to investigate the relationship between TRN activity during wake and sleep onset (See figure 5.5). Mice had to be awake for at least 10 seconds and no more than 20 seconds, before the start of light stimulation start and to fall asleep within 80 seconds after the start of stimulation. Additionally, a new value was introduced, **latency,** period between the light stimulation start and the sleep onset, which characterized the speed of falling asleep, putatively, caused by the TRN optogenetic inhibition. We did not include the latencies longer than 80 seconds for analysis, because the 30 seconds long light stimulations were introduced every 90 seconds in our study.

The latency to sleep onset in chapter 4 was calculated when animals were awake for at least 20 seconds before light stimulation (See figure 4.8). In this case, we calculated the latencies of the same mice which were awake for at least 10 seconds and less than 20 seconds (See figure 5.1). The latencies of 10 and 20 seconds wake were compared to understand how the wake stage might affect the latencies of arousal produced by the caudal and rostral tonic inhibition.

The length of the wake stage did not affect Arch and NpHR expressing mice ability to fall asleep. Results were not statistically significant in both cases (See figure 5.6 a, b. *Arch:* 2-way ANOVA, F = 1.05, p = 0.3. Caudal Arch, 20 sec = 70 traces, 10 sec = 8 traces. Rostral Arch, 20 sec = 41 traces, 10 sec = 4 traces. *NpHR:* 2-way ANOVA, 1.15, p = 0.29. Caudal NpHR, 20 sec = 63 traces, 10 sec = 11 traces. Rostral NpHR, 20 sec = 32 traces, 10 sec = 6 traces). The dynamics of the latency to sleep onset were not as similar as in the case with the latency to arousal covered previously. The caudal Arch and NpHR stimulated animals had different latencies to sleep onset during the early wake stages but the dissimilarity was not significant. The rostrally stimulated animals showed similar results (See figure 5.6 c, d. Caudal: 2-way ANOVA, F = 2.78, p = 0.09. Rostral: 2-way ANOVA, F = 0.74, p = 0.79). The Arch and NpHR results were then combined to increase the sample size. The latencies to sleep onset derived from different wake stages appeared identical in the Opsin group (See figure 5.6 e. Opsin:

2-way ANOVA, F = 0.74, p = 0.79. Caudal Opsin, 20 sec = 133 traces, 10 sec = 19 traces. Rostral Opsin, 20 sec = 73 traces, 10 sec = 10 traces).

Lastly, the relationship between the period of time awake before light stimulation and the sleep onset time (latency) were assessed. Several scatter plots for mice expressing various opsins were constructed. As expected, caudally and rostrally stimulated mice expressing Arch and NpHR did not have any relationship between these two periods. Caudally stimulated mice expressing YFP showed a significant correlation, but the number of points is too low to be considered (See figure 5.7). Although, it would be interesting to see how caudal TRN optogenetic activation might induce sleeping state in the animal, which woke up recently.

We can conclude, that TRN optogenetic inhibition does not appear to influence the sleep onset time.

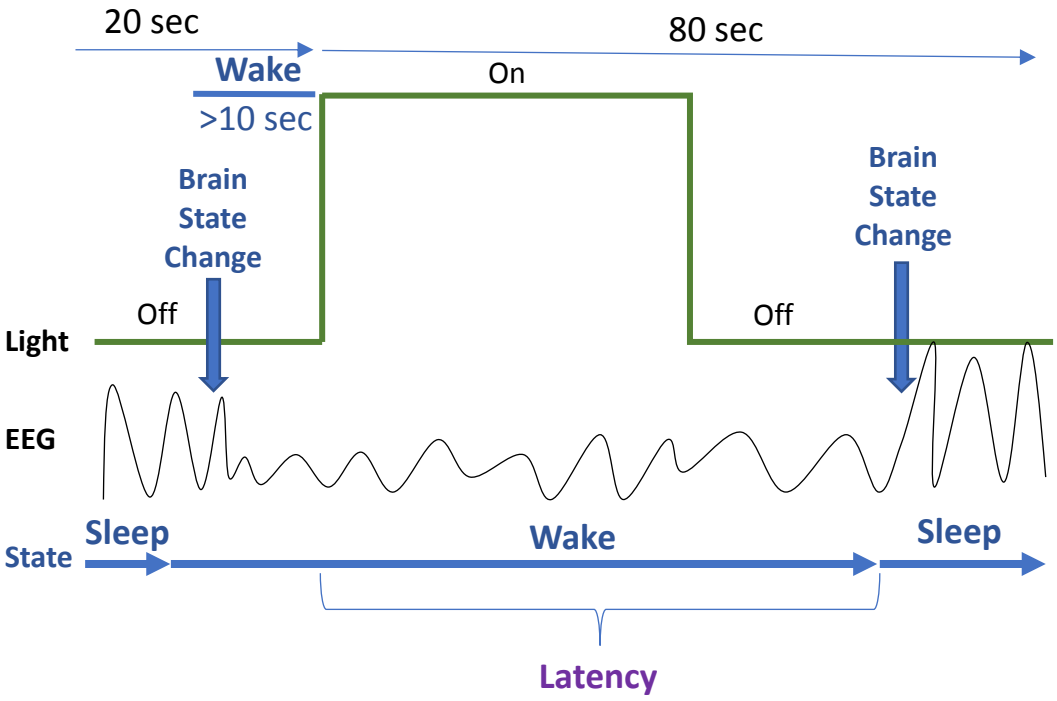

Figure 5.5 The inclusion criteria for the data analysis to investigate the relationship between the optogenetic inhibition of the TRN and falling asleep. The inclusion criteria for latency collection were as follows; animals awake >10 sec but less than 20 sec before the start of the light stimulation and to fall asleep within 80sec after the start of the light stimulation

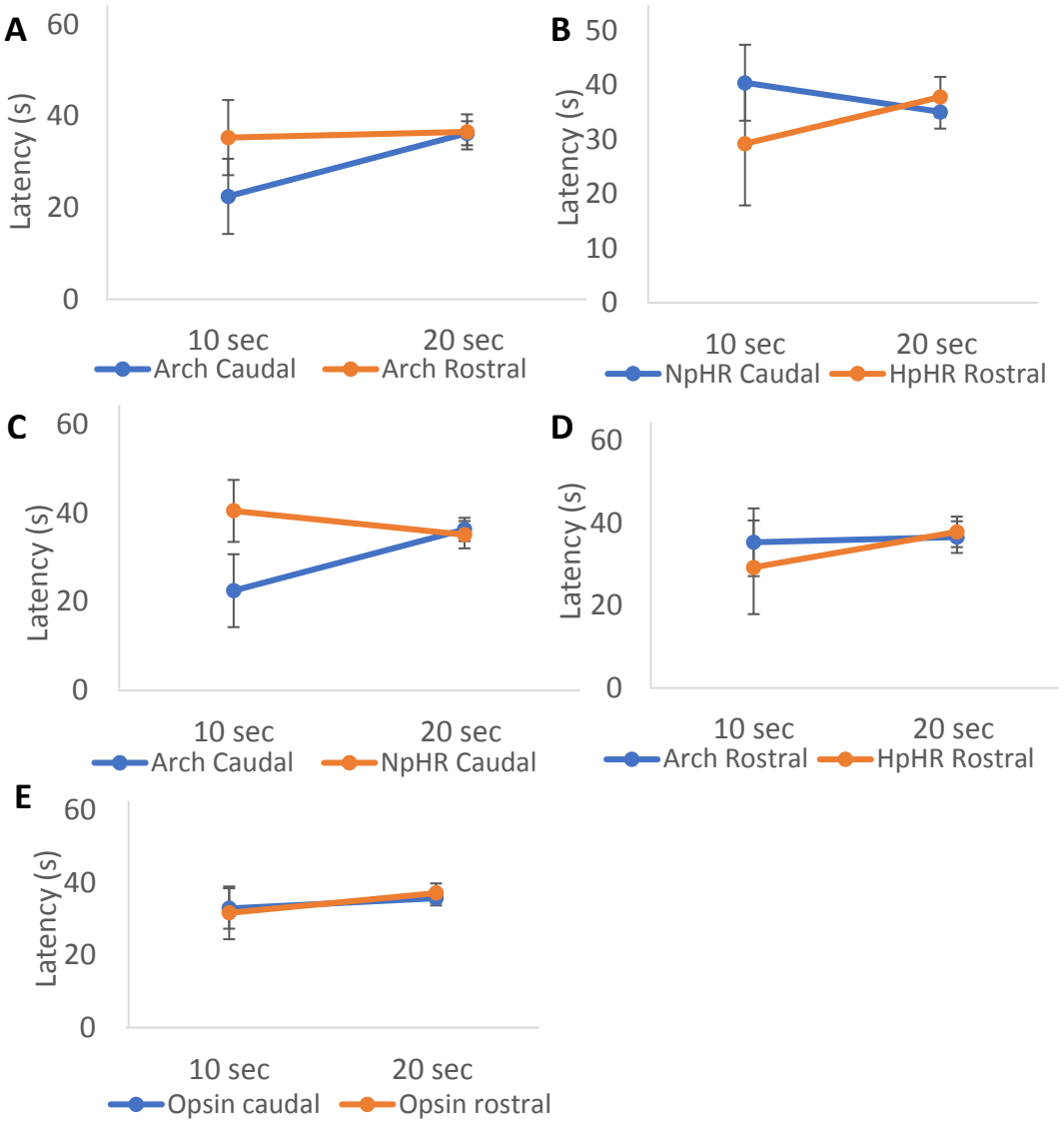

Figure 5.6 Graph portrays changes of the relationship between the latency and wake stage during, which the TRN inhibition occurred. The latency, period between the light activation and sleep onset. Inhibitory opsins were expressed specifically in the caudal (blue) and rostral (yellow) TRN (excluding figures 5.6 c,d). 10 sec – symbolise early wake stage, where the mice had to be awake at least 10 seconds but no more than 20 seconds before light activation. 20 sec – symbolise wake stage, where the same mice had to be awake for at least 20 seconds before light stimulation. **A** Latencies induced during different wake stages in Arch expressing mice. **B** Latencies induced during different wake stages in NpHR expressing mice. **C** Comparison between the latencies induced during different wake stages in caudally stimulated mice expressing inhibitory opsins. **D** Comparison between the latencies induced during different wake stages in rostrally stimulated mice expressing inhibitory opsins. **E** Latencies induced during different sleep stages in Opsin (NpHR + Arch) expressing mice.

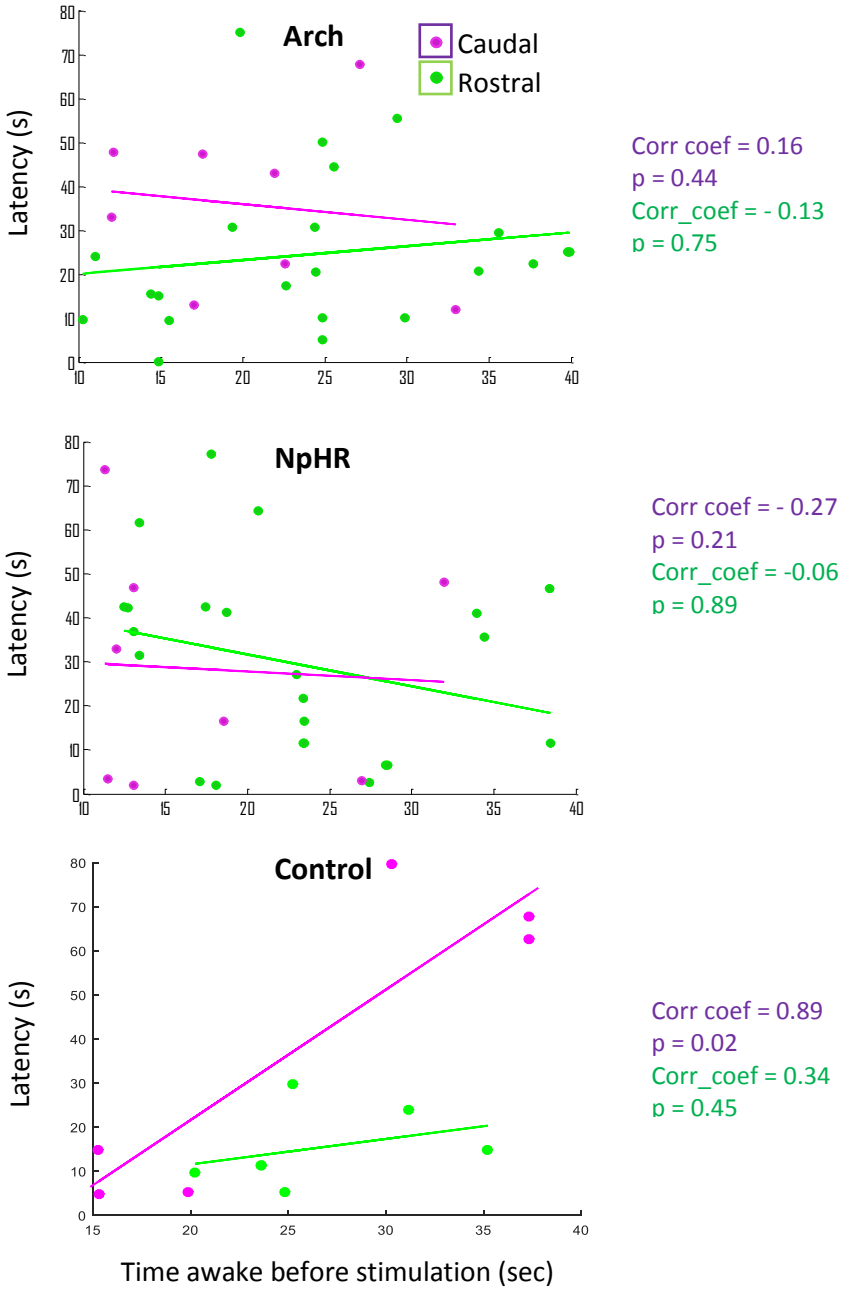

Figure 5.7 Scatter plots portray the relationship between the period awake before the start of light stimulation and the latency to sleep onset in mice expressing Arch (top), NpHR (middle) and YFP (bottom). Caudally (magenta) and rostrally stimulated (green) results are colour coded. Corr_Coef -Correlation coefficient. Green or magenta line – a line of best fit.

5.3.3 Relationship of the sleep pattern to EEG changes during the TRN inhibition

Above (see section 5.3.1) we demonstrated that caudal TRN activity (putatively, sleep spindle activity) during the wake – NREM sleep transition is crucial for sleep initiation. The caudal and rostral TRN inhibition (light stimulation) after 20 seconds of sleep does not produce any significant effect on the latency to wake up (shorter than 80 seconds) in all studied mice (See figure 5.3 and figure 4.16), but the ratio of short sleep episodes (sleep shorter than 80 seconds) in mice with caudally inhibited TRN is two times larger than in mice with rostrally inhibited TRN (See figure 4.17). Potentially, the sleep spindles generated during the middle phase of sleep in the caudal TRN stabilize the state and the malfunctioned sleep spindles induce not rapid but frequent arousal, whereas the rostral TRN activity (putatively, slow sleep spindles) seems to be important for the arousal and its inhibition might lead to reduced frequency of arousal/prolonged sleep episodes.

In order to find out which oscillation band frequencies are involved during frequent or rare arousal, we compared power band differences with corresponding ratios and latencies produced during TRN inhibition. Sleep spindle oscillation were expected to have an effect on the waking up ratios and latencies in the caudally light stimulated animals.

For that we used two different types of the EEG traces. The first trace type, which was named **Sleep_Sleep**, was derived using inclusion criteria introduced in the chapter 3 (See figure 3.1, A or 5.8, A). The trace was included in the analysis if mice were asleep for at least 90 seconds: 30 seconds before stimulation, 30 seconds during stimulation and 30 second after stimulation. The second trace type, which was called **Sleep_Wake**, was derived using criteria introduced in chapter 4 (See figure 4.6, A or figure 5.8, B) in which mice slept at least 20 seconds before the start of light stimulation start and to wake up during 80 seconds after the beginning of the light stimulation. The average change in frequency band (delta, theta, alpha, beta, gamma and high gamma) power of 10 seconds before and 10 seconds during stimulation was used to quantify the band power difference in each animal. All Sleep_Wake traces

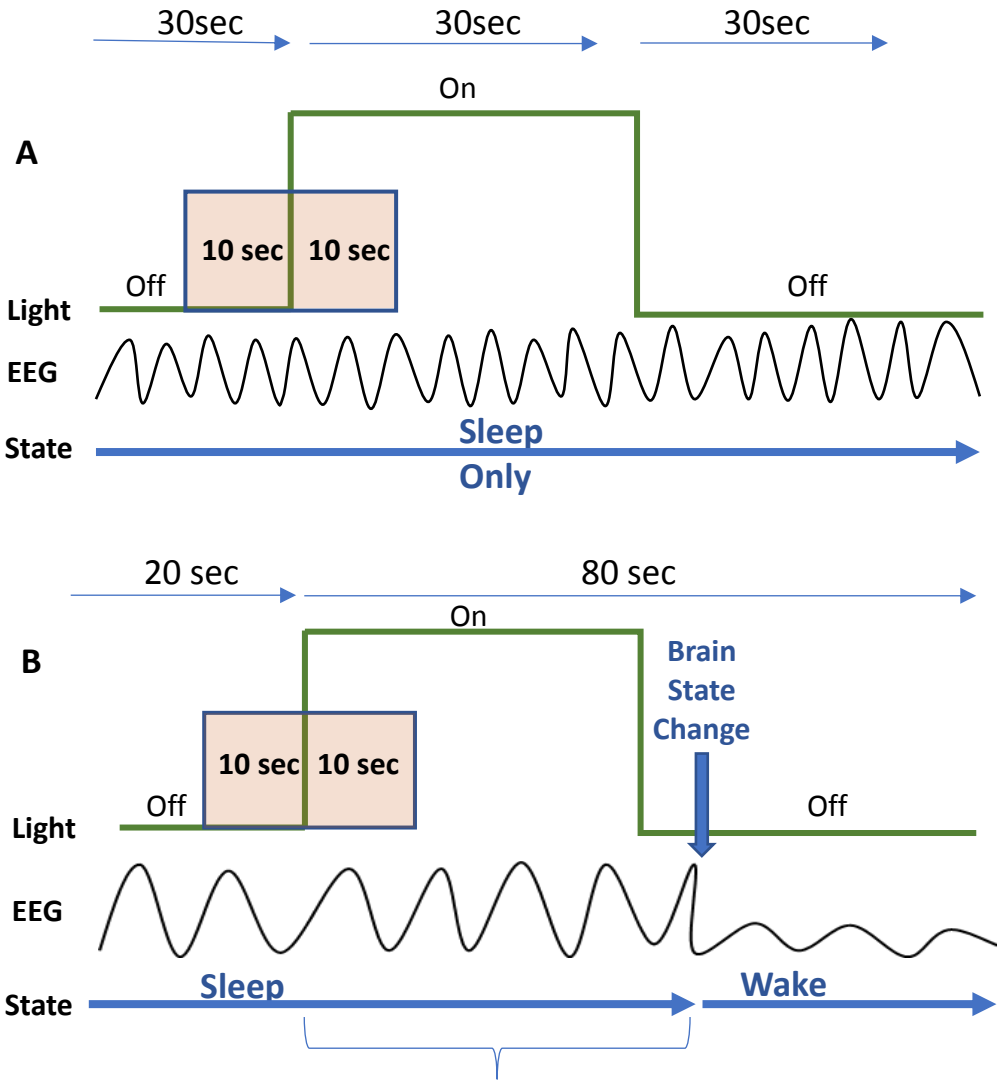

Figure 5.8 Graph demonstrates two inclusion criteria of the EEG traces used for quantification of the band power difference. **A** Sleep_Sleep trace was included in the analysis if mice were asleep for at least 90 seconds: 30 seconds before stimulation, 30 seconds during stimulation and 30 second after stimulation. **B** Sleep _Wake traces were included in the analysis, if mice slept at least 20 seconds, before light stimulation start and to wake up during 80 seconds after the beginning of the light stimulation. All Sleep_Wake traces used in the analysis had latency longer than 10 seconds, to make sure that the brain state transition was not taking place in this period. The average change in frequency band power of 10 seconds before and 10 seconds during stimulation was used to quantify the band power difference in each animal.

used in the analysis had a latency longer than 10 seconds, in order to make sure that we compared the power change caused by light stimulation and that the brain state transition was not taking place in this period.

Latency correlation with EEG power difference

The band power differences derived from Sleep_Wake traces were compared with the averaged latencies for each animal to find out the relationship between the latency change and frequency band change during light stimulation. No significant results were obtained, apart from the relationship between the high gamma power difference and the latency for the rostrally inhibited animals (See figure 5.13).

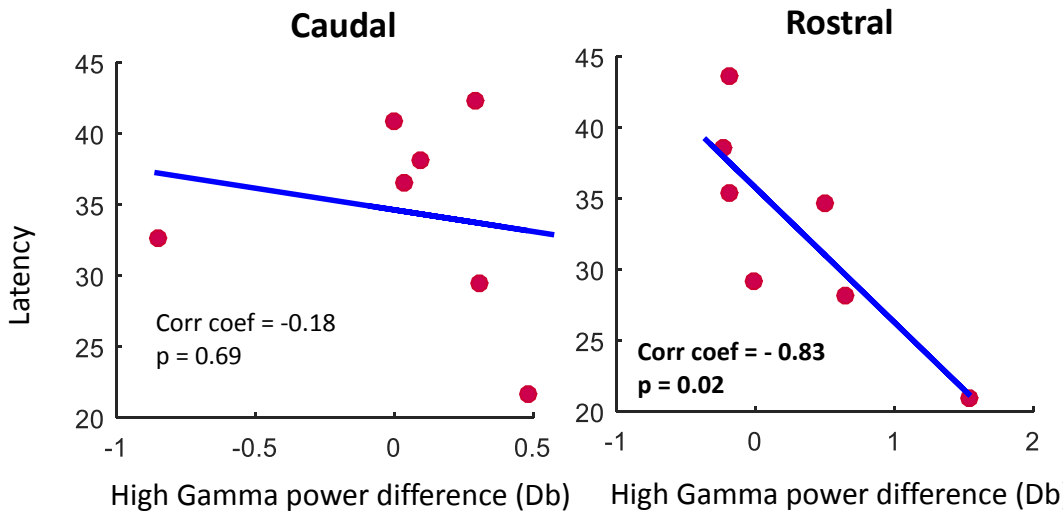

Figure 5.9 Scatter plots display the relationships between the latency and beta, gamma and high gamma power differences derived from Sleep_Wake traces. Each red dot represents the result from single animal. Left scatter is dedicated to the caudal mice expressing inhibitory opsin in the caudal TRN and the right row is dedicated to the rostrally targeted animals. Corr_coef – correlation coefficient. Blue line – a line of best fit. Caudal Opsin = 7 mice. Rostral Opsin = 7 mice.

Instead, the more accurate scatter plots using single trace results were constructed, as the band power differences and the latencies were known for each trace.

Single Sleep_Wake traces generated a strong relationship between the latencies and theta, alpha, and high gamma power differences. Interestingly, the alpha frequency band showed a significant positive correlation with arousal latencies only in the mice with caudally inhibited TRN (See figure 5.10). Arch animals showed a strong

correlation between the latencies and alpha oscillation change (See figure 5.11). The theta oscillation difference showed a positive correlation with arousal latencies whereas high gamma showed a negative correlation. The significant linear correlation between latencies and band power differences was not detected in control and Arch animals without stimulation (No stim). Although, the number of traces used from these animals was smaller (See figure 5.12 and 5.13. Control: caudal = 20 traces, 2 mice; rostral = 17 traces, 3 mice. No stim (Arch) mice = 28, 5 mice).

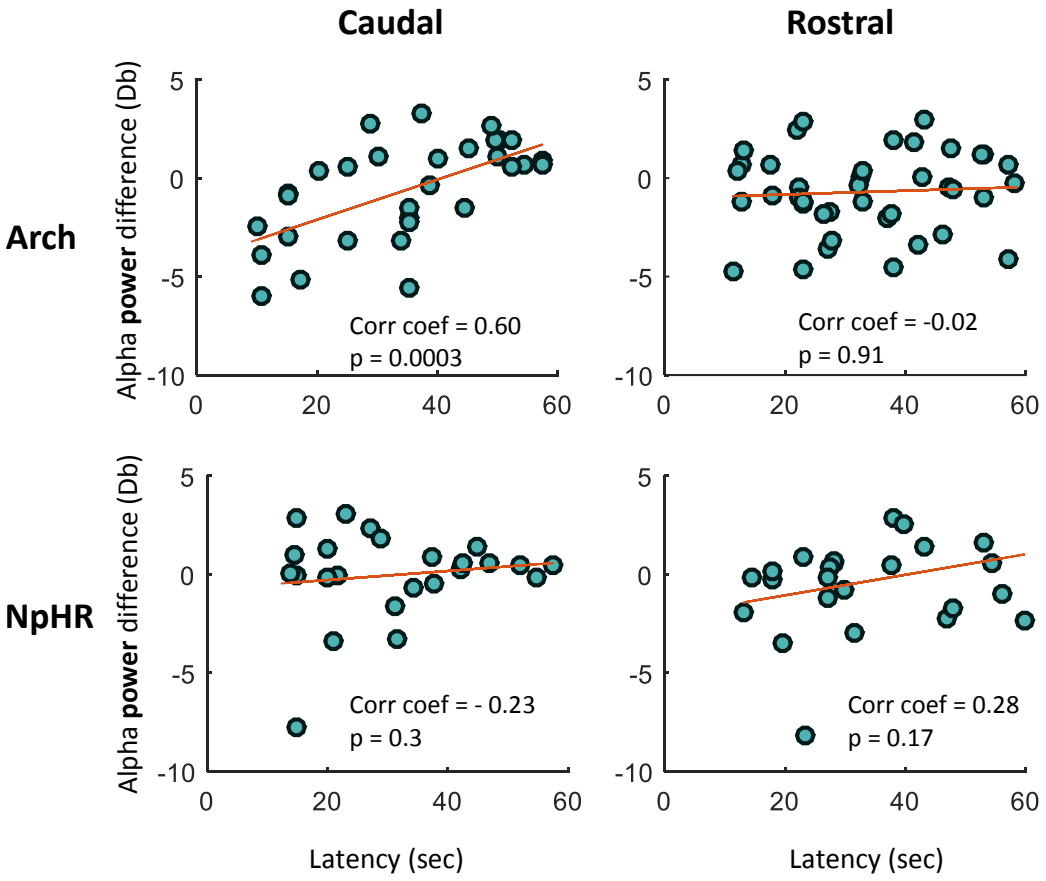

Figure 5.10 Scatter plots display linear relationships between latency and alpha power differences derived from Sleep_Wake traces. Each green dot represents the latency of single trace. Left row is dedicated to the mice expressing inhibitory opsin in the caudal TRN and the right row is dedicated to the rostrally targeted animals. Results for Arch expressing mice are in the top row and the results for NpHR animals in bottom row. Corr_coef – correlation coefficient. Red line – a line of best fit. Arch: caudal n = 39, 3 mice; rostral n = 51, 3 mice. NpHR: caudal n = 29, 4 mice; rostral n = 30, 4 mice.

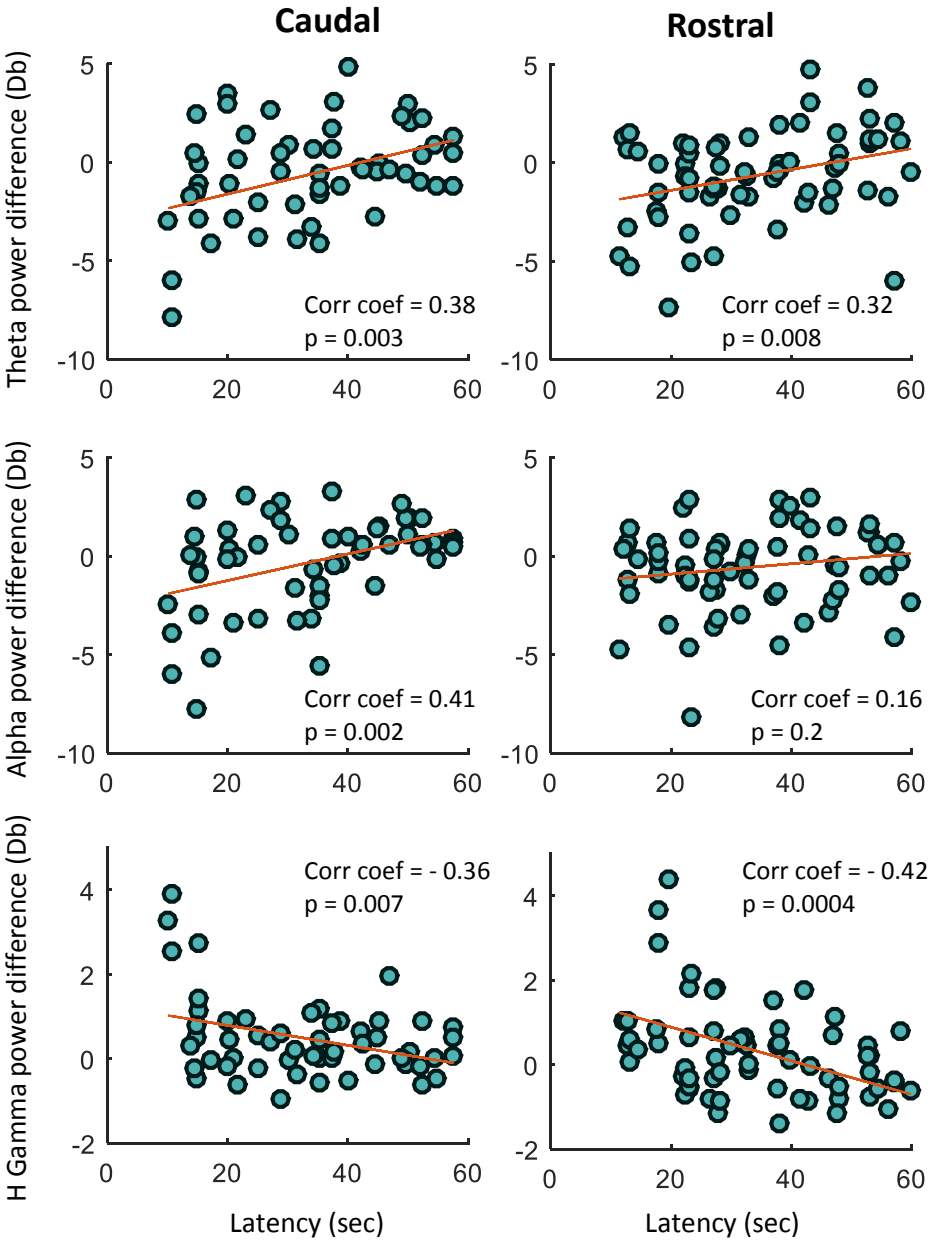

Figure 5.11 Scatter plots display linear relationships between latencies and theta, alpha and high gamma power differences derived from Sleep_Wake traces. Each green dot represents the latency of single trace. Left row is dedicated to the mice expressing inhibitory opsin in the caudal TRN and the right row is dedicated to the rostrally targeted animals. Corr_coef – correlation coefficient. Red line – a line of best fit. Opsin: caudal = 72 traces, 7 mice; rostral = 81 trace, 7 mice.

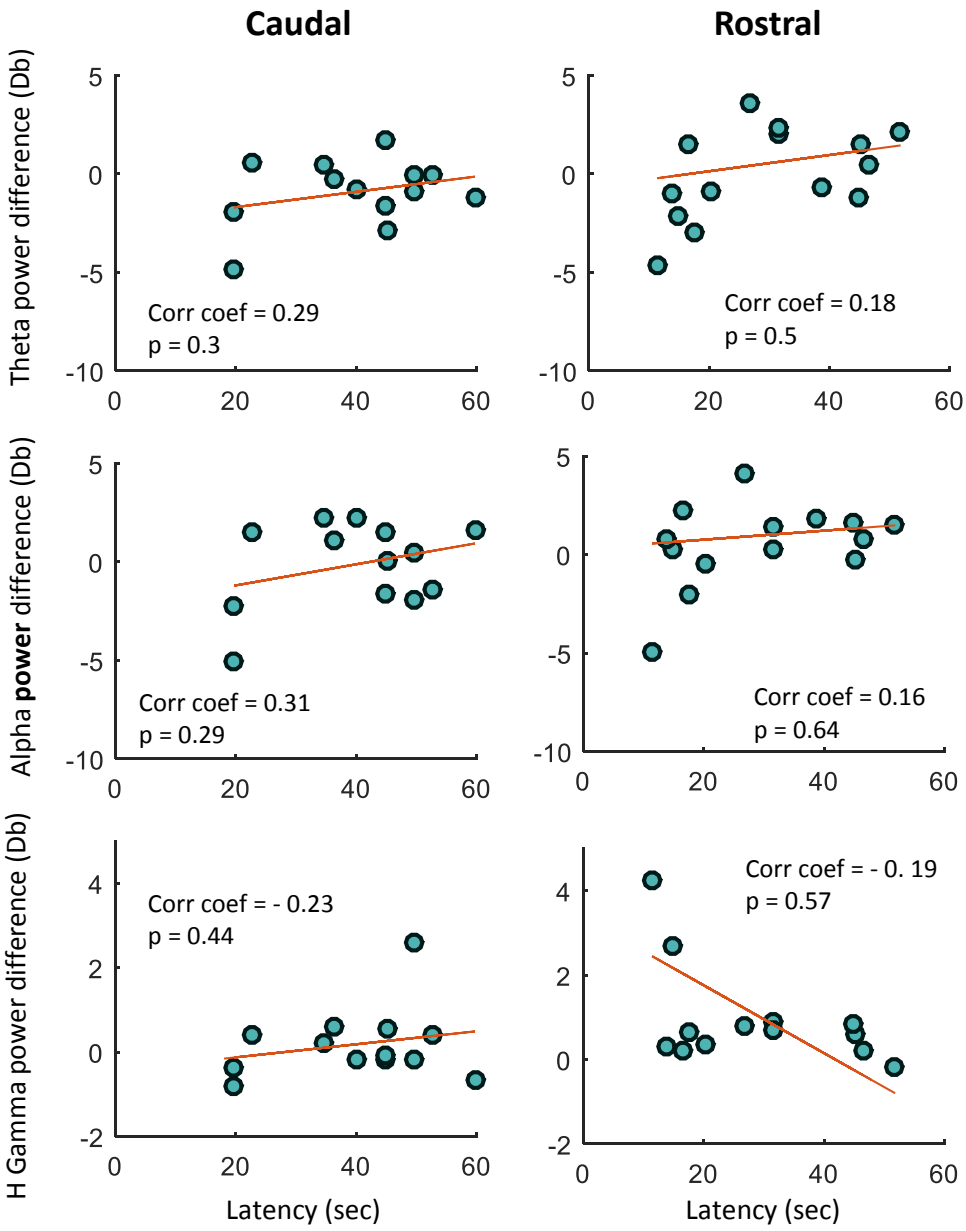

Figure 5.12 Scatter plots display linear relationships between latencies and theta, alpha and high gamma power differences derived from Sleep_Wake traces YFP (control) expressing animals without stimulation. Each green dot represents the latency of single trace. Left row is dedicated to the mice expressing YFP (control) in the caudal TRN and the right row is dedicated to the rostrally targeted control animals. Corr_coef – correlation coefficient. Red line – a line of best fit. Control: caudal = 20 traces, 2 mice; rostral = 17 traces, 3 mice.

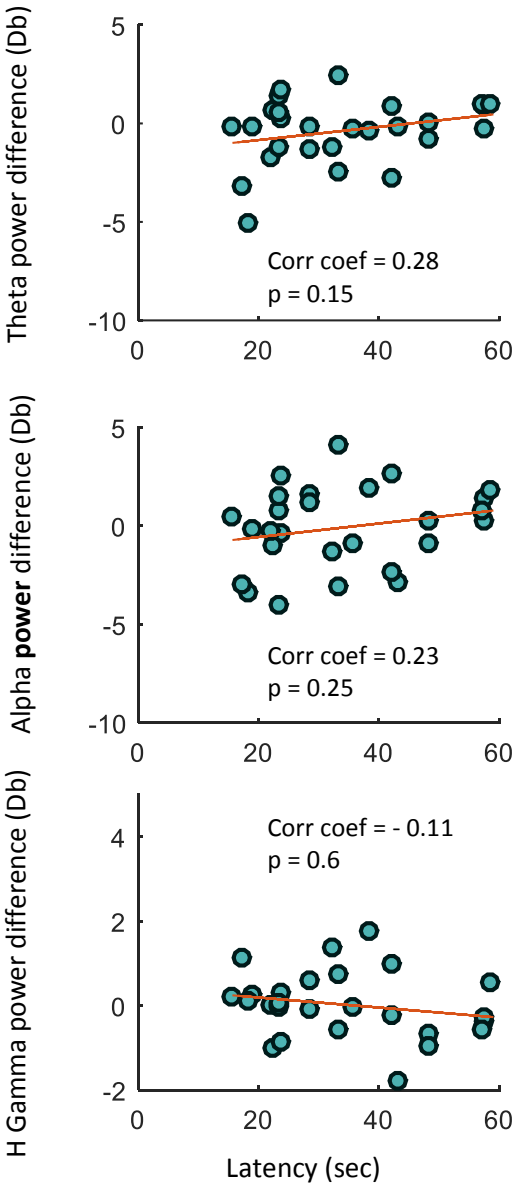

Figure 5.13 Scatter plots display linear relationships between the latency and theta, alpha and high gamma power differences derived from Sleep_Wake traces in Arch expressing animals without stimulation (No stim). Each green dot represents the latency of single trace. The results were derived from Arch animals without TRN light stimulation (No stim sessions). Corr_coef – correlation coefficient. Red line – a line of best fit. No stim (Arch) mice = 28 n, 5 mice.

Correlation of the theta and high gamma power difference

Lastly, we noticed that the theta and high gamma power differences during TRN inhibition have a negative relationship and hence might be important for arousal. We therefore compared the correlation between these frequency bands in different animals during the deep sleep stage (Sleep_Sleep traces, see figure 5.8 A) and during pre-arousal sleep (Sleep_Wake traces, see figure 5.8 B). Mice expressing inhibitory opsins in the caudal and rostral TRN showed a strong correlation between theta and high gamma power differences during pre-arousal sleep. A significant relationship between these power changes were not found in control mice and animals without TRN light stimulation. Although, the two latter animal groups had a lower number of traces for analysis (See figure 5.14. Opsin: caudal n = 72, 7 mice; rostral n = 81, 7 mice. Control: caudal n = 20, 2mice; rostral n = 17, 3 mice. No stim: n = 28, 5 mice). The number of the traces derived from the deep sleep (Sleep_Sleep) were significantly larger, but the correlation of theta and high gamma power was smaller and was not as significant as during pre-sleep stages (See figure 5.15. Opsin: caudal n = 170, 10 mice; rostral n = 347, 10 mice. Control: caudal n = 78, 2mice; rostral n = 83, 3 mice).

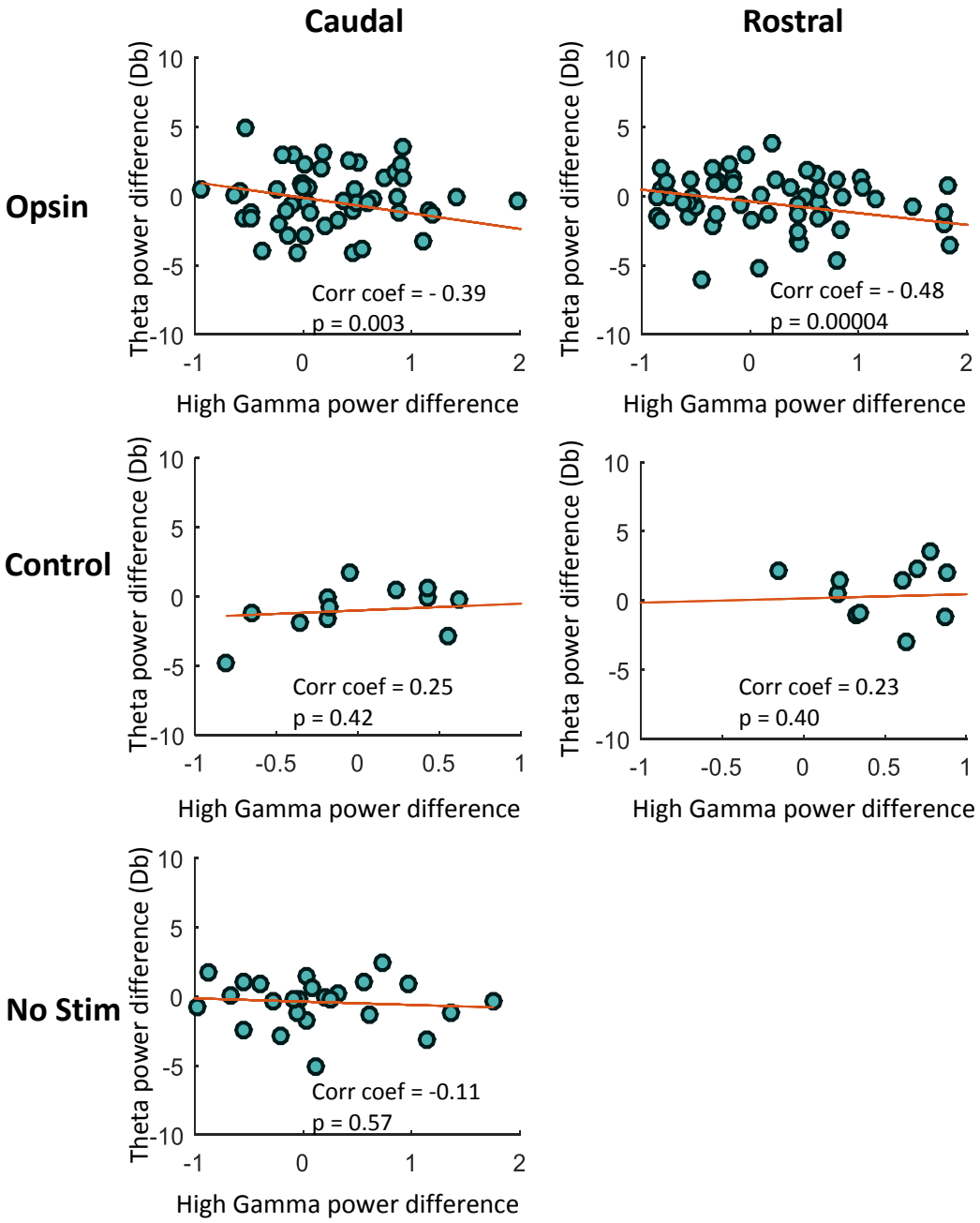

Figure 5.14 Scatter plots display linear relationships between the high gamma and theta differences derived from Sleep_Wake traces (pre-wake sleep). Each green dot represents the power difference caused by light stimulation over 10 seconds in single trace. Results were derived from mice expressing inhibitory opsins (Opsin = Arch and NpHR, top row), from YFP (control) expressing animals (middle row) and from the animals without TRN light stimulation (No stim sessions, bottom row). Corr_coef – correlation coefficient. Red line – a line of best fit. Opsin: caudal n = 72, 7 mice; rostral n = 81, 7 mice. Control: caudal n = 20, 2mice; rostral n = 17, 3 mice. No stim: n = 28, 5 mice.

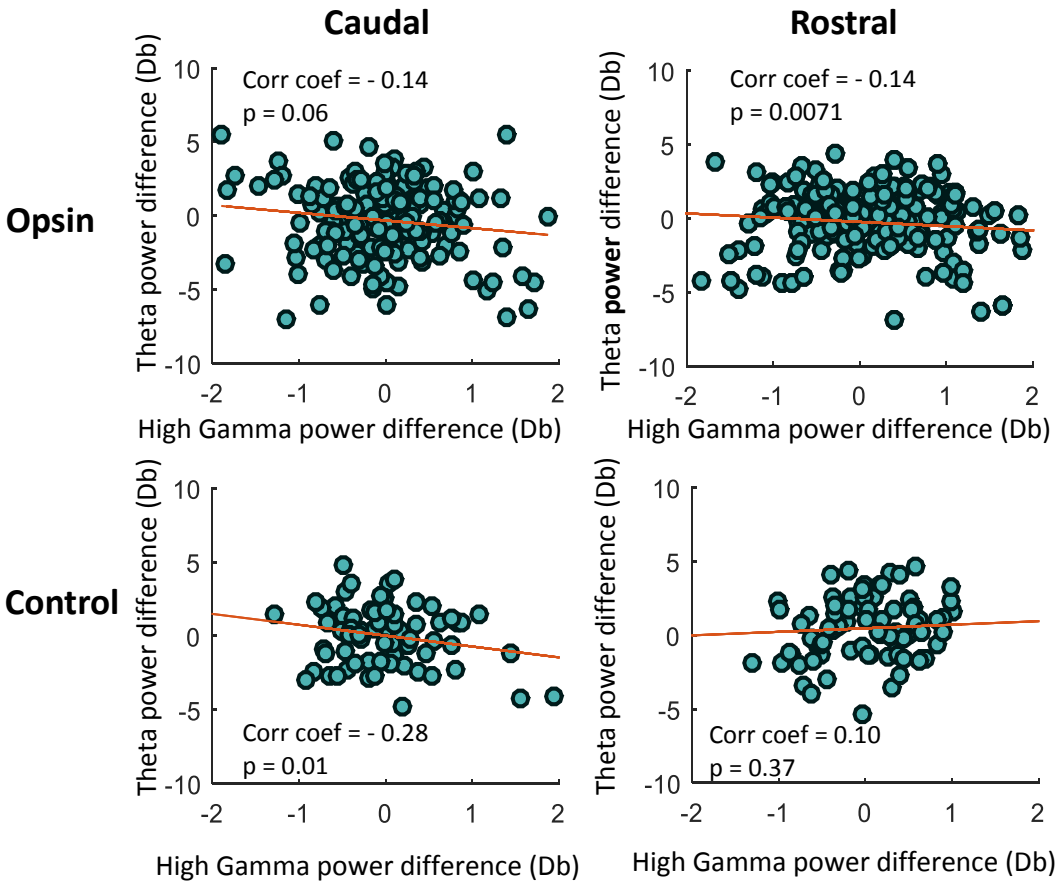

Figure 5.15 Scatter plots display linear relationships between the high gamma and theta differences derived from Sleep_Sleep traces (deep sleep). Each green dot represents the power difference caused by the light stimulation over 10 seconds in single trace. Results were derived from mice expressing inhibitory opsins (Opsin = Arch and NpHR, top row) and from YFP (control) expressing animals (bottom row). Corr_coef – correlation coefficient. Red line – a line of best fit. Opsin: caudal n = 170, 10 mice; rostral n = 347, 10 mice. Control: caudal n = 78, 2mice; rostral n = 83, 3 mice.

Can the pre-wake trace can be counted as a sleep trace?

We conducted one control analysis to confirm that the pre-wake sleep traces (Sleep_Wake) can be counted as sleep traces. Additionally, we compared EEG frequencies of the early (latency < 16 seconds) and late (latency > 16 sec) arousal traces. For that we filtered Sleep_Wake traces into two groups: less than 16 sec and more than 16 secs, based on the criteria mentioned below (See figure 5.16).

The EEG used for comparison was calculated from the period of 10 seconds before the start of the light stimulation. Initially, we compared the power of the frequency bands between early (less than 16 sec) and late (more than 16 seconds) traces. In caudally inhibited rodents, all frequency bands were similar, apart from the high gamma band. Seemingly, the high gamma band might be a good marker between the light and deep sleep. The averaged high gamma band in the late arousal traces was reduced relative to early arousal traces but this was not statistically significant. Multiple T tests were performed and p values in the high gamma case barely showed weak significance, which could be undermined by the Bonferroni correction (was not applied) (See figure 5.17, A. Caudal: two sample test, Delta, p = 0.86; Theta, p = 0.71; Alpha, p = 0.96; Beta, p = 0.51; Gamma, p = 0.08; High Gamma, p = 0.03, CI = 0.08/2, tstats = 2.2. n = 7, less than 16 sec = 24 traces, more than 16 sec = 68 traces.). The rostrally targeted mice displayed the tendency to rise in theta and alpha oscillations in traces with late arousal (See figure 5.17, B. Rostral: two sample t test, Delta, p = 0.13; Theta, p = 0.02, CI = -2.53/-0.13, tstats = -2.2; Alpha, p = 0.04, CI = -2.75/-0.68, tstats = -2.08; Beta, p = 0.22; Gamma, p = 0.36; High Gamma, p = 0.10. n = 7, less than 16 sec = 24 traces, more than 16 sec = 74 traces). Most importantly, when we compared the EEG band powers derived from traces with late and early arousal between caudal and rostral animals, no variance was discovered (See figure 5.18, A. Less than 16 sec: Delta, p = 0.54; Theta, p = 0.65; Alpha, p = 0.59; Beta, p = 0.61; Gamma, p = 0.68; High Gamma, p = 0.61. n = 7, caudal = 24 traces, rostral = 24 traces. B. More than 16 seconds Delta, p = 0.51; Theta, p = 0.26; Alpha, p = 0.10; Beta, p = 0.09; Gamma, p = 0.39; High Gamma, p = 0.97. n = 7, caudal = 68 traces, rostral = 74 traces).

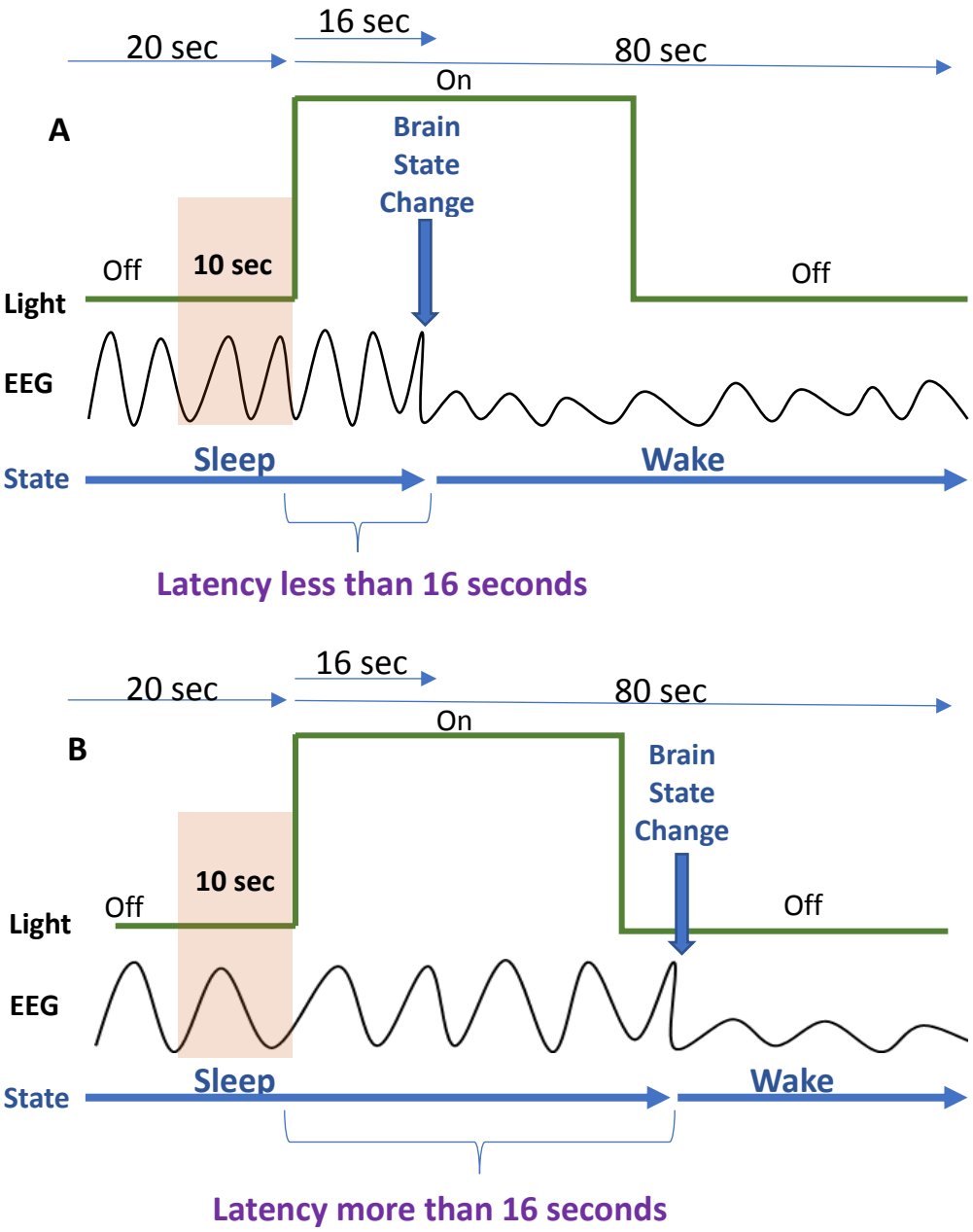

Figure 5.16 Data filtering criteria for pre-wake sleep traces (Sleep_Wake). Sleep _Wake traces were included in the analysis, if mice slept at least 20 seconds, before light stimulation start and to wake up during 80 seconds after the beginning of the light stimulation. In this analysis traces were not filtered from low (10 sec) latency value. Traces were divided into early (latency < 16 seconds) and late (latency > 16 seconds) arousal. **A**. Inclusion criteria for early arousal Sleep_Wake traces. **B** Inclusion criteria for late arousal Sleep_Wake traces. Shaded area (10 sec) shows which part of the EEG was used for analysis, 10 seconds before stimulation

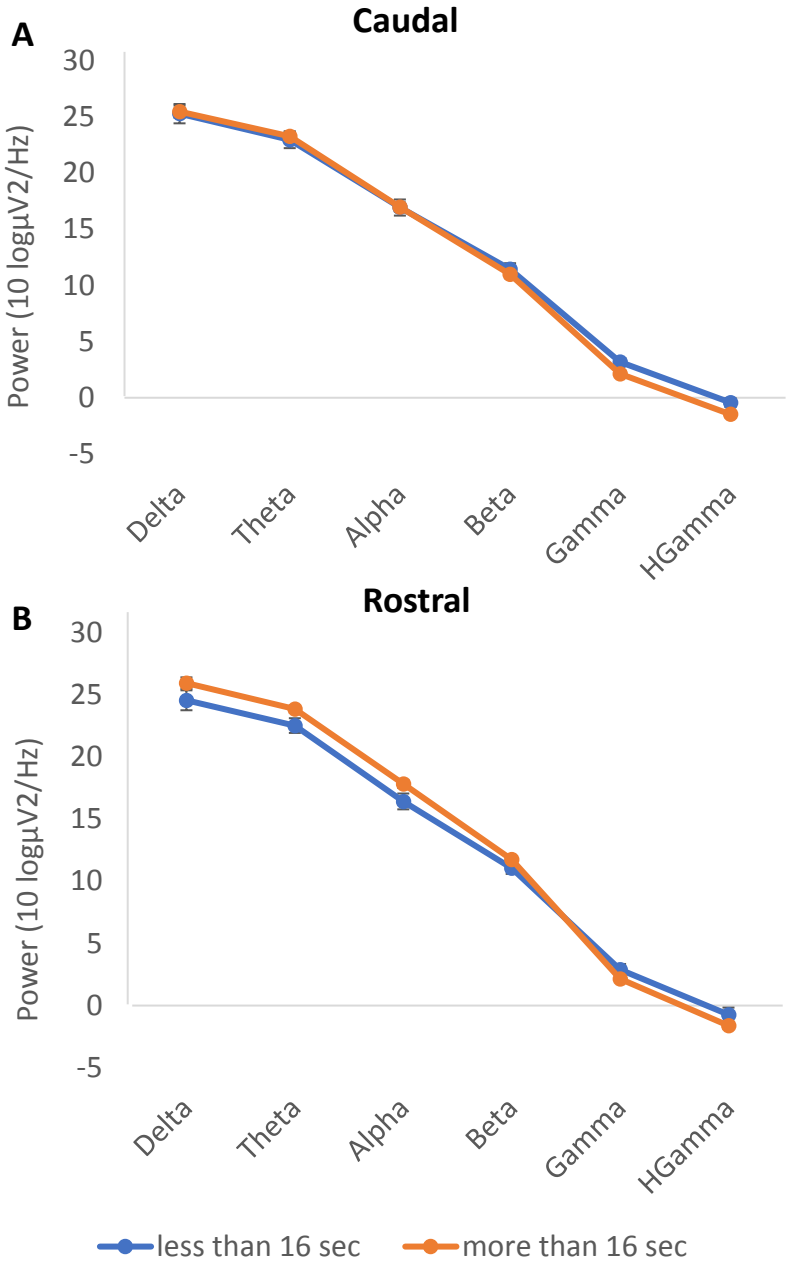

Figure 5.17 The EEG powers of the frequency bands from the traces with early (less than 16 seconds) and late (more than 16 seconds) arousal. Multiple two sample t test were employed in this analysis, therefore shown statistical significance can be easily undermined by the Bonferroni correction (was not applied). *$p < 0.05$ without Bonferroni correction (not significant)

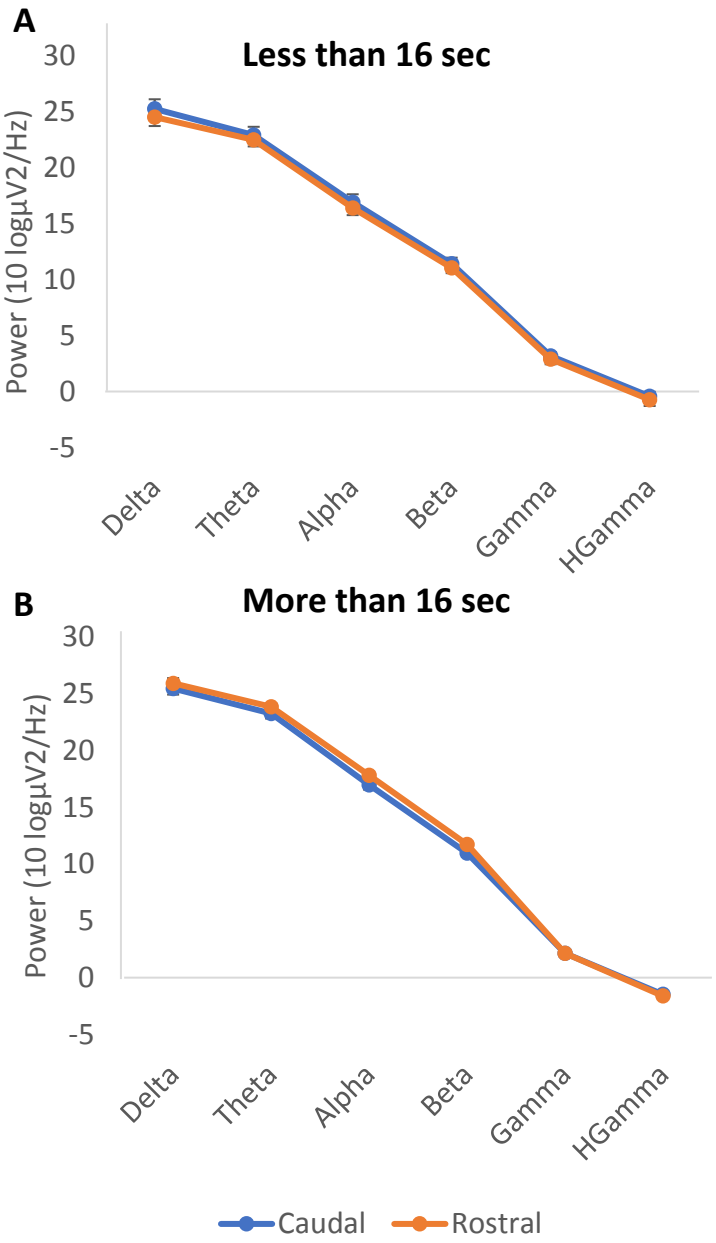

Figure 5.18 The EEG powers of the frequency bands from the traces with early (less than 16 seconds) and late (more than 16 seconds) arousal. Multiple two sample t test were employed in this analysis, therefore shown statistical significance can be easily undermined by the Bonferroni correction (was not applied). *$p < 0.05$ without Bonferroni correction (not significant)

5.3.4 TRN activity balance is shifted to the rostral TRN during the pre-wake period

In chapter 3, we showed that inhibition of the caudal TRN over 5 seconds during sleep (Sleep_Sleep traces) had a tendency to produce a stronger reduction in delta power oscillation than in the rostral TRN. Furthermore, caudal TRN optogenetic inhibition over 10 seconds led to the significant reduction of the alpha and beta oscillations. The significant reductions in EEG power bands mentioned above might be produced due to characteristic activity of the caudal (sensory) TRN during sleep, whereas the non-significant results obtained from the rostral TRN (cognitive) might mirror neuronal silence during sleep. Previously, Halassa et al. (2014) using in vivo electrophysiology discovered the same principles of the TRN, only for sensory and limbic associated TRN cells. Based on the weak evidence from the previous work of Winsky-Sommerer et al. (2008) we hypothesized that sleep spindles of the rostral TRN (slow sleep spindles) are important for arousal, therefore we expected that the balance of the TRN activity should shift to the rostral TRN during the pre-wake period (NREM – wake transition). Putatively, the slow sleep spindles (with lower frequency) appear during NREM - wake transition and the inhibition of these spindles induce prolonged sleep.

We used Sleep_Wake traces to assess the activity in the rostral and caudal TRN (See figure 5.8, B). Traces were included in the analysis if mice slept at least 20 seconds, before light stimulation start and to wake up during 80 seconds after the beginning of the light stimulation. Traces with the latency shorter than 10 seconds were discarded. This way, we could compare the band power difference between 10 seconds before and 10 seconds during light stimulation in the NREM – wake transition.

Caudal TRN optogenetic inhibition over 10 seconds did not produce a significant reduction of delta and alpha oscillations, whereas optogenetic inhibition of the rostral TRN produced a strong and significant reduction of the delta and alpha oscillations (See figure 5.19. Caudal: paired t test, delta, $p = 0.09$; alpha, $p = 0.09$; 72

traces, 7 mice; Rostral: paired t test, delta, p = 0.03; alpha, p = 0.02; 81 traces, 7 mice). Interestingly, in control animals, the rostral stimulation significantly increased delta, beta and gamma oscillations (See figure 5.20, Rostral: paired t test, delta, p = 0.04; beta, p = 0.04; gamma, p = 0.04) Additionally, we divided and tested alpha oscillations for slow (7 – 10 Hz) and fast (10 – 15 Hz) sleep spindle oscillations. There was no significant effect in the fast sleep spindle oscillation in mice with rostral inhibition of the TRN during deep sleep (Sleep_Sleep) and in the caudally inhibited mice during the pre-wake (Sleep_Wake) period (See figure 5.21. Rostral: Sleep_Sleep, paired t test, p = 0.43. Caudal: Sleep_Wake, paired t test, p = 0.16). The same analysis applied to control animals showed a tendency to increase the fast sleep spindle oscillation of the rostrally stimulated animals (See figure 5.22) A summary table portraying band powers modulation caused by TRN inhibition during deep sleep (Sleep_Sleep) and sleep-wake (Sleep_Wake) transition is in the Appendix (See figure 8.27 and 8.28). Theta oscillation, unfairly omitted from pre-wake sleep analysis, also showed strong reduction during optogenetic inhibition.

The averaged values for delta and alpha oscillations were collected from traces with deep sleep (Sleep_Sleep) and pre-wake sleep (Sleep_Wake). Optogenetic inhibition of the caudal TRN during deep sleep (Sleep_Sleep) produced a strong reduction of delta and alpha power, while rostral TRN inhibition had smaller impact, whereas during pre-sleep the TRN sides changed their roles and the strongest reduction in delta and alpha oscillation was generated by the rostral TRN. Whilst deep sleep and pre-wake results were not significantly different from each other, the graph is useful to display the concept of the TRN site dependant inhibition and the TRN balance shift during the change in sleeping stages (See figure 5.23, A *Opsin:* Sleep_Sleep. Caudal, n = 170, 10 mice; Rostral = 347, 10 mice. Sleep_Wake. Caudal, n = 72, 7 mice. Rostral, n = 81, 7 mice). In mice expressing YFP (control) light stimulation did not produce such a band power flip-flop pattern that was dependent on the sleep state (See figure 5.23, B *Control:* Sleep_Sleep. Caudal, n = 78, 2 mice; Rostral = 83, 3 mice. Sleep_Wake. Caudal, n = 20, 2 mice. Rostral, n = 17, 3 mice).

In summary, we demonstrated that the rostral TRN is strongly inhibited during sleep-wake transition, whereas the caudal TRN inhibition demonstrate similar EEG activity during stable NREM sleep. The pattern of the inhibition might reflect the neuronal activity, where the caudal TRN is the most active during sleep, whereas the rostral TRN could be active during sleep-wake transition. Additionally, we showed that fast and slow spindle oscillations are optogenetically reduced (found) in both types of the stimulations.

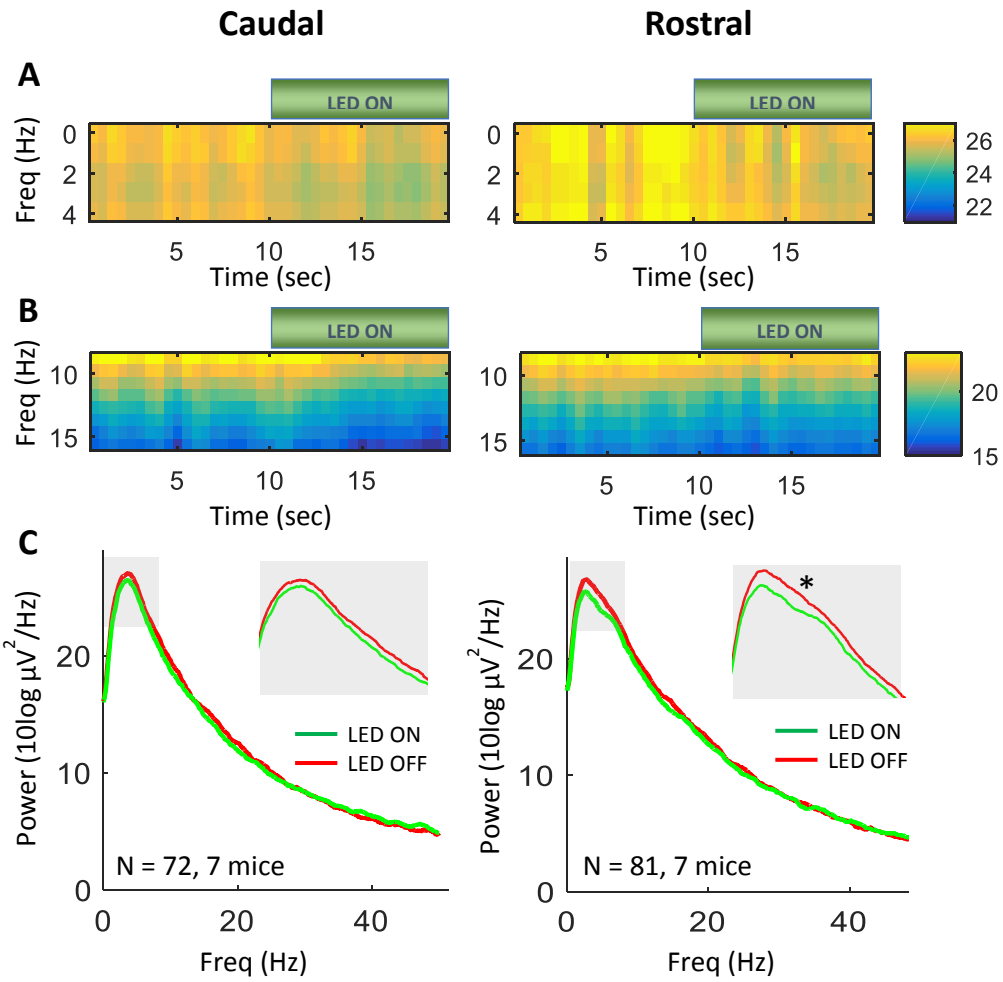

Figure 5.19 Light stimulation effect on Delta and Alpha oscillation in mice expressing inhibitory opsin. Left column show results for mice expressing inhibitory opsins in the caudal part of the TRN, right column shows results for rostrally inhibited TRN. A Mean spectrogram of 0 – 4 Hz over 20 seconds. Green bar (LED ON) symbolize light stimulation, which starts at 10 seconds. B Mean spectrogram of 9 – 15 Hz over 20 seconds. C The power spectrum of 10 seconds before (red) and 10 seconds during (green) light stimulation. Delta, theta and alpha powers were strongly and significantly reduced during light activation over 10 seconds in the rostral mice expressing opsins. (Caudal: N = 72, 7 mice. Rostral: N = 81, 7 mice. Student paired test. *p < 0.05. Right frontal (RF) was used for analysis).

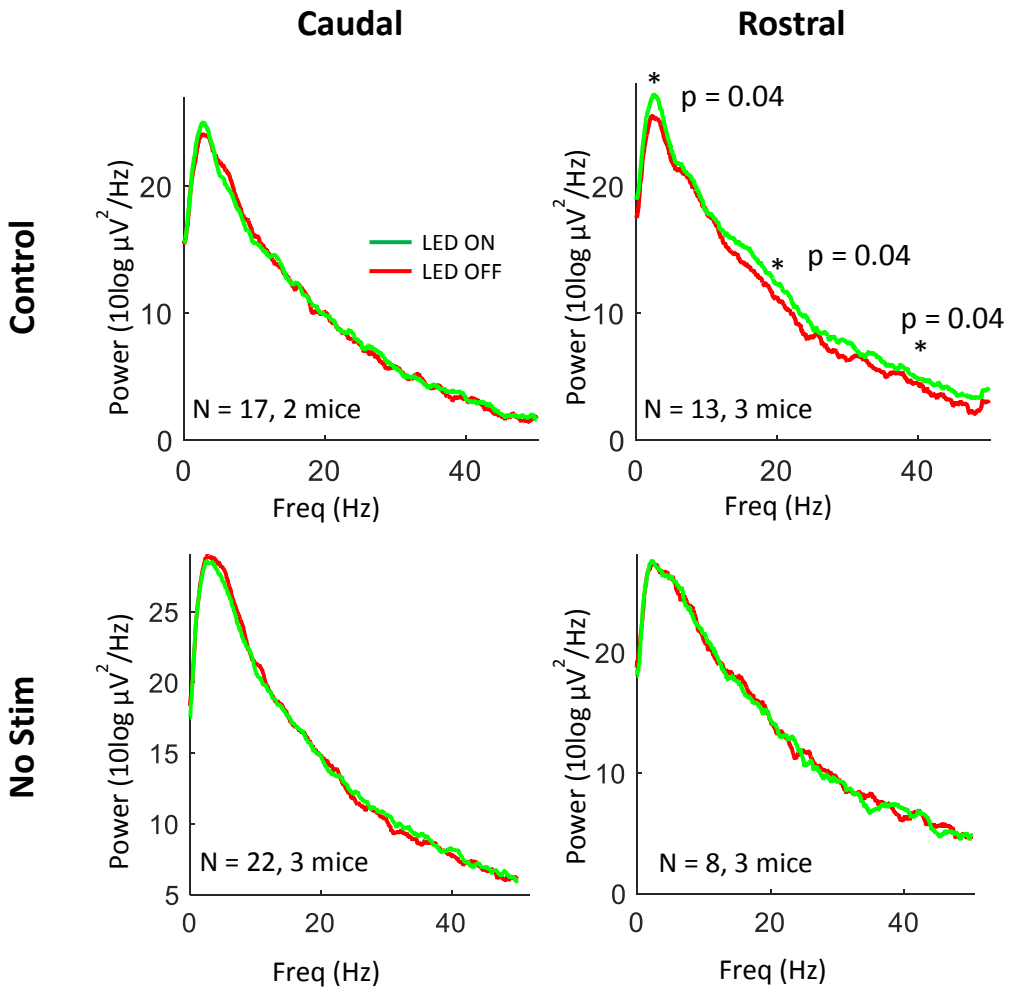

Figure 5.20 The power spectrum of 10 seconds before (red) and 10 seconds during (green) light stimulation in animals expressing YFP (control, top row) and in No Stim mice (bottom). Delta, beta and gamma powers were significantly increased during light activation over 10 seconds in the rostrally stimulated mice. (Control: Caudal, N = 17, 2 mice; Rostral, N = 13, 3 mice. No Stim: Caudal, N = 22, 3 mice; Rostral, N = 8, 3 mice. Student paired test. *p < 0.05. Right frontal (RF) was used for analysis).

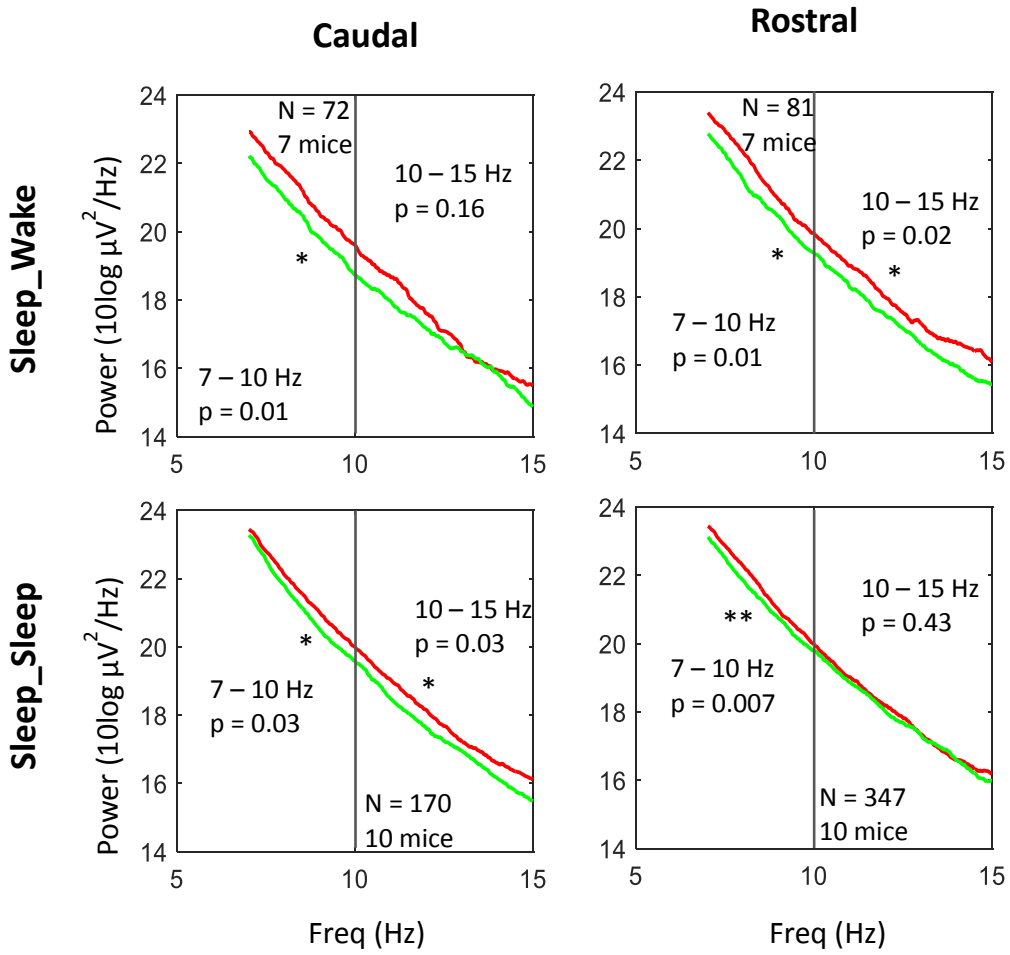

Figure 5.21 Graphs display the changes of the slow (7-10 Hz) and fast (10 -15 Hz) sleep spindle oscillation during deep sleep (Sleep_Sleep) and pre-wake sleep (Sleep_Wake) in the opsin expressing animals. Line portrays the power spectrum of 10 seconds before (red) and 10 seconds during (green) light stimulation. Left column is generated for the caudally inhibited TRN and right column belongs to rostrally inhibited TRN. In most cases, fast and slow sleep spindle oscillations reduction were significant. Caudally stimulated animals failed to reduce fast spindles during pre-wake phase, and vice versa rostrally stimulated animals did not have any reduction in the fast spindle oscillation in deeply sleeping stages. (Opsin: Sleep_Sleep. Caudal: paired t test, p = 0.03 (fast and slow), n = 170, 10 mice; Rostral: paired t test, p = 0.007 (slow), p = 0.43 (fast), n= 347, 10 mice. Sleep_Wake. Caudal: paired t test, p = 0.01 (slow), p = 0.16 (fast), n = 72, 7 mice. Rostral: paired t test, p = 0.01 (slow), p = 0.02 (fast), n = 81, 7 mice.

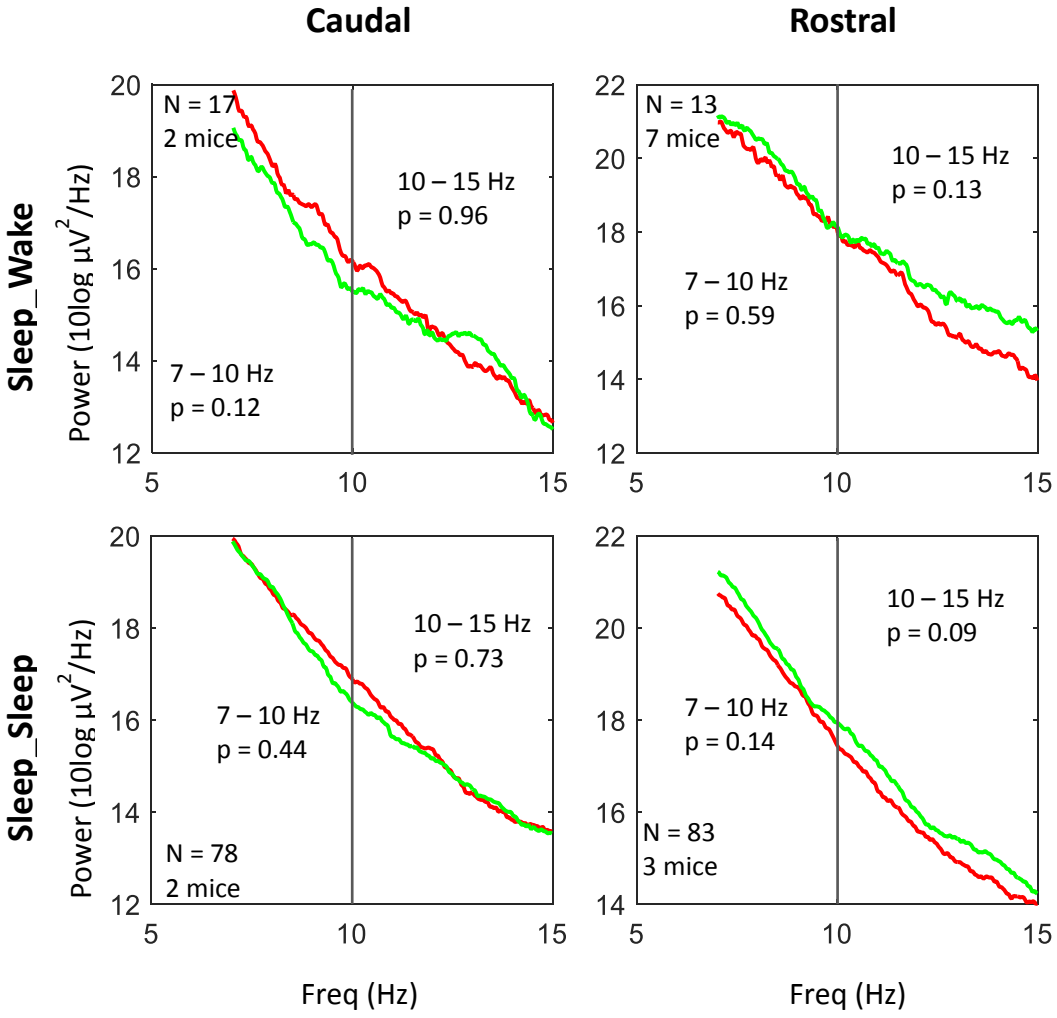

Figure **5.22** Graphs display the changes of the slow (7-10 Hz) and fast (10 -15 Hz) sleep spindle oscillation during deep sleep (Sleep_Sleep) and pre-wake sleep (Sleep_Wake) in the YFP (control) expressing animals. Line portrays the power spectrum of 10 seconds before (red) and 10 seconds during (green) light stimulation. Left column is generated for the caudally stimulated TRN and right column belongs to rostrally stimulated TRN. Fast and slow sleep spindle oscillations were not modulated significantly during light stimulation. Rostrally stimulated animals during deep and pre-wake sleep showed the tendency to the fast spindle increase (Opsin: Sleep_Sleep. Caudal: paired t test, p = 0.03 (fast and slow), n = 170, 10 mice; Rostral: paired t test, p = 0.007 (slow), p = 0.43 (fast), n= 347, 10 mice. Sleep_Wake. Caudal: paired t test, p = 0.01 (slow), p = 0.16 (fast), n = 72, 7 mice. Rostral: paired t test, p = 0.01 (slow), p = 0.02 (fast), n = 81, 7 mice.

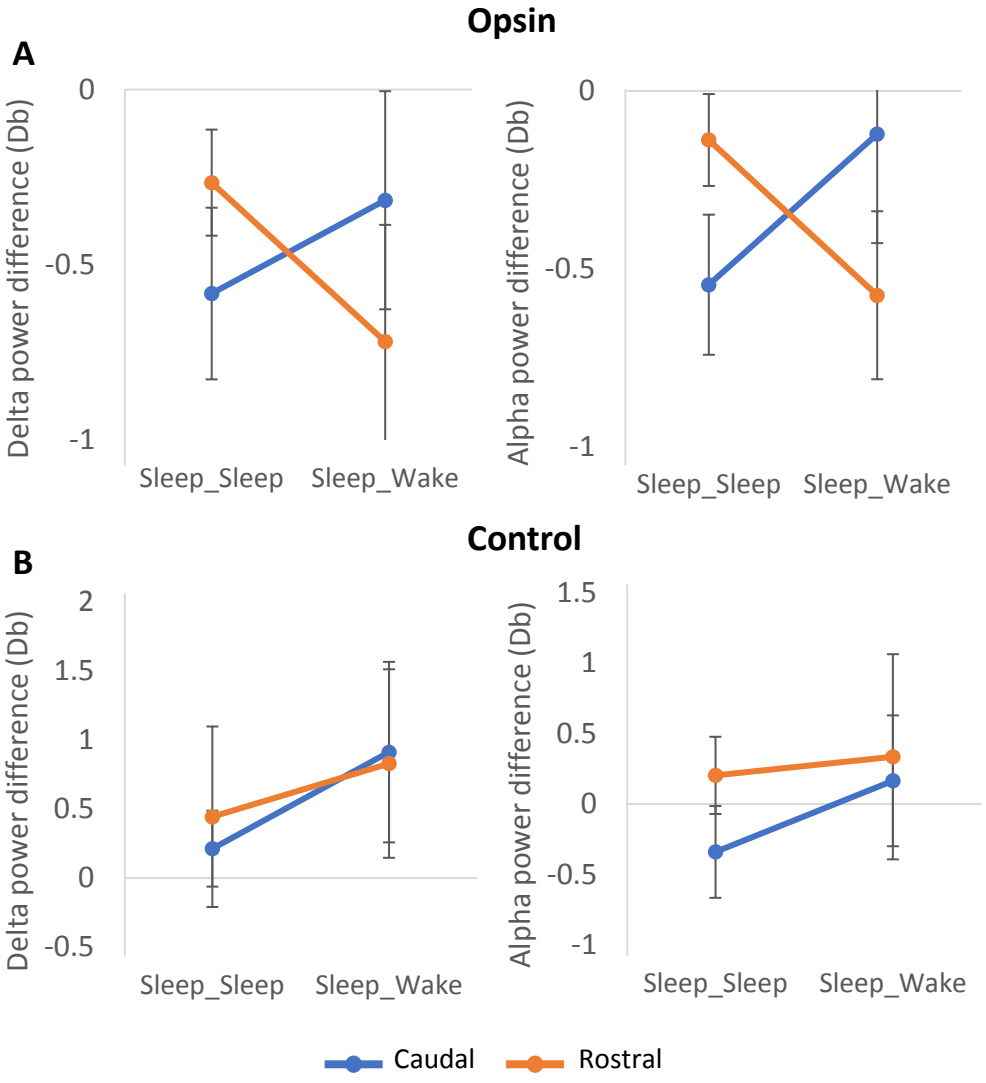

Figure 5.23 Graphs display the changes of the delta and alpha oscillation during diverse sleeping stages. Sleep_Sleep symbolize deep sleep and Sleep-wake symbolize pre-wake sleep. Changes were explored in the caudally light stimulated animals (blue) and rostrally targeted mice (orange). Top row contains graphs with results from mice expressing inhibitory opsins, bottom row covers results from YFP expressing mice (control). Opsin expressing mice show distinct patterns of change in both oscillations during various stages of sleep. Control mice do not show any pattern in the delta and alpha reduction/increase during different sleep stages (Opsin: Sleep_Sleep. Caudal, n = 170, 10 mice; Rostral = 347, 10 mice. Sleep_Wake. Caudal, n = 72, 7 mice. Rostral, n = 81, 7 mice. Control: Sleep_Sleep. Caudal, n = 78, 2 mice; Rostral = 83, 3 mice. Sleep_Wake. Caudal, n = 20, 2 mice. Rostral, n = 17, 3 mice).

5.4 Discussion

5.4.1 The TRN is a functionally heterogenous structure

In the first chapter we hypothesized that the caudal TRN segment is dealing with sensory data modulation, whereas the rostral TRN could be involved in motor and cognitive information control. Based on this hypothesis, we anticipated that the rostral and caudal parts of the TRN might show a dissimilar pattern of activity during brain state transition periods.

In this chapter, we demonstrated that the caudal TRN activity is vital for the wake – NREM sleep transition, whereas rostral TRN inhibition does not have any effect on the wake-NREM transition. The inhibition of the caudal TRN during the first 20 seconds of sleep induces rapid arousal. Additionally, the caudal TRN tonic inhibition during deeper and stable sleep (> 20 seconds sleep) induces frequent arousal (See chapter 4), whereas the rostral TRN tonic inhibition generated rare arousal. According to the correlation studies using the EEG band power differences, the ratio of short sleep and the latencies to arousal, the frequent arousal was caused by the reduction of the alpha/beta oscillations, markers of the fast sleep spindles. The prolonged sleep (rare arousal) was mostly related to the theta oscillations differences (slow spindles?) and to a minor extent the beta oscillation reduction/increase. Lastly, we established that the rostral TRN neuronal activity is significantly inhibited (neurons activated?) during sleep-wake transition, whereas the caudal TRN, apparently, is the most active during stable NREM sleep. The rostral TRN inhibition in the pre-wake period of sleep induced a significant reduction of the fast-alpha oscillation (10 – 15 Hz), which matches with the frequency of the proposed slow spindles in mice (11 – 13 Hz).

So, we can state, that the rostral and caudal parts of the TRN are distinct segments of the nucleus responsible for different functions during sleep. Caudal TRN activity (sleep spindles) are required for wake-sleep transition and for sleep stability, whereas rostral TRN seems to be involved in the sleep-wake transition.

5.4.2 Tumbler or flip-flop mechanism of the TRN during sleep

The Francis Crick searchlight hypothesis and the TRN action during sleep show similar roots. During attention, the modality specific TRN neurons moderately inhibit the relay neurons not involved in the behaviourally required attention and the TRN neurons associated with limbic thalamic nuclei do not show an overall change of firing (Halassa et al., 2014). So, the sensory TRN acts as a searchlight in the dusk, by prioritizing specific information for propagation to the cortex and reducing that not required to relay to the cortex. During different sleep stages the TRN may act like a tumbler or a flip flop mechanism. At NREM sleep initiation and maintenance, the caudal TRN (sensory) neurons are coupled and fire strongly to inhibit sensory propagation, whereas in the pre-wake sleep stages the balance of the activity shifts to the rostral TRN, and this activity promotes arousal. It is also important to note, that TRN activity is dependent on more hierarchically significant brain areas for sleep such as the hypothalamus, brainstem and forebrain (cortex for wake). Apparently, during sleep the TRN acts one of the forebrain arms, which controls thalamus and cortex, whereas during wake it is a modulatory arm (inhibitory feedback) of the cortex. The caudal TRN function during sleep is a complete cessation of the outside information propagation or so-called induced unconsciousness. It is well established that abnormal TRN oscillations lead to absence epilepsy (Cheong & Shin, 2014) and that sleep spindle activity elevates the arousal level (Wimmer et al. 2012). The role of the rostral TRN is still mysterious, but its low activity during sleep might facilitate offline memory formations (Latchoumane et al., 2017).

5.4.3 NREM differentiation in mice

As mentioned in the introduction, NREM sleep is subdivided into three stages: N1, N2 and N3. N1 or drowsiness, is characterized by the slowed down EEG, alpha activity at posterior sites and theta activity at anterior sites, whereas sleep spindles and K-complexes are prevalent during N2 stage, light sleep. In mice, NREM sleep is not divided into stages, even though sleep is a very old, evolutional mechanism of the brain, which is common in most mammalian species, with slight evolutionary modifications (Phillips et al., 2010).

We established that during the first 10-20 seconds of sleep that caudal TRN activity is vital for sleep maintenance and that the effect of TRN inhibition during the first 10-20 seconds and during the sleep stage after 20 seconds of sleep is different. There is a similarity between our results and human EEG outcomes, where during N1 phase in the posterior sites alpha oscillation is recorded. Additionally, the strong alpha oscillation is associated with the start of unconsciousness during general anaesthesia induction (Ching & Brown, 2014). Therefore, we can hypothesize that mice do have N1/N2 sleep phases, which are shorter (no longer than 20 seconds) and are associated with caudal TRN activity (alpha oscillation). Further experiments employing finer tools than EEG are required to establish the different phases in the mice NREM sleep. Future sleeping studies should be aware and cautious of these substages in mice sleep, as they can significantly affect the outcomes and interpretations.

5.4.4 Misalignment between results in Arch and NpHR mice

Archaerhodopsin and halorhodopsin are both inhibitory opsins with different mechanisms of neuronal modulation. Arch is a proton pump (outward current) and NpHR is chloride pump (inward current), thus it was expected that some of the results between these opsins will be different due to diverse effects on the extracellular ionic homeostasis. Results for the EEG power modulation (chapter 3) and sleep/wake cycle effect (chapter 4) were almost identical, but the relationship between the latency and the time slept before stimulation (See figure 5.4 c,d) and the relationship between the alpha oscillation reduction and the latency was different (figure 5.14). Seemingly, the Arch light stimulation led to a stronger neuronal inhibition relatively to NpHR inhibition. Neuronal silencing caused by the Arch activation managed to significantly decrease scored sleep spindles over 10 and 15 seconds of stimulation, whereas NpHR activation led to a strong reduction of the alpha oscillation frequency, while the reduced sleep spindles remained insignificant (See appendix figure 8.29). However, the sleep spindle scoring method might be a problem instead. Based on our experience, future studies aiming to reduce sleep spindles optogenetically should use archaerhodopsin.

5.4.5 Neuronal light activation

Light induced neuronal activation of the rostral TRN in the mice expressing YFP (Control) was more unexpected, than expected. We used a very low light intensity (less than 3 mW), but the light activation time (30 seconds) might play a role in causing the changes observed. Previously, we recorded strong delta activation in caudally and rostrally stimulated mice (See figure 3.4). In this chapter, we recorded a behavioural manifestation of the EEG power increase caused by light stimulation. Rostrally stimulated mice during wake-NREM transition periods induced a rapid arousal (less than 5 seconds) and had almost similar latency dynamics, as mice with caudally inhibited TRN (See figures 5.2, 5.3, 5.4). During the pre-wake period, rostral light stimulation induced a strong and significant increase in the delta, beta and gamma oscillation (See figure 5.24). A simultaneous increase in delta oscillations (sleeping frequency) from one side and the beta/gamma powers (wake frequency) from the other side is strange and might be caused by the activation of the distinct circuitries in the rostral TRN responsible for sensory (motor) and limbic information modulation.

According to Lewis et al. (2015) caudal TRN tonic activation also induced a massive delta increase and facilitated a sleep-like state, but reduced beta and gamma oscillation. So, the rostral TRN tonic activation, by increasing beta/gamma oscillations led to arousal, while the same side inhibition generated longer sleep episodes. With the caudal TRN there is a mirror situation, the inhibition induces arousal and a tonic activation led to sleep-like state or deeper sleep. This antagonistic nature of TRN activity fits well with Halassa's proposed plan: during awake periods, the caudal (sensory) and rostral (limbic) TRN sides are balanced, whereas the sleep state is characterized by the shift of the activity balance to the caudal TRN. We can add to this picture the following statements: sleep is induced by the fast (less than 20 seconds) balance shift to the caudal TRN and wake is induced by the balance shift to the rostral TRN. Additionally, we provided strong evidences that the sensory TRN is mostly located in the caudal TRN and cognitive (limbic) part of it is found in the rostral TRN.

An interesting question is whether a hierarchy exists between the caudal and rostral TRN? Is the mechanism of mutual inhibition during sleep, which is lost during wakefulness or is everything controlled by the incoming synapses from the sleep centres? The rostral TRN is well known for an abundant number of afferents from sleep centres and its relatively more complicated morphologically (See Chapter 1). Wimmer et al. (2015) demonstrated that modulation of the prefrontal cortex (PFC) induces errors in a visual attention task through TRN modulation. A question for future research is how can PFC- sensory TRN functional modulation exist, when the PFC has anatomical connections only with the rostral TRN?

5.4.6 Sleep spindle story

We boldly hypothesized that fast spindles (10 – 15 Hz) in mice are mostly produced in the caudal TRN and that the slow spindles (10 – 13 Hz) are generated in the rostral TRN. We tested the hypothesis but failed to find any frequency difference between rostrally and caudally inhibited sleep spindle oscillations. Additionally, the EEG spectrum analysis is not sensitive enough for such analysis. We managed to show that the fast sleep spindle oscillation is reduced during caudal TRN inhibition in deep sleep and is not affected during pre-wake sleep, whereas the rostral TRN inhibition had a mirror effect and only decreased the fast sleep spindle oscillation during pre-wake sleep. So, the fast sleep spindle oscillation did follow the flip-flop mechanism. According to our data sleep spindles might take place in diverse processes such as sleep initiation, sleep prolongation and sleep termination, depending on the TRN initiation site. However, further studies involving electrophysiology are required to determine the real nature of the different sleep spindles in mice.

One Korean lab optogenetically induced sleep spindles in the rostral TRN with 8 Hz frequency and these sleep spindles were never higher that 10 Hz (Kim et al., 2012; Latchoumane et al., 2017c), therefore we have chosen such low frequency (7-10 Hz) for slow spindle detection. All tested (pre-wake and deep sleep) traces contained the reduction of these oscillation, thereby location of the optogenetic modulation did not have a strong effect on the modulation of the ‘slow spindles’.

The sleep spindle story is more complicated. These strange waves discovered first by the inventor of the EEG technique (Bremer, 1935), appear to be involved not only in sleep, but also important for memory consolidation and neuronal development (Astori et al., 2013) The spindle type detection, apparently, should be done in a semi manual way to precisely understand the existing dynamics and the types of the possible spindles. Contreras & Steriade (1996) for example, detected slow spindles (7-8 Hz) and fast spindles (10-20 Hz) in the cat and we characterized beta oscillation involvement in TRN inhibition, therefore we might be missing a more realistic picture of the sleep spindle change, by exploiting only the power spectrum analysis. Raw EEG data analysis should be performed in the upcoming spindle studies.

5.4.7 Summary

Sleep spindle activity from the caudal and rostral TRN is important for brain state transitions and for sleep maintenance. Caudal TRN activity (putatively, sleep spindles) takes part in the wake-NREM transition and is important for the sleep maintenance, whereas rostral TRN activation accompanies the sleep-wake transition.

Chapter 6: Summary

After the characterization of the thalamic reticular nucleus (TRN) interconnections with the thalamus, afferents from different brain areas, neurochemical diversity, morphology, electrophysiological properties and physiological functions came the understanding, that the caudal and rostral parts of the TRN are diverse in these characteristics. We hypothesized that the caudal segment of the TRN is dealing with sensory information control and that the rostral segment of the TRN is involved in motor and cognitive information modulation. This led us to propose that modulation of distinct neuroanatomical sites within the TRN would differentially impact on components of the sleep-wake cycle and the transition between brain states. In particular that:

1) The optogenetic inhibition of the caudal TRN should have a stronger impact on sleep spindles (alpha band) and slow/delta waves than the rostral TRN inhibition.

2) The optogenetic inhibition of the different parts of the TRN should produce distinct effects on the sleep/wake cycle.

3) The rostral/caudal parts of the TRN might show dissimilar activity patterns during brain state change.

In order to test these predictions, we used optogenetics with the cre-lox system, which allowed us to target only parvalbumin containing neurons in the TRN with precise spatial and temporal resolution. We expressed light sensitive ion pumps (archaerhodopsin, Arch) and chloride channel (halorhodopsin, NpHR) in the parvalbumin neurons by injecting the virus in the rostral (AP -0.8 mm) or caudal TRN (AP-1.6 mm) area of the genetically modified mice, containing Cre recombinase protein only in the parvalbumin expressing neurons. The light, delivered through intracranially introduced optic fiber probes, activated the proton pumps/chloride and hyperpolarized TRN neurons. The EMG and EEG recordings were used to assess the effect of the various TRN site inhibition in freely moving animals.

Tonic stimulations during awake states did not produce any significant change in EEG, whereas stimulations during sleep significantly affected several frequency bands

associated with TRN functions. The delta oscillation was decreased significantly during optogenetic inhibition in the rostral and caudal TRN. The sleep spindles, and alpha waves, were significantly diminished only during caudal TRN inhibition. Additionally, the beta waves showed different tendencies to change during optogenetic modulations of the rostral and caudal TRN. Hence the EEG results supported the idea that the caudal TRN is responsible for the modulation of the alpha and beta (sleep spindle) oscillations during deep sleep, whereas both parts of the TRN can modulate delta oscillations.

Previous studies demonstrated that the malfunctioned sleep spindles oddly affect architecture of the sleep: total sleeping time is not changed, but the time of sleeping bouts is reduced. The optogenetic inhibition of the sensory TRN led to a reduction of sleep spindle oscillations and consequently, the sleep became less stable, discontinuous and contained a larger number of the short sleeping episodes. Optogenetic inhibition of the rostral TRN did not have an effect on sleep spindles and according to previous studies, most likely because it contains arousal correlated neurons. Basically, the same modulation in different parts of the nucleus is expected to produce opposite results. We demonstrated that the rostrally inhibited animals had a tendency for longer sleep and had a reduced proportion of the short sleep episodes relatively to the mice with caudally inhibited TRN. According to the correlation studies, employing the EEG band power differences, optogenetic manipulations of the caudal TRN which resulted frequent arousal was caused by the reduction of the alpha/beta (sleep spindle) oscillations, whereas rostral TRN inhibition was associated with prolonged sleep (rare arousal) was mostly related to the theta and beta oscillations differences.

Lastly, we demonstrated that the caudal and rostral TRN are taking part in transition between brain states. The caudal part of the nucleus is vital for the wake – NREM sleep transition and the rostral TRN activation is associated with the sleep-wake transition. Hence, TRN may act like a tumbler at the different sleep stages. According to Halassa et al. (2014), during wake the activity of both TRN sides (limbic and sensory

nuclei in actual paper) are balanced, while during sleep the balance is shifted to the sensory part of the TRN (caudal). We verified that the wake-sleep transition and sleep maintenance is possible only if the activity balance is shifted to the caudal part of the TRN, when the rostral TRN should remain silent. The balance shift to the rostral TRN, accompanies the sleep-wake transition period. These results support the simple notion, to fall asleep you should reduce emotions and thoughts, which, putatively, might be modulated by the rostral TRN activity. Additionally, we propose introduce the NREM stages in mice sleep, which could be differentiated by the TRN activity.

Although, it was a crude way to test the hypothesis, we concluded that rostral and caudal TRN consist of distinct subnetworks which have different activity level during sleep. The evidence discussed above support the hypothesis, that the caudal segment of TRN is dealing with sensory information control and the rostral segment of the TRN is involved with limbic/cognitive information modulation. We described the TRN heterogeneity by using location principles and draw attention to the issue, that the optogenetic targeting of the TRN segments in future should be seriously considered during the design of novel optogenetic experiments.

Chapter 7: Further work

Although, our results matched with previous reports (Halassa et al., 2014; Lewis et al., 2015), we still require data from single unit activity to confirm that the light caused inhibition of the TRN neurons. The TRN is not a simple structure for electrophysiological characterization, therefore the approach used by the Clemente-Perez et al. (2017) should be employed, where they combined electrophysiological and neurochemical methods to characterize cell diversity *in vivo*.

Site dependent activation of the TRN would also clarify our results. We showed, that control light stimulation on the rostral TRN did have an effect on the EEG and behaviour of mice, but the study of Lewis et al. (2015) with tonic optogenetic activation of the caudal TRN produced opposite results. So, further conformational studies, employing excitatory opsins, are required to provide evidence for the concept of the TRN tumbler like action during sleep.

Additionally, the introduction of extra control results would help us to clarify YFP only stimulations, which caused unexpected impact on EEG and behavioural data. Experiments without YFP introduction could be used to understand YFP influence on the gained results. The increase in n number of the control YFP would provide us with stronger significance and would allow us to state the importance of the extra control experiments in optogenetics studies.

Even though, spindles were detected almost a century ago, it appears that numerous labs around the world are detecting sleep spindles with different oscillations (Contreras & Steriade, 1996; Halassa et al., 2011; Kim et al., 2012; Latchoumane et al., 2017). Before the quantification of sleep spindles, we require to understand, which spindle types are generated by the rostral and caudal TRN activity. The spindle type detection could be done in semi manual way to precisely characterize the existing dynamics and types of spindle waves. Raw EEG data analysis should be performed in the upcoming studies characterizing spindles.

To the best of my knowledge, there is no study investigating the effect of the BF on the TRN neuronal firing. Additionally, there are limited numbers of *in vivo* studies characterizing brainstem and hypothalamic nuclei effect on the TRN cells during sleep

and wake states. The previous tracing studies, confirming the abundant number synapses between these brain areas and the TRN, allow us to hypothesise, that these connections should be critical for brain state modulations. More quality *in vivo* studies are required to understand the nature of the relationship between the TRN and sleeping/arousal centres.

References

Adrian, E.D., 1926. The impulses produced by sensory nerve endings: Part I. *The Journal of Physiology*, 61(1), pp.49–72.

Adrian, E.D. & Mattews, B.H.C., 1934. The berger rhythm: potential changes from the occipital lobes in man. *Brain*, 57(4), pp.355–385.

Aggleton, J.P. et al., 2010. Hippocampal-anterior thalamic pathways for memory: uncovering a network of direct and indirect actions. *European Journal of Neuroscience*, 31(12), pp.2292–2307.

Ahlsén, G. & Lindström, S., 1982. Mutual inhibition between perigeniculate neurones. *Brain Research*, 236(2), pp.482–6.

Ahrens, S. et al., 2015. ErbB4 regulation of a thalamic reticular nucleus circuit for sensory selection. *Nature Neuroscience*, 18(1), pp.104–11.

Alam, M.A. et al., 2014. Neuronal activity in the preoptic hypothalamus during sleep deprivation and recovery sleep. *Journal of Neurophysiology*, 111(2), pp.287–99.

Alam, M.A. et al., 2014. Neuronal activity in the preoptic hypothalamus during sleep deprivation and recovery sleep. *Journal of Neurophysiology*, 111(2), pp.287–299.

Albéri, L. et al., 2013. The calcium-binding protein parvalbumin modulates the firing properties of the reticular thalamic nucleus bursting neurons. *Journal of Neurophysiology*, 109(11), pp.2827–2841.

Ali, T. et al., 2013. Sleep, immunity and inflammation in gastrointestinal disorders. *World Journal of Gastroenterology*, 19(48), p.9231.

Allen, Y.S. et al., 1983. Neuropeptide Y distribution in the rat brain. *Science (New York, N.Y.)*, 221(4613), pp.877–9.

Alshelh, Z. et al., 2016. Chronic Neuropathic Pain: It's about the Rhythm. *The Journal of Neuroscience*, 36(3), pp.1008–18.

Ambardekar, A. V et al., 1999. Distribution and properties of GABA(B) antagonist [3H]CGP 62349 binding in the rhesus monkey thalamus and basal ganglia and the influence of lesions in the reticular thalamic nucleus. *Neuroscience*, 93(4), pp.1339–47.

Amzica, F. & Steriade, M., 1997. The K-complex: its slow. *Neurology*, 49(4), pp.952–9.

Anacker, A.M.J., Smith, M.L. & Ryabinin, A.E., 2014. Establishment of stable dominance interactions in prairie vole peers: Relationships with alcohol drinking and activation of the paraventricular nucleus of the hypothalamus. *Social Neuroscience*, 9(5), pp.484–494.

Anaclet, C. et al., 2015. Basal forebrain control of wakefulness and cortical rhythms. *Nature Communications*, 6(1), p.8744

Anaya-Martinez, V. et al., 2006. Substantia nigra compacta neurons that innervate the reticular thalamic nucleus in the rat also project to striatum or globus pallidus: implications for abnormal motor behavior. *Neuroscience*, 143(2), pp.477–86.

Anaya-Martinez, V. et al., 2006. Substantia nigra compacta neurons that innervate the reticular thalamic nucleus in the rat also project to striatum or globus pallidus: Implications for abnormal motor behavior. *Neuroscience*, 143(2), pp.477–486.

Andrillon, T. et al., 2011. Sleep spindles in humans: insights from intracranial EEG and unit recordings. *The Journal of Neuroscience*, 31(49), pp.17821–34.

Arai, R., Jacobowitz, D. & Deura, S., 1994. Distribution of calretinin, calbindin-D28k, and parvalbumin in the rat thalamus. *Brain research bulletin*, 33(5), pp.595–614.

Arai, R., Jacobowitz, D.M. & Deura, S., 1994. Distribution of calretinin, calbindin-D28k,

and parvalbumin in the rat thalamus. *Brain research bulletin*, 33(5), pp.595–614.

Aravanis, A.M. et al., 2007. An optical neural interface: *in vivo* control of rodent motor cortex with integrated fiberoptic and optogenetic technology. *Journal of Neural Engineering*, 4(3), pp.S143–S156.

Arenkiel, B.R. et al., 2007. In Vivo Light-Induced Activation of Neural Circuitry in Transgenic Mice Expressing Channelrhodopsin-2. *Neuron*, 54(2), pp.205–218.

Asanuma, C., 1989. Axonal arborizations of a magnocellular basal nucleus input and their relation to the neurons in the thalamic reticular nucleus of rats. *Proceedings of the National Academy of Sciences of the United States of America*, 86(12), pp.4746–50.

Asanuma, C., 1992. Noradrenergic innervation of the thalamic reticular nucleus: a light and electron microscopic immunohistochemical study in rats. *The Journal of Comparative Neurology*, 319(2), pp.299–311.

Asanuma, C. & Porter, L.L., 1990. Light and electron microscopic evidence for a GABAergic projection from the caudal basal forebrain to the thalamic reticular nucleus in rats. *The Journal of Comparative Neurology*, 302(1), pp.159–172.

Astori, S. et al., 2011. The Ca(V)3.3 calcium channel is the major sleep spindle pacemaker in thalamus. *Proceedings of the National Academy of Sciences of the United States of America*, 108(33), pp.13823–8.

Astori, S., Wimmer, R.D. & Lüthi, A., 2013. Manipulating sleep spindles - expanding views on sleep, memory, and disease. *Trends in Neurosciences*, 36(12), pp.738–48.

Avoli, M., 2012. A brief history on the oscillating roles of thalamus and cortex in absence seizures. *Epilepsia*, 53(5), pp.779–89.

Bal, T., von Krosigk, M. & McCormick, D. a, 1995. Role of the ferret perigeniculate nucleus in the generation of synchronized oscillations in vitro. *The Journal of Physiology*, 483, Pt 3, pp.665–85.

Bal, T. & McCormick, D., 1993. Mechanisms of oscillatory activity in guinea-pig nucleus reticularis thalami in vitro: a mammalian pacemaker. *The Journal of Physiology*, pp.669–691.

Baraban, S.C. & Tallent, M.K., 2004. Interneuron Diversity series: Interneuronal neuropeptides--endogenous regulators of neuronal excitability. *Trends in neurosciences*, 27(3), pp.135–42.

Barnard, E.A. et al., 1998. International Union of Pharmacology. XV. Subtypes of gamma-aminobutyric acidA receptors: classification on the basis of subunit structure and receptor function. *Pharmacological Reviews*, 50(2), pp.291–313.

Barone, F.C., Cheng, J.T. & Wayner, M.J., 1994. GABA inhibition of lateral hypothalamic neurons: role of reticular thalamic afferents. *Brain research bulletin*, 33(6), pp.699–708.

Barrionuevo, G., Benoit, O. & Tempier, P., 1981. Evidence for two types of firing pattern during the sleep-waking cycle in the reticular thalamic nucleus of the cat. *Experimental Neurology*, 72(2), pp.486–501.

Barthó, P., Freund, T.F. & Acsády, L., 2002. Selective GABAergic innervation of thalamic nuclei from zona incerta. *The European journal of Neuroscience*, 16(6), pp.999–1014

Bartlett, E.L., 2013. The organization and physiology of the auditory thalamus and its role in processing acoustic features important for speech perception. *Brain and Language*, 126(1), pp.29–48.

Başar, E., 1972. A study of the time and frequency characteristics of the potentials evoked in the acoustical cortex. *Kybernetik*, 10(2), pp.61–4.

Başar, E., 1999. *Brain Function and Oscillations : Integrative Brain Function. Neurophysiology and Cognitive Processes*, Springer Berlin Heidelberg.

Batini, C. et al., 1958. Presistent patterns of wakefulness in the pretrigeminal midpontine preparation. *Science (New York, N.Y.)*, 128(3314), pp.30–2.

Bazhenov, M. et al., 1999. Self-sustained rhythmic activity in the thalamic reticular nucleus mediated by depolarizing GABAA receptor potentials. *Nature Neuroscience*, 2(2), pp.168–74.

Bender, D.B., 1983. Visual activation of neurons in the primate pulvinar depends on cortex but not colliculus. *Brain Research*, 279(1–2), pp.258–61.

Bendotti, C. et al., 1990. Developmental expression of somatostatin in mouse brain. II. In situ hybridization. *Brain Research. Developmental brain research*, 53(1), pp.26–39.

Berendse, H.W. & Groenewegen, H.J., 1990. Organization of the thalamostriatal projections in the rat, with special emphasis on the ventral striatum. *The Journal of Comparative Neurology*, 299(2), pp.187–228.

Berendse, H.W. & Groenewegen, H.J., 1991. Restricted cortical termination fields of the midline and intralaminar thalamic nuclei in the rat. *Neuroscience*, 42(1), pp.73–102.

Berger, H., 1930. Über das Elektrenkephalogramm des Menschen.Zweite Mitteilung. *J.Psychol.Neurol.*, (40), pp.160–179.

Berger, H., 1929. Über das Elektrenkephalogramm des Menschen. *Archiv für Psychiatrie und Nervenkrankheiten*, 87(1), pp.527–570.

Bester, H. et al., 1999. Differential projections to the intralaminar and gustatory thalamus from the parabrachial area: a PHA-L study in the rat. *The Journal of Comparative Neurology*, 405(4), pp.421–49.

Bhatnagar, S. et al., 2002. Lesions of the posterior paraventricular thalamus block habituation of hypothalamic-pituitary-adrenal responses to repeated restraint. *Journal of Neuroendocrinology*, 14(5), pp.403–10.

Bi, A. et al., 2006. Ectopic expression of a microbial-type rhodopsin restores visual responses in mice with photoreceptor degeneration. *Neuron*, 50(1), pp.23–33.

Bickford, M.E. et al., 1994. GABAergic projection from the basal forebrain to the visual

sector of the thalamic reticular nucleus in the cat. *Journal of Comparative Neurology*, 348(4), pp.481–510.

Bland, B.H., 1986. The physiology and pharmacology of hippocampal formation theta rhythms. *Progress in Neurobiology*, 26(1), pp.1–54.

Blevins, J.E. & Baskin, D.G., 2009. Hypothalamic-Brainstem Circuits Controlling Eating. In *Frontiers in Eating and Weight Regulation*. Basel: KARGER, pp. 133–140.

Blum, P.S. et al., 1979. Thalamic components of the ascending vestibular system. *Experimental Neurology*, 64(3), pp.587–603.

Bonjean, M. et al., 2011. Corticothalamic feedback controls sleep spindle duration in vivo. *The Journal of Neuroscience*, 31(25), pp.9124–34.

Bosch-Bouju, C., Hyland, B.I. & Parr-Brownlie, L.C., 2013. Motor thalamus integration of cortical, cerebellar and basal ganglia information: implications for normal and parkinsonian conditions. *Frontiers in computational neuroscience*, 7, p.163.

Boutros, N.N. et al., 2008. The status of spectral EEG abnormality as a diagnostic test for schizophrenia. *Schizophrenia Research*, 99(1–3), pp.225–237.

Boyden, E., 2011. A history of optogenetics: the development of tools for controlling brain circuits with light. *F1000 Biology Reports*, 3(May), pp.1–12.

Boyden, E.S. et al., 2005a. Millisecond-timescale, genetically targeted optical control of neural activity. *Nature neuroscience*, 8(9), pp.1263–8.

Boyden, E.S. et al., 2005b. Millisecond-timescale, genetically targeted optical control of neural activity. *Nature Neuroscience*, 8(9), pp.1263–1268.

Brankačk, J. et al., 2010. EEG gamma frequency and sleep–wake scoring in mice: Comparing two types of supervised classifiers. *Brain Research*, 1322, pp.59–71.

Bremer, F., 1935. Cerveau “isole” et physiologie du sommeil. *Comptes Rendus de la Societe de Biologie*, (118), pp.1235–1241.

Brewer, J. & Porter, R., 2013. *Consumption and the World of Goods*, Routledge.

Brill, J., Kwakye, G. & Huguenard, J.R., 2007. NPY signaling through Y1 receptors modulates thalamic oscillations. *Peptides*, 28(2), pp.250–6.

Broberger, C. & McCormick, D.A., 2005. Excitatory Effects of Thyrotropin-Releasing Hormone in the Thalamus. *Journal of Neuroscience*, 25(7), pp.1664–1673.

Brodmann, K., 1909. *Vergleichende Lokalisationslehre der Grosshirnhide*.

Brown, A.R. et al., 2015. Developmentally regulated neurosteroid synthesis enhances GABAergic neurotransmission in mouse thalamocortical neurones. *The Journal of Physiology*, 593(1), pp.267–284.

Brown, E.N., Purdon, P.L. & Van Dort, C.J., 2011. General Anesthesia and Altered States of Arousal: A Systems Neuroscience Analysis. *Annual Review of Neuroscience*, 34(1), pp.601–628.

Brown, R.E. et al., 2012. Control of Sleep and Wakefulness. *Physiological Reviews*, 92(3), pp.1087–1187.

Browning, P.G.F., Chakraborty, S. & Mitchell, A.S., 2015. Evidence for Mediodorsal Thalamus and Prefrontal Cortex Interactions during Cognition in Macaques. *Cerebral cortex (New York, N.Y. : 1991)*, 25(11), pp.4519–34.

Brunton, J. & Charpak, S., 1997. Heterogeneity of cell firing properties and opioid sensitivity in the thalamic reticular nucleus. *Neuroscience*, 78(2), pp.303–307.

Brzezinski, A. et al., 2005. Effects of exogenous melatonin on sleep: a meta-analysis. *Sleep medicine reviews*, 9(1), pp.41–50.

Bubser, M. & Deutch, A.Y., 1999. Stress induces Fos expression in neurons of the thalamic paraventricular nucleus that innervate limbic forebrain sites. *Synapse (New York, N.Y.)*, 32(1), pp.13–22.

Bubser, M. & Deutch, A.Y., 1998. Thalamic paraventricular nucleus neurons collateralize to innervate the prefrontal cortex and nucleus accumbens. *Brain Research*, 787(2), pp.304–10.

Burgunder, J.-M. & Taylor, T., 1989. Ontogeny of Thyrotropin-Releasing Hormone Gene Expression in the Rat Diencephalon. *Neuroendocrinology*, 49(6), pp.631–640.

Burgunder, J.M., Heyberger, B. & Lauterburg, T., 1999a. Thalamic reticular nucleus parcellation delineated by VIP and TRH gene expression in the rat. *Journal of Chemical Neuroanatomy*, 17(3), pp.147–52.

Burgunder, J.M., Heyberger, B. & Lauterburg, T., 1999b. Thalamic reticular nucleus parcellation delineated by VIP and TRH gene expression in the rat. *Journal of Chemical Neuroanatomy*, 17(3), pp.147–52.

Burgunder, J.M. & Young, W.S., 1992. Expression of cholecystokinin and somatostatin genes in the human thalamus. *The Journal of Comparative Neurology*, 324(1), pp.14–22.

Butler, A.B., 2008a. Evolution of brains, cognition, and consciousness. *Brain Research Bulletin*, 75(2–4), pp.442–449.

Butler, A.B., 2008b. Evolution of the thalamus: A morphological and functional review. *Thalamus and Related Systems*, 4(1), pp.35–58.

Buzsaki, G. et al., 1988. Nucleus basalis and thalamic control of neocortical activity in the freely moving rat. *The Journal of Neuroscience*, 8(11), pp.4007–26.

Buzsáki, G., 2002. Theta oscillations in the hippocampus. *Neuron*, 33(3), pp.325–40.

Cain, S.M. et al., 2017. GABA $_B$ receptors suppress burst-firing in reticular thalamic neurons. *Channels*, 11(6), pp.574–586.

Callaway, E.M. & Katz, L.C., 1993. Photostimulation using caged glutamate reveals functional circuitry in living brain slices. *Proceedings of the National Academy of Sciences of the United States of America*, 90(16), pp.7661–7665.

Campbell, C.B., 1972. Evolutionary patterns in mammalian diencephalic visual nuclei and their fiber connections. *Brain, behavior and evolution*, 6(1), pp.218–36.

Canavan, A.G., Nixon, P.D. & Passingham, R.E., 1989. Motor learning in monkeys (Macaca fascicularis) with lesions in motor thalamus. *Experimental Brain Research*, 77(1), pp.113–26.

Cardin, J.A. et al., 2009. Driving fast-spiking cells induces gamma rhythm and controls sensory responses. *Nature*, 459(7247), pp.663–667.

Carman, J.B., Cowan, W.M. & Powell, T.P., 1964. Cortical Connexions of the Thalamic Reticular Nucleus. *Journal of Anatomy*, 98, pp.587–98.

Carter, M.E. et al., 2010. Tuning arousal with optogenetic modulation of locus coeruleus neurons. *Nature Neuroscience*, 13(12), pp.1526–33.

Casagrande, V.A., 1994. A third parallel visual pathway to primate area V1. *Trends in Neurosciences*, 17(7), pp.305–10.

Cavdar, S. et al., 2006. Connections of the zona incerta to the reticular nucleus of the thalamus in the rat. *Journal of Anatomy*, 209(2), pp.251–258.

Çavdar, S. et al., 2008. The pathways connecting the hippocampal formation, the thalamic reuniens nucleus and the thalamic reticular nucleus in the rat. *Journal of Anatomy*, 212(3), pp.249–256.

Celio, M.R., 1990. Calbindin D-28k and parvalbumin in the rat nervous system. *Neuroscience*, 35(2), pp.375–475.

Celio, M.R., 1986. Parvalbumin in most gamma-aminobutyric acid-containing neurons of the rat cerebral cortex. *Science (New York, N.Y.)*, 231(4741), pp.995–7.

Celio, M.R., Pauls, T.L. & Schwaller, B., 1996. *Guidebook to the calcium-binding proteins*, Sambrook & Tooze Publication at Oxford University Press.

Chard, P.S. et al., 1993. Calcium buffering properties of calbindin D28k and parvalbumin in rat sensory neurones. *The Journal of Physiology*, 472, pp.341–57.

Chatila, M. et al., 1993. Alpha rhythm in the cat thalamus. *Comptes rendus de l'Academie des sciences. Serie III, Sciences de la vie*, 316(1), pp.51–8.

Cheong, E. & Shin, H.-S., 2014. T-type Ca2+ channels in absence epilepsy. *Pflügers Archiv - European Journal of Physiology*, 466(4), pp.719–734.

Ching, S. & Brown, E.N., 2014. Modeling the dynamical effects of anesthesia on brain circuits. *Current Opinion in Neurobiology*, 25, pp.116–122.

Cholvin, T. et al., 2013. The ventral midline thalamus contributes to strategy shifting in a memory task requiring both prefrontal cortical and hippocampal functions. *The Journal of Neuroscience*, 33(20), pp.8772–83.

Cholvin, T. et al., 2013. The Ventral Midline Thalamus Contributes to Strategy Shifting in a Memory Task Requiring Both Prefrontal Cortical and Hippocampal Functions. *Journal of Neuroscience*, 33(20), pp.8772–8783.

Chow, B.Y. et al., 2010. High-Performance Genetically Targetable Optical Neural Silencing via Light-Driven Proton Pumps Brian. , 463(7277), pp.98–102.

Choy, E.H.S., 2015. The role of sleep in pain and fibromyalgia. *Nature Reviews Rheumatology*, 11(9), pp.513–520.

Christian, C.A. & Huguenard, J.R., 2013. Astrocytes potentiate GABAergic transmission in the thalamic reticular nucleus via endozepine signaling. *Proceedings of the National Academy of Sciences*, 110(50), pp.20278–20283.

Chrobak, J.J. & Buzsáki, G., 1996. High-frequency oscillations in the output networks of the hippocampal-entorhinal axis of the freely behaving rat. *The Journal of Neuroscience*, 16(9), pp.3056–66.

Clark, B.J. & Harvey, R.E., 2016. Do the anterior and lateral thalamic nuclei make distinct contributions to spatial representation and memory? *Neurobiology of Learning and Memory*, 133, pp.69–78.

Clayton, M.S., Yeung, N. & Cohen Kadosh, R., 2015. The roles of cortical oscillations in sustained attention. *Trends in Cognitive Sciences*, 19(4), pp.188–195.

Clemente-perez, A. et al., 2017. Distinct Thalamic Reticular Cell Types Differentially Modulate Normal and Pathological Cortical Rhythms Article Distinct Thalamic Reticular Cell Types Differentially Modulate Normal and Pathological Cortical Rhythms. *Cell reports*, pp.2130–2142.

Coleman, K.A. & Mitrofanis, J., 1996. Organization of the visual reticular thalamic nucleus of the rat. *The European journal of Neuroscience*, 8(2), pp.388–404.

Comai, S., Ochoa-Sanchez, R. & Gobbi, G., 2013. Sleep–wake characterization of double MT1/MT2 receptor knockout mice and comparison with MT1 and MT2 receptor knockout mice. *Behavioural Brain Research*, 243, pp.231–238.

Conley, M. & Diamond, I.T., 1990. Organization of the Visual Sector of the Thalamic Reticular Nucleus in Galago. *The European journal of Neuroscience*, 2(3), pp.211–226.

Connolly, C.N. et al., 1996. Assembly and cell surface expression of heteromeric and homomeric gamma-aminobutyric acid type A receptors. *The Journal of Biological Chemistry*, 271(1), pp.89–96.

Contreras-Rodríguez, J. et al., 2003. Neurochemical heterogeneity of the thalamic reticular and perireticular nuclei in developing rabbits: patterns of calbindin expression. *Brain research. Developmental brain research*, 144(2), pp.211–21.

Contreras-Rodríguez, J. et al., 2002. The thalamic reticular and perireticular nuclei in developing rabbits: patterns of parvalbumin expression. *Brain Research. Developmental brain research*, 136(2), pp.123–33.

Contreras, D., Curró Dossi, R. & Steriade, M., 1992. Bursting and tonic discharges in two classes of reticular thalamic neurons. *Journal of Neurophysiology*, 68(3), pp.973–7.

Contreras, D., Destexhe, A. & Steriade, M., 1997. Intracellular and computational characterization of the intracortical inhibitory control of synchronized thalamic inputs in vivo. *Journal of Neurophysiology*, 78(1), pp.335–50.

Contreras, D., Dossi, R. & Steriade, M., 1993. Electrophysiological properties of cat reticular thalamic neurones in vivo. *The Journal of Physiology*, pp.273–294.

Contreras, D. & Steriade, M., 1995. Cellular basis of EEG slow rhythms: a study of dynamic corticothalamic relationships. *The Journal of Neuroscience*, 15(1 Pt 2), pp.604–22.

Contreras, D. & Steriade, M., 1996a. Spindle oscillation in cats: the role of corticothalamic feedback in a thalamically generated rhythm. *The Journal of Physiology*, 490, Pt 1, pp.159–79.

Contreras, D. & Steriade, M., 1996b. Spindle oscillation in cats: the role of corticothalamic feedback in a thalamically generated rhythm. *The Journal of Physiology*, 490 (Pt 1), pp.159–79.

Copeland, C.S. et al., 2017. Astrocytes modulate thalamic sensory processing via mGlu2 receptor activation. *Neuropharmacology*, 121, pp.100–110.

Cornwall, J., Cooper, J.D. & Phillipson, O.T., 1990a. Afferent and efferent connections of the laterodorsal tegmental nucleus in the rat. *Brain Research Bulletin*, 25(2), pp.271–84.

Cornwall, J., Cooper, J.D. & Phillipson, O.T., 1990b. Projections to the rostral reticular thalamic nucleus in the rat. *Experimental Brain Research*, 80(1), pp.157–71.

Cornwall, J., Cooper, J.D. & Phillipson, O.T., 1990c. Projections to the rostral reticular thalamic nucleus in the rat. *Experimental Brain Research*, 80(1), pp.157–71.

Cornwall, J., Cooper, J.D. & Phillipson, O.T., 1990d. Projections to the rostral reticular thalamic nucleus in the rat. *Experimental Brain Research*, 80(1), pp.157–71.

Coulon, P. et al., 2009. Burst discharges in neurons of the thalamic reticular nucleus are shaped by calcium-induced calcium release. *Cell Calcium*, 46(5–6), pp.333–46.

Cox, C. & Sherman, S., 1999. Glutamate inhibits thalamic reticular neurons. *The Journal of Neuroscience*, 19(15), pp.6694–6699.

Cox, C.L., Huguenard, J.R. & Prince, D. a, 1997. Peptidergic modulation of intrathalamic circuit activity in vitro: actions of cholecystokinin. *The Journal of Neuroscience*, 17(1), pp.70–82.

Cox, C.L., Huguenard, J.R. & Prince, D.A., 1995. Cholecystokinin depolarizes rat thalamic reticular neurons by suppressing a K+ conductance. *Journal of Neurophysiology*, 74(3), pp.990–1000.

Cox, C.L., Huguenard, J.R. & Prince, D.A., 1996. Heterogeneous axonal arborizations of rat thalamic reticular neurons in the ventrobasal nucleus. *The Journal of Comparative Neurology*, 366(3), pp.416–30.

Cox, C.L., Huguenard, J.R. & Prince, D.A., 1997. Nucleus reticularis neurons mediate diverse inhibitory effects in thalamus. *Proceedings of the National Academy of Sciences of the United States of America*, 94(16), pp.8854–9.

Crabtree, J., 1999. Intrathalamic sensory connections mediated by the thalamic reticular nucleus. *Cellular and Molecular Life Sciences CMLS*, 56(7–8), pp.683–700.

Crabtree, J., 1992. The somatotopic organization within the rabbit's thalamic reticular nucleus. *European Journal of Neuroscience*, 4(12), pp.1343–1351.

Crabtree, J. & Killackey, H., 1989. The topographic organization and axis of projection within the visual sector of the rabbit's thalamic reticular nucleus. *European Journal of Neuroscience*, 1(1), pp.94–109.

Crabtree, J.W., 1998. Organization in the auditory sector of the cat's thalamic reticular nucleus. *The Journal of Comparative Neurology*, 390(2), pp.167–82.

Crabtree, J.W., 1996. Organization in the somatosensory sector of the cat's thalamic reticular nucleus. *The Journal of Comparative Neurology*, 366(2), pp.207–22.

Crabtree, J.W., 1992. The Somatotopic Organization Within the Cat's Thalamic Reticular Nucleus. *The European Journal of Neuroscience*, 4(12), pp.1352–1361.

Crabtree, J.W. & Isaac, J.T.R., 2002. New intrathalamic pathways allowing modality-

related and cross-modality switching in the dorsal thalamus. *The Journal of Neuroscience*, 22(19), pp.8754–61.

Crandall, S.R., Cruikshank, S.J. & Connors, B.W., 2015. A corticothalamic switch: controlling the thalamus with dynamic synapses. *Neuron*, 86(3), pp.768–82.

Crick, F., 1984. Function of the thalamic reticular complex: the searchlight hypothesis. *Proceedings of the National Academy of Sciences*, 81(14), pp.4586–4590.

Crunelli, V. et al., 1988. Cl- - and K+-dependent inhibitory postsynaptic potentials evoked by interneurones of the rat lateral geniculate nucleus. *The Journal of Physiology*, 399, pp.153–76.

Crunelli, V. & Hughes, S.W., 2010. The slow (<1 Hz) rhythm of non-REM sleep: a dialogue between three cardinal oscillators. *Nature Neuroscience*, 13(1), pp.9–17.

Csillik, B. et al., 2005. GABAergic parvalbumin-immunoreactive large calyciform presynaptic complexes in the reticular nucleus of the rat thalamus. *Journal of Chemical Neuroanatomy*, 30(1), pp.17–26.

Cueni, L. et al., 2008. T-type Ca2+ channels, SK2 channels and SERCAs gate sleep-related oscillations in thalamic dendrites. *Nature Neuroscience*, 11(6), pp.683–92.

Dalrymple-Alford, J.C. et al., 2015. Anterior thalamic nuclei lesions and recovery of function: Relevance to cognitive thalamus. *Neuroscience and Biobehavioral Reviews*, 54, pp.145–160.

Dan, Y. & Poo, M.-M., 2004. Spike timing-dependent plasticity of neural circuits. *Neuron*, 44(1), pp.23–30.

Dang-Vu, T.T., 2012. Neuronal oscillations in sleep: insights from functional neuroimaging. *Neuromolecular Medicine*, 14(3), pp.154–67.

Dang-Vu, T.T. et al., 2010. Spontaneous brain rhythms predict sleep stability in the face of noise. *Current Biology : CB*, 20(15), pp.R626-7.

David, F. et al., 2013. Essential thalamic contribution to slow waves of natural sleep. *The Journal of Neuroscience*, 33(50), pp.19599–610.

David, F. et al., 2013. Essential Thalamic Contribution to Slow Waves of Natural Sleep. *Journal of Neuroscience*, 33(50), pp.19599–19610.

Davidson, B.L. & Breakefield, X.O., 2003. Neurological diseases: Viral vectors for gene delivery to the nervous system. *Nature Reviews Neuroscience*, 4(5), pp.353–364.

Deisseroth, K. et al., 2010. Next generation optical technology for illuminating genetically targeted brain circuits. *Journal of Neuroscience*, 26(41). pp.10380–6.

Deleuze, C. & Huguenard, J.R., 2016. Two classes of excitatory synaptic responses in rat thalamic reticular neurons. *Journal of Neurophysiology*, 116(3), pp.995–1011.

Deschênes, M., Madariaga-Domich, A. & Steriade, M., 1985. Dendrodendritic synapses in the cat reticularis thalami nucleus: a structural basis for thalamic spindle synchronization. *Brain Research*, 334(1), pp.165–8.

Destexhe, A. & Contreras, D., 1996. In vivo, in vitro, and computational analysis of dendritic calcium currents in thalamic reticular neurons. *The Journal of Neuroscience*, 16(1), pp.169–185.

Dewulf, A. et al., 1969. [Cytometric studies of the normal human thalamus]. *Giornale di psichiatria e di neuropatologia*, 97(3), pp.361–73.

Diamond, M.E. et al., 1992. Somatic sensory responses in the rostral sector of the posterior group (POm) and in the ventral posterior medial nucleus (VPM) of the rat thalamus: dependence on the barrel field cortex. *The Journal of Comparative Neurology*, 319(1), pp.66–84.

Ditz, H.M. & Nieder, A., 2016. Sensory and Working Memory Representations of Small and Large Numerosities in the Crow Endbrain. *The Journal of Neuroscience*, 36(47), pp.12044–12052.

Du, J. et al., 1996. Developmental expression and functional characterization of the

potassium-channel subunit Kv3.1b in parvalbumin-containing interneurons of the rat hippocampus. *The Journal of Neuroscience*, 16(2), pp.506–18.

Eccles, J.C., 1961. "Chairman's opening remarks". In *Foundation Symposium on the Nature of Sleep*.

von Economo, C., 1930. Sleep as a problem of localization. *J Nerv Ment Dis.*, (71), pp.249–259.

Eguchi, K. & Satoh, T., 1980. Characterization of the neurons in the region of solitary tract nucleus during sleep. *Physiology & Behavior*, 24(1), pp.99–102.

Ekstrand, A.J. et al., 2003. Deletion of neuropeptide Y (NPY) 2 receptor in mice results in blockage of NPY-induced angiogenesis and delayed wound healing. *Proceedings of the National Academy of Sciences of the United States of America*, 100(10), pp.6033–8.

Elena Erro, M., Lanciego, J.L. & Gimenez-Amaya, J.M., 2002. Re-examination of the thalamostriatal projections in the rat with retrograde tracers. *Neuroscience Research*, 42(1), pp.45–55.

Erickson, S.L., Melchitzky, D.S. & Lewis, D.A., 2004. Subcortical afferents to the lateral mediodorsal thalamus in cynomolgus monkeys. *Neuroscience*, 129(3), pp.675–690.

Erlij, D. et al., 2012. Dopamine D4 receptor stimulation in GABAergic projections of the globus pallidus to the reticular thalamic nucleus and the substantia nigra reticulata of the rat decreases locomotor activity. *Neuropharmacology*, 62(2), pp.1111–8.

Erro, M.E. et al., 2001. Striatal input from the ventrobasal complex of the rat thalamus. *Histochemistry and Cell Biology*, 115(6), pp.447–54.

Espinosa, F. et al., 2008. Ablation of Kv3.1 and Kv3.3 potassium channels disrupts thalamocortical oscillations in vitro and in vivo. *The Journal of Neuroscience*, 28(21), pp.5570–81.

Everyvector.com, 2009. No Title. *everyvector.com*. Available at: http://www.everyvector.com/sequences/show_public/40772 [Accessed March 24, 2014].

Eyles, D.W., McGrath, J.J. & Reynolds, G.P., 2002. Neuronal calcium-binding proteins and schizophrenia. *Schizophrenia Research*, 57(1), pp.27–34.

Fernández-Alacid, L. et al., 2009. Subcellular compartment-specific molecular diversity of pre- and post-synaptic GABA $_B$ -activated GIRK channels in Purkinje cells. *Journal of Neurochemistry*, 110(4), pp.1363–1376.

Ferrarelli, F. et al., 2007. Reduced sleep spindle activity in schizophrenia patients. *The American journal of psychiatry*, 164(3), pp.483–92.

Ferrarelli, F. & Tononi, G., 2011. The thalamic reticular nucleus and schizophrenia. *Schizophrenia Bulletin*, 37(2), pp.306–15.

von Fersen, L. et al., 1990. Deductive reasoning in pigeons. *Die Naturwissenschaften*, 77(11), pp.548–9.

Fischer, C. et al., 1995. Auditory evoked potentials in a patient with a unilateral lesion of the inferior colliculus and medial geniculate body. *Electroencephalography and Clinical Neurophysiology*, 96(3), pp.261–7.

Fitch, W.T., 2011. Speech Perception: A Language-Trained Chimpanzee Weighs In. *Current Biology*, 21(14), pp.R543–R546.

FitzGibbon, T., Solomon, S. & Goodchild, A., 2000. Distribution of calbindin, parvalbumin, and calretinin immunoreactivity in the reticular thalamic nucleus of the marmoset: evidence for a medial leaflet of incertal. *Experimental Neurology*, 164(2), pp.371–383.

FitzGibbon, T., Solomon, S.G. & Goodchild, A.K., 2000. Distribution of Calbindin, Parvalbumin, and Calretinin Immunoreactivity in the Reticular Thalamic Nucleus of the Marmoset: Evidence for a Medial Leaflet of Incertal Neurons. *Experimental Neurology*, 164(2), pp.371–383.

Florán, B. et al., 2004. Activation of dopamine D4 receptors modulates [3H]GABA release in slices of the rat thalamic reticular nucleus. *Neuropharmacology*, 46(4), pp.497–503.

Fork, R.L., 1971. Laser Stimulation of Nerve Cells in Aplysia. *Science*, 171(3974), pp.907–908.

Fortin, M. et al., 1998. Calretinin-immunoreactive neurons in the human thalamus. *Neuroscience*, 84(2), pp.537–48.

Fortin, M., Asselin, M.C. & Parent, A., 1996. Calretinin immunoreactivity in the thalamus of the squirrel monkey. *Journal of Chemical Neuroanatomy*, 10(2), pp.101–17.

Fowler, M., Medina, L. & Reiner, A., 1999. Immunohistochemical localization of NMDA- and AMPA-type glutamate receptor subunits in the basal ganglia of red-eared turtles. *Brain, Behavior and Evolution*, 54(5), pp.276–89.

Freeman, A. et al., 2001. Nigrostriatal collaterals to thalamus degenerate in parkinsonian animal models. *Annals of Neurology*, 50(3), pp.321–9.

Freeman, W.J., 1975. *Mass Action in the Nervous System* Academic Press., New York.

Fries, P., 2009. Neuronal Gamma-Band Synchronization as a Fundamental Process in Cortical Computation. *Annual Review of Neuroscience*, 32(1), pp.209–224.

Fritschy, J.M. & Mohler, H., 1995. GABAA-receptor heterogeneity in the adult rat brain: differential regional and cellular distribution of seven major subunits. *The Journal of Comparative Neurology*, 359(1), pp.154–94.

Froemke, R.C., Merzenich, M.M. & Schreiner, C.E., 2007. A synaptic memory trace for cortical receptive field plasticity. *Nature*, 450(7168), pp.425–9.

Fuentealba, P. et al., 2004. Experimental evidence and modeling studies support a synchronizing role for electrical coupling in the cat thalamic reticular neurons in vivo. *The European journal of neuroscience*, 20(1), pp.111–9.

Fuentealba, P. et al., 2005. Membrane bistability in thalamic reticular neurons during spindle oscillations. *Journal of Neurophysiology*, 93(1), pp.294–304.

Fuentealba, P. & Steriade, M., 2005. The reticular nucleus revisited: Intrinsic and network properties of a thalamic pacemaker. *Progress in Neurobiology*, 75(2), pp.125–41.

Funke, K. & Eysel, U.T., 1993. Modulatory effects of acetylcholine, serotonin and noradrenaline on the activity of cat perigeniculate neurons. *Experimental Brain Research*, 95(3), pp.409–20.

Galvani, L., 1791. De viribus electricitatis in motu musculari commentarius. *Typographia Instituti Scientiarum*.

Gandia, J. a et al., 1993. Afferent projections to the reticular thalamic nucleus from the globus pallidus and the substantia nigra in the rat. *Brain Research Bulletin*, 32(4), pp.351–8.

Gandia, J.A. et al., 1993. Afferent projections to the reticular thalamic nucleus from the globus pallidus and the substantia nigra in the rat. *Brain Research Bulletin*, 32(4), pp.351–8.

García-Cabezas, M.A. et al., 2007. Distribution of the dopamine innervation in the macaque and human thalamus. *NeuroImage*, 34(3), pp.965–84.

Garcia-Lopez, P., Garcia-Marin, V. & Freire, M., 2010. The histological slides and drawings of cajal. *Frontiers in Neuroanatomy*, 4, p.9.

Gasca-Martinez, D. et al., 2010. Dopamine inhibits GABA transmission from the globus pallidus to the thalamic reticular nucleus via presynaptic D4 receptors. *Neuroscience*, 169(4), pp.1672–81.

Geiger, J.R. et al., 1995. Relative abundance of subunit mRNAs determines gating and Ca2+ permeability of AMPA receptors in principal neurons and interneurons in rat CNS. *Neuron*, 15(1), pp.193–204.

Gent, T.C. et al., 2018. Thalamic dual control of sleep and wakefulness. *Nature*

Neuroscience, 21(7), pp.974–984.

Ghodrati, M., Khaligh-Razavi, S.-M. & Lehky, S.R., 2017a. Towards building a more complex view of the lateral geniculate nucleus: Recent advances in understanding its role. *Progress in Neurobiology*, 156, pp.214–255.

Ghodrati, M., Khaligh-Razavi, S.-M. & Lehky, S.R., 2017b. Towards building a more complex view of the lateral geniculate nucleus: Recent advances in understanding its role. *Progress in Neurobiology*, 156, pp.214–255.

Gibbs, E.L. & Gibbs, F.A., 1962. Extreme spindles: correlation of electroencephalographic sleep pattern with mental retardation. *Science (New York, N.Y.)*, 138(3545), pp.1106–7.

Girardeau, G. & Zugaro, M., 2011. Hippocampal ripples and memory consolidation. *Current Opinion in Neurobiology*, 21(3), pp.452–9.

Golshani, P., Liu, X.B. & Jones, E.G., 2001. Differences in quantal amplitude reflect GluR4- subunit number at corticothalamic synapses on two populations of thalamic neurons. *Proceedings of the National Academy of Sciences of the United States of America*, 98(7), pp.4172–7.

González-Rueda, A. et al., 2018. Activity-Dependent Downscaling of Subthreshold Synaptic Inputs during Slow-Wave-Sleep-like Activity In Vivo. *Neuron*.

Gonzalo-Ruiz, a. & Lieberman, A., 1995. GABAergic projections from the thalamic reticular nucleus to the anteroventral and anterodorsal thalamic nuclei of the rat. *Journal of Chemical Neuroanatomy*, 9(3), pp.165–174.

Gonzalo-Ruiz, a & Lieberman, a R., 1995. Topographic organization of projections from the thalamic reticular nucleus to the anterior thalamic nuclei in the rat. *Brain Research Bulletin*, 37(1), pp.17–35.

Govindaiah & Cox, C.L., 2004. Synaptic activation of metabotropic glutamate receptors regulates dendritic outputs of thalamic interneurons. *Neuron*, 41(4), pp.611–23.

Govindaiah, G. et al., 2010. Regulation of inhibitory synapses by presynaptic D_4 dopamine receptors in thalamus. *Journal of Neurophysiology*, 104(5), pp.2757–65.

Graber, M. & Burgunder, J.M., 1996. Ontogeny of vasoactive intestinal peptide gene expression in rat brain. *Anatomy and Embryology*, 194(6), pp.595–605.

Gradinaru, V., Thompson, K.R. & Deisseroth, K., 2008. eNpHR: A Natronomonas halorhodopsin enhanced for optogenetic applications. *Brain Cell Biology*, 36(1–4), pp.129–139.

Gray, C.M. & McCormick, D.A., 1996. Chattering cells: superficial pyramidal neurons contributing to the generation of synchronous oscillations in the visual cortex. *Science (New York, N.Y.)*, 274(5284), pp.109–13.

Grieve, K.L., Acuña, C. & Cudeiro, J., 2000. The primate pulvinar nuclei: vision and action. *Trends in Neurosciences*, 23(1), pp.35–9.

Van Groen, T. & Wyss, J.M., 1995. Projections from the anterodorsal and anteroventral nucleus of the thalamus to the limbic cortex in the rat. *The Journal of Comparative Neurology*, 358(4), pp.584–604.

Groenewegen, H.J., 1988. Organization of the afferent connections of the mediodorsal thalamic nucleus in the rat, related to the mediodorsal-prefrontal topography. *Neuroscience*, 24(2), pp.379–431.

Gu, W. et al., 2004. The Prolactin-Releasing Peptide Receptor (GPR10) Regulates Body Weight Homeostasis in Mice. *Journal of Molecular Neuroscience*, 22(1–2), pp.93–104.

Gu, Z. et al., 2012. Regulation of *N* -Methyl-d-aspartic Acid (NMDA) Receptors by Metabotropic Glutamate Receptor 7. *Journal of Biological Chemistry*, 287(13), pp.10265–10275.

Guetg, N. et al., 2009. The GABAB1a isoform mediates heterosynaptic depression at hippocampal mossy fiber synapses. *The Journal of Neuroscience*, 29(5),

pp.1414–23.

Guilbaud, G., 1986. [Role of the ventrobasal complex of the thalamus in nociception and pain: data obtained in the normal rat and in a model of clinical pain]. *Revue Neurologique*, 142(4), pp.291–6.

Guillery, R., Feig, S. & Lozsadi, D., 1998. Paying attention to the thalamic reticular nucleus. *Trends in Neurosciences*, 2236(97), pp.28–32.

Guillery, R. & Harting, J., 2003. Structure and connections of the thalamic reticular nucleus: advancing views over half a century. *Journal of Comparative Neurology*, 463(4), pp.360–371.

Guillery, R.W., 1995. Anatomical evidence concerning the role of the thalamus in corticocortical communication: a brief review. *Journal of Anatomy*, 187, Pt 3, pp.583–92.

Gustin, S.M. et al., 2014. Thalamic activity and biochemical changes in individuals with neuropathic pain after spinal cord injury. *Pain*, 155(5), pp.1027–36.

Halassa, M.M. et al., 2011a. Selective optical drive of thalamic reticular nucleus generates thalamic bursts and cortical spindles. *Nature Neuroscience*, 14(9), pp.1118–20.

Halassa, M.M. et al., 2011b. Selective optical drive of thalamic reticular nucleus generates thalamic bursts and cortical spindles. *Nature Neuroscience*, 14(9), pp.1118–20.

Halassa, M.M. et al., 2014. State-Dependent Architecture of Thalamic Reticular Subnetworks. *Cell*, 158(4), pp.808–821.

Halassa, M.M. & Acsády, L., 2016. Thalamic Inhibition: Diverse Sources, Diverse Scales. *Trends in Neurosciences*, 39(10), pp.680–693.

Hallanger, A.E. et al., 1987a. The origins of cholinergic and other subcortical afferents to the thalamus in the rat. *The Journal of Comparative Neurology*, 262(1), pp.105–24.

Hallanger, A.E. et al., 1987b. The origins of cholinergic and other subcortical afferents to the thalamus in the rat. *The Journal of Comparative Neurology*, 262(1), pp.105–24.

Han, X., 2012. Optogenetics in the nonhuman primate. *Progress in Brain Research*, 196, pp.215–33.

Han, X. & Boyden, E.S., 2007. Multilpe-color optical activation, silencing, and desynchronization of neural activity, with single-spike temporal resolution. *PLoS ONE*, 2(3).

Hansel, D.E., Eipper, B.A. & Ronnett, G. V., 2001. Neuropeptide Y functions as a neuroproliferative factor. *Nature*, 410(6831), pp.940–944.

Harris, K.D. & Thiele, A., 2011. Cortical state and attention. *Nature Reviews Neuroscience*, 12(9), pp.509–523.

Harris, R.M., 1987. Axon collaterals in the thalamic reticular nucleus from thalamocortical neurons of the rat ventrobasal thalamus. *The Journal of Comparative Neurology*, 258(3), pp.397–406.

Hartings, J. a, Temereanca, S. & Simons, D.J., 2000. High responsiveness and direction sensitivity of neurons in the rat thalamic reticular nucleus to vibrissa deflections. *Journal of Neurophysiology*, 83(5), pp.2791–801.

Hartings, J.A., Temereanca, S. & Simons, D.J., 2003. State-dependent processing of sensory stimuli by thalamic reticular neurons. *The Journal of Neuroscience*, 23(12), pp.5264–71.

Hasenstaub, A. et al., 2005. Inhibitory Postsynaptic Potentials Carry Synchronized Frequency Information in Active Cortical Networks. *Neuron*, 47(3), pp.423–435.

Häusler, R. & Levine, R.A., 2000. Auditory dysfunction in stroke. *Acta oto-laryngologica*, 120(6), pp.689–703.

Hayama, T., Hashimoto, K. & Ogawa, H., 1994. Anatomical location of a taste-related region in the thalamic reticular nucleus in rats. *Neuroscience Research*, 18(4),

pp.291–9.

Hazrati, L.N. & Parent, A., 1991a. Contralateral pallidothalamic and pallidotegmental projections in primates: an anterograde and retrograde labeling study. *Brain Research*, 567(2), pp.212–23.

Hazrati, L.N. & Parent, A., 1991b. Projection from the external pallidum to the reticular thalamic nucleus in the squirrel monkey. *Brain Research*, 550(1), pp.142–6.

Hazrati, L.N., Pinault, D. & Parent, A., 1995. The thalamic reticular nucleus does not send commissural projection to the contralateral parafascicular nucleus in the rat. *Brain Research*, 679(1), pp.123–34.

Heath, C.J. & Jones, E.G., 1971. An experimental study of ascending connections from the posterior group of thalamic nuclei in the cat. *The Journal of Comparative Neurology*, 141(4), pp.397–425.

Hembrook, J.R., Onos, K.D. & Mair, R.G., 2012. Inactivation of ventral midline thalamus produces selective spatial delayed conditional discrimination impairment in the rat. *Hippocampus*, 22(4), pp.853–60.

Hembrook, J.R., Onos, K.D. & Mair, R.G., 2012. Inactivation of ventral midline thalamus produces selective spatial delayed conditional discrimination impairment in the rat. *Hippocampus*, 22(4), pp.853–860.

Henderson, L.A. et al., 2013. Chronic Pain: Lost Inhibition? *Journal of Neuroscience*, 33(17), pp.7574–7582.

Henderson, L.A. & Di Pietro, F., 2016. How do neuroanatomical changes in individuals with chronic pain result in the constant perception of pain? *Pain Management*, 6(2), pp.147–159.

Henkel, C.K., 1983. Evidence of sub-collicular auditory projections to the medial geniculate nucleus in the cat: an autoradiographic and horseradish peroxidase study. *Brain Research*, 259(1), pp.21–30.

Henley, J.M. & Wilkinson, K.A., 2013. AMPA receptor trafficking and the mechanisms underlying synaptic plasticity and cognitive aging. *Dialogues in Clinical Neuroscience*, 15(1), pp.11–27.

Herkenham, M., 1978. The connections of the nucleus reuniens thalami: evidence for a direct thalamo-hippocampal pathway in the rat. *The Journal of Comparative Neurology*, 177(4), pp.589–610.

Herrera, C.G. et al., 2015a. Hypothalamic feedforward inhibition of thalamocortical network controls arousal and consciousness. *Nature Neuroscience*, 19(December), pp.1–12.

Herrera, C.G. et al., 2015b. Hypothalamic feedforward inhibition of thalamocortical network controls arousal and consciousness. *Nature Neuroscience*, (December), pp.1–12.

Herron, P., 1983. The connections of cortical somatosensory areas I and II with separate nuclei in the ventroposterior thalamus in the raccoon. *Neuroscience*, 8(2), pp.243–57.

Hinuma, S. et al., 1998. A prolactin-releasing peptide in the brain. *Nature*, 393(6682), pp.272–276.

Hirai, T. & Jones, E.G., 1989. A new parcellation of the human thalamus on the basis of histochemical staining. *Brain Research. Brain research reviews*, 14(1), pp.1–34.

Hobson, J.A., Pace-Schott, E.F. & Stickgold, R., 2000. Dreaming and the brain: toward a cognitive neuroscience of conscious states. *The Behavioral and Brain Sciences*, 23(6), pp.793-842.

Hodgkin, A.L., 1976. Chance and design in electrophysiology: an informal account of certain experiments on nerve carried out between 1934 and 1952. *The Journal of Physiology*, 263(I), pp.1–21.

Hodgkin, A.L. & Huxley, A.F., 1952. A quantitative description of membrane current

and its application to conduction and excitation in nerve. *The Journal of Physiology*, 117(4), pp.500–44.

Hollis, D.M. & Boyd, S.K., 2005. Distribution of GABA-Like Immunoreactive Cell Bodies in the Brains of Two Amphibians. *Brain, Behavior and Evolution*, 65(2), pp.127–142.

Hoogland, P. V, Welker, E. & Van der Loos, H., 1987. Organization of the projections from barrel cortex to thalamus in mice studied with Phaseolus vulgaris-leucoagglutinin and HRP. *Experimental Brain Research*, 68(1), pp.73–87.

Hoover, W.B. & Vertes, R.P., 2007. Anatomical analysis of afferent projections to the medial prefrontal cortex in the rat. *Brain Structure & Function*, 212(2), pp.149–79.

Hou, G., Smith, A.G. & Zhang, Z.-W., 2016. Lack of Intrinsic GABAergic Connections in the Thalamic Reticular Nucleus of the Mouse. *The Journal of neuroscience*, 36(27), pp.7246–52.

Hsu, D.T. et al., 2014. Contributions of the paraventricular thalamic nucleus in the regulation of stress, motivation, and mood. *Frontiers in Behavioral Neuroscience*, 8, p.73.

Huang, Q. et al., 1992. Immunohistochemical localization of the D1 dopamine receptor in rat brain reveals its axonal transport, pre- and postsynaptic localization, and prevalence in the basal ganglia, limbic system, and thalamic reticular nucleus. *Proceedings of the National Academy of Sciences of the United States of America*, 89(24), pp.11988–92.

Hughes, S.W. & Crunelli, V., 2005. Thalamic mechanisms of EEG alpha rhythms and their pathological implications. *The Neuroscientist: a review journal bringing neurobiology, neurology and psychiatry*, 11(4), pp.357–72.

Huguenard, J. & McCormick, D., 2007. Thalamic synchrony and dynamic regulation of global forebrain oscillations. *Trends in Neurosciences*, 30(7), pp.350–356.

Huguenard, J.R., 1996. Low-threshold calcium currents in central nervous system neurons. *Annual Review of Physiology*, 58, pp.329–48.

Huguenard, J.R. & Prince, D. a, 1992. A novel T-type current underlies prolonged Ca(2+)-dependent burst firing in GABAergic neurons of rat thalamic reticular nucleus. *The Journal of Neuroscience*, 12(10), pp.3804–17.

Huntsman, M.M. et al., 1999. Reciprocal inhibitory connections and network synchrony in the mammalian thalamus. *Science (New York, N.Y.)*, 283(5401), pp.541–3.

Huntsman, M.M. & Huguenard, J.R., 2000. Nucleus-Specific Differences in GABA $_A$ -Receptor-Mediated Inhibition Are Enhanced During Thalamic Development. *Journal of Neurophysiology*, 83(1), pp.350–358.

Huntsman, M.M., Leggio, M.G. & Jones, E.G., 1996. Nucleus-specific expression of GABA(A) receptor subunit mRNAs in monkey thalamus. *The Journal of Neuroscience*, 16(11), pp.3571–89.

Ibata, Y. et al., 2000. Morphological survey of prolactin-releasing peptide and its receptor with special reference to their functional roles in the brain. *Neuroscience Research*, 38(3), pp.223–30.

Ikeda, H. et al., 2015. Inhibition of opioid systems in the hypothalamus as well as the mesolimbic area suppresses feeding behavior of mice. *Neuroscience*, 311, pp.9–21.

Ishizuka, T. et al., 2006. Kinetic evaluation of photosensitivity in genetically engineered neurons expressing green algae light-gated channels. *Neuroscience Research*, 54(2), pp.85–94.

Ito, H. et al., 2013. Analysis of sleep disorders under pain using an optogenetic tool: possible involvement of the activation of dorsal raphe nucleus-serotonergic neurons. *Molecular Brain*, 6(1), p.59.

Jaeger, D. & Kita, H., 2011. Functional connectivity and integrative properties of

globus pallidus neurons. *Neuroscience*, 198, pp.44–53.

Jagannath, A., Peirson, S.N. & Foster, R.G., 2013. Sleep and circadian rhythm disruption in neuropsychiatric illness. *Current Opinion in Neurobiology*, 23(5), pp.888–894.

James, M.H. et al., 2011. Propensity to "relapse" following exposure to cocaine cues is associated with the recruitment of specific thalamic and epithalamic nuclei. *Neuroscience*, 199, pp.235–42.

Jankowski, M.M. et al., 2013. The anterior thalamus provides a subcortical circuit supporting memory and spatial navigation. *Frontiers in Systems Neuroscience*, 7, p.45.

Jasper, P.H. & Andrews, H.., 1938. Electroencephalography.III Normal differentiation of occipital and precentral regions in man. *Archives of Neurology & Psychiatry*, 39(1), p.96.

Jin, C.Y., Kalimo, H. & Panula, P., 2002. The histaminergic system in human thalamus: correlation of innervation to receptor expression. *The European Journal of Neuroscience*, 15(7), pp.1125–38.

Jones, B.E., 2005. From waking to sleeping: neuronal and chemical substrates. *Trends in Pharmacological Sciences*, 26(11), pp.578–586.

Jones, E., 1985. *The thalamus*.

Jones, E.G., 1975. Some aspects of the organization of the thalamic reticular complex. *The Journal of Comparative Neurology*, 162(3), pp.285–308.

Jones, E.G., 1991. The anatomy of sensory relay functions in the thalamus. *Progress in Brain Research*, 87, pp.29–52.

Jones, E.G. & Powell, T.P., 1971. An analysis of the posterior group of thalamic nuclei on the basis of its afferent connections. *The Journal of Comparative Neurology*, 143(2), pp.185–216.

Jordan, H., 1973. The structure of the medial geniculate nucleus (MGN): A cyto- and myeloarchitectonic study in the squirrel monkey. *The Journal of Comparative Neurology*, 148(4), pp.469–479.

Jouvet, M., 1969. Biogenic amines and the states of sleep. *Science (New York, N.Y.)*, 163(3862), pp.32–41.

Karavanova, I. et al., 2007. Novel regional and developmental NMDA receptor expression patterns uncovered in NR2C subunit-beta-galactosidase knock-in mice. *Molecular and Cellular Neurosciences*, 34(3), pp.468–80.

Katz, B. & Miledi, R., 1969. Spontaneous and evoked activity of motor nerve endings in calcium Ringer. *The Journal of Physiology*, 203(3), pp.689–706.

Kaufman, A.B., Colbert-White, E.N. & Burgess, C., 2013. Higher-order semantic structures in an African Grey parrot's vocalizations: evidence from the hyperspace analog to language (HAL) model. *Animal Cognition*, 16(5), pp.789–801.

Kawaguchi, Y. et al., 1987. Fast spiking cells in rat hippocampus (CA1 region) contain the calcium-binding protein parvalbumin. *Brain Research*, 416(2), pp.369–74.

Kayahara, T. & Nakano, K., 1998. The globus pallidus sends axons to the thalamic reticular nucleus neurons projecting to the centromedian nucleus of the thalamus: a light and electron microscope study in the cat. *Brain Research Bulletin*, 45(6), pp.623–30.

Keifer, O.P. et al., 2015. A comparative analysis of mouse and human medial geniculate nucleus connectivity: a DTI and anterograde tracing study. *NeuroImage*, 105, pp.53–66.

Kenigfest, N. et al., 2005. The turtle thalamic anterior entopeduncular nucleus shares connectional and neurochemical characteristics with the mammalian thalamic reticular nucleus. *Journal of Chemical Neuroanatomy*, 30(2–3), pp.129–143.

Khan, Z.U. et al., 1998. Differential regional and cellular distribution of dopamine D2-

like receptors: an immunocytochemical study of subtype-specific antibodies in rat and human brain. *The Journal of Comparative Neurology*, 402(3), pp.353–71.

Kilner, J.M. et al., 2000. Human cortical muscle coherence is directly related to specific motor parameters. *The Journal of Neuroscience*, 20(23), pp.8838–45.

Kim, A. et al., 2012. Optogenetically induced sleep spindle rhythms alter sleep architectures in mice. *Proceedings of the National Academy of Sciences of the United States of America*, 109(50), pp.20673–8.

Kim, D. et al., 2015. Characterization of Topographically Specific Sleep Spindles in Mice. *Sleep*, 38(1), pp.85–96.

Kim, J.A. & Connors, B.W., 2012. High temperatures alter physiological properties of pyramidal cells and inhibitory interneurons in hippocampus. *Frontiers in Cellular Neuroscience*, 6, p.27.

Kim, U. & Mccormick, D., 1998. Functional and ionic properties of a slow afterhyperpolarization in ferret perigeniculate neurons in vitro. *Journal of Neurophysiology*, pp.1222–1235.

Kimura, A. et al., 2007. Axonal projections of single auditory neurons in the thalamic reticular nucleus: implications for tonotopy-related gating function and cross-modal modulation. *European Journal of Neuroscience*, 26(12), pp.3524–3535.

Kinney, H.C. & Samuels, M.A., 1994. Neuropathology of the persistent vegetative state. A review. *Journal of Neuropathology and Experimental neurology*, 53(6), pp.548–58.

Kirouac, G.J., Parsons, M.P. & Li, S., 2005. Orexin (hypocretin) innervation of the paraventricular nucleus of the thalamus. *Brain Research*, 1059(2), pp.179–88.

Klimesch, W., 1999. EEG alpha and theta oscillations reflect cognitive and memory performance: a review and analysis. *Brain Research. Brain research reviews*, 29(2–3), pp.169–95.

Klockgether, T. et al., 1986. The rat ventromedial thalamic nucleus and motor control:

role of N-methyl-D-aspartate-mediated excitation, GABAergic inhibition, and muscarinic transmission. *The Journal of Neuroscience : the official journal of the Society for Neuroscience*, 6(6), pp.1702–11.

Koella, W.P. & Czicman, J., 1966. Mechanism of the EEG-synchronizing action of serotonin. *The American Journal of Physiology*, 211(4), pp.926–34.

Köhr, G., Lambert, C.E. & Mody, I., 1991. Calbindin-D28K (CaBP) levels and calcium currents in acutely dissociated epileptic neurons. *Experimental Brain Research*, 85(3), pp.543–51.

Kolmac, C. & Mitrofanis, J., 1999. Distribution of various neurochemicals within the zona incerta: an immunocytochemical and histochemical study. *Anatomy and Embryology*, 199(3), pp.265–280.

Kolmac, C.I. & Mitrofanis, J., 1997a. Organisation of the reticular thalamic projection to the intralaminar and midline nuclei in rats. *The Journal of Comparative Neurology*, 377(2), pp.165–78.

Kolmac, C.I. & Mitrofanis, J., 1997b. Organisation of the reticular thalamic projection to the intralaminar and midline nuclei in rats. *The Journal of Comparative Neurology*, 377(2), pp.165–78.

Kolmac, C.I. & Mitrofanis, J., 1998. Patterns of brainstem projection to the thalamic reticular nucleus. *The Journal of Comparative Neurology*, 396(4), pp.531–43.

Krol, A. et al., 2018. Thalamic Reticular Dysfunction as a Circuit Endophenotype in Neurodevelopmental Disorders. *Neuron*, 98(2), pp.282–295.

Krout, K.E., Belzer, R.E. & Loewy, A.D., 2002. Brainstem projections to midline and intralaminar thalamic nuclei of the rat. *The Journal of Comparative Neurology*, 448(1), pp.53–101.

Kudo, M. & Niimi, K., 1980. Ascending projections of the inferior colliculus in the cat: An autoradiographic study. *The Journal of Comparative Neurology*, 191(4), pp.545–556.

Kudrimoti, H.S., Barnes, C.A. & McNaughton, B.L., 1999. Reactivation of hippocampal cell assemblies: effects of behavioral state, experience, and EEG dynamics. *The Journal of Neuroscience*, 19(10), pp.4090–101.

Kultas-Ilinsky, K., Yi, H. & Ilinsky, I., 1995. Nucleus reticularis thalami input to the anterior thalamic nuclei in the monkey: a light and electron microscopic study. *Neuroscience Letters*, 186(1), pp.25–28.

Kuramoto, E. et al., 2011. Complementary distribution of glutamatergic cerebellar and GABAergic basal ganglia afferents to the rat motor thalamic nuclei. *The European Journal of Neuroscience*, 33(1), pp.95–109.

De La Mothe, L.A. et al., 2006. Thalamic connections of the auditory cortex in marmoset monkeys: Core and medial belt regions. *The Journal of Comparative Neurology*, 496(1), pp.72–96.

Lacoste, B. et al., 2015. Anatomical and cellular localization of melatonin MT_1 and MT_2 receptors in the adult rat brain. *Journal of Pineal Research*, 58(4), pp.397–417.

Landisman, C.E. et al., 2002. Electrical synapses in the thalamic reticular nucleus. *The Journal of Neuroscience*, 22(3), pp.1002–9.

Landisman, C.E. & Connors, B.W., 2005. Long-Term Modulation of Electrical Synapses in the Mammalian Thalamus. *Science*, 310(5755), pp.1809–1813.

Landolt, H.-P. et al., 2006. Sleep-wake disturbances in sporadic Creutzfeldt-Jakob disease. *Neurology*, 66(9), pp.1418–24.

Laroche, S., Davis, S. & Jay, T.M., 2000. Plasticity at hippocampal to prefrontal cortex synapses: dual roles in working memory and consolidation. *Hippocampus*, 10(4), pp.438–46.

Lasiter, P.S., 1985. Thalamocortical relations in taste aversion learning: II. Involvement of the medial ventrobasal thalamic complex in taste aversion learning. *Behavioral Neuroscience*, 99(3), pp.477–95.

Latchoumane, C.-F. V. et al., 2017. Thalamic Spindles Promote Memory Formation during Sleep through Triple Phase-Locking of Cortical, Thalamic, and Hippocampal Rhythms. *Neuron*, 95(2), p.424–435.

Lau, D. et al., 2000. Impaired fast-spiking, suppressed cortical inhibition, and increased susceptibility to seizures in mice lacking Kv3.2 K+ channel proteins. *The Journal of Neuroscience*, 20(24), pp.9071–85.

Lazarus, M. et al., 2013. Role of the basal ganglia in the control of sleep and wakefulness. *Curr. Opin. Neurobiol*, 23(5), pp.780–785.

Lechner, J., Leah, J.D. & Zimmermann, M., 1993. Brainstem peptidergic neurons projecting to the medial and lateral thalamus and zona incerta in the rat. *Brain Research*, 603(1), pp.47–56.

Ledoux, J.E. et al., 1987. Topographic organization of convergent projections to the thalamus from the inferior colliculus and spinal cord in the rat. *The Journal of Comparative Neurology*, 264(1), pp.123–146.

LeDoux, J.E., Farb, C. & Ruggiero, D.A., 1990. Topographic organization of neurons in the acoustic thalamus that project to the amygdala. *The Journal of Neuroscience*, 10(4), pp.1043–54.

LeDoux, J.E., Sakaguchi, A. & Reis, D.J., 1984. Subcortical efferent projections of the medial geniculate nucleus mediate emotional responses conditioned to acoustic stimuli. *The Journal of Neuroscience*, 4(3), pp.683–98.

Lee, K.H. & McCormick, D. a, 1997. Modulation of spindle oscillations by acetylcholine, cholecystokinin and 1S,3R-ACPD in the ferret lateral geniculate and perigeniculate nuclei in vitro. *Neuroscience*, 77(2), pp.335–50.

Lee, K.H. & McCormick, D.A., 1995. Acetylcholine excites GABAergic neurons of the ferret perigeniculate nucleus through nicotinic receptors. *Journal of Neurophysiology*, 73(5), pp.2123–8.

Lee, S.-H. & Cox, C.L., 2003. Vasoactive intestinal peptide selectively depolarizes

thalamic relay neurons and attenuates intrathalamic rhythmic activity. *Journal of Neurophysiology*, 90(2), pp.1224–34.

Lee, S.-H., Govindaiah, G. & Cox, C.L., 2007. Heterogeneity of firing properties among rat thalamic reticular nucleus neurons. *The Journal of Physiology*, 582(1), pp.195–208.

Lee, S. et al., 2011. Bidirectional modulation of fear extinction by mediodorsal thalamic firing in mice. *Nature Neuroscience*, 15(2), pp.308–314.

Lee, S.A. et al., 2015. Working memory and reference memory tests of spatial navigation in mice (Mus musculus). *Journal of Comparative Psychology*, 129(2), pp.189–197.

Leonard, C., 1969. The prefrontal cortex of the rat. I. Cortical projection of the mediodorsal nucleus. II. Efferent connections. *Brain research*, 10021, pp.321–343.

Lesica, N. a et al., 2006. Dynamic encoding of natural luminance sequences by LGN bursts. *PLoS biology*, 4(7), p.e209.

Levenga, J. et al., 2018. Sleep Behavior and EEG Oscillations in Aged Dp(16)1Yey/+ Mice: A Down Syndrome Model. *Neuroscience*, 376, pp.117–126.

Lewis, L.D. et al., 2015. Thalamic reticular nucleus induces fast and local modulation of arousal state. *eLife*, 4(October).

Li, D. et al., 2006. Meta-analysis shows significant association between dopamine system genes and attention deficit hyperactivity disorder (ADHD). *Human Molecular Genetics*, 15(14), pp.2276–2284.

Li, H. & Mizuno, N., 1997. Collateral projections from single neurons in the dorsal column nuclei to the inferior colliculus and the ventrobasal thalamus: a retrograde double-labeling study in the rat. *Neuroscience Letters*, 225(1), pp.21–4.

Li, S. & Kirouac, G.J., 2008. Projections from the paraventricular nucleus of the

thalamus to the forebrain, with special emphasis on the extended amygdala. *The Journal of Comparative Neurology*, 506(2), pp.263–87.

Li, X. et al., 2005. Fast noninvasive activation and inhibition of neural and network activity by vertebrate rhodopsin and green algae channelrhodopsin. *Proceedings of the National Academy of Sciences of the United States of America*, 102(49), pp.17816–17821.

Liao, L.-D. et al., 2013. Imaging of temperature dependent hemodynamics in the rat sciatic nerve by functional photoacoustic microscopy. *Biomedical Engineering Online*, 12, p.120.

Lin, S. et al., 2002. Prolactin-releasing peptide (PrRP) promotes awakening and suppresses absence seizures. *Neuroscience*, 114(1), pp.229–238.

Lisman, J.E. & Idiart, M.A., 1995. Storage of 7 +/- 2 short-term memories in oscillatory subcycles. *Science (New York, N.Y.)*, 267(5203), pp.1512–5.

Liu, J. et al., 2017. Activation of Parvalbumin Neurons in the Rostro-Dorsal Sector of the Thalamic Reticular Nucleus Promotes Sensitivity to Pain in Mice. *Neuroscience*, 366, pp.113–123.

Liu, K. et al., 2017. Corrigendum: Lhx6-positive GABA-releasing neurons of the zona incerta promote sleep. *Nature*, 550(7677), pp.548–548.

Livingstone, M. & Hubel, D., 1988. Segregation of form, color, movement, and depth: anatomy, physiology, and perception. *Science (New York, N.Y.)*, 240(4853), pp.740–9.

Lizier, C., Spreafico, R. & Battaglia, G., 1997. Calretinin in the thalamic reticular nucleus of the rat: distribution and relationship with ipsilateral and contralateral efferents. *Journal of Comparative Neurology*, 377(2), pp.217–233.

Llinás, R.R., Grace, A.A. & Yarom, Y., 1991. In vitro neurons in mammalian cortical layer 4 exhibit intrinsic oscillatory activity in the 10- to 50-Hz frequency range. *Proceedings of the National Academy of Sciences*, 88(3).

Llinás, R.R. & Steriade, M., 2006. Bursting of thalamic neurons and states of vigilance. *Journal of Neurophysiology*, 95(6), pp.3297–308.

Lo, C.-C. et al., 2004. Common scale-invariant patterns of sleep-wake transitions across mammalian species. *Proceedings of the National Academy of Sciences of the United States of America*, 101(50), pp.17545–8.

Long, M. a, Landisman, C.E. & Connors, B.W., 2004. Small clusters of electrically coupled neurons generate synchronous rhythms in the thalamic reticular nucleus. *The Journal of Neuroscience : the official journal of the Society for Neuroscience*, 24(2), pp.341–9.

Long, M.A. & Fee, M.S., 2008. Using temperature to analyse temporal dynamics in the songbird motor pathway. *Nature*, 456(7219), pp.189–94.

Lozsádi, D.A., 1995. Organization of connections between the thalamic reticular and the anterior thalamic nuclei in the rat. *The Journal of Comparative Neurology*, 358(2), pp.233–46.

Lozsádi, D.A., 1994. Organization of cortical afferents to the rostral, limbic sector of the rat thalamic reticular nucleus. *The Journal of Comparative Neurology*, 341(4), pp.520–33.

Lu, J. et al., 2000. Effect of lesions of the ventrolateral preoptic nucleus on NREM and REM sleep. *The Journal of Neuroscience*, 20(10), pp.3830–42.

Lübke, J., 1993. Morphology of neurons in the thalamic reticular nucleus (TRN) of mammals as revealed by intracellular injections into fixed brain slices. *The Journal of Comparative Neurology*, 329(4), pp.458–71.

Lukas, W. & Jones, K.A., 1994. Cortical neurons containing calretinin are selectively resistant to calcium overload and excitotoxicity in vitro. *Neuroscience*, 61(2), pp.307–16.

Luo, M. & Perkel, D.J., 1999. A GABAergic, strongly inhibitory projection to a thalamic nucleus in the zebra finch song system. *The Journal of Neuroscience*, 19(15),

pp.6700–11.

M'Harzi, M. et al., 1991. Selective fimbria and thalamic lesions differentially impair forms of working memory in rats. *Behavioral and neural biology*, 56(3), pp.221–39.

MacLean, J.N. et al., 2005. Internal Dynamics Determine the Cortical Response to Thalamic Stimulation. *Neuron*, 48(5), pp.811–823.

Magistretti, P.J., 1986. Intercellular communication mediated by VIP in the cerebral cortex. *Peptides*, 7 Suppl 1, pp.169–73.

Magistretti, P.J., 1990. VIP neurons in the cerebral cortex. *Trends in Pharmacological Sciences*, 11(6), pp.250–4.

Mair, R.G., Burk, J.A. & Porter, M.C., 1998. Lesions of the frontal cortex, hippocampus, and intralaminar thalamic nuclei have distinct effects on remembering in rats. *Behavioral Neuroscience*, 112(4), pp.772–92.

Mair, R.G. & Hembrook, J.R., 2008. Memory enhancement with event-related stimulation of the rostral intralaminar thalamic nuclei. *The Journal of Neuroscience*, 28(52), pp.14293–300.

Majak, K. et al., 1998. Parvalbumin immunoreactivity changes in the thalamic reticular nucleus during the maturation of the rat's brain. *Folia Neuropathologica*, 36(1), pp.7–14.

Mallet, N. et al., 2012. Dichotomous Organization of the External Globus Pallidus. *Neuron*, 74(6), pp.1075–1086.

Manning, K.A., Wilson, J.R. & Uhlrich, D.J., 1996. Histamine-immunoreactive neurons and their innervation of visual regions in the cortex, tectum, and thalamus in the primate Macaca mulatta. *The Journal of Comparative Neurology*, 373(2), pp.271–82.

Manshanden, I. et al., 2002. Source localization of MEG sleep spindles and the relation to sources of alpha band rhythms. *Clinical Neurophysiology*, 113(12),

pp.1937–47.

Marchant, N.J., Furlong, T.M. & McNally, G.P., 2010. Medial dorsal hypothalamus mediates the inhibition of reward seeking after extinction. *The Journal of Neuroscience*, 30(42), pp.14102–15.

Marco-Pallares, J. et al., 2008. Human oscillatory activity associated to reward processing in a gambling task. *Neuropsychologia*, 46(1), pp.241–248.

Marks, G. & Roffwarg, H., 1993. Spontaneous activity in the thalamic reticular nucleus during the sleep/wake cycle of the freely-moving rat. *Brain Research*, 623, pp.241–248.

McAlonan, K., 2006. Attentional modulation of thalamic reticular neurons. *The Journal of neuroscience*, 26(16), pp.4444–4450.

McAlonan, K., Cavanaugh, J. & Wurtz, R., 2008. Guarding the gateway to cortex with attention in visual thalamus. *Nature*, 456(7220), pp.391–394.

McCormick, D. & Prince, D., 1986. Acetylcholine induces burst firing in thalamic reticular neurones by activating a potassium conductance. *Nature*, pp.402–405.

McCormick, D. & Wang, Z., 1991. Serotonin and noradrenaline excite GABAergic neurones of the guinea-pig and cat nucleus reticularis thalami. *The Journal of Physiology*, pp.235–255.

McCormick, D.A. & Bal, T., 1997. Sleep and arousal: thalamocortical mechanisms. *Annual Review of Neuroscience*, 20(1), pp.185–215.

McCormick, D.A. & Pape, H.C., 1990. Noradrenergic and serotonergic modulation of a hyperpolarization-activated cation current in thalamic relay neurones. *The Journal of Physiology*, 431, pp.319–42.

McGinty, D.J. & Sterman, M.B., 1968. Sleep suppression after basal forebrain lesions in the cat. *Science (New York, N.Y.)*, 160(3833), pp.1253–5.

McHugh, P.C. & Buckley, D.A., 2015. The Structure and Function of the Dopamine

Transporter and its Role in CNS Diseases. In *Vitamins and Hormones*. pp. 339–369.

Melloni, L. et al., 2007. Synchronization of neural activity across cortical areas correlates with conscious perception. *The Journal of Neuroscience : the official journal of the Society for Neuroscience*, 27(11), pp.2858–65.

Mena-Segovia, J., 2016. Structural and functional considerations of the cholinergic brainstem. *Journal of Neural Transmission*, 123(7), pp.731–736.

Mesulam, M.-M. et al., 1983. Cholinergic innervation of cortex by the basal forebrain: Cytochemistry and cortical connections of the septal area, diagonal band nuclei, nucleus basalis (Substantia innominata), and hypothalamus in the rhesus monkey. *The Journal of Comparative Neurology*, 214(2), pp.170–197.

Min, B.-K., 2010. A thalamic reticular networking model of consciousness. *Theoretical Biology and Medical Modelling*, 7(1), p.10.

Mineff, E.M. & Weinberg, R.J., 2000. Differential synaptic distribution of AMPA receptor subunits in the ventral posterior and reticular thalamic nuclei of the rat. *Neuroscience*, 101(4), pp.969–82.

Mitrofanis, J., 1992a. Calbindin immunoreactivity in a subset of cat thalamic reticular neurons. *Journal of Neurocytology*, 21(7), pp.495–505.

Mitrofanis, J., 1992b. Patterns of antigenic expression in the thalamic reticular nucleus of developing rats. *The Journal of Comparative Neurology*, 320(2), pp.161–81.

Mitrofanis, J., 2005. Some certainty for the “zone of uncertainty”? Exploring the function of the zona incerta. *Neuroscience*, 130(1), pp.1–15.

Molinari, M., Hendry, S.H. & Jones, E.G., 1987. Distributions of certain neuropeptides in the primate thalamus. *Brain Research*, 426(2), pp.270–89.

Montero, V., Guillery, R. & Woolsey, C., 1977. Retinotopic organization within the thalamic reticular nucleus demonstrated by a double label autoradiographic

technique. *Brain Research*, 138, pp.407–421.

Montero, V.M. & Scott, G.L., 1981. Synaptic terminals in the dorsal lateral geniculate nucleus from neurons of the thalamic reticular nucleus: a light and electron microscope autoradiographic study. *Neuroscience*, 6(12), pp.2561–77.

Moriizumi, T. & Hattori, T., 1992. Ultrastructural morphology of projections from the medial geniculate nucleus and its adjacent region to the basal ganglia. *Brain Research Bulletin*, 29(2), pp.193–8.

Morin, L.P. & Studholme, K.M., 2014. Retinofugal projections in the mouse. *Journal of Comparative Neurology*, 522(16), pp.3733–3753.

Morris, B.J., 1989. Neuronal localisation of neuropeptide Y gene expression in rat brain. *The Journal of Comparative Neurology*, 290(3), pp.358–68.

Morrison, J.H. & Foote, S.L., 1986. Noradrenergic and serotoninergic innervation of cortical, thalamic, and tectal visual structures in Old and New World monkeys. *The Journal of Comparative Neurology*, 243(1), pp.117–38.

Moruzzi, G. & Magoun, H.W., 1949. Brain stem reticular formation and activation of the EEG. *Electroencephalography and Clinical Neurophysiology*, 1(4), pp.455–73.

Moser, M.& A., 1993. Association Between Brain Temperature and Dentate Field Potentials in Exploring and Swimming Rats. *Science*, p.Volume: 259, Issue: 5099, Pages: 1324-1326.

Motomura, K. & Kosaka, T., 2011a. Medioventral part of the posterior thalamus in the mouse. *Journal of Chemical Neuroanatomy*, 42(3), pp.192–209.

Motomura, K. & Kosaka, T., 2011b. Medioventral part of the posterior thalamus in the mouse. *Journal of Chemical Neuroanatomy*, 42(3), pp.192–209.

Mrzljak, L. et al., 1996. Localization of dopamine D4 receptors in GABAergic neurons of the primate brain. *Nature*, 381, pp.245–248.

Mukhametov, LM, Rizzolatti, G, , Tradardi, V., 1970. Spontaneous activity of neurones

of nucleus reticularis thalami in freely moving cats. *The Journal of Physiology*, pp.651–667.

Mulholland, T.B., 1965. Occurrence of the electroencephalographic alpha rhythm with eyes open. *Nature*, 206(985), p.746.

Nagel, G. et al., 2003. Channelrhodopsin-2, a directly light-gated cation-selective membrane channel. *Proceedings of the National Academy of Sciences of the United States of America*, 100(24), pp.13940–5.

Nanobashvili, Z.I., Khizanishvili, N.A. & Bilanishvili, I.G., 2009. [Influence of solitary tract nucleus stimulation on activity of thalamic reticular nucleus and mesencephalic reticular formation of the brain]. *Georgian medical news*, (169), pp.74–8.

Nanobashvili, Z.I. & Narikashvili, S.P., 1985. [The locus coeruleus and neuronal activity of the thalamic reticular nucleus]. *Fiziologicheskii zhurnal SSSR imeni I. M. Sechenova*, 71(1), pp.15–21.

Nanobashvili, Z.I. & Narikashvili, S.P., 1986. Locus ceruleus and neuronal activity of the reticular nucleus of the thalamus. *Neuroscience and Behavioral Physiology*, 16(5), pp.430–6.

Nedeltcheva, A. V. & Scheer, F.A.J.L., 2014. Metabolic effects of sleep disruption, links to obesity and diabetes. *Current Opinion in Endocrinology & Diabetes and Obesity*, 21(4), pp.293–298.

Ni, K.-M. et al., 2016a. Selectively driving cholinergic fibers optically in the thalamic reticular nucleus promotes sleep. *eLife*, 5.

Ni, K.-M. et al., 2016b. Selectively driving cholinergic fibers optically in the thalamic reticular nucleus promotes sleep. *eLife*, 5.

Nishino, S. et al., 1997. Effects of thyrotropin-releasing hormone and its analogs on daytime sleepiness and cataplexy in canine narcolepsy. *The Journal of Neuroscience : the official journal of the Society for Neuroscience*, 17(16),

pp.6401–8.

Nissl, F., 1913. Die Grosshirnanteile des Kaninchens. *Arch. Psychiat.*, 2, pp.867–953.

Nusser, Z., Sieghart, W. & Somogyi, P., 1998. Segregation of different GABAA receptors to synaptic and extrasynaptic membranes of cerebellar granule cells. *The Journal of Neuroscience : the official journal of the Society for Neuroscience*, 18(5), pp.1693–703.

Nutt, D., 2006. GABAA receptors: subtypes, regional distribution, and function. *Journal of clinical sleep medicine : JCSM : official publication of the American Academy of Sleep Medicine*, 2(2), pp.S7-11.

Ochoa-Sanchez, R. et al., 2011. Promotion of non-rapid eye movement sleep and activation of reticular thalamic neurons by a novel MT2 melatonin receptor ligand. *The Journal of Neuroscience : the official journal of the Society for Neuroscience*, 31(50), pp.18439–52.

Ohara, P.T. & Havton, L.A., 1996. Dendritic arbors of neurons from different regions of the rat thalamic reticular nucleus share a similar orientation. *Brain Research*, 731(1–2), pp.236–40.

Ohara, P.T. & Lieberman, A.R., 1985a. The thalamic reticular nucleus of the adult rat: experimental anatomical studies. *Journal of Neurocytology*, 14(3), pp.365–411.

Ohtake, T. & Yamada, H., 1989. Efferent connections of the nucleus reuniens and the rhomboid nucleus in the rat: an anterograde PHA-L tracing study. *Neuroscience Research*, 6(6), pp.556–68.

Olivéras, J.L. & Montagne-Clavel, J., 1994. The GABAA receptor antagonist picrotoxin induces a “pain-like” behavior when administered into the thalamic reticular nucleus of the behaving rat: a possible model for “central” pain? *Neuroscience Letters*, 179(1–2), pp.21–4.

Olsen, R.W. & Sieghart, W., 2009a. GABAA receptors: Subtypes provide diversity of function and pharmacology. *Neuropharmacology*, 56(1), pp.141–148.

Olsen, R.W. & Sieghart, W., 2009b. GABAA receptors: Subtypes provide diversity of function and pharmacology. *Neuropharmacology*, 56(1), pp.141–148.

Otmakhova, N.A. & Lisman, J.E., 2004. Contribution of Ih and GABAB to synaptically induced afterhyperpolarizations in CA1: a brake on the NMDA response. *Journal of Neurophysiology*, 92(4), pp.2027–39.

Ottersen, O.P. & Ben-Ari, Y., 1979. Afferent connections to the amygdaloid complex of the rat and cat. I. Projections from the thalamus. *The Journal of Comparative Neurology*, 187(2), pp.401–24.

Pape, H.-C., Munsch, T. & Budde, T., 2004. Novel vistas of calcium-mediated signalling in the thalamus. *Pflugers Archiv : European journal of physiology*, 448(2), pp.131–8.

Papez, J.W., 1937. A proposed mechanism of emotion. *The Journal of Neuropsychiatry and Clinical Neurosciences*, 7(1), pp.103–112.

Paré, D. et al., 1987. Physiological characteristics of anterior thalamic nuclei, a group devoid of inputs from reticular thalamic nucleus. *Journal of Neurophysiology*, 57(6), pp.1669–85.

Paré, D. et al., 1988. Projections of brainstem core cholinergic and non-cholinergic neurons of cat to intralaminar and reticular thalamic nuclei. *Neuroscience*, 25(1), pp.69–86.

Paré, D. et al., 1990. Substantia nigra pars reticulata projects to the reticular thalamic nucleus of the cat: a morphological and electrophysiological study. *Brain Research*, 535(1), pp.139–46.

Paré, D. & Steriade, M., 1993. The reticular thalamic nucleus projects to the contralateral dorsal thalamus in macaque monkey. *Neuroscience Letters*, 154(1–2), pp.96–100.

Parent, A. et al., 1988. Basal forebrain cholinergic and noncholinergic projections to the thalamus and brainstem in cats and monkeys. *Journal of Comparative*

Neurology, 277(2), pp.281–301.

Park, A. et al., 2017. Presynaptic and extrasynaptic regulation of posterior nucleus of thalamus. pp.507–519.

Parker, R.M. & Herzog, H., 1999. Regional distribution of Y-receptor subtype mRNAs in rat brain. *The European Journal of Neuroscience*, 11(4), pp.1431–48.

Parnaudeau, S., O'Neill, P. & Bolkan, S., 2013. Inhibition of mediodorsal thalamus disrupts thalamofrontal connectivity and cognition. *Neuron*, 77(6), pp.1151–1162.

Pavlov, I.P., 1923. Address on "The Identity of Inhibition with Hypnosis and Sleep." *Quarterly Journal of Experimental Physiology*, 13(suppl), pp.39–43.

Paxinos, G. & Watson, C., 2007. *The rat brain in stereotaxic coordinates*, Elsevier.

Paz, J.T. et al., 2011. A new mode of corticothalamic transmission revealed in the Gria4−/− model of absence epilepsy. *Nature Neuroscience*, 14(9), pp.1167–1173.

Pazo, J.H. et al., 2013. Electrophysiologic study of globus pallidus projections to the thalamic reticular nucleus. *Brain Research Bulletin*, 94, pp.82–89.

Peng, Z.-C. & Bentivoglio, M., 2004. The thalamic paraventricular nucleus relays information from the suprachiasmatic nucleus to the amygdala: a combined anterograde and retrograde tracing study in the rat at the light and electron microscopic levels. *Journal of Neurocytology*, 33(1), pp.101–16.

Perez, A.C. et al., 2017. Normal and Pathological Cortical Rhythms. , 19(10), pp.2130–2142.

Périer, C. et al., 2002. Behavioral consequences of bicuculline injection in the subthalamic nucleus and the zona incerta in rat. *The Journal of Neuroscience : the official journal of the Society for Neuroscience*, 22(19), pp.8711–9.

Peschanski, M., Guilbaud, G. & Gautron, M., 1980. Neuronal responses to cutaneous

electrical and noxious mechanical stimuli in the nucleus reticularis thalami of the rat. *Neuroscience Letters*, 20(2), pp.165–70.

Petersen, C.C.H. et al., 2003. Interaction of sensory responses with spontaneous depolarization in layer 2/3 barrel cortex. *Proceedings of the National Academy of Sciences*, 100(23), pp.13638–13643.

Petralia, R.S. et al., 1997. A monoclonal antibody shows discrete cellular and subcellular localizations of mGluR1 alpha metabotropic glutamate receptors. *Journal of Chemical Neuroanatomy*, 13(2), pp.77–93.

Peyrache, A., Battaglia, F.P. & Destexhe, A., 2011. Inhibition recruitment in prefrontal cortex during sleep spindles and gating of hippocampal inputs. *Proceedings of the National Academy of Sciences of the United States of America*, 108(41), pp.17207–12.

Phillips, A.J.K. et al., 2010. Mammalian sleep dynamics: how diverse features arise from a common physiological framework. *PLoS computational biology*, 6(6), p.e1000826.

Piccolino, M. & Bresadola, M., 2013. *Shocking Frogs: Galvani, Volta, and the Electric Origins of Neuroscience*, Oxford University Press.

Pinard, A., Seddik, R. & Bettler, B., 2010a. GABAB Receptors: Physiological Functions and Mechanisms of Diversity. In *Advances in pharmacology (San Diego, Calif.)*. pp. 231–255.

Pinard, A., Seddik, R. & Bettler, B., 2010b. GABAB Receptors: Physiological Functions and Mechanisms of Diversity. In *Advances in Pharmacology (San Diego, Calif.)*. pp. 231–255.

Pinault, D., 2003. Cellular interactions in the rat somatosensory thalamocortical system during normal and epileptic 5–9 Hz oscillations. *The Journal of Physiology*, 552(3), pp.881–905.

Pinault, D., 2004b. The thalamic reticular nucleus: structure, function and concept.

Brain Research Reviews, 46(1), pp.1–31.

Pinault, D. & Deschênes, M., 1998a. Anatomical evidence for a mechanism of lateral inhibition in the rat thalamus. *The European Journal of Neuroscience*, 10(11), pp.3462–9.

Pinault, D. & Deschênes, M., 1992. Control of 40-Hz firing of reticular thalamic cells by neurotransmitters. *Neuroscience*, 51(2), pp.259–68.

Pinault, D. & Deschênes, M., 1998b. Projection and innervation patterns of individual thalamic reticular axons in the thalamus of the adult rat: a three-dimensional, graphic, and morphometric analysis. *The Journal of comparative neurology*, 391(2), pp.180–203.

Pinault, D., Smith, Y. & Deschênes, M., 1997. Dendrodendritic and axoaxonic synapses in the thalamic reticular nucleus of the adult rat. *The Journal of Neuroscience : the official journal of the Society for Neuroscience*, 17(9), pp.3215–33.

Pinto, L. et al., 2013. Fast modulation of visual perception by basal forebrain cholinergic neurons. *Nature Neuroscience*, 16(12), pp.1857–1863.

Pita-Almenar, J.D. et al., 2014. Mechanisms underlying desynchronization of cholinergic-evoked thalamic network activity. *The Journal of Neuroscience : the official journal of the Society for Neuroscience*, 34(43), pp.14463–74.

Pollin, B. & Rokyta, R., 1982. Somatotopic organization of nucleus reticularis thalami in chronic awake cats and monkeys. *Brain Research*, 250(2), pp.211–21.

Powe, C.E. et al., 2011. Effects of Recombinant Human Prolactin on Breast Milk Composition. *PEDIATRICS*, 127(2), pp.e359–e366.

Powell, S.K., Rivera-Soto, R. & Gray, S.J., 2015. Viral expression cassette elements to enhance transgene target specificity and expression in gene therapy. *Discovery Medicine*, 19(102), pp.49–57.

Power, B.D., Kolmac, C.I. & Mitrofanis, J., 1999. Evidence for a large projection from

the zona incerta to the dorsal thalamus. *The Journal of Comparative Neurology*, 404(4), pp.554–65.

Power, B.D., Leamey, C.A. & Mitrofanis, J., 2001. Evidence for a visual subsector within the zona incerta. *Visual Neuroscience*, 18(2), pp.179–86.

Prasad, J.A., Macgregor, E.M. & Chudasama, Y., 2013. Lesions of the thalamic reuniens cause impulsive but not compulsive responses. *Brain Structure & Function*, 218(1), pp.85–96.

Práwdicz-Neminski, W.W., 1925. Zur Kenntnis der elektrischen und der Innervationsvorgänge in den funktionellen Elementen und Geweben des tierischen Organismus. Elektrocerebrogramm der Säugetiere. *Pflügers Archiv für die Gesamte Physiologie des Menschen und der Tiere*, 209(1), pp.362–382.

Pritz, M.B., 1995. The thalamus of reptiles and mammals: similarities and differences. *Brain, Behavior and Evolution*, 46(4–5), pp.197–208.

Pritz, M.B., 1995. The Thalamus of Reptiles and Mammals: Similarities and Differences. *Brain, Behavior and Evolution*, 46(4–5), pp.197–208.

Pritz, M.B. & Stritzel, M.E., 1991. Calcium binding protein immunoreactivity in a reptilian thalamic reticular nucleus. *Brain Research*, 554(1–2), pp.325–8.

Pritz, M.B. & Stritzel, M.E., 1993. Neuronal subpopulations in a reptilian thalamic reticular nucleus. *Neuroreport*, 4(6), pp.791–4.

Qiu, M.-H. et al., 2010. Basal ganglia control of sleep-wake behavior and cortical activation. *The European Journal of Neuroscience*, 31(3), pp.499–507.

Rabbitt, R.D. et al., 2016. Heat pulse excitability of vestibular hair cells and afferent neurons. *Journal of Neurophysiology*, 116(2), pp.825–43.

Raffaele, R., Sapienza, S. & Urbano, A., 1969. [Fastigial nucleus projections in the pars magnocellularis of the medial geniculate body of the cat]. *Bollettino della Societa italiana di biologia sperimentale*, 45(20), pp.1296–8.

Raghavachari, S. et al., 2001. Gating of human theta oscillations by a working memory task. *The Journal of Neuroscience : the official journal of the Society for Neuroscience*, 21(9), pp.3175–83.

Randall, A.D. & Tsien, R.W., 1997. Contrasting biophysical and pharmacological properties of T-type and R-type calcium channels. *Neuropharmacology*, 36(7), pp.879–93.

Rasch, B. & Born, J., 2013. About sleep's role in memory. *Physiological reviews*, 93(2), pp.681–766.

Ray, J.P. & Price, J.L., 1993. The organization of projections from the mediodorsal nucleus of the thalamus to orbital and medial prefrontal cortex in macaque monkeys. *The Journal of Comparative Neurology*, 337(1), pp.1–31.

Reese, B.E., 1988. "Hidden lamination" in the dorsal lateral geniculate nucleus: the functional organization of this thalamic region in the rat. *Brain Research Reviews*, 13(2), pp.119–137.

Reig, R. et al., 2010. Temperature modulation of slow and fast cortical rhythms. *Journal of Neurophysiology*, 103(3), pp.1253–61.

Résibois, A. & Rogers, J.H., 1992. Calretinin in rat brain: an immunohistochemical study. *Neuroscience*, 46(1), pp.101–34.

Rikhye, R. V., Wimmer, R.D. & Halassa, M.M., 2018. Toward an Integrative Theory of Thalamic Function. *Annual Review of Neuroscience*, 41(1), pp. 62144.

Rinvik, E. & Wiberg, M., 1990. Demonstration of a reciprocal connection between the periaqueductal gray matter and the reticular nucleus of the thalamus. *Anatomy and Embryology*, 181(6), pp.577–84.

Risold, P.Y., Canteras, N.S. & Swanson, L.W., 1994. Organization of projections from the anterior hypothalamic nucleus: a Phaseolus vulgaris-leucoagglutinin study in the rat. *The Journal of Comparative Neurology*, 348(1), pp.1–40.

Rodrigo-Angulo, M.L. & Reinoso-Suárez, F., 1988. Connections to the lateral

posterior-pulvinar thalamic complex from the reticular and ventral lateral geniculate thalamic nuclei: a topographical study in the cat. *Neuroscience*, 26(2), pp.449–59.

Rodríguez, J.J. et al., 2011. Serotonergic projections and serotonin receptor expression in the reticular nucleus of the thalamus in the rat. *Synapse (New York, N.Y.)*, 65(9), pp.919–28.

Rogers, J. & Resibois, A., 1992. Calretinin and calbindin-D 28k in rat brain: Patterns of partial co-localization. *Neuroscience*, 51(4).

Roland, B.L. et al., 1999. Anatomical distribution of prolactin-releasing peptide and its receptor suggests additional functions in the central nervous system and periphery. *Endocrinology*, 140(12), pp.5736–45.

Romanowski, C.A., Mitchell, I.J. & Crossman, A.R., 1985. The organisation of the efferent projections of the zona incerta. *Journal of Anatomy*, 143, pp.75–95.

Ros, H. et al., 2009. Neocortical networks entrain neuronal circuits in cerebellar cortex. *The Journal of Neuroscience : the official journal of the Society for Neuroscience*, 29(33), pp.10309–20.

Rose, J.E. & Woolsey, C.N., 1948. Structure and relations of limbic cortex and anterior thalamic nuclei in rabbit and cat. *The Journal of Comparative neurology*, 89(3), pp.279–347.

Roth, G., 2015. Convergent evolution of complex brains and high intelligence. *Philosophical transactions of the Royal Society of London. Series B, Biological sciences*, 370(1684).

Roth, M.M. et al., 2016. Thalamic nuclei convey diverse contextual information to layer 1 of visual cortex. *Nature Neuroscience*, 19(2), pp.299–307.

Rouiller, E.M. et al., 1985. Projections of the reticular complex of the thalamus onto physiologically characterized regions of the medial geniculate body. *Neuroscience Letters*, 53(2), pp.227–32.

Rowe, D.L., Robinson, P.A. & Gordon, E., 2005. Stimulant drug action in attention deficit hyperactivity disorder (ADHD): inference of neurophysiological mechanisms via quantitative modelling. *Clinical Neurophysiology*, 116(2), pp.324–335.

Rudy, B. & Mcbain, C.J., 2001. Kv3 channels : voltage-gated K + channels designed for high-frequency repetitive firing. , 24(9), pp.517–526.

Saab, C.Y. & Barrett, L.F., 2016. Thalamic Bursts and the Epic Pain Model. *Frontiers in Computational Neuroscience*, 10, p.147.

Sakata, S. & Harris, K.D., 2009. Laminar Structure of Spontaneous and Sensory-Evoked Population Activity in Auditory Cortex. *Neuron*, 64(3), pp.404–418.

Salas, M., Torrero, C. & Pulido, S., 1986. Undernutrition induced by early pup separation delays the development of the thalamic reticular nucleus in rats. *Experimental Neurology*, pp.447–455.

Sanchez-Vives, M. V & McCormick, D.A., 2000. Cellular and network mechanisms of rhythmic recurrent activity in neocortex. *Nature Neuroscience*, 3(10), pp.1027–34.

Saper, C.B. et al., 2011. Sleep State Swithcing. *Neuron*, 68(6), pp.1023–1042.

Saper, C.B., Chou, T.C. & Scammell, T.E., 2001. The sleep switch: hypothalamic control of sleep and wakefulness. *Trends in Neurosciences*, 24(12), pp.726–31.

Scheib, C.M., 2017. Brainstem Influence on Thalamocortical Oscillations during Anesthesia Emergence. *Frontiers in Systems Neuroscience*, 11, p.66.

Scheibel, M. & Scheibel, A., 1972. Specialized organizational patterns within the nucleus reticularis thalami of the cat. *Experimental Neurology*, 316322.

Scheibel, M.E. & Scheibel, A.B., 1965. Activity cycles in neurons of the reticular formation. *Recent advances in biological psychiatry*, 8, pp.283–93.

Scheibel, M.E. & Scheibel, A.B., 1972. Input-Output Relations of the Thalamic

Nonspecific System (Part 1 of 2). *Brain, Behavior and Evolution*, 6(1–6), pp.332–345.

Scheibel, M.E. & Scheibel, A.B., 1971. Thalamus and body image--a model. *Biological Psychiatry*, 3(1), pp.71–6.

Schmalbach, B. et al., 2015. Age-dependent loss of parvalbumin-expressing hippocampal interneurons in mice deficient in CHL1, a mental retardation and schizophrenia susceptibility gene. *Journal of Neurochemistry*, 135(4), pp.830–844.

Schmitt, L.I. et al., 2017. Thalamic amplification of cortical connectivity sustains attentional control. *Nature*, 545(7653), pp.219–223.

Schwaller, B. et al., 2004. Parvalbumin deficiency affects network properties resulting in increased susceptibility to epileptic seizures. *Molecular and Cellular Neurosciences*, 25(4), pp.650–63.

Schwartz, M.D. & Kilduff, T.S., 2015. The Neurobiology of Sleep and Wakefulness. *Psychiatric Clinics of North America*, 38(4), pp.615–644.

Sesack, S.R. et al., 1989a. Topographical organization of the efferent projections of the medial prefrontal cortex in the rat: an anterograde tract-tracing study with Phaseolus vulgaris leucoagglutinin. *The Journal of Comparative Neurology*, 290(2), pp.213–42.

Shammah-Lagnado, S.J., Alheid, G.F. & Heimer, L., 1996. Efferent connections of the caudal part of the globus pallidus in the rat. *The Journal of Comparative Neurology*, 376(3), pp.489–507.

Shaw, V. & Mitrofanis, J., 2002. Anatomical evidence for somatotopic maps in the zona incerta of rats. *Anatomy and Embryology*, 206(1–2), pp.119–30.

Sherin, J.E. et al., 1998. Innervation of histaminergic tuberomammillary neurons by GABAergic and galaninergic neurons in the ventrolateral preoptic nucleus of the rat. *The Journal of Neuroscience : the official journal of the Society for*

Neuroscience, 18(12), pp.4705–21.

Sherman, S.M., 2005. Thalamic relays and cortical functioning. In *Progress in Brain Research*. pp. 107–126.

Sherman, S.M., 2014. The Function of Metabotropic Glutamate Receptors in Thalamus and Cortex. *The Neuroscientist : a review journal bringing neurobiology, neurology and psychiatry*, 20(2), p.136.

Sherman, S.M. & Guillery, R.W., 2002a. The role of the thalamus in the flow of information to the cortex. *Philosophical transactions of the Royal Society of London. Series B, Biological sciences*, 357(1428), pp.1695–708.

Sheroziya, M. & Timofeev, I., 2014. Global Intracellular Slow-Wave Dynamics of the Thalamocortical System. *Journal of Neuroscience*, 34(26), pp.8875–8893.

Shibata, H., 1992. Topographic organization of subcortical projections to the anterior thalamic nuclei in the rat. *Journal of Comparative Neurology*, 323(1), pp.117–127.

Shinotoh, H. et al., 2000. Progressive loss of cortical acetylcholinesterase activity in association with cognitive decline in Alzheimer's disease: a positron emission tomography study. *Annals of Neurology*, 48(2), pp.194–200.

Shosaku, a, 1985. A comparison of receptive field properties of vibrissa neurons between the rat thalamic reticular and ventro-basal nuclei. *Brain Research*, 347(1), pp.36–40.

Sieghart, W. & Sperk, G., 2002. Subunit composition, distribution and function of GABA(A) receptor subtypes. *Current Topics in Medicinal Chemistry*, 2(8), pp.795–816.

da Silva, F.H. et al., 1973. Organization of thalamic and cortical alpha rhythms: spectra and coherences. *Electroencephalography and Clinical Neurophysiology*, 35(6), pp.627–39.

Sineshchekov, O.A., Jung, K.-H. & Spudich, J.L., 2002. Two rhodopsins mediate

phototaxis to low- and high-intensity light in Chlamydomonas reinhardtii. *Proceedings of the National Academy of Sciences of the United States of America*, 99(13), pp.8689–94.

Sirota, A. & Buzsáki, G., 2005. Interaction between neocortical and hippocampal networks via slow oscillations. *Thalamus and Related Systems*, 3(04), p.245.

Sirota, A. & Csicsvari, J., 2003. Communication between neocortex and hippocampus during sleep in rodents. *Proceedings of the National Academy of Sciences of the United States of America*, 100(4).

Smith, J.C. et al., 2013. Brainstem respiratory networks: building blocks and microcircuits. *Trends in Neurosciences*, 36(3), pp.152–162.

So, Y.T. & Shapley, R., 1979. Spatial properties of X and Y cells in the lateral geniculate nucleus of the cat and conduction veolcities of their inputs. *Experimental Brain Research*, 36(3), pp.533–50.

Sofroniew, M. V et al., 1985. Cholinergic projections from the midbrain and pons to the thalamus in the rat, identified by combined retrograde tracing and choline acetyltransferase immunohistochemistry. *Brain Research*, 329(1–2), pp.213–23.

Sohal, V.S., Cox, C.L. & Huguenard, J.R., 1998. Localization of CCK receptors in thalamic reticular neurons: a modeling study. *Journal of Neurophysiology*, 79(5), pp.2820–4.

Sohal, V.S. & Huguenard, J.R., 2003. Inhibitory interconnections control burst pattern and emergent network synchrony in reticular thalamus. *The Journal of Neuroscience : the official journal of the Society for Neuroscience*, 23(26), pp.8978–88.

de Sousa, A.A. et al., 2013. Lamination of the lateral geniculate nucleus of catarrhine primates. *Brain, Behavior and Evolution*, 81(2), pp.93–108.

Sparta, D.R. et al., 2012. Construction of implantable optical fibers for long-term optogenetic manipulation of neural circuits. *Nature Protocols*, 7(1), pp.12–23.

Spellman, T. et al., 2015. Hippocampal-prefrontal input supports spatial encoding in working memory. *Nature*, 522(7556), pp.309–14.

Spreafico, R. et al., 1993. Branching projections from mesopontine nuclei to the nucleus reticularis and related thalamic nuclei: A double labelling study in the rat. *The Journal of Comparative Neurology*, 336(4), pp.481–492.

Spreafico, R. et al., 1988. Electrophysiological characteristics of morphologically identified reticular thalamic neurons from rat slices. *Neuroscience*, 27(2), pp.629–638.

Spreafico, R., Battaglia, G. & Frassoni, C., 1991. The reticular thalamic nucleus (RTN) of the rat: Cytoarchitectural, Golgi, immunocytochemical, and horseradish peroxidase study. *The Journal of Comparative Neurology*, 304(3), pp.478–490.

Stehberg, J. et al., 2001. The visceral sector of the thalamic reticular nucleus in the rat. *Neuroscience*, 106(4), pp.745–755.

Steriade, M., Parent, A., et al., 1987. Cholinergic and non-cholinergic neurons of cat basal forebrain project to reticular and mediodorsal thalamic nuclei. *Brain Research*, 408(1–2), pp.372–6.

Steriade, M., 2006. Grouping of brain rhythms in corticothalamic systems. *Neuroscience*, 137(4), pp.1087–106.

Steriade, M. et al., 1988. Projections of cholinergic and non-cholinergic neurons of the brainstem core to relay and associational thalamic nuclei in the cat and macaque monkey. *Neuroscience*, 25(1), pp.47–67.

Steriade, M., 1994a. Sleep oscillations and their blockage by activating systems. *Journal of Psychiatry & Neuroscience : JPN*, 19(5), pp.354–8.

Steriade, M., 1994b. Sleep oscillations and their blockage by activating systems. *Journal of Psychiatry & Neuroscience : JPN*, 19(5), pp.354–8.

Steriade, M., Domich, L., et al., 1987. The deafferented reticular thalamic nucleus generates spindle rhythmicity. *Journal of Neurophysiology*, 57(1), pp.260–73.

Steriade, M., Contreras, D., et al., 1993. The slow (< 1 Hz) oscillation in reticular thalamic and thalamocortical neurons: scenario of sleep rhythm generation in interacting thalamic and neocortical networks. *The Journal of Neuroscience : the official journal of the Society for Neuroscience*, 13(8), pp.3284–99.

Steriade, M. & Amzica, F., 1996. Intracortical and corticothalamic coherency of fast spontaneous oscillations. *Proceedings of the National Academy of Sciences*, 93(6).

Steriade, M., Domich, L. & Oakson, G., 1986. Reticularis thalami neurons revisited: activity changes during shifts in states of vigilance. *The Journal of Neuroscience*, 6(l).

Steriade, M., Dossi, R.C. & Nuñez, A., 1991. Network modulation of a slow intrinsic oscillation of cat thalamocortical neurons implicated in sleep delta waves: cortically induced synchronization and brainstem cholinergic suppression. *The Journal of Neuroscience : the official journal of the Society for Neuroscience*, 11(10), pp.3200–17.

Steriade, M., McCormick, D.A. & Sejnowski, T.J., 1993. Thalamocortical oscillations in the sleeping and aroused brain. *Science (New York, N.Y.)*, 262(5134), pp.679–85.

Steriade, M., Nuñez, A. & Amzica, F., 1993a. A novel slow (1 Hz) oscillation of neocortical neurons in vivo: depolarizing and hyperpolarizing components. *The Journal of Neuroscience : the official journal of the Society for Neuroscience*, 13(8), pp.3252–65.

Steullet, P. et al., 2017. The thalamic reticular nucleus in schizophrenia and bipolar disorder: role of parvalbumin-expressing neuron networks and oxidative stress. *Molecular Psychiatry*.

Stone, J.L. & Hughes, J.R., 2013. Early History of Electroencephalography and Establishment of the American Clinical Neurophysiology Society. *Journal of Clinical Neurophysiology*, 30(1), pp.28–44.

Stroud, L.M. et al., 2005. Neuropeptide Y suppresses absence seizures in a genetic rat model. *Brain Research*, 1033(2), pp.151–156.

Stujenske, J.M., Spellman, T. & Gordon, J.A., 2015. Modeling the Spatiotemporal Dynamics of Light and Heat Propagation for In Vivo Optogenetics. *Cell Reports*, 12(3), pp.525–534.

Sun, Q.-Q. et al., 2003. Target-specific neuropeptide Y-ergic synaptic inhibition and its network consequences within the mammalian thalamus. *The Journal of Neuroscience : the official journal of the Society for Neuroscience*, 23(29), pp.9639–49.

Sun, Q., Huguenard, J. & Prince, D., 2002. Somatostatin inhibits thalamic network oscillations in vitro: actions on the GABAergic neurons of the reticular nucleus. *The Journal of Neuroscience*, 22(13), pp.5374–5386.

Sun, Q.Q., Akk, G., et al., 2001. Differential regulation of GABA release and neuronal excitability mediated by neuropeptide Y1 and Y2 receptors in rat thalamic neurons. *The Journal of Physiology*, 531(Pt 1), pp.81–94.

Sun, Q.Q., Huguenard, J.R. & Prince, D.A., 2001. Neuropeptide Y receptors differentially modulate G-protein-activated inwardly rectifying K+ channels and high-voltage-activated Ca2+ channels in rat thalamic neurons. *The Journal of Physiology*, 531(Pt 1), pp.67–79.

Sun, Y.-G. et al., 2013a. Biphasic cholinergic synaptic transmission controls action potential activity in thalamic reticular nucleus neurons. *The Journal of Neuroscience : the official journal of the Society for Neuroscience*, 33(5), pp.2048–59.

Sun, Y.-G. et al., 2013b. Biphasic cholinergic synaptic transmission controls action potential activity in thalamic reticular nucleus neurons. *The Journal of Neuroscience : the official journal of the Society for Neuroscience*, 33(5), pp.2048–59.

Sun, Y.-G. et al., 2011. Target-dependent control of synaptic inhibition by endocannabinoids in the thalamus. *The Journal of Neuroscience : the official journal of the Society for Neuroscience*, 31(25), pp.9222–30.

Swanson, L.W., 1981. A direct projection from Ammon's horn to prefrontal cortex in the rat. *Brain Research*, 217(1), pp.150–4.

Tai, Y. et al., 1995. Nucleus reticularis thalami connections with the mediodorsal thalamic nucleus: a light and electron microscopic study in the monkey. *Brain Research Bulletin*, 38(5), pp.475–88.

Takahashi, K. et al., 2010a. Locus coeruleus neuronal activity during the sleep-waking cycle in mice. *Neuroscience*, 169(3), pp.1115–1126.

Tallon-Baudry, C. et al., 1998. Induced gamma-band activity during the delay of a visual short-term memory task in humans. *The Journal of Neuroscience : the official journal of the Society for Neuroscience*, 18(11), pp.4244–54.

Thakkar, M.M., 2011. Histamine in the regulation of wakefulness. *Sleep Medicine Reviews*, 15(1), pp.65–74.

Thompson, S.M., Masukawa, L.M. & Prince, D.A., 1985. Temperature dependence of intrinsic membrane properties and synaptic potentials in hippocampal CA1 neurons in vitro. *The Journal of Neuroscience : the official journal of the Society for Neuroscience*, 5(3), pp.817–24.

Thompson, S.M. & Robertson, R.T., 1987. Organisation of subcortical pathways for sensory projections to the limbic cortex. I. Subcortical projections to the medial limbic cortex in the rat. *The Journal of Comparative Neurology*, 265(2), pp.175–188.

Timbie, C. & Barbas, H., 2015. Pathways for Emotions: Specializations in the Amygdalar, Mediodorsal Thalamic, and Posterior Orbitofrontal Network. *The Journal of Neuroscience : the official journal of the Society for Neuroscience*, 35(34), pp.11976–87.

Timofeev, I. & Chauvette, S., 2011. Thalamocortical oscillations: local control of EEG slow waves. *Current topics in Medicinal Chemistry*, 11(19), pp.2457–71.

Timofeev, I. & Steriade, M., 1996. Low-frequency rhythms in the thalamus of intact-cortex and decorticated cats. *Journal of Neurophysiology*, 76(6), pp.4152–4168.

Tonelli, L. & Chiaraviglio, E., 1993. Enhancement of water intake in rats after lidocaine injection in the zona incerta. *Brain Research Bulletin*, 31(1–2), pp.1–5.

Traynelis, S.F. et al., 2010. Glutamate receptor ion channels: structure, regulation, and function. *Pharmacological Reviews*, 62(3), pp.405–96.

Turner, B.H., Mishkin, M. & Knapp, M., 1980. Organization of the amygdalopetal projections from modality-specific cortical association areas in the monkey. *The Journal of Comparative Neurology*, 191(4), pp.515–543.

Ujihara, H. et al., 1991. Inhibition by thyrotropin-releasing hormone of epileptic seizures in spontaneously epileptic rats. *European Journal of Pharmacology*, 196(1), pp.15–9.

Ulfig, N., Nickel, J. & Bohl, J., 1998. Transient features of the thalamic reticular nucleus in the human foetal brain. *The European Journal of Neuroscience*, 10(12), pp.3773–84.

Ulrich, D., Besseyrias, V. & Bettler, B., 2007. Functional Mapping of $GABA_B$-Receptor Subtypes in the Thalamus. *Journal of Neurophysiology*, 98(6), pp.3791–3795.

Vanderwolf, C.H., 1969. Hippocampal electrical activity and voluntary movement in the rat. *Electroencephalography and Clinical Neurophysiology*, 26(4), pp.407–18.

Vanderwolf, C.H. & Stewart, D.J., 1988. Thalamic control of neocortical activation: a critical re-evaluation. *Brain Research Bulletin*, 20(4), pp.529–38.

Varela, C. et al., 2014. Anatomical substrates for direct interactions between hippocampus, medial prefrontal cortex, and the thalamic nucleus reuniens. *Brain Structure & Function*, 219(3), pp.911–29.

Velayos, J.L., Jiménez-Castellanos, J. & Reinoso-Suárez, F., 1989. Topographical organization of the projections from the reticular thalamic nucleus to the intralaminar and medial thalamic nuclei in the cat. *Journal of Comparative Neurology*, 279(3), pp.457–469.

Vertes, R.P., 2002. Analysis of projections from the medial prefrontal cortex to the thalamus in the rat, with emphasis on nucleus reuniens. *The Journal of Comparative Neurology*, 442(2), pp.163–87.

Vertes, R.P., 2004. Differential projections of the infralimbic and prelimbic cortex in the rat. *Synapse (New York, N.Y.)*, 51(1), pp.32–58.

Vertes, R.P. & Hoover, W.B., 2008. Projections of the paraventricular and paratenial nuclei of the dorsal midline thalamus in the rat. *The Journal of Comparative Neurology*, 508(2), pp.212–37.

Vertes, R.P., Hoover, W.B. & Rodriguez, J.J., 2012. Projections of the central medial nucleus of the thalamus in the rat: Node in cortical, striatal and limbic forebrain circuitry. *Neuroscience*, 219, pp.120–136.

Vertes, R.P. & Kocsis, B., 1997. Brainstem-diencephalo-septohippocampal systems controlling the theta rhythm of the hippocampus. *Neuroscience*, 81(4), pp.893–926.

Vertes, R.P., Linley, S. & Hoover, W.B., 2016. Limbic Circuitry of the midline thalamus. *Neurosci Biobehav Rev*, (54), pp.89–107.

Vidal, L., Blanchard, J. & Morin, L.P., 2005. Hypothalamic and zona incerta neurons expressing hypocretin, but not melanin concentrating hormone, project to the hamster intergeniculate leaflet. *Neuroscience*, 134(3), pp.1081–90.

Villalobos, N. et al., 2016. Striatum and globus pallidus control the electrical activity of reticular thalamic nuclei. *Brain Research*, 1644, pp.258–266.

Volgushev, M. et al., 2000. Synaptic transmission in the neocortex during reversible cooling. *Neuroscience*, 98(1), pp.9–22.

Vyazovskiy, V. V. & Delogu, A., 2014. NREM and REM Sleep. *The Neuroscientist*, 20(3), pp.203–219.

Vyazovskiy, V. V et al., 2004. The dynamics of spindles and EEG slow-wave activity in NREM sleep in mice. *Archives italiennes de biologie*, 142(4), pp.511–23.

Walker, A.E., 1937. The Projection of the Medial Geniculate Body to the Cerebral Cortex in the Macaque Monkey. *Journal of Anatomy*, 71(Pt 3), pp.319–31.

Walter, W.G., 1936. The location of cerebral tumours by electroencephalography. *Lancet*, (2), pp.305–308.

Wan, X., Mathers, D.A. & Puil, E., 2003. Pentobarbital modulates intrinsic and GABA-receptor conductances in thalamocortical inhibition. *Neuroscience*, 121(4), pp.947–58.

Warburton, E.C. et al., 2000. Disconnecting hippocampal projections to the anterior thalamus produces deficits on tests of spatial memory in rats. *The European Journal of Neuroscience*, 12(5), pp.1714–26.

Wass, C. et al., 2012. Covariation of learning and "reasoning" abilities in mice: Evolutionary conservation of the operations of intelligence. *Journal of Experimental Psychology: Animal Behavior Processes*, 38(2), pp.109–124.

Watson, C., Lind, C.R.P. & Thomas, M.G., 2014. The anatomy of the caudal zona incerta in rodents and primates. *Journal of Anatomy*, 224(2), pp.95–107.

Weese, G.D., Phillips, J.M. & Brown, V.J., 1999. Attentional orienting is impaired by unilateral lesions of the thalamic reticular nucleus in the rat. *The Journal of Neuroscience*, 19(22), pp.10135–9.

Weiergräber, M. et al., 2008. Altered thalamocortical rhythmicity in Ca(v)2.3-deficient mice. *Molecular and Cellular Neurosciences*, 39(4), pp.605–18.

Wells, M.F. et al., 2016. Thalamic reticular impairment underlies attention deficit in Ptchd1(Y/-) mice. *Nature*, 532(7597), pp.58–63.

Van der Werf, Y.D., Witter, M.P. & Groenewegen, H.J., 2002. The intralaminar and midline nuclei of the thalamus. Anatomical and functional evidence for participation in processes of arousal and awareness. *Brain Research. Brain research reviews*, 39(2–3), pp.107–40.

Wiegand, M. et al., 1991. Brain morphology and sleep EEG in patients with Huntington's disease. *European Archives of Psychiatry and Clinical Neuroscience*, 240(3), pp.148–52.

Willis, W.D. et al., 2001. Projections from the marginal zone and deep dorsal horn to the ventrobasal nuclei of the primate thalamus. *Pain*, 92(1–2), pp.267–76.

Wilson, C.J. & Groves, P.M., 1981. Spontaneous firing patterns of identified spiny neurons in the rat neostriatum. *Brain Research*, 220(1), pp.67–80.

Wilton, L. et al., 2001. Excitotoxic lesions of the rostral thalamic reticular nucleus do not affect the performance of spatial learning and memory tasks in the rat. *Behavioural Brain Research*, 120(2), pp.177–187.

Wimmer, R., Astori, S. & Bond, C., 2012. Sustaining sleep spindles through enhanced SK2-channel activity consolidates sleep and elevates arousal threshold. *The Journal of Neuroscience*, 32(40), pp.13917–13928.

Wimmer, R.D. et al., 2015. Thalamic control of sensory selection in divided attention. *Nature*.

Winsky-Sommerer, R. et al., 2008. Normal sleep homeostasis and lack of epilepsy phenotype in GABAA receptor α3 subunit-knockout mice. *Neuroscience*, 154(2), pp.595–605.

Witter, M.P. & Groenewegen, H.J., 2004. *Thalamus. In: Paxinos, G., editor. The Rat Nervous System. third ed*,

Wolak, M.L. et al., 2003. Comparative distribution of neuropeptide Y Y1 and Y5 receptors in the rat brain by using immunohistochemistry. *The Journal of Comparative Neurology*, 464(3), pp.285–311.

Woodruff, D.S., 1975. Relationships among EEG alpha frequency, reaction time, and age: a biofeedback study. *Psychophysiology*, 12(6), pp.673–81.

Wouterlood, F.G., Saldana, E. & Witter, M.P., 1990. Projection from the nucleus reuniens thalami to the hippocampal region: light and electron microscopic tracing study in the rat with the anterograde tracer Phaseolus vulgaris-leucoagglutinin. *The Journal of Comparative Neurology*, 296(2), pp.179–203.

Wright, K.P., Badia, P. & Wauquier, A., 1995. Topographical and temporal patterns of brain activity during the transition from wakefulness to sleep. *Sleep*, 18(10), pp.880–9.

Xia, Y.-F. & Arai, a C., 2011. Prolactin-releasing peptide enhances synaptic transmission in rat thalamus. *Neuroscience*, 172, pp.1–11.

Xiao, D., Zikopoulos, B. & Barbas, H., 2009. Laminar and modular organization of prefrontal projections to multiple thalamic nuclei. *Neuroscience*, 161(4), pp.1067–81.

Xu, M. et al., 2015. Basal forebrain circuit for sleep-wake control. *Nature Neuroscience*, 18(11), pp.1641–1647.

Yen, C.-T. & Lu, P.-L., 2013. Thalamus and pain. *Acta Anaesthesiologica Taiwanica*, 51(2), pp.73–80.

Yen, C.-T. & Shaw, F.-Z., 2003. Reticular thalamic responses to nociceptive inputs in anesthetized rats. *Brain Research*, 968(2), pp.179–91.

Yen, C. & Conley, M., 1985. The morphology of physiologically identified GABAergic neurons in the somatic sensory part of the thalamic reticular nucleus in the cat. *The Journal of Neuroscience,* 5(8), pp.2254-68.

Yoshida, M., Sasa, M. & Takaori, S., 1984. Serotonin-mediated inhibition from dorsal raphe nucleus of neurons in dorsal lateral geniculate and thalamic reticular nuclei. *Brain Research*, 290(1), pp.95–105.

Yu, Y., Hill, A.P. & McCormick, D.A., 2012. Warm body temperature facilitates energy

efficient cortical action potentials. *PLoS Computational Biology*, 8(4), p.e1002456.

Zaborszky, L. et al., 2015. Neurons in the Basal Forebrain Project to the Cortex in a Complex Topographic Organization that Reflects Corticocortical Connectivity Patterns: An Experimental Study Based on Retrograde Tracing and 3D Reconstruction. *Cerebral Cortex*, 25(1), pp.118–137.

Zagha, E. & McCormick, D.A., 2014. Neural control of brain state. *Current opinion in neurobiology*, 29, pp.178–86.

Zaman, T. et al., 2011. Cav2.3 channels are critical for oscillatory burst discharges in the reticular thalamus and absence epilepsy. *Neuron*, 70(1), pp.95–108.

Zant, J.C. et al., 2016. Cholinergic Neurons in the Basal Forebrain Promote Wakefulness by Actions on Neighboring Non-Cholinergic Neurons: An Opto-Dialysis Study. *Journal of Neuroscience*, 36(6), pp.2057–2067.

Zemelman, B. V. et al., 2002. Selective photostimulation of genetically chARGed neurons. *Neuron*, 33(1), pp.15–22.

Zhang, F. et al., 2006. Channelrhodopsin-2 and optical control of excitable cells. *Nature Methods*, 3(10), pp.785–792.

Zhang, F., Wang, L.-P., et al., 2007. Multimodal fast optical interrogation of neural circuitry. *Nature*, 446(7136), pp.633–9.

Zhang, F., Aravanis, A.M. & Adamantidis, A., 2007. Circuit-breakers: optical technologies for probing neural signals and systems Feng. , 8(8), pp.577–581.

Zhang, Y.-P. & Oertner, T.G., 2007. Optical induction of synaptic plasticity using a light-sensitive channel. *Nature Methods*, 4(2), pp.139–141.

Zhang, Y., Llinas, R.R. & Lisman, J.E., 2009a. Inhibition of NMDARs in the Nucleus Reticularis of the Thalamus Produces Delta Frequency Bursting. *Frontiers in Neural Circuits*, 3, p.20.

Zhang, Y., Llinas, R.R. & Lisman, J.E., 2009b. Inhibition of NMDARs in the Nucleus Reticularis of the Thalamus Produces Delta Frequency Bursting. *Frontiers in Neural Circuits*, 3, p.20.

Zhou, C. et al., 2015. Altered intrathalamic GABAA neurotransmission in a mouse model of a human genetic absence epilepsy syndrome. *Neurobiology of Disease*, 73, pp.407–417.

Zilles, K. & Amunts, K., 2010. Centenary of Brodmann's map — conception and fate. *Nature Reviews Neuroscience*, 11(2), pp.139–145.

Zimny, R. et al., 1981. The medial geniculate body afferents from the cerebellum in the rabbit as studied with the method of orthograde degeneration. *Journal fur Hirnforschung*, 22(5), pp.573–85.

Znamenskiy, P. & Zador, A.M., 2013. During Auditory Discrimination. *Nature*, 497(7450).

Appendix

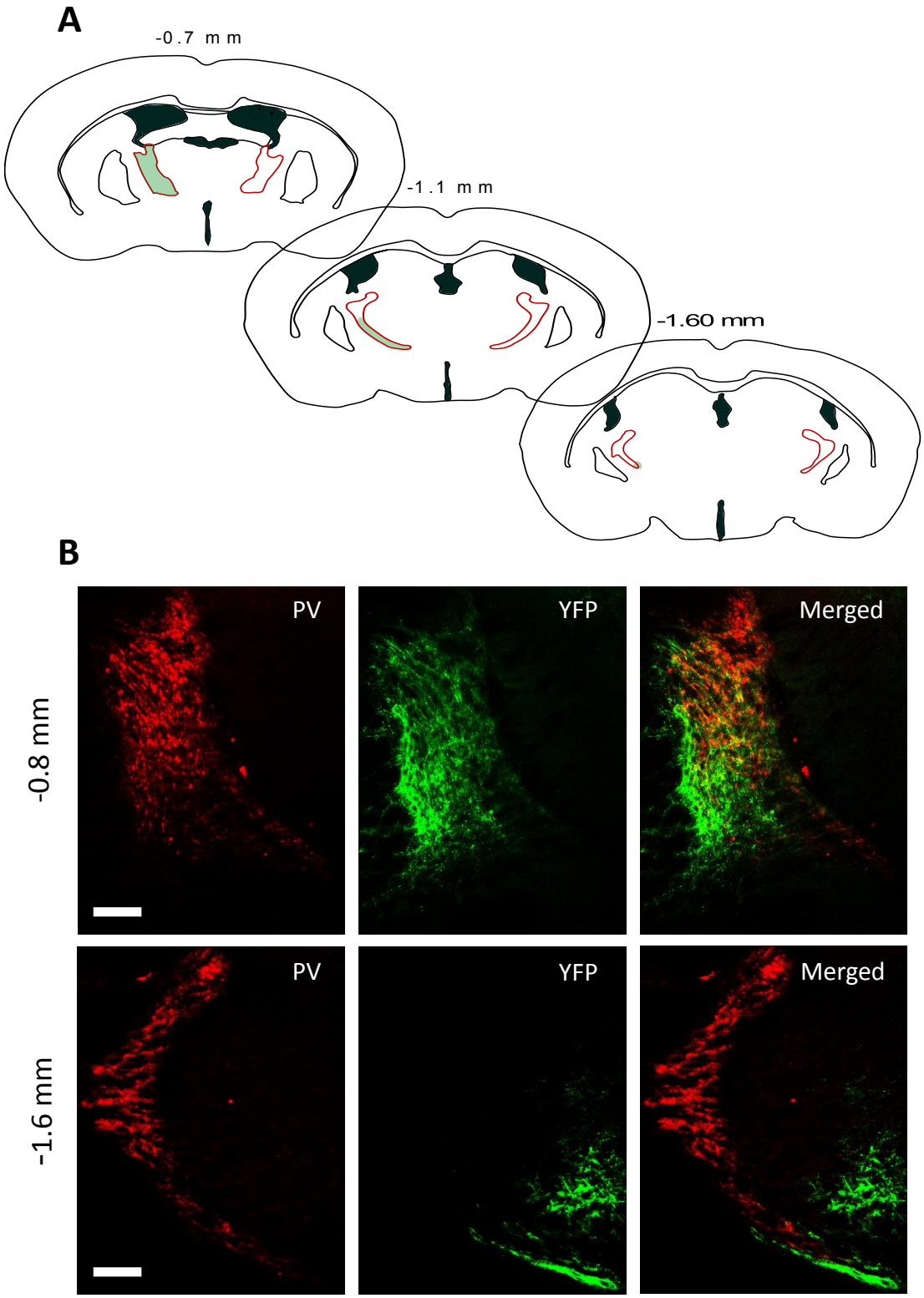

Figure 8.1 Expression pattern of Arch-YFP after bilateral rostral injections of AAV in mouse Arch-1. A. Schematic drawings of coronal sections at three coordinates containing the rostral and caudal TRN. Arch-YFP expression is marked by green shading. The red boundary highlights the TRN. B. Photographs of PV (parvalbumin, red) and YFP (green) expression in the rostral and caudal TRN. Scale bar, 250 µm.

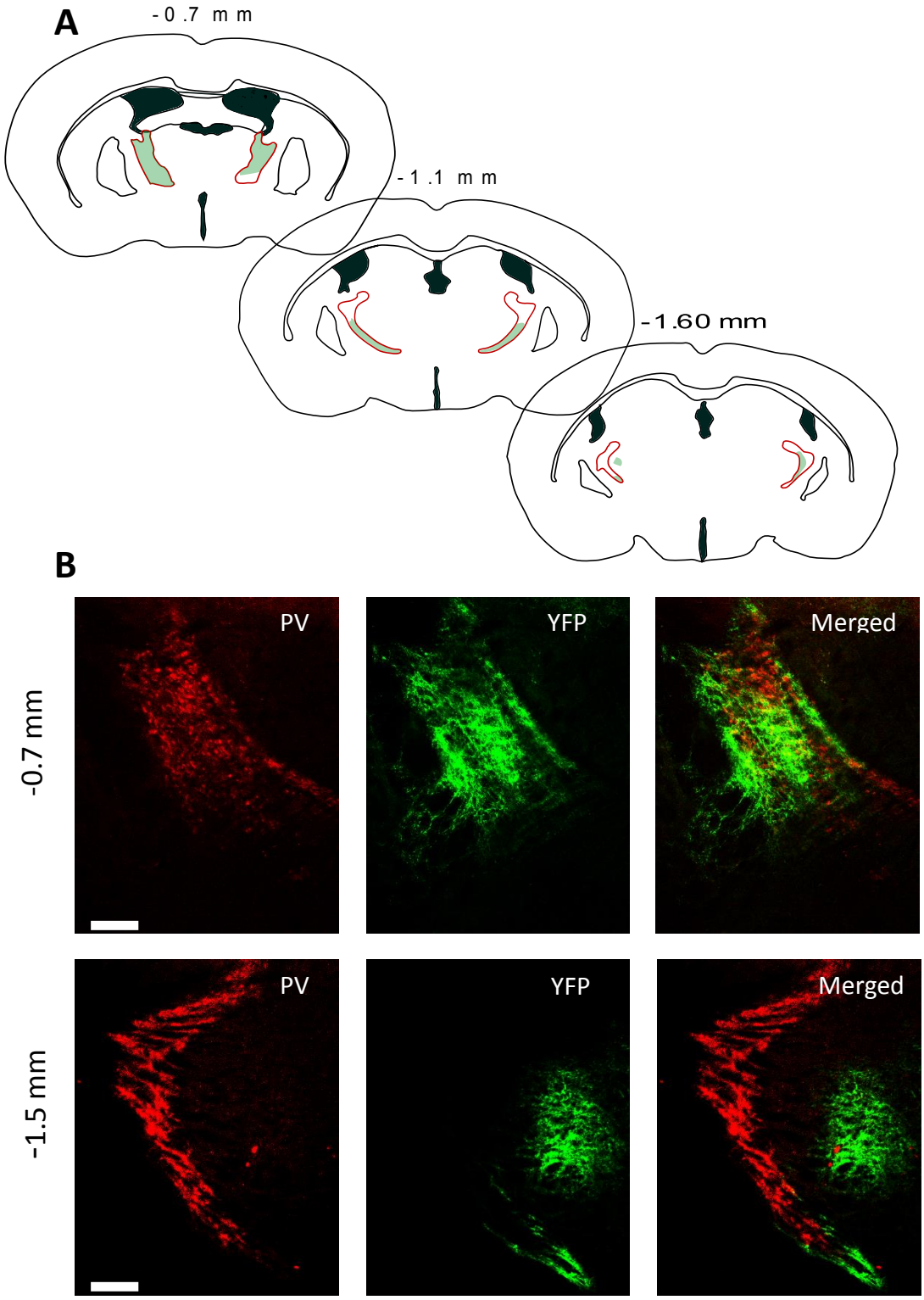

Figure 8.2 Expression pattern of Arch-YFP after bilateral rostral injections of AAV in mouse Arch-2. A. Schematic drawings of coronal sections at three coordinates containing the rostral and caudal TRN. Arch-YFP expression is marked by green shading. The red boundary highlights the TRN. B. Photographs of PV (parvalbumin, red) and YFP (green) expression in the rostral and caudal TRN. Scale bar,250 µm.

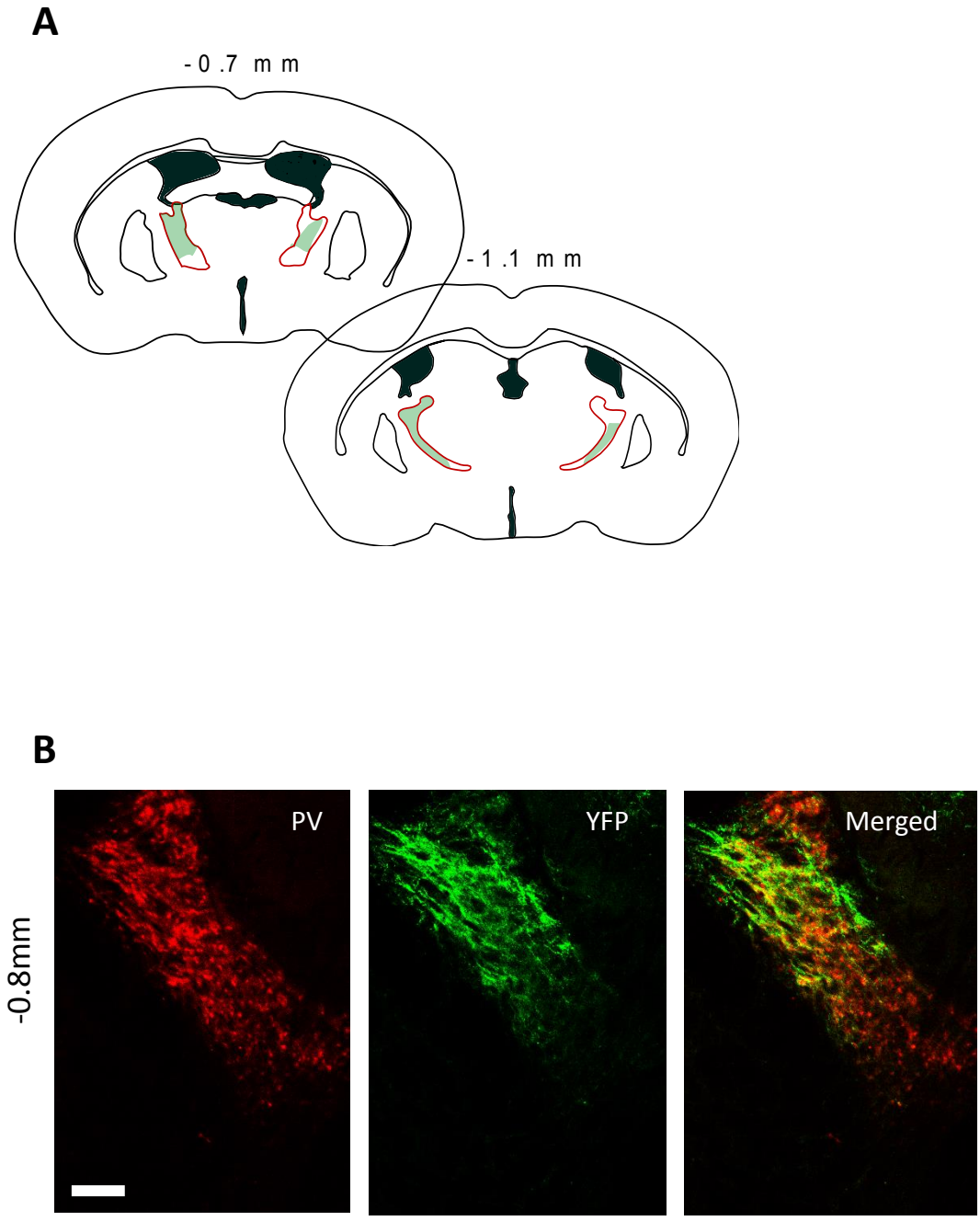

Figure 8.3 Expression pattern of Arch-YFP after bilateral rostral injections of AAV in mouse Arch-3. A. Schematic drawings of coronal sections at two coordinates containing the rostral and middle TRN. Arch-YFP expression is marked by green shading. The red boundary highlights the TRN. B. Photographs of PV (parvalbumin, red) and YFP (green) expression in the rostral and caudal TRN. Scale bar, 250 µm.

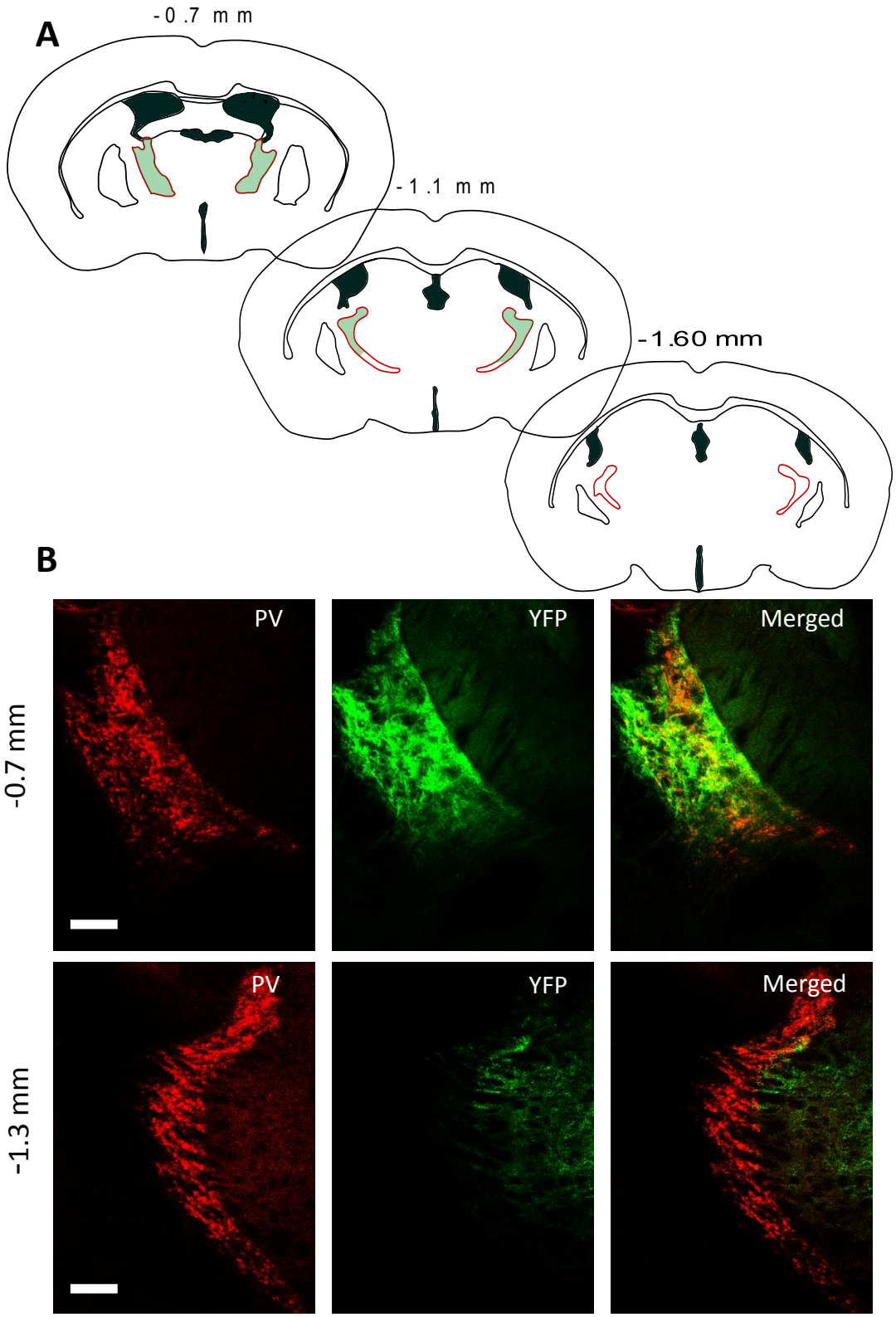

Figure 8.4 Expression pattern of Arch-YFP after bilateral rostral injections of AAV in mouse Arch-4. A. Schematic drawings of coronal sections at three coordinates containing the rostral and caudal TRN. Arch-YFP expression is marked by green shading. The red boundary highlights the TRN. B. Photographs of PV (parvalbumin, red) and YFP (green) expression in the rostral and caudal TRN. Scale bar, 250 µm.

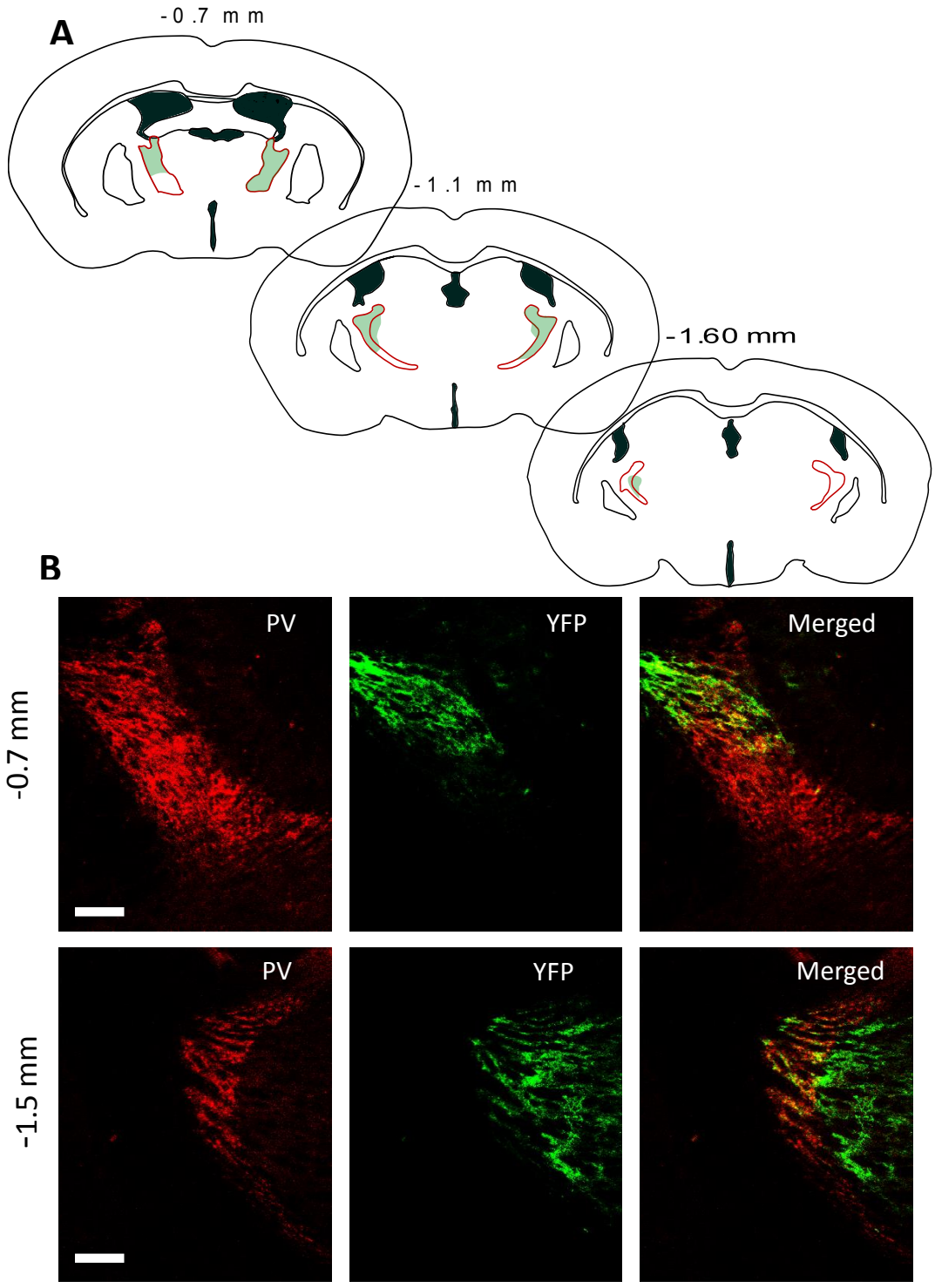

Figure 8.5 Expression pattern of Arch-YFP after bilateral rostral injections of AAV in mouse Arch-5. A. Schematic drawings of coronal sections at three coordinates containing the rostral and caudal TRN. Arch-YFP expression is marked by green shading. The red boundary highlights the TRN. B. Photographs of PV (parvalbumin, red) and YFP (green) expression in the rostral and caudal TRN. Scale bar, 250 µm.

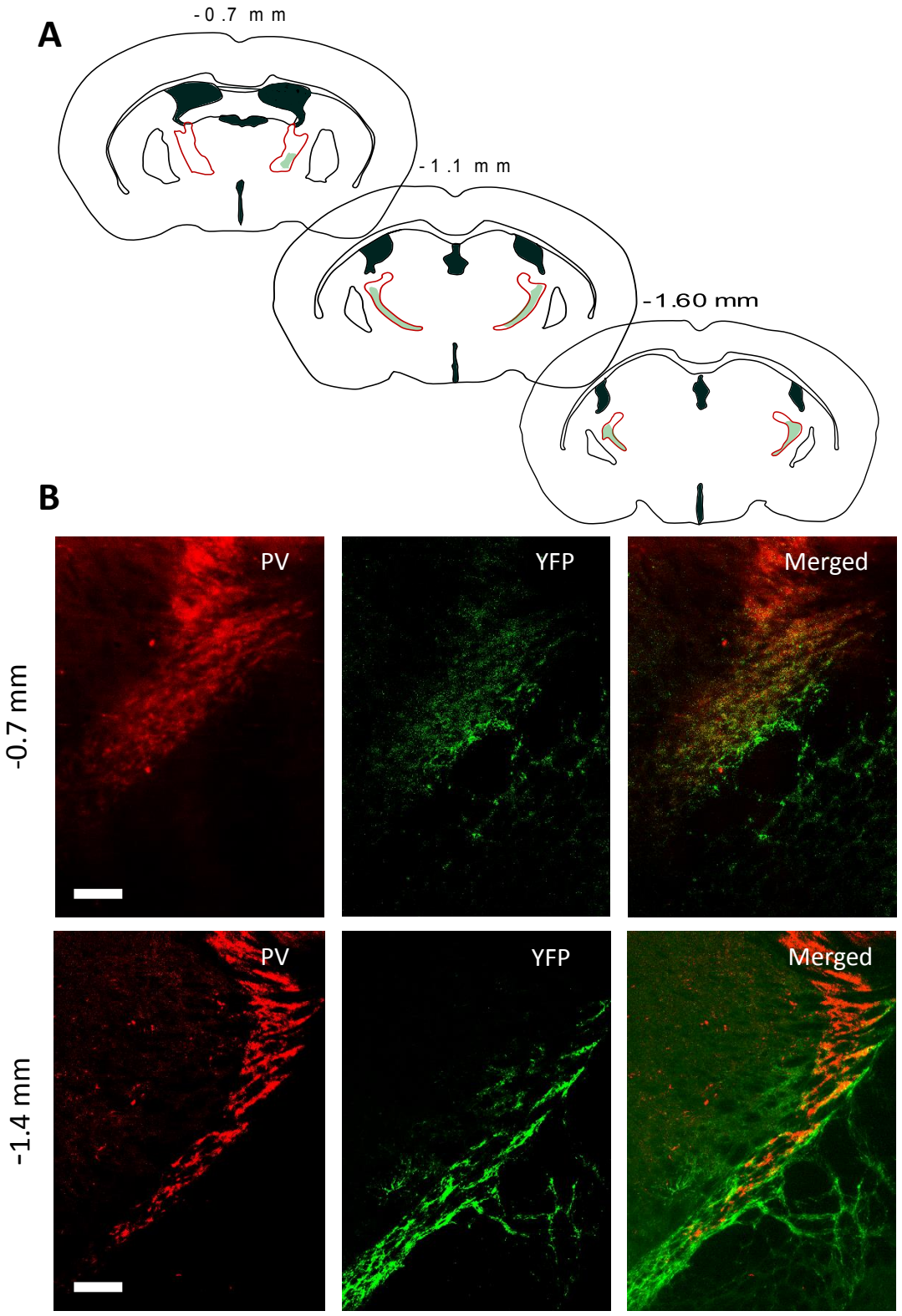

Figure 8.6 Expression pattern of Arch-YFP after bilateral caudal injections of AAV in mouse Arch-6. A. Schematic drawings of coronal sections at three coordinates containing the rostral and caudal TRN. Arch-YFP expression is marked by green shading. The red boundary highlights the TRN. B. Photographs of PV (parvalbumin, red) and YFP (green) expression in the rostral and caudal TRN. Scale bar, 250 µm.

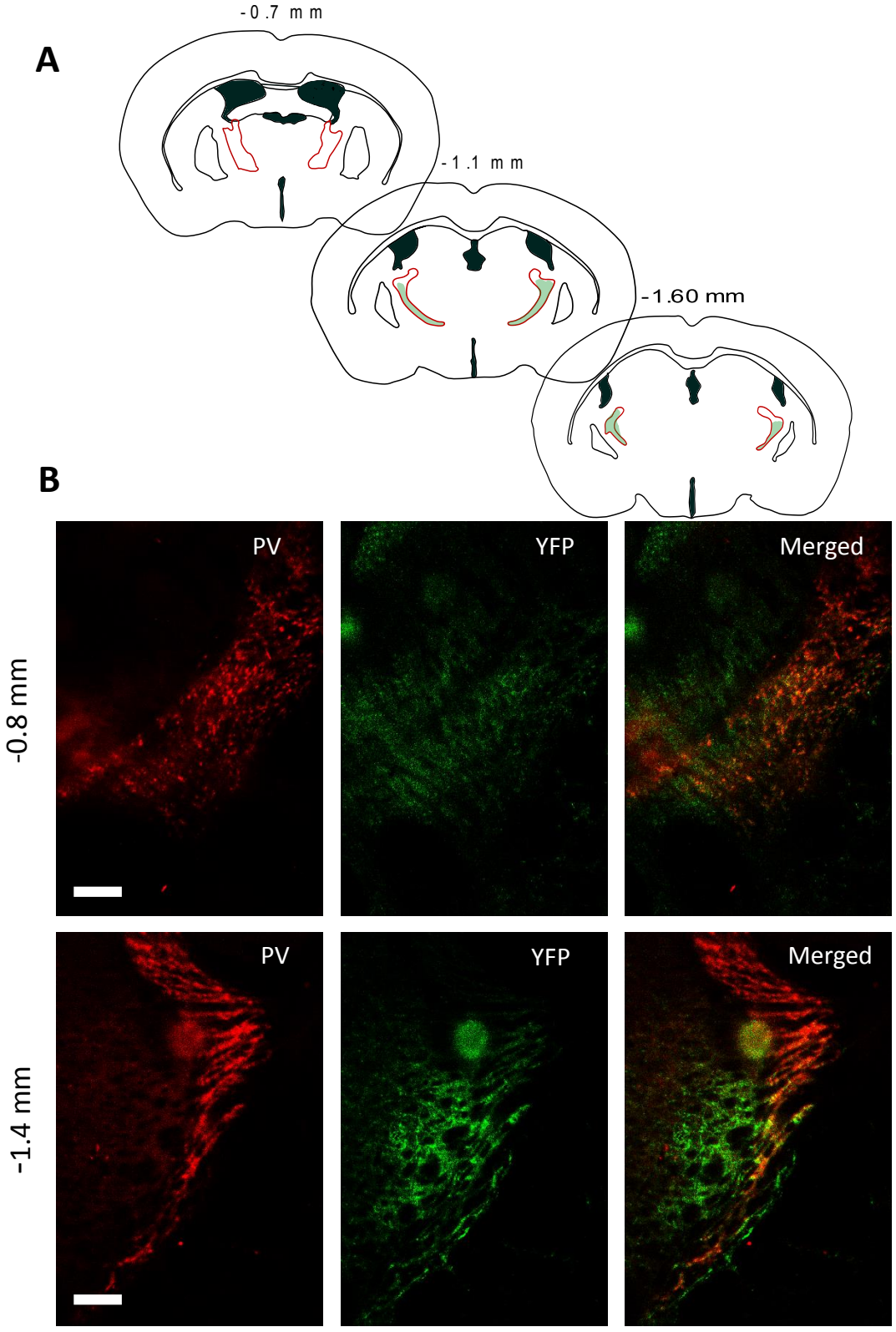

Figure 8.7 Expression pattern of Arch-YFP after bilateral caudal injections of AAV in mouse Arch-7. A. Schematic drawings of coronal sections at three coordinates containing the rostral and caudal TRN. Arch-YFP expression is marked by green shading. The red boundary highlights the TRN. B. Photographs of PV (parvalbumin, red) and YFP (green) expression in the rostral and caudal TRN. Scale bar, 250 µm.

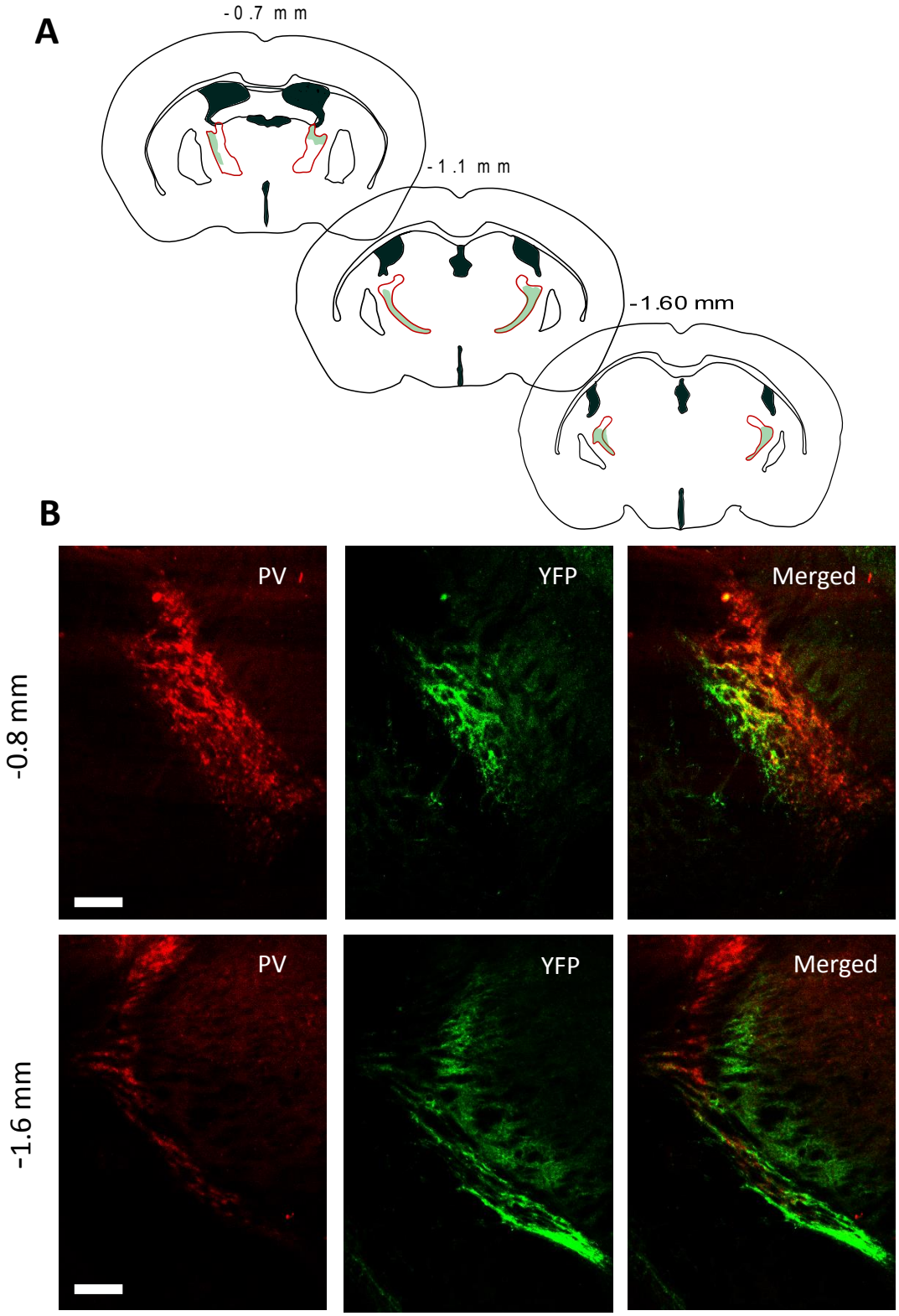

Figure 8.8 Expression pattern of Arch-YFP after bilateral caudal injections of AAV in mouse Arch-8. A. Schematic drawings of coronal sections at three coordinates containing the rostral and caudal TRN. Arch-YFP expression is marked by green shading. The red boundary highlights the TRN. B. Photographs of PV (parvalbumin, red) and YFP (green) expression in the rostral and caudal TRN. Scale bar, 250 µm.

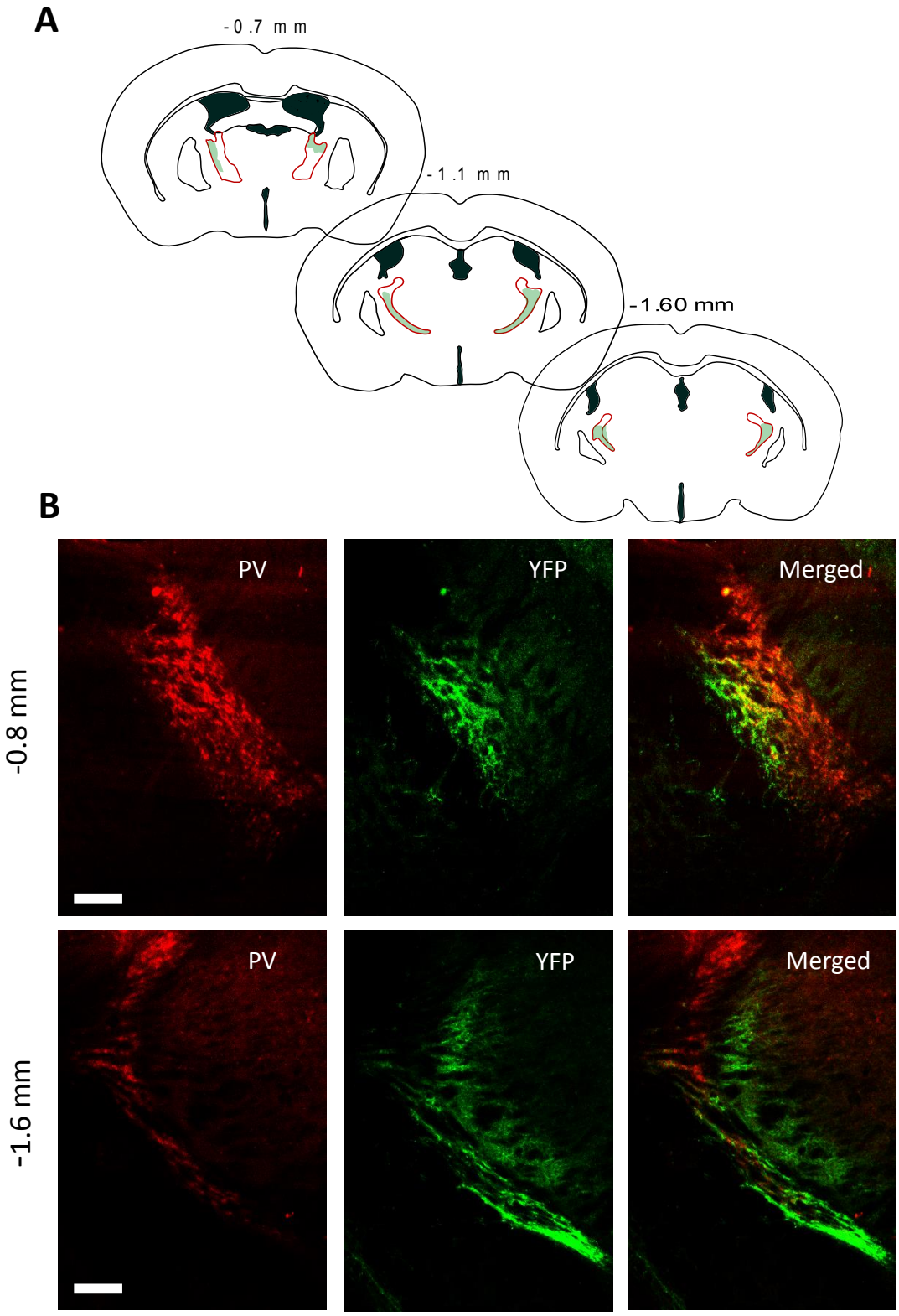

Figure 8.9 Expression pattern of Arch-YFP after bilateral caudal injections of AAV in mouse Arch-8. A. Schematic drawings of coronal sections at three coordinates containing the rostral and caudal TRN. Arch-YFP expression is marked by green shading. The red boundary highlights the TRN. B. Photographs of PV (parvalbumin, red) and YFP (green) expression in the rostral and caudal TRN. Scale bar, 250 µm.

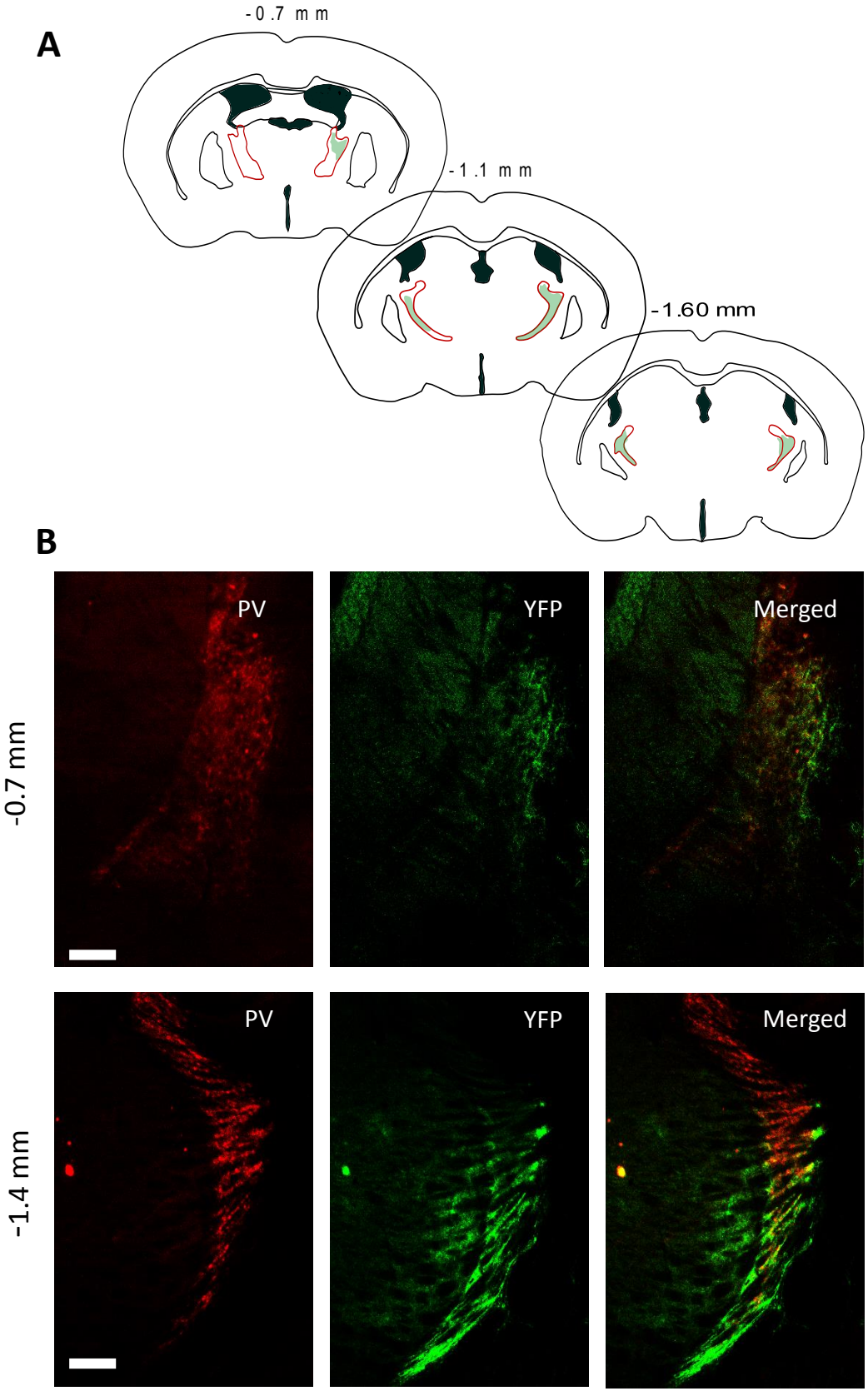

Figure 8.10 Expression pattern of Arch-YFP after bilateral caudal injections of AAV in mouse Arch-10. A. Schematic drawings of coronal sections at three coordinates containing the rostral and caudal TRN. Arch-YFP expression is marked by green shading. The red boundary highlights the TRN. B. Photographs of PV (parvalbumin, red) and YFP (green) expression in the rostral and caudal

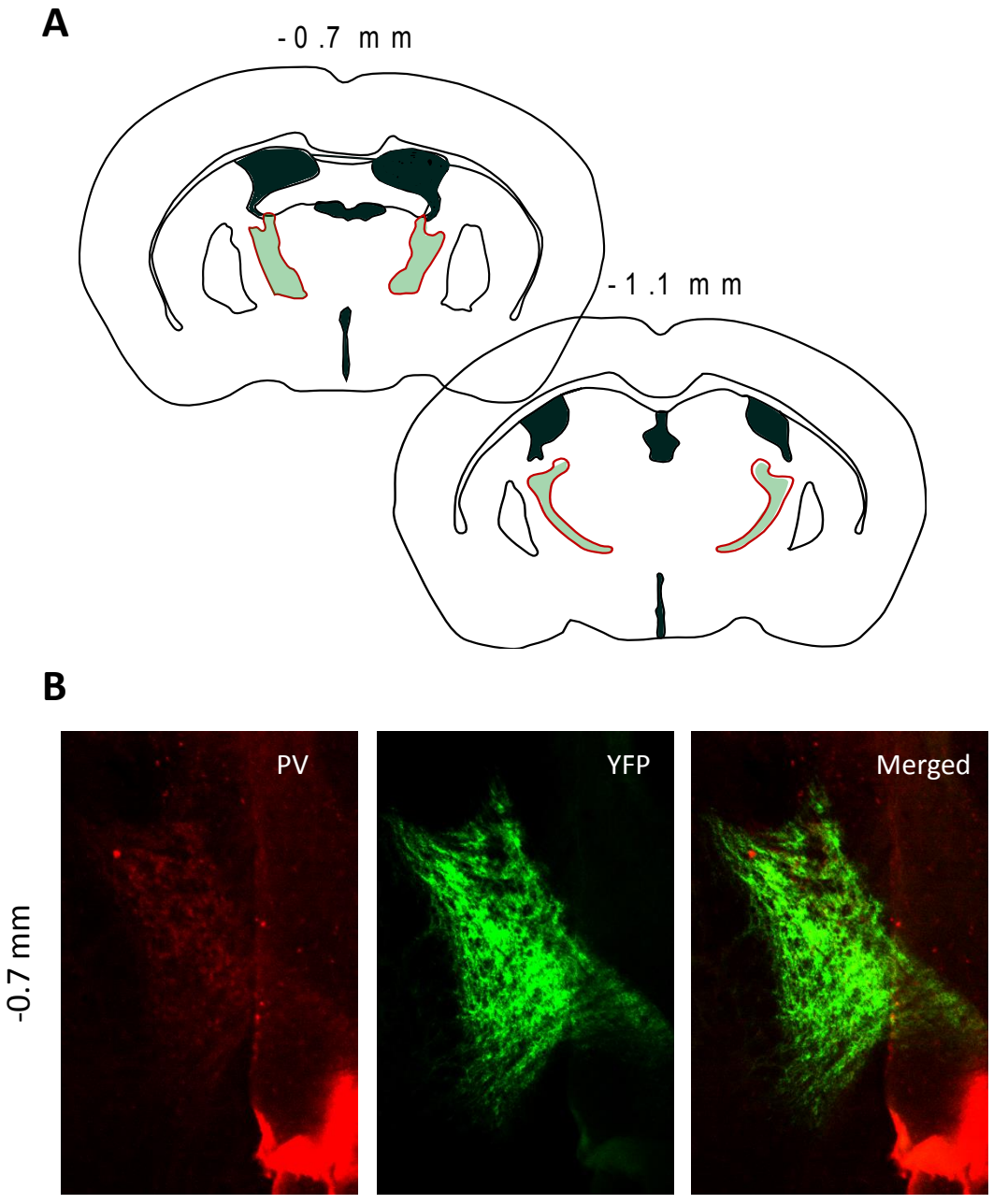

Figure 8.11 Expression pattern of NpHR-YFP after bilateral rostral injections of AAV in mouse NpHR-1. A. Schematic drawings of coronal sections at three coordinates containing the rostral and caudal TRN. NpHR-YFP expression is marked by green shading. The red boundary highlights the TRN. B. Photographs of PV (parvalbumin, red) and YFP (green) expression in the rostral and caudal TRN. Scale bar, 250 µm.

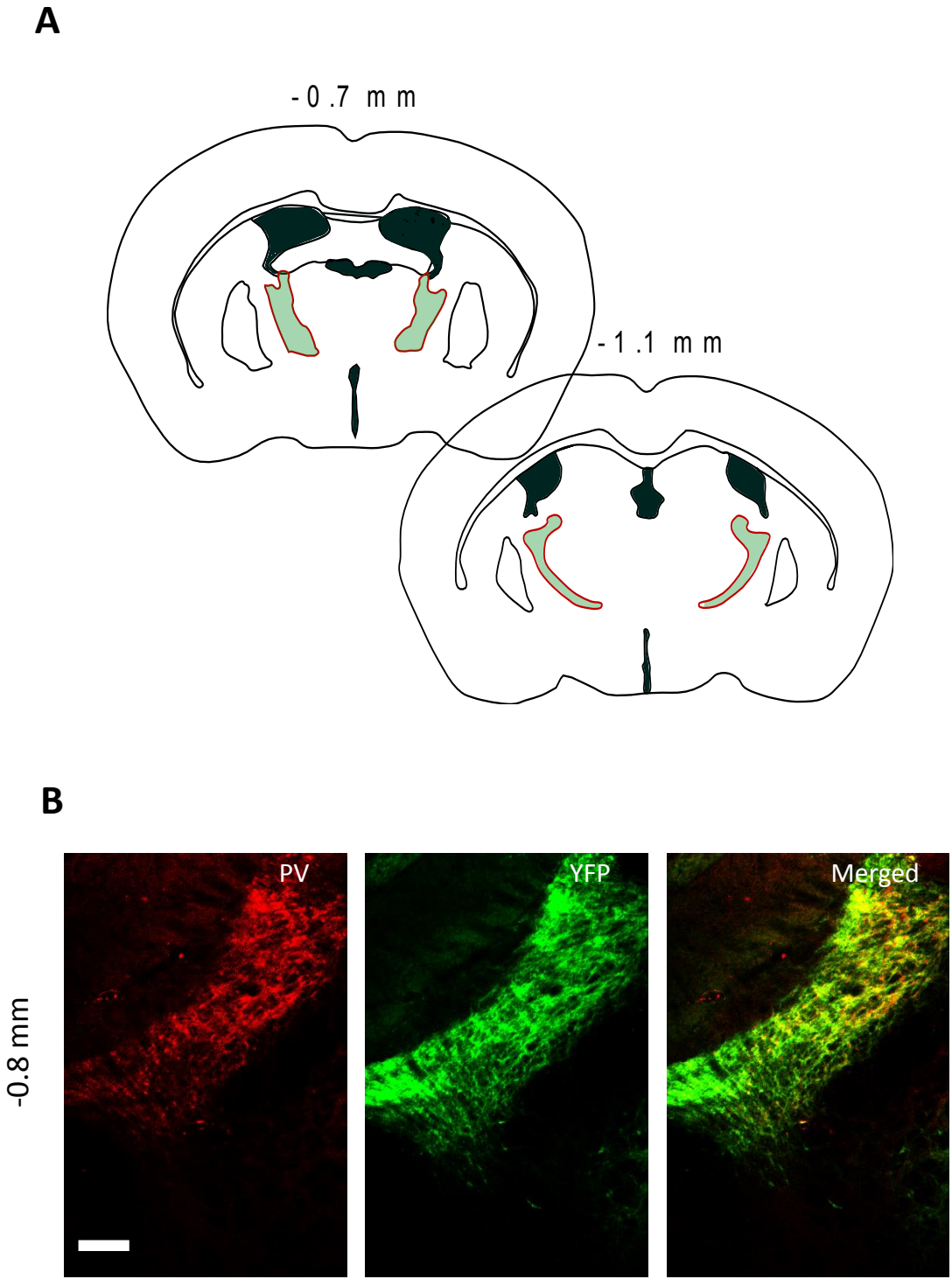

Figure 8.12 Expression pattern of NpHR-YFP after bilateral rostral injections of AAV in mouse NpHR-2. A. Schematic drawings of coronal sections at three coordinates containing the rostral and caudal TRN. NpHR-YFP expression is marked by green shading. The red boundary highlights the TRN. B. Photographs of PV (parvalbumin, red) and YFP (green) expression in the rostral and caudal TRN. Scale bar, 250 µm.

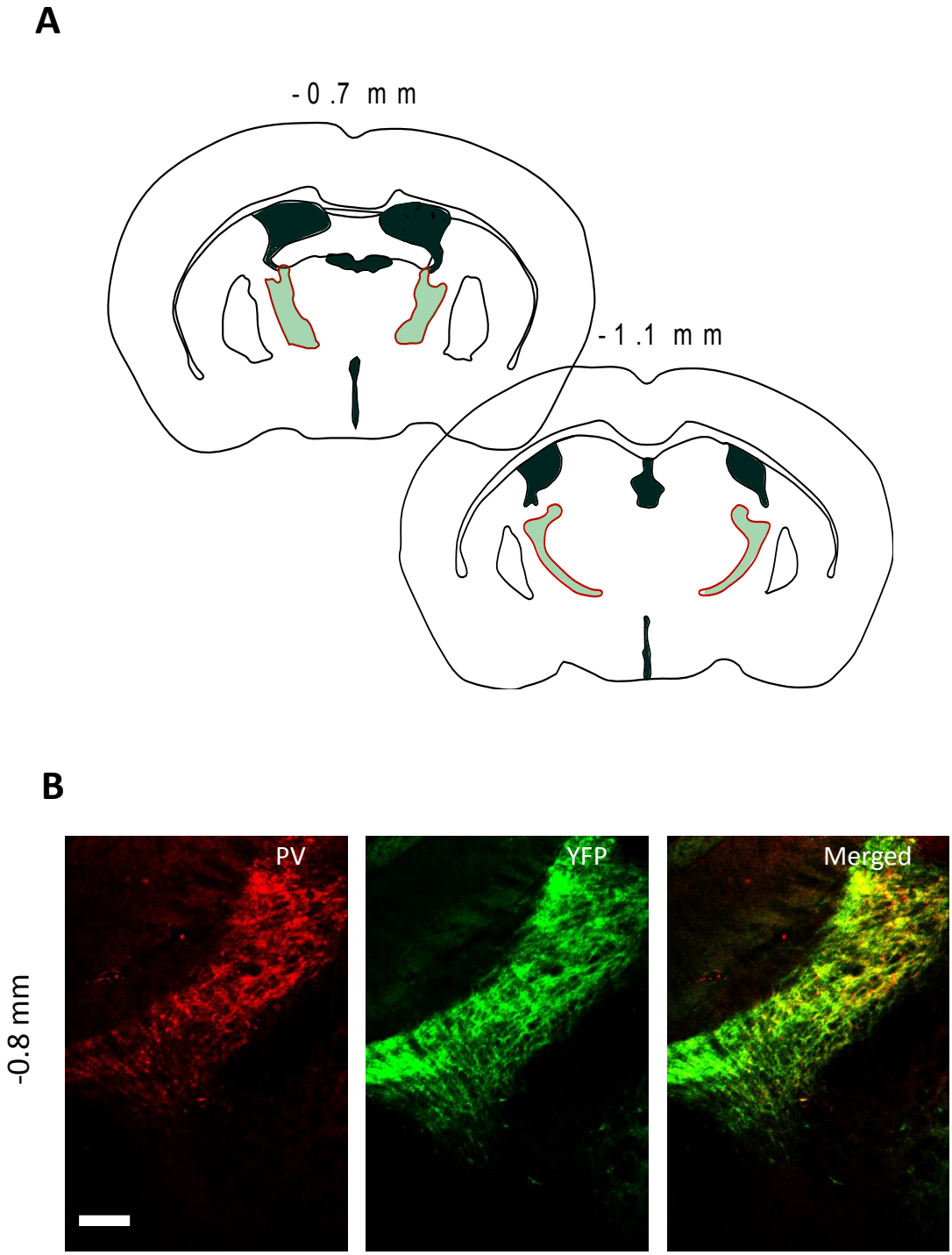

Figure 8.13 Expression pattern of NpHR-YFP after bilateral rostral injections of AAV in mouse NpHR-2. A. Schematic drawings of coronal sections at three coordinates containing the rostral and caudal TRN. NpHR-YFP expression is marked by green shading. The red boundary highlights the TRN. B. Photographs of PV (parvalbumin, red) and YFP (green) expression in the rostral and caudal TRN. Scale bar, 250 µm.

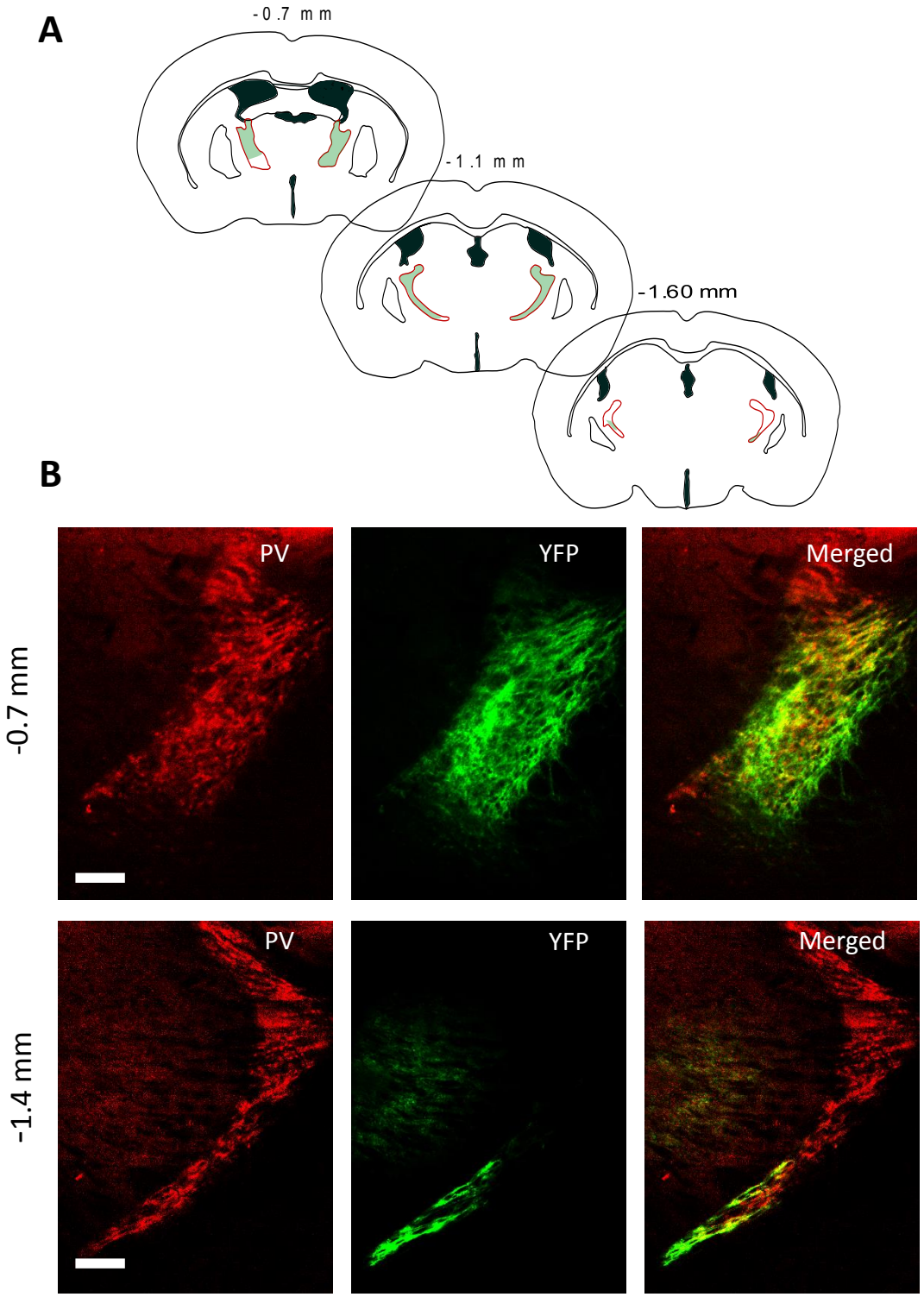

Figure 8.14 Expression pattern of NpHR-YFP after bilateral rostral injections of AAV in mouse NpHR-4. A. Schematic drawings of coronal sections at three coordinates containing the rostral and caudal TRN. NpHR-YFP expression is marked by green shading. The red boundary highlights the TRN. B. Photographs of PV (parvalbumin, red) and YFP (green) expression in the rostral and caudal TRN. Scale bar, 250 µm.

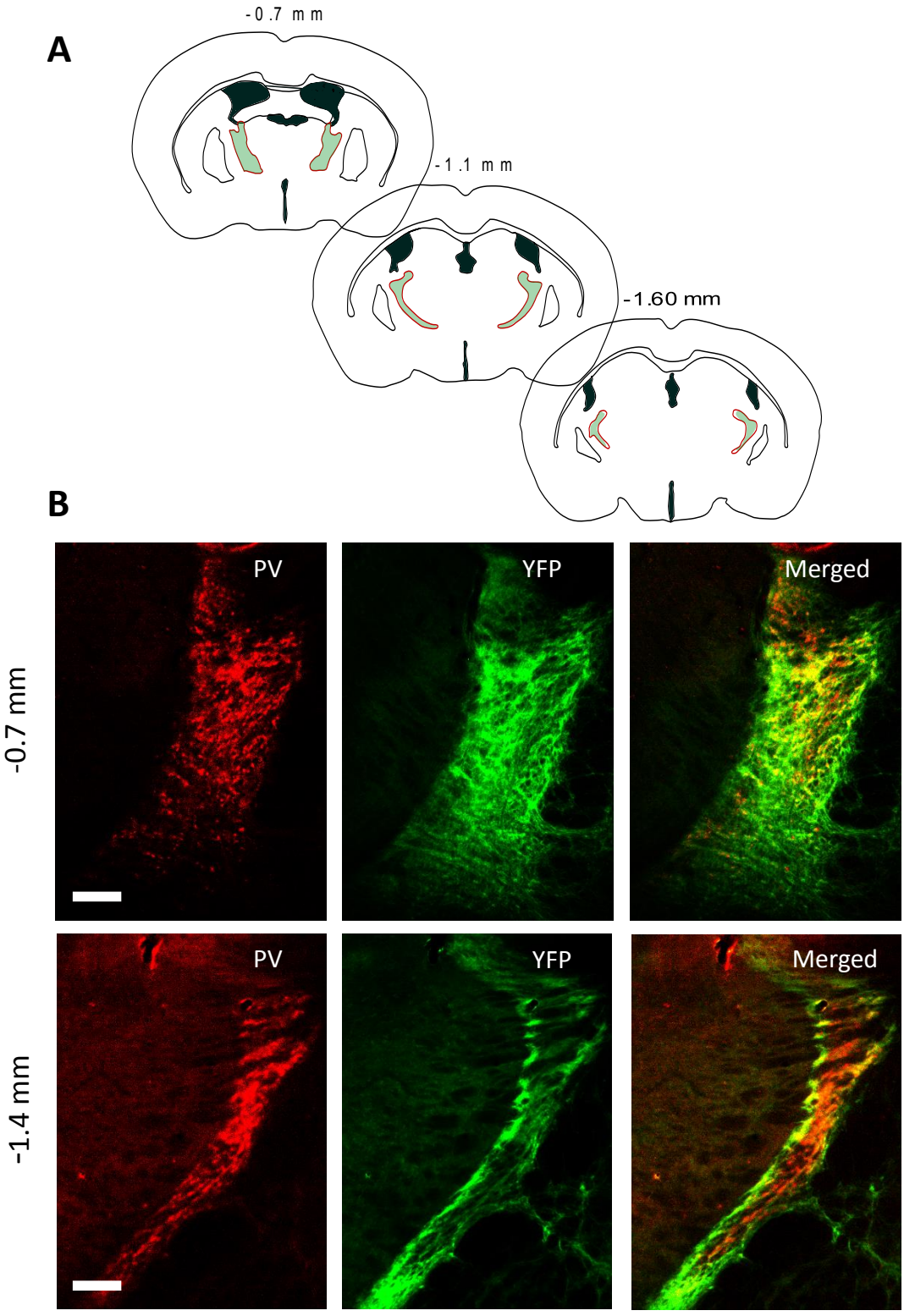

Figure 8.15 Expression pattern of NpHR-YFP after bilateral rostral injections of AAV in mouse NpHR-5. A. Schematic drawings of coronal sections at three coordinates containing the rostral and caudal TRN. NpHR-YFP expression is marked by green shading. The red boundary highlights the TRN. B. Photographs of PV (parvalbumin, red) and YFP (green) expression in the rostral and caudal TRN. Scale bar, 250 µm.

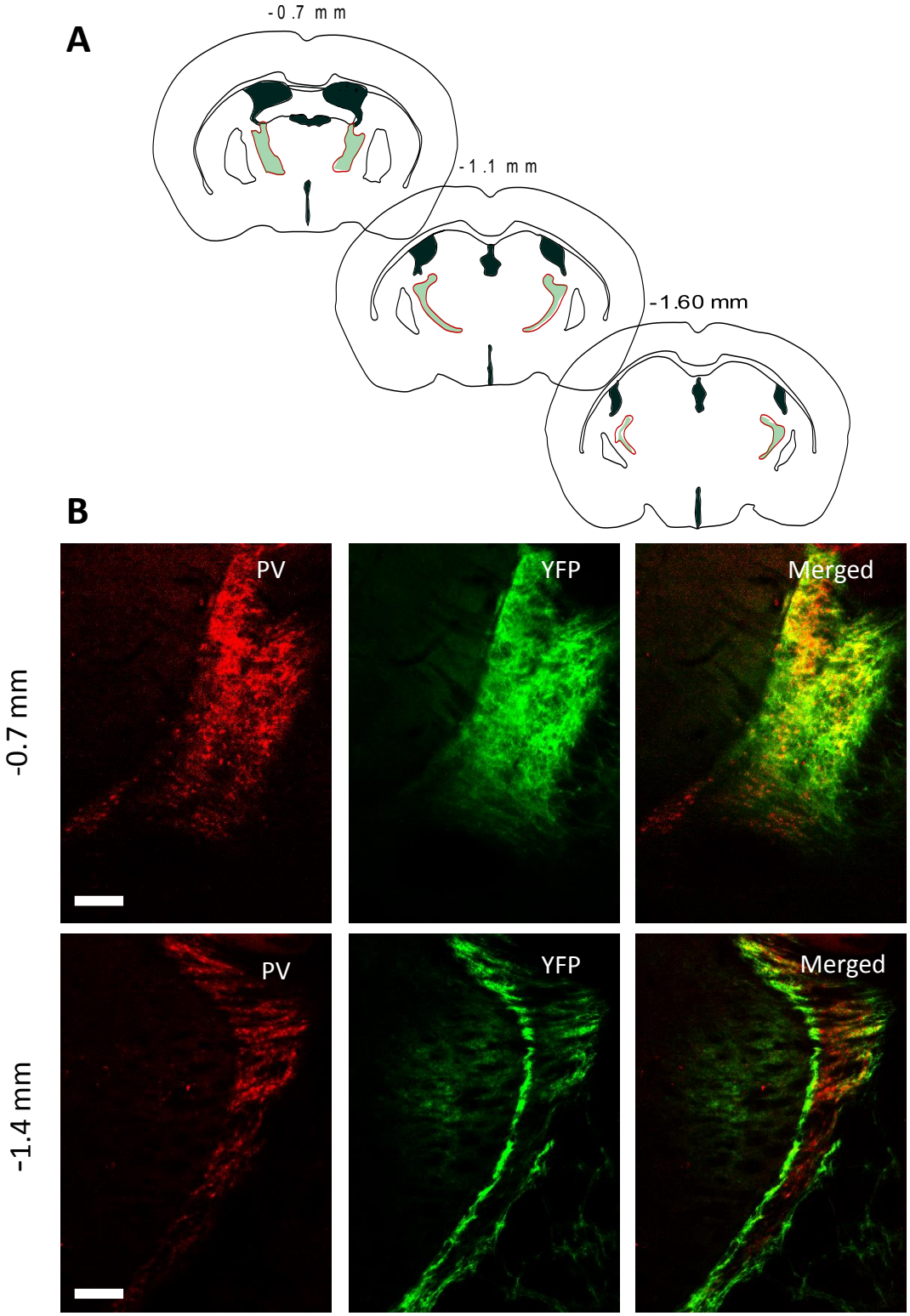

Figure 8.16 Expression pattern of NpHR-YFP after bilateral rostral injections of AAV in mouse NpHR-6. A. Schematic drawings of coronal sections at three coordinates containing the rostral and caudal TRN. NpHR-YFP expression is marked by green shading. The red boundary highlights the TRN. B. Photographs of PV (parvalbumin, red) and YFP (green) expression in the rostral and caudal TRN. Scale bar, 250 µm.

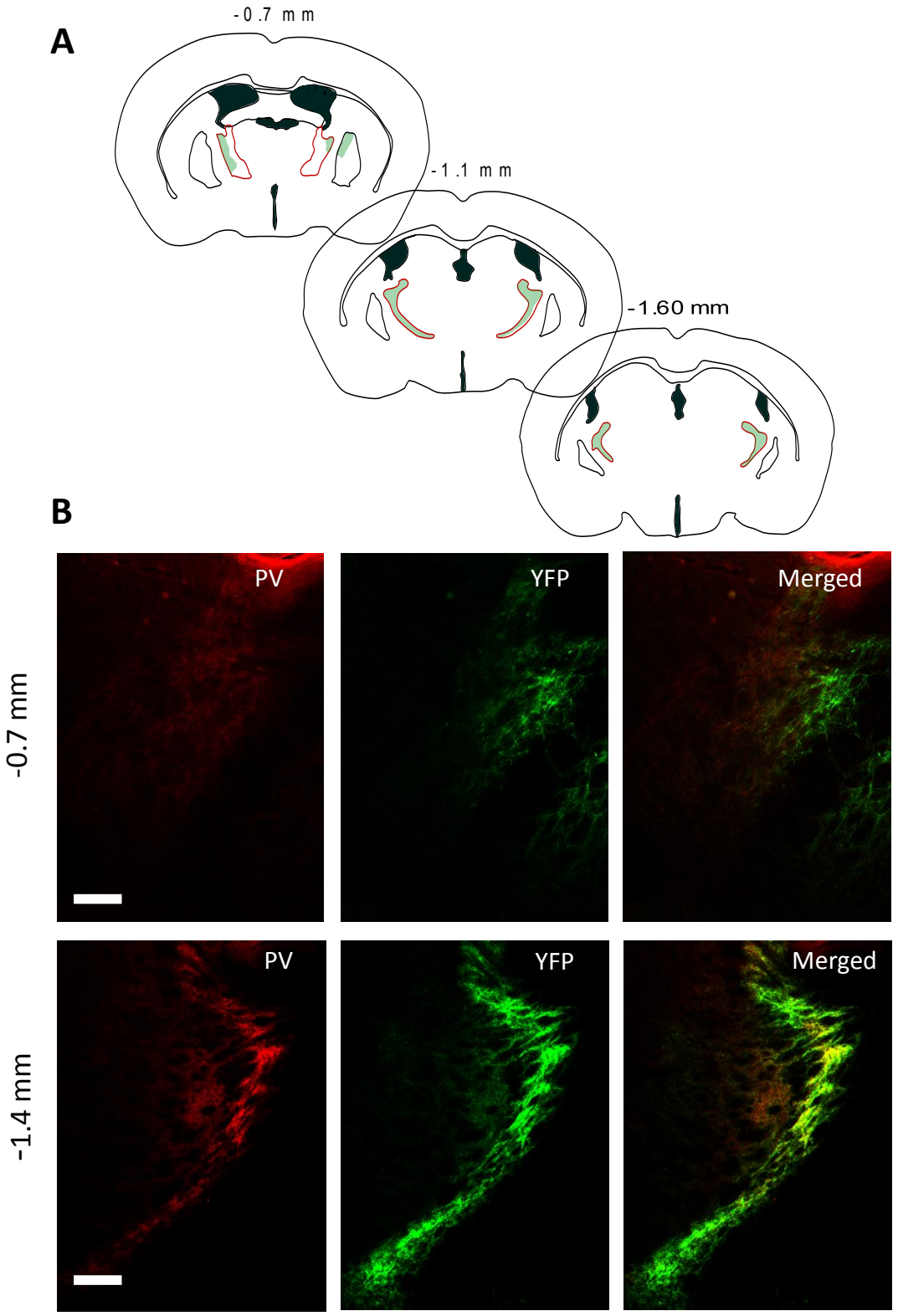

Figure 8.17 Expression pattern of NpHR-YFP after bilateral caudal injections of AAV in mouse NpHR-7. A. Schematic drawings of coronal sections at three coordinates containing the rostral and caudal TRN. NpHR-YFP expression is marked by green shading. The red boundary highlights the TRN. B. Photographs of PV (parvalbumin, red) and YFP (green) expression in the rostral and caudal TRN. Scale bar, 250 µm.

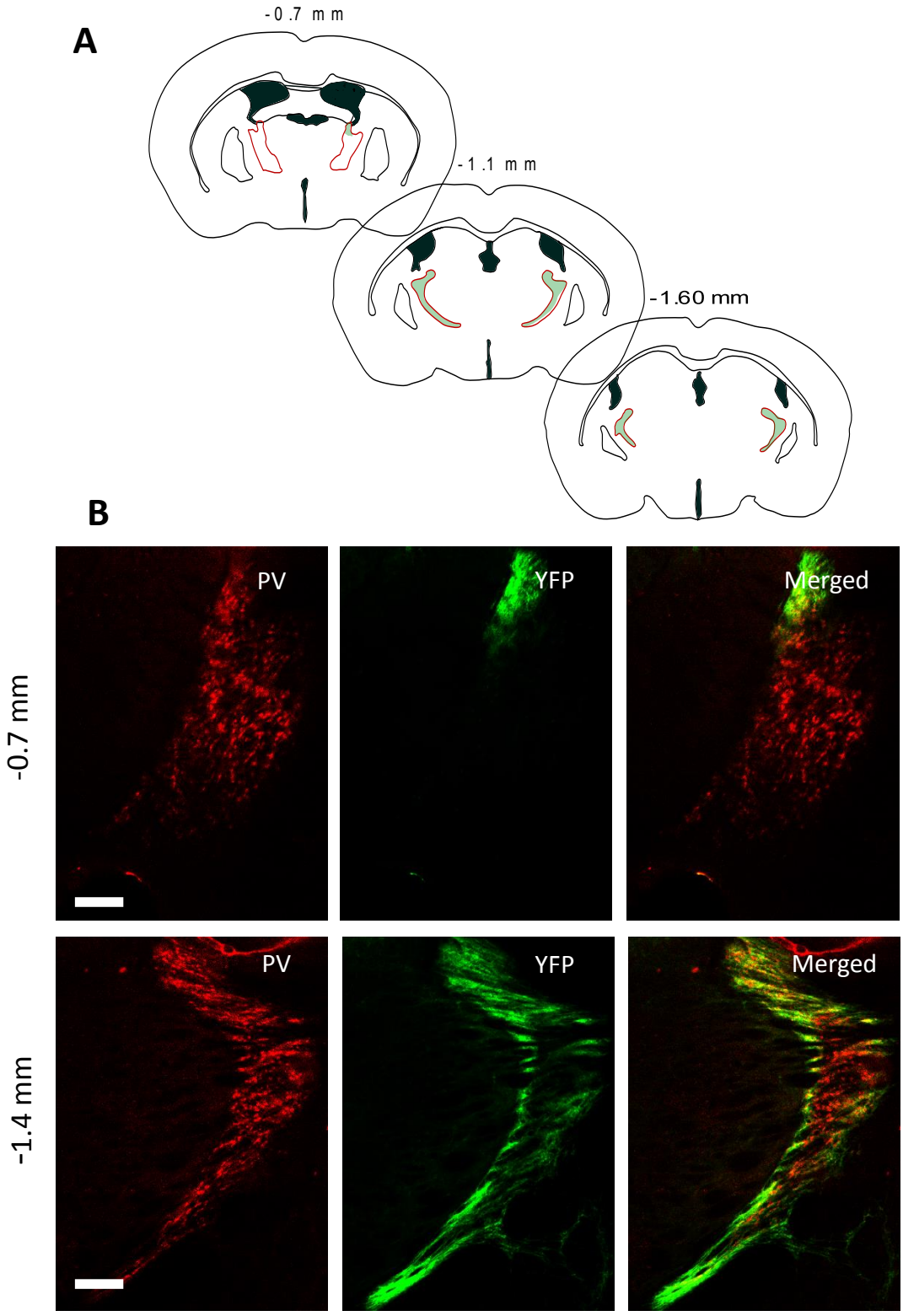

Figure 8.18 Expression pattern of NpHR-YFP after bilateral caudal injections of AAV in mouse NpHR-8. A. Schematic drawings of coronal sections at three coordinates containing the rostral and caudal TRN. NpHR-YFP expression is marked by green shading. The red boundary highlights the TRN. B. Photographs of PV (parvalbumin, red) and YFP (green) expression in the rostral and caudal TRN. Scale bar, 250 µm.

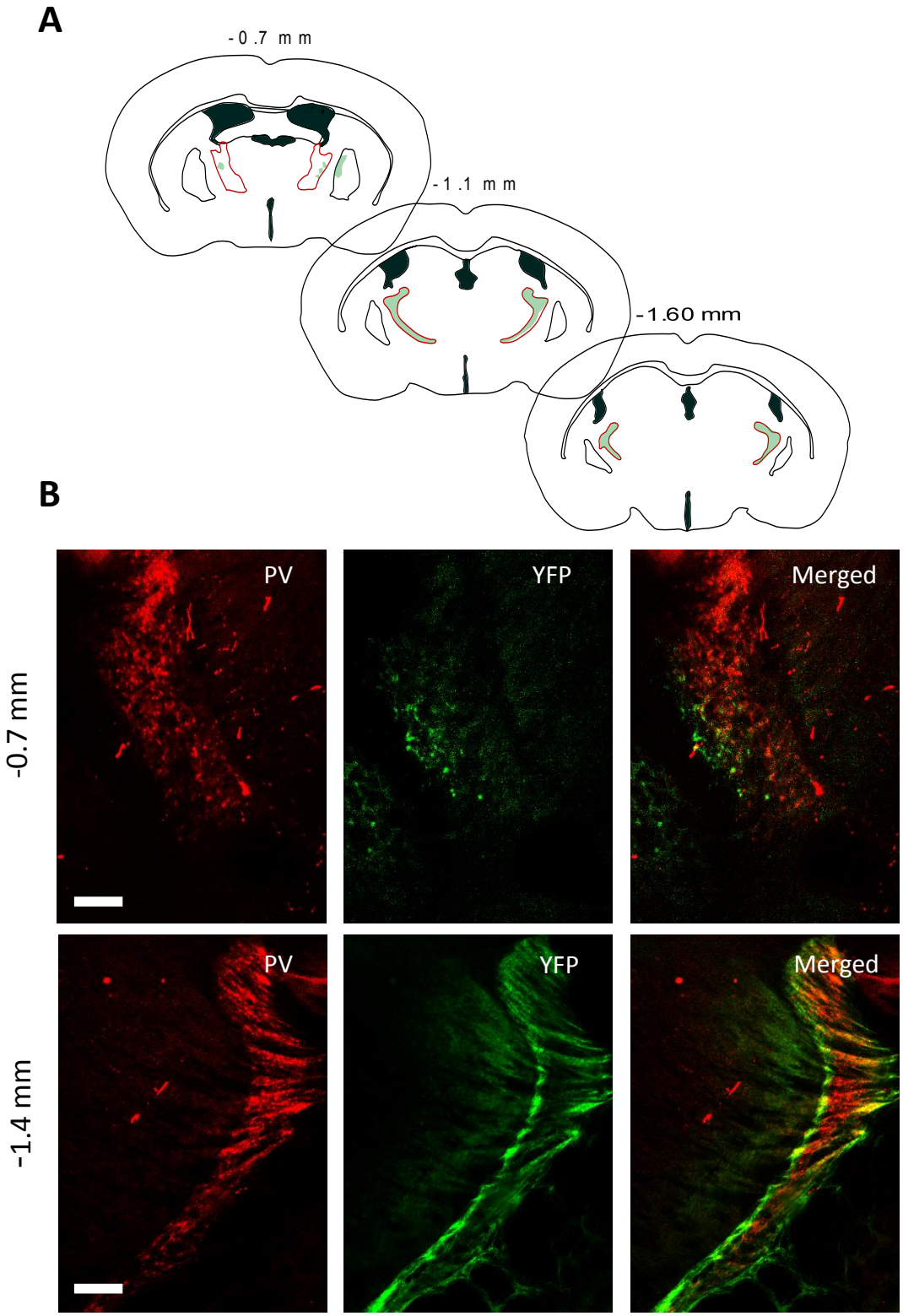

Figure 8.19 Expression pattern of NpHR-YFP after bilateral caudal injections of AAV in mouse NpHR-9. A. Schematic drawings of coronal sections at three coordinates containing the rostral and caudal TRN. NpHR-YFP expression is marked by green shading. The red boundary highlights the TRN. B. Photographs of PV (parvalbumin, red) and YFP (green) expression in the rostral and caudal TRN. Scale bar, 250 µm.

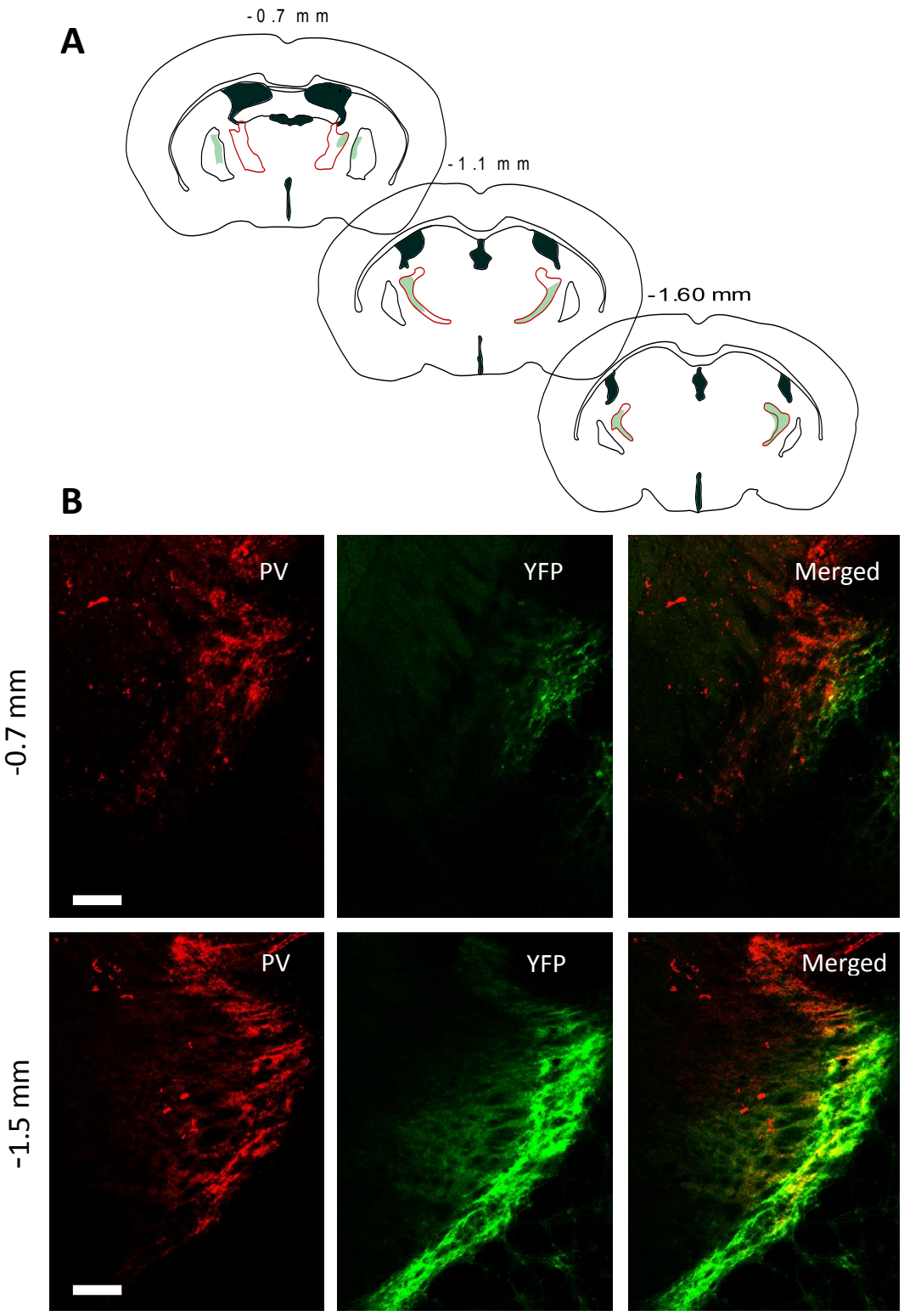

Figure 8.20 Expression pattern of NpHR-YFP after bilateral caudal injections of AAV in mouse NpHR-10. A. Schematic drawings of coronal sections at three coordinates containing the rostral and caudal TRN. NpHR-YFP expression is marked by green shading. The red boundary highlights the TRN. B. Photographs of PV (parvalbumin, red) and YFP (green) expression in the rostral and caudal TRN. Scale bar, 250 µm.

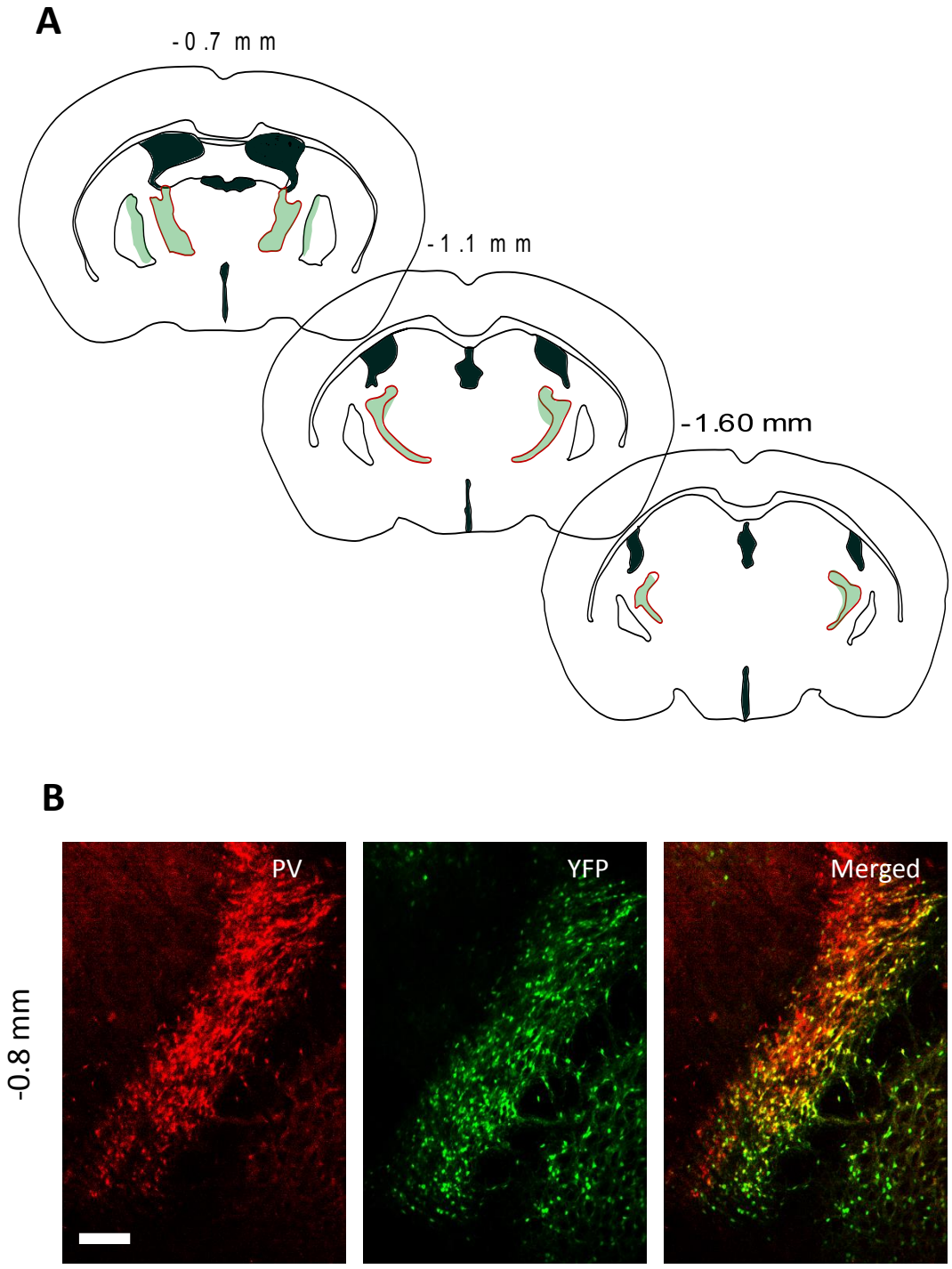

Figure 8.21 Expression pattern of Control-YFP after bilateral rostral injections of AAV in mouse Control-1. A. Schematic drawings of coronal sections at three coordinates containing the rostral and caudal TRN. Control-YFP expression is marked by green shading. The red boundary highlights the TRN. B. Photographs of PV (parvalbumin, red) and YFP (green) expression in the rostral and caudal TRN. Scale bar, 250 µm.

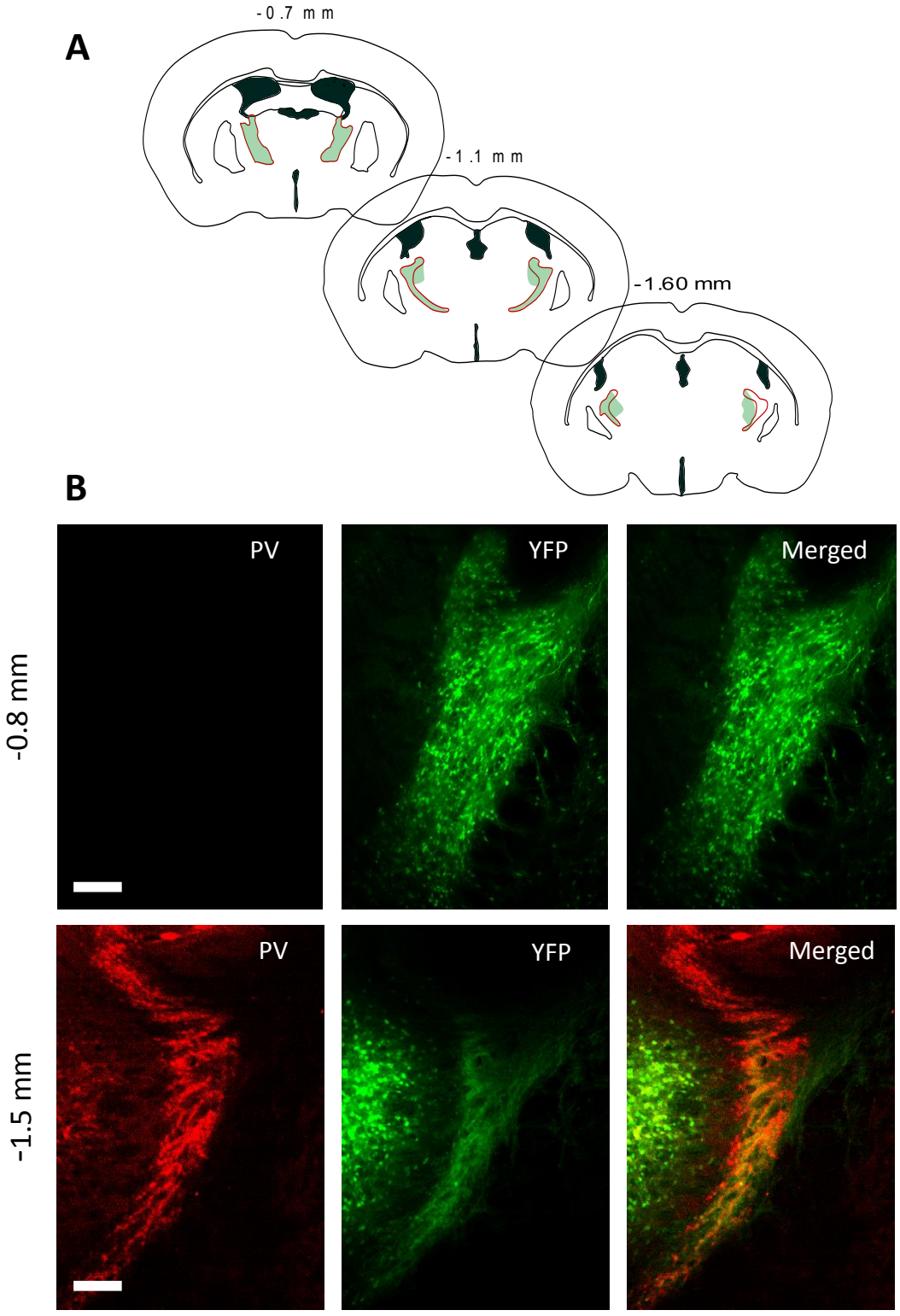

Figure 8.22 Expression pattern of Control-YFP after bilateral rostral injections of AAV in mouse Control-2. A. Schematic drawings of coronal sections at three coordinates containing the rostral and caudal TRN. Control-YFP expression is marked by green shading. The red boundary highlights the TRN. B. Photographs of PV (parvalbumin, red) and YFP (green) expression in the rostral and caudal TRN. Scale bar, 250 µm.

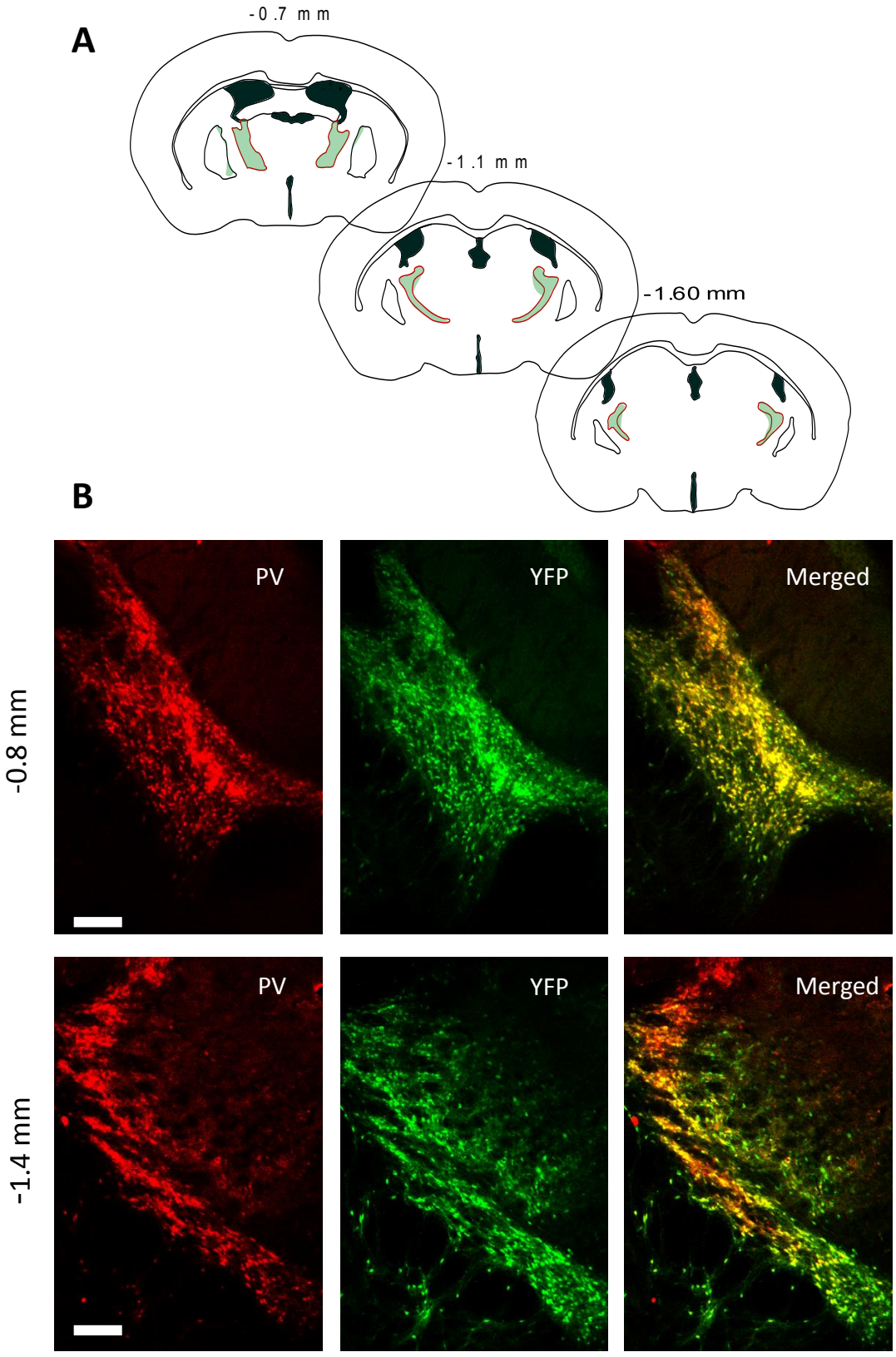

Figure 8.23 Expression pattern of Control-YFP after bilateral rostral injections of AAV in mouse Control-3. A. Schematic drawings of coronal sections at three coordinates containing the rostral and caudal TRN. Control-YFP expression is marked by green shading. The red boundary highlights the TRN. B. Photographs of PV (parvalbumin, red) and YFP (green) expression in the rostral and caudal TRN. Scale bar, 250 µm.

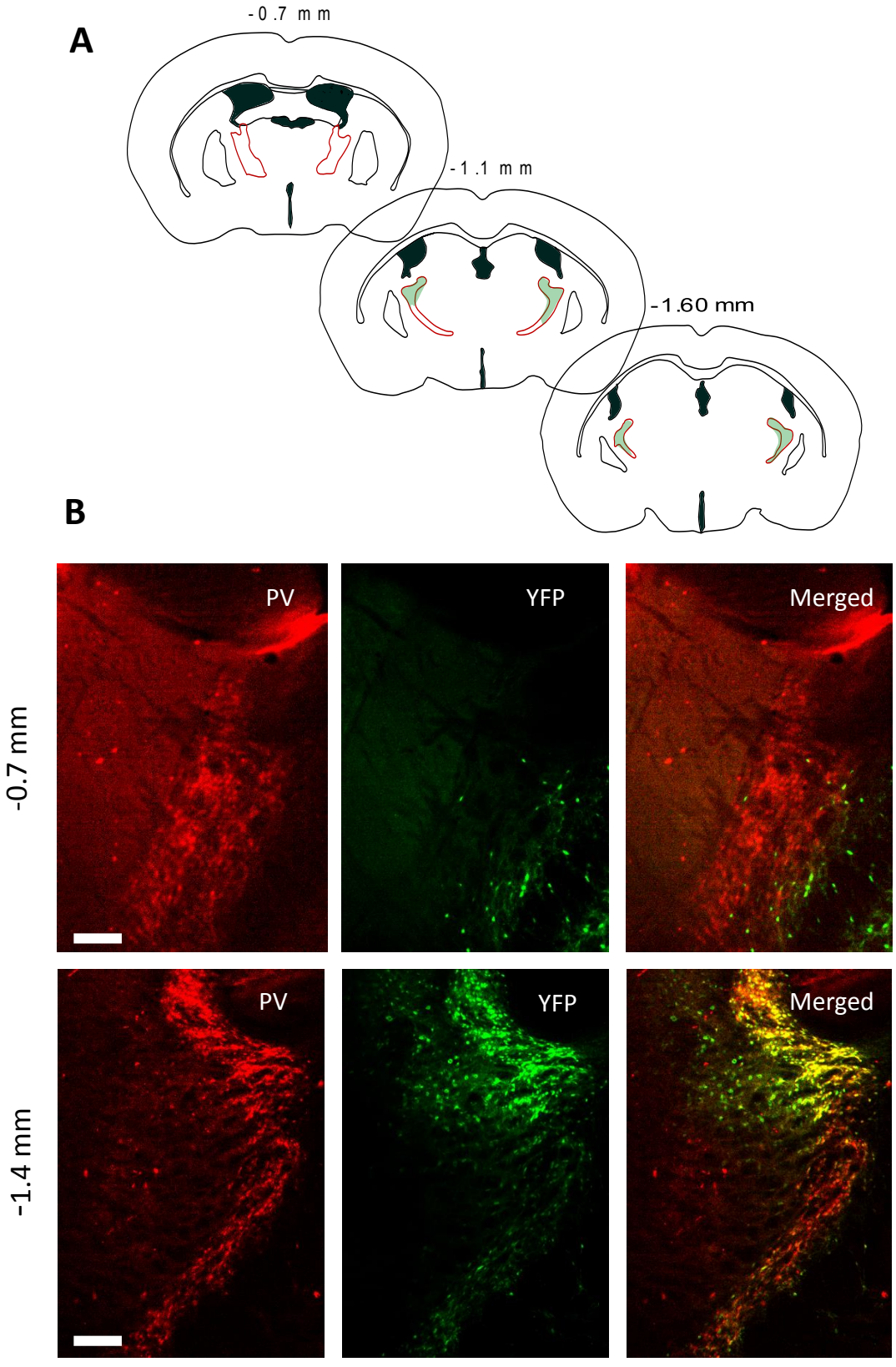

Figure 8.24 Expression pattern of Control-YFP after bilateral caudal injections of AAV in mouse Control-4. A. Schematic drawings of coronal sections at three coordinates containing the rostral and caudal TRN. Control-YFP expression is marked by green shading. The red boundary highlights the TRN. B. Photographs of PV (parvalbumin, red) and YFP (green) expression in the rostral and caudal TRN. Scale bar, 250 µm.

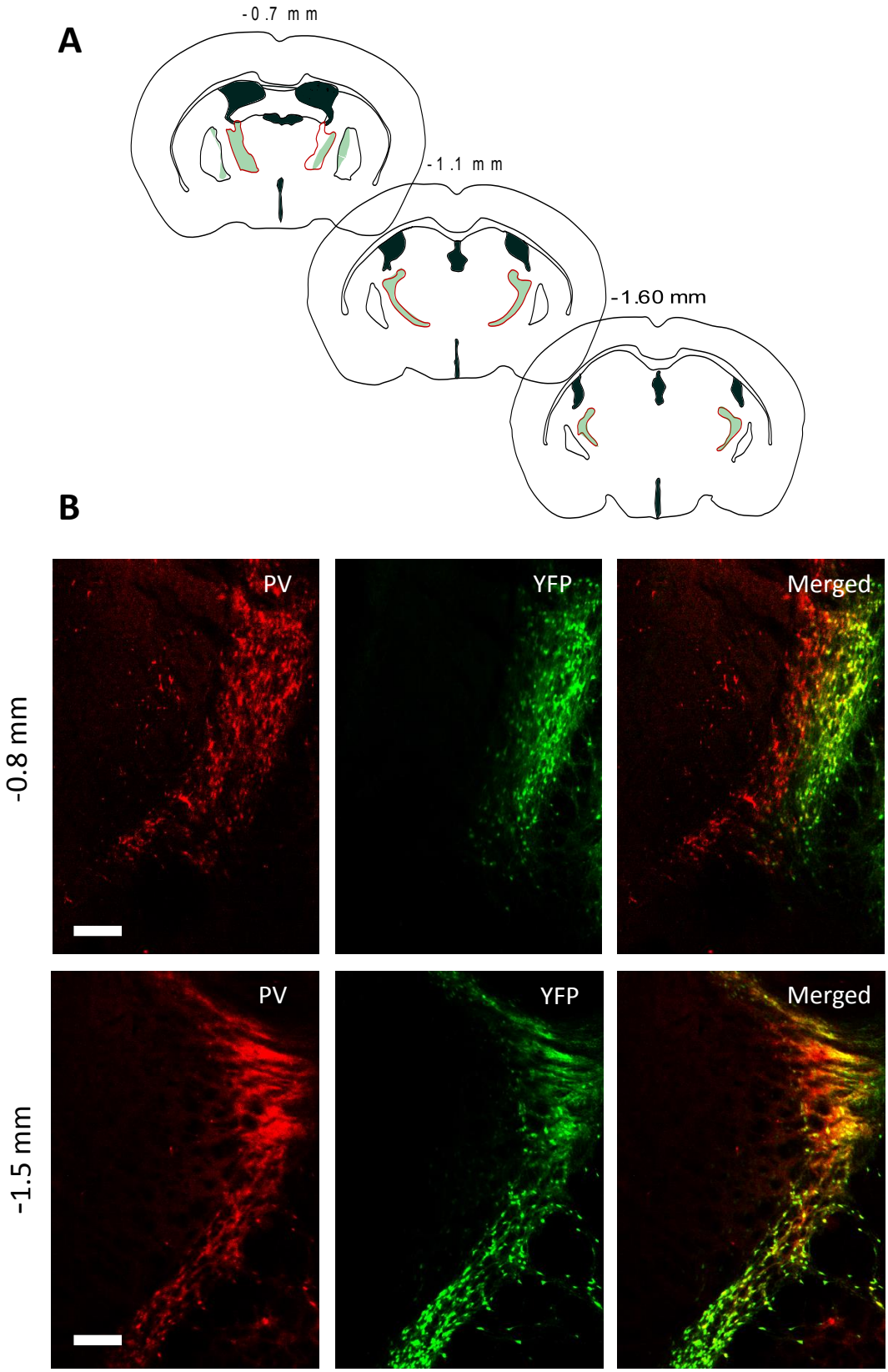

Figure 8.25 Expression pattern of Control-YFP after bilateral caudal injections of AAV in mouse Control-5. A. Schematic drawings of coronal sections at three coordinates containing the rostral and caudal TRN. Control-YFP expression is marked by green shading. The red boundary highlights the TRN. B. Photographs of PV (parvalbumin, red) and YFP (green) expression in the rostral and caudal TRN. Scale bar, 250 µm.

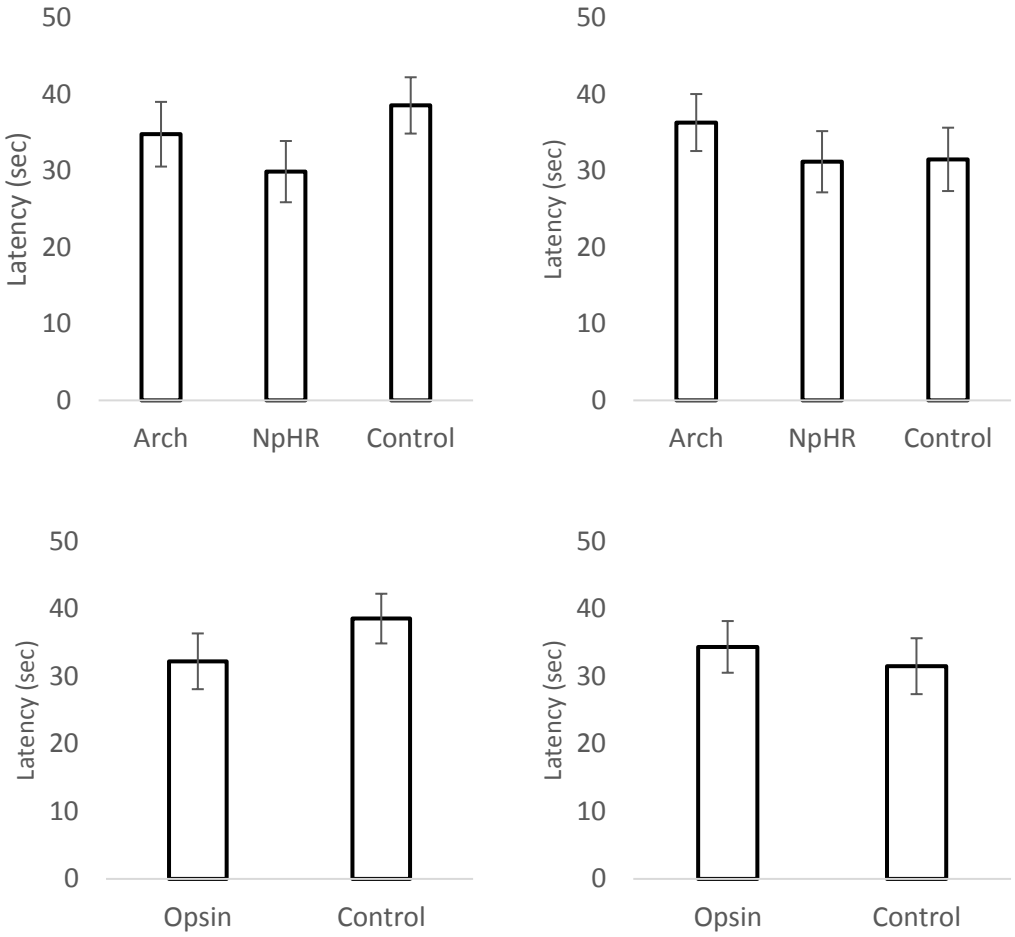

Figure 8.26 Graphs demonstrate the effect of the caudal and rostral TRN light stimulation on the latency in animals expressing Arch, NpHR and YFP (control). The latency is a period between light activation and arousal. Top graphs display the average latency change between Arch, NpHR and YFP (control) mice. Bottom graphs shows the differences in the latencies between mice with inhibitory opsins (Arch + NpHR) and control mice. The latencies were similar. * $p < 0.05$. Error bars – SEM.

Arch Caudal						Arch Rostral					
N = 39	Sleep_Wake					N = 52	Slee_Wake				
AR	5sec	10sec	MES	5sec	10sec	AR	5sec	10sec	MES	5sec	10sec
Delta	-0.30411	-0.24254	Delta	-0.09345	-0.07528	Delta	-1.10084	-0.87659	Delta	-0.30759	-0.25503
Theta	-0.08142	-0.40452	Theta	-0.04299	-0.24058	Theta	-0.4257	-0.57182	Theta	-0.26583	-0.38689
Alpha	0.136557	-0.32427	Alpha	0.07397	-0.2093	Alpha	-0.20101	-0.15287	Alpha	-0.1257	-0.10798
Beta	0.00167	-0.09727	Beta	0.001519	-0.12335	Beta	-0.27657	0.097291	Beta	-0.22219	0.096467
Gamma	0.152027	0.296821	Gamma	0.154993	0.318148	Gamma	0.241937	0.476528	Gamma	0.202987	0.360893
GammaX	0.188037	0.433718	GammaX	0.16476	0.379167	GammaX	0.1486	0.576941	GammaX	0.114649	0.394884
GammaXX	0.040274	0.479354	GammaXX	0.049377	0.455332	GammaXX	0.254349	0.759592	GammaXX	0.177597	0.418307
FR	5sec	10sec		5sec	10sec	FR	5sec	10sec			
Delta	-0.48913	-0.79787	Delta	-0.13337	-0.22244	Delta	-0.95829	-0.94596	Delta	-0.22297	-0.27249
Theta	-0.02839	-0.84946	Theta	-0.00878	-0.29638	Theta	-0.70917	-0.7985	Theta	-0.22853	-0.31039
Alpha	-0.19186	-0.82888	Alpha	-0.06325	-0.30987	Alpha	-0.82583	-0.86043	Alpha	-0.32702	-0.35485
Beta	-0.31257	-0.58817	Beta	-0.12635	-0.27478	Beta	-0.54763	-0.49277	Beta	-0.19558	-0.16479
Gamma	0.056614	0.253235	Gamma	0.035015	0.160514	Gamma	-0.23321	-0.06206	Gamma	-0.12775	-0.04654
GammaX	0.250802	0.386366	GammaX	0.188791	0.274079	GammaX	-0.09732	0.228389	GammaX	-0.05362	0.116243
GammaXX	0.077814	0.646069	GammaXX	0.065731	0.440139	GammaXX	0.242014	0.56722	GammaXX	0.078933	0.233818
N = 112	Sleep_Sleep					N = 207	Sleep_Sleep				
AR	5sec	10sec	MES	5sec	10sec	AR	5sec	10sec	MES	5sec	10sec
Delta	-0.46693	-0.13924	Delta	-0.13768	-0.04114	Delta	-0.32573	-0.27981	Delta	-0.11254	-0.1006
Theta	-0.48074	-0.28921	Theta	-0.23855	-0.16384	Theta	-0.32659	-0.29562	Theta	-0.21567	-0.21148
Alpha	-0.33361	-0.18562	Alpha	-0.16391	-0.109	Alpha	-0.1749	-0.15905	Alpha	-0.11101	-0.11062
Beta	-0.16122	-0.11386	Beta	-0.09578	-0.08106	Beta	0.045144	0.104207	Beta	0.036523	0.096488
Gamma	0.03774	-0.01753	Gamma	0.032297	-0.01688	Gamma	-0.04742	0.106747	Gamma	-0.03571	0.083957
GammaX	-0.07362	-0.01575	GammaX	-0.07049	-0.01675	GammaX	-0.04697	0.155781	GammaX	-0.03506	0.121023
GammaXX	-0.0195	-0.05883	GammaXX	-0.01971	-0.05785	GammaXX	0.018601	0.329755	GammaXX	0.01283	0.219367
FR	5sec	10sec	MES	5sec	10sec	FR	5sec	10sec	MES	5sec	10sec
Delta	-0.41773	-0.21449	Delta	-0.11996	-0.06412	Delta	-0.20414	-0.08646	Delta	-0.05593	-0.02473
Theta	-0.33307	-0.2614	Theta	-0.10216	-0.08737	Theta	-0.10391	-0.2194	Theta	-0.03876	-0.09003
Alpha	-0.51668	-0.48178	Alpha	-0.1608	-0.16078	Alpha	-0.11826	-0.09533	Alpha	-0.04233	-0.03713
Beta	-0.34823	-0.34537	Beta	-0.11807	-0.12639	Beta	-0.10863	-0.04702	Beta	-0.04898	-0.02346
Gamma	-0.18814	-0.17426	Gamma	-0.08237	-0.08078	Gamma	-0.03313	0.062266	Gamma	-0.02104	0.043514
GammaX	-0.04761	-0.04019	GammaX	-0.02527	-0.02165	GammaX	-0.15529	0.064208	GammaX	-0.08984	0.040906
GammaXX	0.026008	-0.06678	GammaXX	0.016244	-0.04087	GammaXX	0.061735	0.207486	GammaXX	0.030728	0.110124
Paired t test						Measure effec size (MES)					
p < 0.05	P < 0.01										

Figure 8.27 Table shows the oscillation bands differences caused by 5 and 10 seconds stimulation of the rostral and caudal TRN in mice expressing Arch. Top row is dedicated to the traces from pre-wake sleep (Sleep_Wake). Bottom row is dedicated to the traces from deep sleep (Sleep_Sleep). Left column shows results from the caudally stimulated animals (Arch Caudal) and right column results are from the rostrally stimulated animals (Arch Rostral). Paired t test p value changes are colour coded (left bottom corner). Measure effect values (MES) is displayed opposite to the power difference changes and are colour coded (bottom). N – number of traces. Arch Caudal = 7 mice. Arch Rostral = 7 mice.

Halo Caudal

N = 38	Sleep_Wake				
AR	5sec	10sec	MES	5sec	10sec
Delta	0.05151	-0.14121	Delta	0.006512	-0.01769
Theta	-0.19415	0.138883	Theta	-0.02835	0.02081
Alpha	-0.34942	-0.16387	Alpha	-0.05117	-0.02402
Beta	0.102184	0.14397	Beta	0.018124	0.02506
Gamma	0.073628	0.155648	Gamma	0.016036	0.033129
GammaX	0.000438	0.098302	GammaX	9.85E-05	0.021749
GammaXX	0.236201	0.240444	GammaXX	0.056017	0.057615
FR	5sec	10sec		5sec	10sec
Delta	-0.0586	-0.4092	Delta	-0.01212	-0.08519
Theta	-0.25027	-0.37645	Theta	-0.07427	-0.1227
Alpha	-0.01668	0.023476	Alpha	-0.00501	0.00722
Beta	0.140767	-0.00394	Beta	0.048106	-0.00143
Gamma	0.244149	0.184187	Gamma	0.145346	0.118286
GammaX	0.134838	0.279536	GammaX	0.122614	0.273519
GammaXX	0.133351	0.244742	GammaXX	0.157601	0.310569

N = 64	Sleep_Sleep				
AR	5sec	10sec	MES	5sec	10sec
Delta	-0.59344	-0.525	Delta	-0.08322	-0.07289
Theta	-0.30885	0.045926	Theta	-0.05077	0.007556
Alpha	0.023215	0.117325	Alpha	0.003675	0.018478
Beta	0.211833	0.202585	Beta	0.03992	0.038388
Gamma	0.080886	0.156353	Gamma	0.017448	0.033666
GammaX	0.075358	0.256133	GammaX	0.016852	0.057418
GammaXX	-0.03154	0.227318	GammaXX	-0.0073	0.05347
FR	5sec	10sec	MES	5sec	10sec
Delta	-0.83883	-0.58934	Delta	-0.19523	-0.1467
Theta	-0.65426	-0.40957	Theta	-0.18473	-0.12341
Alpha	-0.61345	-0.38623	Alpha	-0.17029	-0.11085
Beta	-0.59987	-0.4704	Beta	-0.1835	-0.15108
Gamma	-0.15385	0.002869	Gamma	-0.049	0.000946
GammaX	-0.04526	0.080008	GammaX	-0.01411	0.025768
GammaXX	0.053071	0.284107	GammaXX	0.018645	0.104692

Halo Rostral

N = 31	Slee_Wake				
AR	5sec	10sec	MES	5sec	10sec
Delta	-0.64438	-0.91366	Delta	-0.10111	-0.14677
Theta	-0.35366	-0.68086	Theta	-0.06363	-0.12883
Alpha	-0.24723	-0.13838	Alpha	-0.04832	-0.028
Beta	0.462126	0.571973	Beta	0.102836	0.132541
Gamma	0.63907	0.76636	Gamma	0.148088	0.187746
GammaX	0.254379	0.895357	GammaX	0.057849	0.2236
GammaXX	-0.05973	0.633167	GammaXX	-0.01611	0.182634
FR	5sec	10sec			
Delta	-0.63464	-1.00287	Delta	-0.11925	-0.19736
Theta	-0.70771	-0.83068	Theta	-0.19098	-0.27057
Alpha	-0.22649	-0.24349	Alpha	-0.06447	-0.07551
Beta	0.0908	-0.11391	Beta	0.03571	-0.04741
Gamma	0.56647	0.342264	Gamma	0.299963	0.204338
GammaX	0.559995	0.596673	GammaX	0.312161	0.35665
GammaXX	0.619662	0.854847	GammaXX	0.293407	0.416879

N = 155	Sleep_Sleep				
AR	5sec	10sec	MES	5sec	10sec
Delta	-0.60221	-0.45168	Delta	-0.12339	-0.09416
Theta	0.017371	0.121939	Theta	0.0043	0.03068
Alpha	-0.09837	-0.04032	Alpha	-0.02376	-0.00995
Beta	0.081965	0.026126	Beta	0.023807	0.007849
Gamma	-0.10083	-0.12242	Gamma	-0.04126	-0.04959
GammaX	-0.07957	-0.0058	GammaX	-0.02724	-0.002
GammaXX	-0.17557	-0.08842	GammaXX	-0.0593	-0.02942
FR	5sec	10sec	MES	5sec	10sec
Delta	-0.60603	-0.30234	Delta	-0.12725	-0.06211
Theta	-0.13285	0.050537	Theta	-0.04366	0.018604
Alpha	0.013194	-0.02702	Alpha	0.004393	-0.00978
Beta	0.047693	0.084928	Beta	0.018905	0.037664
Gamma	-0.18557	-0.05559	Gamma	-0.12455	-0.03977
GammaX	0.001326	0.019973	GammaX	0.000941	0.014887
GammaXX	-0.13598	-0.12262	GammaXX	-0.08758	-0.0837

Paired t test		Measure effec size (MES)
p < 0.05	P < 0.01	

Figure 8.28 Table shows the oscillation bands differences caused by 5 and 10 seconds stimulation of the rostral and caudal TRN in mice expressing NpHR (Halo). Top row is dedicated to the traces from pre-wake sleep (Sleep_Wake). Bottom row is dedicated to the traces from deep sleep (Sleep_Sleep). Left column shows results from the caudally stimulated animals (Halo Caudal) and right column results are from the rostrally stimulated animals. Paired t test p value changes are colour coded (left bottom corner). Measure effect values (MES) are displayed opposite to the power difference changes and are colour coded (bottom). N – number of traces. NpHR (Halo) Caudal = 7 mice. NpHR (Halo) Rostral = 7 mice.

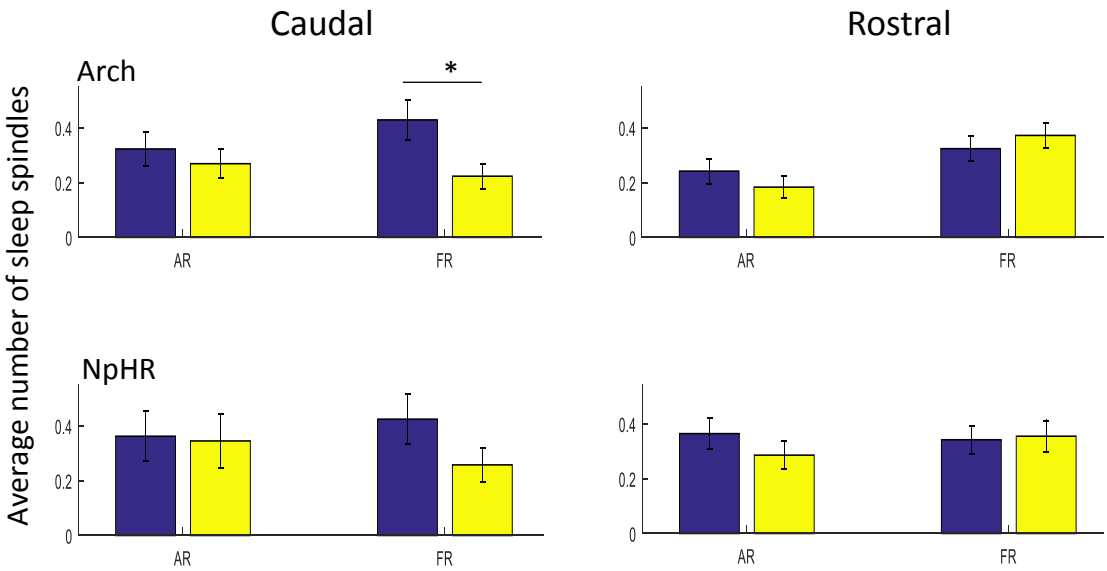

Figure 8.29 Sleep spindle change during light stimulation in Arch (top) and NpHR (bottom) expressing animals. Figure portrays an average number of sleep spindles over 10 seconds period before (blue) and during (yellow) light stimulation detected in auditory right (AR) and frontal right (FR) EEG channels. The light stimulation of the caudal TRN in Arch expressing animals reduce significantly the average number of sleep spindles recorded in FR channel. Paired t test, * $p < 0.05$. Error bars – SEM.